FINAL REPORT

FHWA/IN/JTRP-2006/15

IMPLEMENTATION OF A NON-METALLIC REINFORCED BRIDGE DECK

Volume 1: Bond Behavior

By

Robert J. Frosch
Associate Professor of Civil Engineering
Principal Investigator

and

A. Cihan Pay
Graduate Research Assistant

School of Civil Engineering
Purdue University

Joint Transportation Research Program
Project No. C-36-56HHH
File No. 7-4-59
SPR-2491

Project No. C-36-56SSS
File No. 7-4-70
FHWA 2004001

Conducted in Cooperation with the
Indiana Department of Transportation
and the
Federal Highway Administration

Purdue University
West Lafayette, IN 47907
May 2006

TECHNICAL REPORT STANDARD TITLE PAGE

1. Report No.	2. Government Accession No.	3. Recipient's Catalog No.
FHWA/IN/JTRP-2006/15		

4. Title and Subtitle	5. Report Date
Implementation of a Non-Metallic Reinforced Bridge Deck	May 2006
	6. Performing Organization Code

7. Author(s)	8. Performing Organization Report No.
Robert J. Frosch and A. Cihan Pay	FHWA/IN/JTRP-2006/15

9. Performing Organization Name and Address	10. Work Unit No.
Joint Transportation Research Program 550 Stadium Mall Drive Purdue University West Lafayette, Indiana 47907-2051	
	11. Contract or Grant No. SPR-2491 & FHWA-2004001

12. Sponsoring Agency Name and Address	13. Type of Report and Period Covered
Indiana Department of Transportation State Office Building 100 North Senate Avenue Indianapolis, IN 46204	Final Report
	14. Sponsoring Agency Code

15. Supplementary Notes

Prepared in cooperation with the Indiana Department of Transportation and Federal Highway Administration.

16. Abstract

The primary maintenance problem with bridges in Indiana has been deterioration of the concrete deck which is often related to corrosion of the reinforcing steel. While a corrosion protection system consisting of epoxy-coated reinforcement in combination with 2-1/2 in. of Class C concrete cover has been used in Indiana, research and experience have demonstrated that this system can be compromised. As an alternative solution to the corrosion problem in reinforced concrete, fiber reinforced polymer (FRP) bars which are corrosion resistant can be provided as reinforcement. This research was divided into two phases directed towards the implementation of a nonmetallic reinforced bridge deck. The first phase evaluated the bond strength of fiber reinforced polymer reinforcement with the goal of developing a design expression for the calculation of development and splice lengths. Forty-six glass FRP, carbon FRP, and steel reinforced concrete beams with unconfined tension lap splices were tested. The second phase consisted of the design, construction, and performance evaluation of a glass FRP bar reinforced concrete bridge deck. Based on this study, design recommendations are provided for the calculation of development and splice lengths of both FRP and steel reinforcement. Furthermore, the behavior of the FRP reinforced bridge deck is assessed and compared with its design assumptions. The findings of this study provide design tools and behavioral data that will assist in the future development and deployment of this technology.

17. Key Words	18. Distribution Statement
Bond, Bridge Deck, Bridges, Concrete, Development Length, Durability, Fiber Reinforced Polymer (FRP) Reinforcement, Nonmetallic Reinforcement, Splice Length	No restrictions. This document is available to the public through the National Technical Information Service, Springfield, VA 22161

19. Security Classif. (of this report)	20. Security Classif. (of this page)	21. No. of Pages	22. Price
Unclassified	Unclassified	309+106	

Form DOT F 1700.7 (8-69)

ACKNOWLEDGEMENTS

This work was supported by the Joint Transportation Research Program (JTRP) administered by the Indiana Department of Transportation (INDOT) and Purdue University through contract SPR-2491 and FHWA 2004001. The support of the Indiana Department of Transportation (INDOT) and the Federal Highway Administration (FHWA) are gratefully acknowledged. The authors would like to extend thanks to Dr. Tommy Nantung, Project Administrator, for his support throughout the project. In addition, thanks are extended to members of the Study Advisory Committee for their participation and thoughtful comments throughout the project. These members include Tom Byrne, Keith Hoernschemeyer, Don Leonard, and George Synder. Finally, thanks are extended to Hughes Brothers and Pultrall for their support of this research study through their donations of materials required for the bond study. Special thanks are extended to Doug Gremel of Hughes Brothers and Sam Steere of Concrete Protection Products Inc. for their continual support of our research into fiber reinforced polymer reinforcement.

TABLE OF CONTENTS

LIST OF TABLES

LIST OF FIGURES

CHAPTER 1

INTRODUCTION

1.1 Background

Corrosion of steel reinforcement in concrete structures subjected to an aggressive environment ultimately causes deterioration of concrete and loss of serviceability of structures. Concrete deterioration due to steel corrosion occurs as the corroded steel reinforcement occupies a greater volume and causes high radial stresses around the reinforcing bar resulting in cracking and spalling of the surrounding concrete. Ultimately, the area of the steel bar reduces, and the reinforcement may lose bond between the concrete and the steel, affecting the performance of the structure. Bridge decks, parking garages, and marine structures are susceptible to deterioration because deicing and marine salts accelerate corrosion of the steel reinforcement due to the presence of chloride ions. Several methods have been used to prevent corrosion including improving the impermeability of concrete, increasing the cover thickness, providing cathodic protection, epoxy coating the reinforcement. Among them, the most common application for corrosion prevention is the use of epoxy coated reinforcement. Nevertheless, extensive premature corrosion of epoxy coated steel reinforcement has been found in bridges, indicating the shortcomings of this protection method (Ehsani, Saadatmanesh, and Tao (1996)).

Recently, fiber reinforced polymer (FRP) bars have become an alternative solution for structures susceptible to corrosion problems. FRP bars have also been used where low electric conductivity or electromagnetic transparency is required. FRP bars have some advantages over steel bars because of their physical and mechanical properties such as high tensile strength to weight ratio (4-8 times higher than that of steel), high

ultimate tensile strength, and low unit weight (one fourth that of steel). FRP bars, however, have disadvantages that must be carefully considered. FRP materials are linear-elastic until failure. They are anisotropic and provide primarily tensile strength. The modulus of elasticity of glass and aramid FRP bars are about one-fifth that of steel. Even though carbon FRP bars have a higher modulus of elasticity than glass FRP bars, their stiffness is about two-thirds that of steel reinforcing bars. Lower stiffness causes larger deflections and crack widths for FRP reinforced members which can affect serviceability (Toutanji and Saafi (2000)). FRP reinforcing bars are also not suitable for structures that have a potential for exposure to high temperatures. The strength of the FRP reinforcing bars decreases significantly at temperatures in excess of 400 $^{\circ}$F (Brown and Bartholomew (1993)).

Because the physical and mechanical properties of FRP bars are different from those of steel reinforcement, especially the surface deformation and the modulus of elasticity of the reinforcement, the bond behavior of FRP reinforced concrete specimens is expected to be quite different than steel reinforced specimens. Therefore, the bond behavior of FRP reinforced specimens is of interest in this investigation.

1.2 Bond Behavior

In reinforced concrete structures, successful transfer of stresses between concrete and reinforcement is required for satisfactory design. Therefore, appropriate development and splice lengths must be provided.

1.2.1 Bond Forces

1.2.1.1 Steel Reinforced Specimens

Three mechanisms can be identified as transferring forces from the deformed steel reinforcement to surrounding concrete:

- Chemical adhesion between the bar and the concrete
- Frictional forces due to the roughness of the interface and the relative slip between the reinforcing bar and the surrounding concrete

- Mechanical anchorage of the bar lugs bearing against the concrete

As a deformed bar slips with respect to the concrete along its length, chemical adhesion is lost while friction and bearing forces are mobilized. Because the forces interact with each other, it is difficult to quantify their contribution to the overall bond behavior. These forces on the bar surface create hoop tensile stresses and shear stresses on the surrounding concrete which can result in cracking in planes that are both perpendicular and parallel to the reinforcement. The failure mode depends primarily on the cover, spacing of reinforcement, transverse reinforcement, and concrete strength. If the concrete cover, bar spacing, and transverse reinforcement are sufficient, the specimen fails in a pullout mode by shearing along the surface of the bar. Otherwise, the specimen fails in a splitting mode due to the hoop tensile stresses. If anchorage of the concrete is adequate, it is possible that the bar may develop its ultimate tensile strength.

In the case of plain bar reinforced specimens, forces are transferred from the reinforcement to surrounding concrete through chemical adhesion and friction. Pullout failures are the most likely failure mechanism for these types of specimens.

1.2.1.2 FRP Bar Reinforced Specimens

For FRP bar reinforced specimens, chemical adhesion and friction play an important role in bond behavior. While the effect of mechanical interlock on bond strength has been studied for FRP reinforced specimens, the effect of the deformation pattern on bond strength is not fully understood because of the wide range of deformation patterns produced. Nanni et al. (1995) and Larralde and Silva-Rodriquez (1993) tested pullout specimens to investigate the main parameters that control bond behavior and found that at the time of pullout failure, very little localized cracking was observed in the specimens. This result indicated that the bearing stresses on the deformations were not very high. However, Malvar (1994), Kanakubo et al. (1993), and Makinati et al. (1993) concluded that the bond transfer mechanism in pullout specimens can be governed primarily by mechanical interlock for deformed FRP bars.

While the bond mechanisms are of the interest for FRP bars, it must be considered that variations in surface deformations can change their relative contribution. Wambeke

(2003) investigated the effect of surface deformation on bond strength by evaluating 91 pullout specimens reinforced with bars having surface deformations including helical lugs, spiral wraps, and sand coatings. Wambeke (2003) found that deformation patterns have minimal influence on the average unit bond strength for the deformation patterns investigated. Makinati et al. (1993) investigated the effect of smoothness of the bar surface and concluded that the bond strength of uncoated FRP bars are much lower than the bar having a surface deformation of spiral and sand coating.

1.2.2 Bond Tests

The bond behavior of steel and FRP reinforced specimens has been investigated using mainly four types of tests, namely, pullout, beam-end, beam anchorage, and splice tests (Figure 1.1). It is important to note that a test method representing the direct measurement of bond stresses in actual reinforced concrete members does not exists due to the difficulty in duplicating the behavior of actual structural members in a laboratory environment.

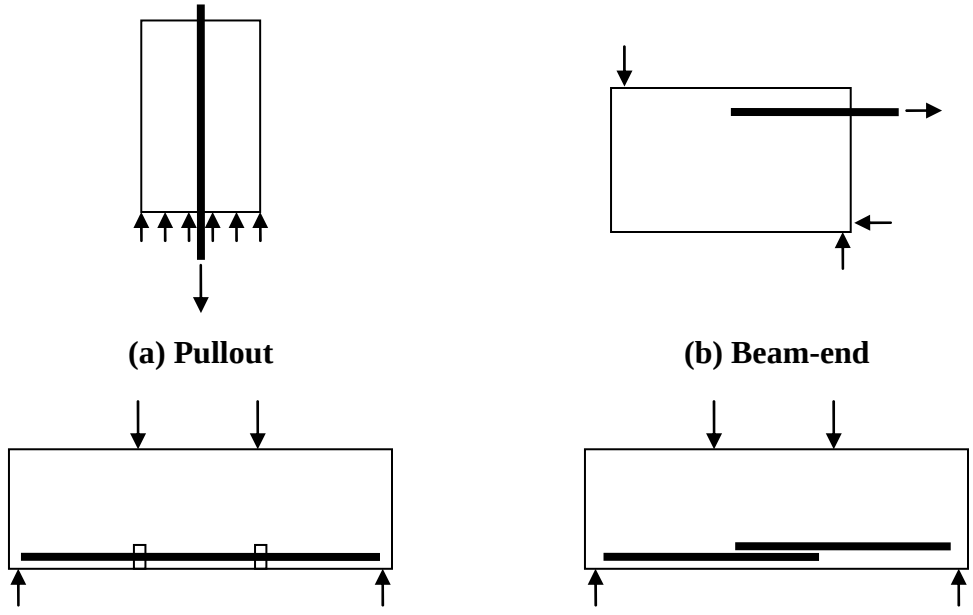

(a) Pullout **(b) Beam-end**

(c) Beam Anchorage **(d) Splice**

Figure 1.1 Types of Test Methods

Two simple and inexpensive test methods are the pullout and beam-end tests. The pullout test is widely used because it is easy and inexpensive to fabricate and the test procedure is simple. In pullout tests, however, compressive stresses in the concrete eliminate transverse tension cracking. Friction on the loaded end bearing retards splitting locally. As a result, bond stresses obtained from pullout tests are higher than that measured from beam tests (Ferguson (1966), Tastani and Pantazopoulou (2002)). Although pullout tests do not reflect the state of stresses in reinforced concrete structures, they are very useful in evaluating the load-slip relationship of reinforcing bars. The beam-end test is also fairly inexpensive; nonetheless, evaluation of the data becomes complicated because both flexural and anchorage bond stresses are present around the reinforcing bar.

Beam anchorage and splice tests are designed to measure development and splice strengths in full-size flexural members. These tests are considered to be most realistic for representing actual beam behavior because the flexural stresses are not affected by the loading configuration. In addition, specimens allow random distribution of flexural cracking. Therefore, comparison can be made regarding overall structural performance. However, slip between the bar and concrete cannot be measured because the bars are fully embedded in concrete. The majority of data in the literature for steel reinforced beams are based on splice tests because the specimens are easy to fabricate and the test yields results similar to those of beam anchorage specimens (ACI 408R-03). It is important to note that the bond behavior of steel reinforced specimens has been under investigation for more than a century. Consequently, extensive literature is available regarding the bond performance of steel reinforced concrete.

The bond behavior of FRP bars has been primarily studied by testing pullout specimens. Only limited data are available for tension lap splice tests which are considered best representative for flexural members in which the reinforcement is located in the tension zone of a reinforced concrete member. A noticeable trend, however, is observed from the test results of pullout and splice tests conducted to-date. Pullout tests by Benmokrane, Tighiouart, and Chaallal (1996), and Brown and Bartholomew (1993)

and splice tests by Mosley (2000) show that the bond strength of glass FRP bars are lower than that of steel reinforcement.

1.2.3 Types of Failures

There are generally three types of failures in bond tests: bar failure, bar pullout, and concrete splitting failures. Among the failure types, two of them, bar pullout and concrete splitting, are desired failure types for investigating bond strength. Test specimens are generally designed so that the specimen fails in bond rather than by failure of the reinforcement because limited information is obtained regarding required development length and bond strength if failure is controlled by the reinforcement. Failure of the bar indicates that the bar had sufficient development length and the limits of bond strength have not been tested.

As the bar slips inside the concrete, surface adhesion is lost and force is transferred primarily through friction between the concrete and the reinforcement and the bearing forces acting on the deformations. The forces on the surface of the bar are balanced by compressive and shear stresses on the surrounding concrete surface. These forces can be resolved into tensile stresses that can result in cracking planes both horizontal and perpendicular to the reinforcement. The type of failure is dictated mainly by the cover and spacing dimensions, concrete strength, and presence of transverse reinforcement.

Splitting failure occurs if the concrete cover and spacing of the bars are small enough for a splitting plane to develop. The potential failure planes for a splitting failure are shown in Figure 1.2 and develop depending on the cover and bar spacing.

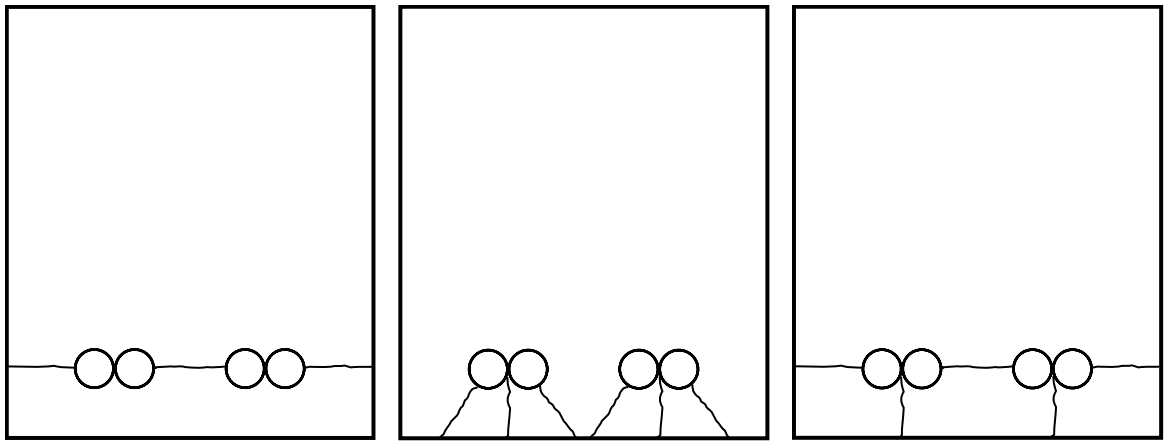

(a) Side Splitting **(b) Face Splitting** **(c) Face and Side Splitting**

Figure 1.2 Splitting Cracks

If the concrete cover, bar spacing, and presence of transverse reinforcement is sufficient to provide enough strength to prevent splitting, the reinforcement can fail in a pullout mode (Figure 1.3). A pullout failure occurs as the concrete shears along the top surface of the ribs for deformed reinforcing steel. For FRP bars, the pullout strength is likely to be governed by shearing of concrete along the reinforcement, the shearing of the bar deformations, or both (Boothby et al. (1995)).

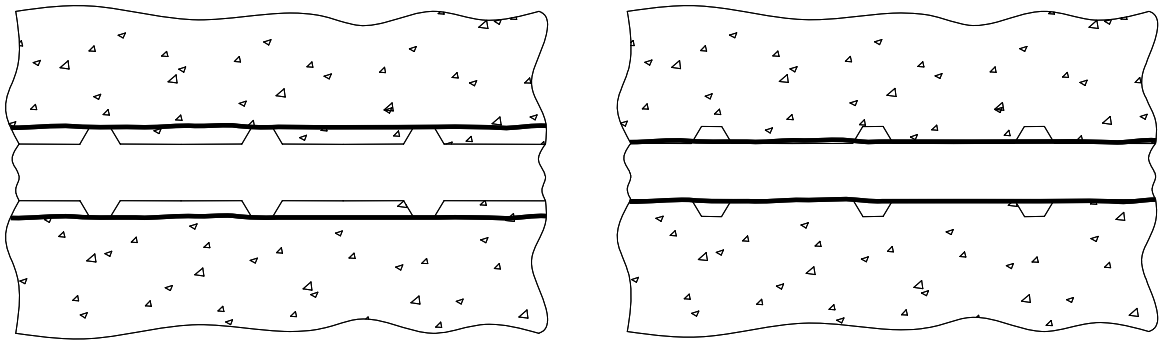

(a) Shearing of Concrete **(b) Shearing of Concrete and Deformation**

Figure 1.3 Pullout Failure

1.2.4 Factors Influencing Bond Behavior

Bond between reinforcement and concrete is affected by many factors. The major factors influencing the bond behavior of steel and FRP reinforced concrete are as follows:

1.2.4.1 Concrete Cover and Bar Spacing

The bond strength of steel reinforced beams increases with wider spacing of the reinforcing bar until the bond capacity is reached by yielding of the reinforcement (Chamberlin (1958), Chinn, Ferguson, and Thompson (1955)). Chinn et al. also found that an increase in the cover dimension increases bond strength especially for short splices. However, Ferguson and Thompson (1962) found that the increase in bond strength with an increase in cover is less for larger diameter bars. Thompson et al. (1975) studied the effect of the ratio of the cover to clear spacing on splice strength. Thompson (1975) concluded that the strength of the splice is increased as the ratio of the cover to bar spacing increased.

The failure mode depends on the cover and bar spacing of the specimen. The types of splitting failures are shown in Figure 1.2. Side splitting occurs when a horizontal crack develops at the level of the bars while face splitting occurs when a vertical crack develops along the length on the tension face of the beam. It is generally assumed that side splitting is a function of side cover and bar spacing while face splitting is controlled by the face cover. Splitting failure occurs as the weaker splitting plane reaches its ultimate tensile capacity. A pullout failure is also possible if large covers and bar spacings are provided.

For small covers and bar spacings, a splitting failure occurs if transverse reinforcement is not present (Chinn et al. (1955), Orangun et al. (1977), and Darwin et al. (1996a, b)). "The presence of transverse reinforcement prevents the progression of splitting cracks; however, the failure mode depends on the amount of transverse reinforcement present in the splice region." The same conclusion is also valid for FRP reinforced specimens (Ehsani (1996)). The effect of transverse reinforcement on bond strength is discussed in Section 1.2.4.5.

1.2.4.2 Concrete Compressive Strength

For deformed steel reinforced specimens, the relationship between concrete strength and bond strength is not fully understood; however, it has generally been accepted that the effect of concrete strength on bond strength is represented using the square root of the concrete compressive strength, $\sqrt{f_c'}$, (Ferguson and Thompson (1962), Orangun et al. (1977), Darwin et al. (1992), and Esfahani and Rangan (1998)). However, various investigators have also suggested expressions for evaluating bond strength which are in terms of various roots of concrete compressive strength, $\sqrt[n]{f_c'}$, with values of n ranging from 2 to 4. Recent studies on steel bars based on a database which also incorporates high strength concrete have shown that the fourth root, $\sqrt[4]{f_c'}$, provides the best representation for the effect of concrete compressive strength to bond strength (Zuo and Darwin (2000), and Canbay and Frosch (2005)).

The effect of concrete strength is not fully understood for FRP specimens as well. There is only limited data available for FRP bar reinforced specimens, and of those, the majority are pullout specimens. Nanni et al. (1995) investigated the effect of concrete strength on bond behavior using pullout specimens and found that concrete strength does not have any influence on pullout failures. However Malvar (1994) found that, for splitting failures, an increase in concrete strength results in an increase in bond strength. In the case of splitting failures, the behavior and failure mechanism of steel and FRP reinforced specimens are similar. In other words, the failure of the concrete around the reinforcing bar is primarily a function of the splitting tensile strength of the concrete; therefore, the contribution of concrete strength on bond behavior should not be affected by the type of reinforcing material.

1.2.4.3 Development and Splice Length

An increase in the development and splice length of a reinforcing bar will increase the total bond force transferred between the concrete and the reinforcement. It has been observed, however, that the unit bond strength decreases as the splice strength increases (Chinn et al. (1955) and Azizinamini (1993)) indicating that the increase in the

bond strength is not proportional to the increase in anchorage length. In another words, the relationship between bond strength and bar length is not linear. The distribution of bond forces along the development or splice region is not uniform. For short splice lengths, the assumption of a uniform distribution of bond stress along the bonded length is fairly accurate for evaluating behavior; however, as the bonded length increases, the effectiveness of the bonded length decreases, thus the relative gain with increase in splice length reduces. This behavior is identical for both deformed steel and FRP bar reinforcement; however, the increase in bond strength (strength gain) with an increase in splice length is different for both materials. Further study is needed to quantify this effect.

1.2.4.4 Bar Casting Position

Bar position during concrete placement has an important effect on the bond strength between concrete and the reinforcement. It is found that the bond strength decreases with an increase in the depth of concrete cast below the reinforcing bar (Jirsa et al. (1982), Devries et al. (1991), Maeda et al. (1991), Azizinamini et al. (1993), Ehsani et al. (1996), Tighiouart et al. (1998)). Jirsa et al. (1982) found that bar size has very little effect on the pattern of the strength reduction with height of the concrete cast below the reinforcement being the major parameter.

The influence of casting position on bond strength may be explained according to the following reasons: settlement of concrete beneath the concrete, bleeding of the concrete around the reinforcing bar, or both. The concrete beneath the reinforcement during casting and curing settles and bleeds. Furthermore, due to bleeding, the concrete surrounding the reinforcement has a high water/cement ratio which results in a reduced concrete compressive and tensile strength. Several researchers have studied the effect of top and bottom cast bars, and it was found that the bond strength of top cast bars decreased with increasing slump (Ferguson and Thompson (1965) and decreasing top cover. The effects of settlement and bleeding of concrete around the reinforcing bar is aggravated by these factors. The influence of cover on settlement and bleeding, however, cannot be easily distinguished for specimens that fail in face splitting as the cover has a

direct influence on bond strength (Ehsani et al. (1996)). The influence of cover on settlement and bleeding can be identified only from specimens which fail in the side splitting mode. Devries et al. (1991) studied the effect of bleeding on the bond strength for top cast bars. It was concluded that while an anti-bleeding agent stopped the bleeding of the concrete; it did not significantly alter the bond strength of the reinforcement.

1.2.4.5 Transverse Reinforcement (Confinement)

The presence of transverse reinforcement in the development and splice region prevents the progression of splitting cracks; therefore, the bond force required to cause failure of the bar increases (Orangun et al. (1977), Tepfers (1982), and Darwin et al. (1996 a, b)). As the bond strength increases with an increase in transverse reinforcement, eventually the failure mode changes from splitting to pullout. Additional transverse reinforcement above that required to cause a pullout failure is unlikely to increase the anchorage capacity of the section (Orangun et al. (1977)).

The effect of transverse reinforcement on bond strength depends on the splitting pattern (Morita and Fujii (1982)). Morita and Fujii observed that transverse reinforcement strains demonstrated abrupt changes at low stress levels in specimens that failed in side splitting while the increase was more gradual when the failure was face splitting. Zuo and Darwin (2000) found that the size and relative rib area of the longitudinal reinforcement also have an influence on the effect provided transverse reinforcement. As the relative rib area and bar cross-sectional area increase, the stress in the stirrups increase, consequently, increasing the confining force and bond strength of the bar.

Kanakuno et al. (1993) investigated the effect of different types of transverse reinforcement on the bond strength of FRP reinforced specimens. Kanakubo et al. found that the increment of bond strength caused by transverse reinforcement can be evaluated in terms of the modulus of elasticity of the developed or spliced bar. He also concluded that as the amount of transverse reinforcement increases, the maximum bond stress of the reinforcing bar increases.

1.2.4.6 Bar Size

Bar size has a direct influence on the bond strength of FRP and steel reinforced beams. As the bar size increases for a given development and splice length, the total bond force developed by the bar increases. However, for steel reinforced specimens the rate of increase in the bond force is lower than the increase in bar area. Consequently, bond stresses are lower for larger diameter bars. (Mathey and Watstein (1961) and Ferguson and Thompson (1965)). The same behavior was observed for FRP bar reinforced specimens; larger diameter bars have a lower pullout stress at ultimate than smaller diameter bars (Nanni et al. (1995) and Tighiouart et al. (1998)). Therefore, longer development or splice lengths are required as the bar size increases. For specimens confined with transverse reinforcement, the contribution of the transverse reinforcement on bond strength increases as the bar size increases (Zuo and Darwin (2000)).

1.2.4.7 Surface Deformation of the Reinforcement

As early as 1913, Abrams studied the effect of the surface deformation of steel on bond strength (Abrams (1993)). Abrams found that deformed bars provided higher bond resistance than plain bars. The bond-slip resistances of plain and deformed bars were similar up to the slip corresponding to the maximum stress achieved in plain bars. As the the bar continues to slip, the stress on the deformed bar increases as the lugs bear against the adjacent concrete, increasing the bond resistance of the bar.

In the case of FRP bars, force transfer is mainly due to chemical adhesion and friction between the concrete and the reinforcement. Bearing of concrete on the surface deformation is minimal. Makinati et al. (1993), Malvar (1994), and Nanni et al. (1995) studied the effect of surface deformation on the bond strength of FRP reinforced specimens. Studies were performed using pullout tests. They concluded that the surface deformation of the bar has an influence on the bond strength. The study by Malvar (1994) also indicated that concrete strength has an effect on bond strength only if the ribs or the indentations have sufficient shear strength.

Darwin and Graham (1993) and Zuo and Darwin (2000) studied the effect of relative rib area on bond strength. They concluded that bond strength is independent of the surface deformation pattern if the bar is under relatively low confinement and the bond strength is governed by a splitting failure in the concrete. However, the splice strength of reinforcement confined by transverse reinforcement increases with an increase in the relative rib area.

1.2.4.8 Modulus of Elasticity of Reinforcing Bars

Until recently, the modulus of elasticity of the reinforcing bars was not considered as a parameter influencing the bond behavior of reinforced concrete structures. This is mainly because research has been conducted on the behavior of steel reinforced structures which has a constant modulus of elasticity. FRP reinforcing bars with different moduli of elasticity make it possible to investigate the effect of modulus of elasticity on bond strength. However, there is no consensus among researchers regarding the effect of the modulus of elasticity of the reinforcing bars on bond performance.

1.3 Objective and Scope

The physical and mechanical properties of FRP bars are different from those of steel reinforcement, especially the surface deformation and the modulus of elasticity; therefore, the bond behavior of FRP reinforced concrete specimens is expected to be different than that of steel reinforced specimens. While substantial research has been conducted on bond behavior of steel reinforced members, limited research has been conducted for FRP bar reinforced members. In particular, extremely limited test results are available for splice tests which are considered most representative of bond behavior in actual structures.

The objective of this research study is to evaluate the effects of the axial stiffness, modulus of elasticity, reinforcement size, surface deformation, splice length, and casting position on the bond behavior of FRP and steel reinforcing bars spliced at tension, as well as to develop a plausible model for the bond strength of FRP and steel bars.

To achieve this objective, an experimental program was developed. Forty-six beam specimens reinforced with spliced reinforcement were designed and tested in the experimental program. While it is hypothesized that the bond strength is effected by the modulus of elasticity, the goals of study were to address the following key questions:

- Is the effect of splice length on bond strength a function of the axial stiffness of the reinforcing bar?
- Is there a relationship between the axial stiffness of the bar and the bar stresses reached at failure?
- What is the effect of surface deformation on the bond strength of different types of reinforcement?
- What is the effect of casting position on splice strength of different types of reinforcing bars?
- Is it possible to develop a plausible model representing the bond behavior of FRP and steel reinforced structures?

CHAPTER 2

EXPERIMENTAL PROGRAM

2.1 Introduction

The experimental program investigated the bond behavior of fiber reinforced polymer (FRP) and steel reinforced concrete beams with tension lap splices. A two phase study was conducted to evaluate the effect of the modulus of elasticity, surface deformation, axial rigidity, bar size, splice length, and casting position of the longitudinal reinforcement on bond. A total of 46 specimens were tested in two phases; sixteen in Phase I and thirty in Phase II. Phase I consisted of two series, and Phase II consisted of three series.

2.2 Specimen Design

The specimens were designed to investigate the bond behavior of FRP and steel reinforced concrete beams. Throughout this experimental program, tests commonly referred to as beam splice tests were conducted. The concrete strength was selected as 4,000 psi, the typical design strength for bridge decks as well as buildings.

Cross-sectional details of the specimens are shown in Figure 2.1. All beams were rectangular in cross section with a total depth of 16 in. All specimens were designed with a clear spacing of 1 in. between the bars located in the splice region and with a 1-1/2 in. side and top clear cover. This limitation represents the minimum clear spacing allowed by ACI 318-05 and the minimum clear cover allowed by ACI 318-05 and AASHTO LRFD for reinforced concrete members where the primary reinforcement is not exposed to weather. Three reinforcing bars were spliced at the center of the constant moment region of the beam. The width of the specimens was dictated by the minimum cover and spacing limitations and the size of the reinforcement. For that reason, the width of

specimens was 8.75 in. for the specimens reinforced with #5 bars and 11 in. for the specimens reinforced with #8 bars.

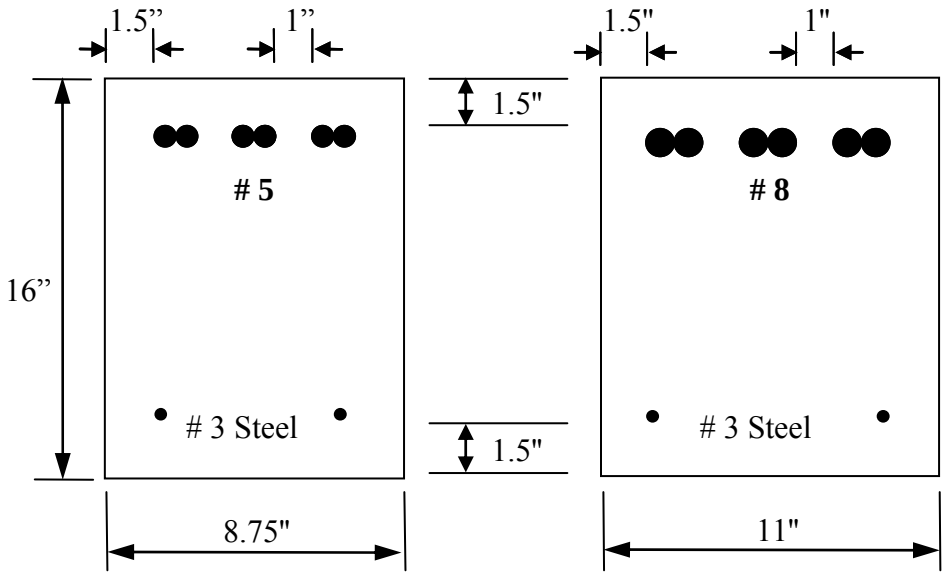

(a) Beams Reinforced with #5 Bars (b) Beams Reinforced with #8 Bars

Figure 2.1 Cross Section Detail at Splice Region

A typical test specimen is illustrated Figure 2.2, while dimensions for each specimen are provided in Table 2.1. The length of the specimens was dictated by three factors: spacing of the holes located in the reaction floor, splice length, and casting area space limitations. In the Kettelhut laboratory, the reaction floor anchor holes are spaced in 6 ft intervals with an exception of one row which is spaced in 4.5 ft while they are spaced at 2 ft intervals in the Bowen Laboratory. As both laboratories were used, both hole spacings needed to be considered.

The specimens were loaded at the ends of the specimen to develop tension at the top surface. With this loading configuration, cracks are formed at the top of the beam which provided ease in both mapping cracks and measuring their widths. The loading frame was located 12 ft apart for the 13.5 ft long specimens in both phases. For the 18 ft specimens, they were located 16.5 ft apart in Phase I (Kettelhut Laboratory) and 16 ft apart in Phase II (Bowen Laborartory). This dimensional change occurred because holes in the reaction floor at the Bowen Laboratory are spaced in 2 ft intervals as previously

mentioned. The constant moment span was adjusted depending on the splice length; the constant moment region was adjusted so that the bars were spliced in the region where the assumption of plane sections remaining plane from flexural theory is applicable. Based on St. Venant's principle, stresses due to bending approach a linear distribution at a distance equal to the overall height of the member, h, away from the section where a load or change in geometry occurs. The span length between the supports was selected such that the splice end was at least 1.5h away from the supports. Consequently, specimens with 12, 18, and 24 in. splices were constructed 13.5 ft long and specimens with 36 and 54 in. splices were constructed 18 ft long.

The shear spans of the beams were reinforced with #3 steel stirrups at 6 in. for specimens having a 3 ft shear span and at 5 in. for specimens having a 3.75 ft shear span to prevent shear a failure prior to bond failure. No stirrups were provided in the constant moment region of the beam. Two #3 longitudinal steel bars were provided in the compression side of the beam to assist with fabrication of the reinforcement cage.

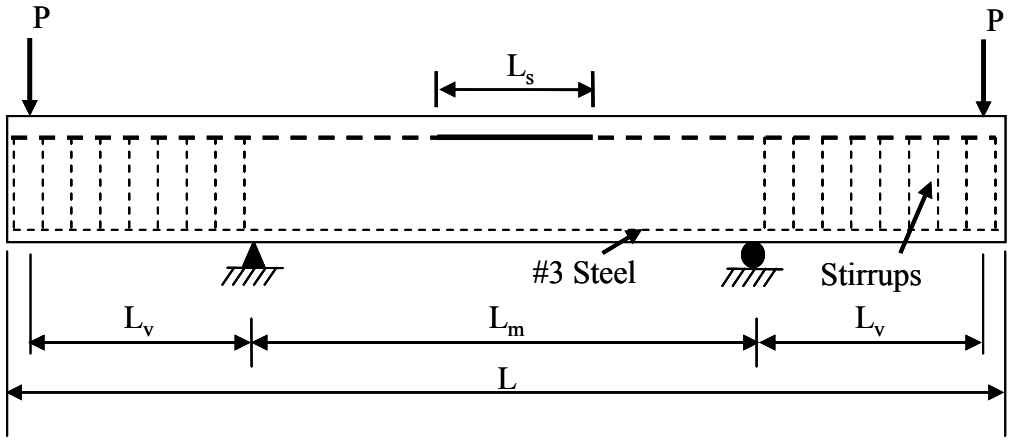

Figure 2.2 Typical Test Specimen

Table 2.1 Specimen Details

Phase	Series	Specimen Length, L (ft)	L_v (ft)	L_m (ft)
I	I	13-1/2	3	6
	II	13-1/2	3	6
		18	3-3/4	9
II	III	13-1/2	3	6
	IV	13-1/2	3	6
	V	13-1/2	3	6
		18	3-3/4	8-1/2

2.3 Test Specimens and Variables

The experimental program consisted of forty-six reinforced concrete beam specimens with tension lap splices located in a constant moment region. The beams were reinforced either with carbon FRP, glass FRP, or steel bars. FRP reinforcing bars were supplied from two manufacturers, Pultrall Inc. and Hughes Brothers Inc., and included #5 and #8 glass FRP bars as well as #5 carbon FRP bars.

Tests were conducted in two phases. In the first phase, sixteen specimens were cast in two series while in the second phase, thirty specimens were cast in three series. Phase I was conducted at the Kettelhut Laboratory and completed in July 2002, while Phase II was conducted at the Bowen Laboratory and completed in February 2005.

Details of the specimens are summarized in Table 2.2 and Table 2.3 for Phase I and Phase II, respectively. A four part notation system is used to identify the specimens. The specimens were identified first by the descriptive label B (bond) followed by the reinforcement type, the bar size (#5, #8), and finally by the splice length. For example, B-C-5-12 stands for a bond test with #5 carbon FRP bars spliced at 12 in. Bottom cast specimens were identified by adding the notation "b" to the splice length. The variables investigated in this program are described in the following.

Table 2.2 Specimen Details (Phase I)

Series	Specimens	Bar Type	Deformation	Bar Size	L_s (in.)	Cast
I	B-S-8-18	Steel	Deformed	#8	18	Top
	B-P-8-18	Glass	Sand Coated	#8	18	Top
	B-H-8-18	Glass	Sand and Wrapped	#8	18	Top
	B-HN-5-18	Glass	Sand and Wrapped	#5	18	Top
	B-HO-5-18	Glass	Sand and Wrapped	#5	18	Top
	B-P-5-18	Glass	Sand Coated	#5	18	Top
	B-S-5-18	Steel	Deformed	#5	18	Top
	B-C-5-18	Carbon	Fabric Texture	#5	18	Top
II	B-C-5-12	Carbon	Fabric Texture	#5	12	Top
	B-S-8-36	Steel	Deformed	#8	36	Top
	B-P-8-36	Glass	Sand Coated	#8	36	Top
	B-H-8-36	Glass	Sand and Wrapped	#8	36	Top
	B-HN-5-36	Glass	Sand and Wrapped	#5	36	Top
	B-HO-5-36	Glass	Sand and Wrapped	#5	36	Top
	B-P-5-36	Glass	Pultrall	#5	36	Top
	B-C-5-36	Carbon	Fabric Texture	#5	36	Top

Table 2.3 Specimen Details (Phase II)

Series	Specimens	Bar Type	Deformation	Bar Size	L_s (in.)	Cast
III	B-S2-8-12	Steel	Deformed	#8	12	Top
	B-S1-8-12	Steel	Deformed	#8	12	Top
	B-S4-8-12	Steel Bar	Plain	1 in.	12	Top
	B-S3-8-12	Steel Pipe	Plain	1 in.	12	Top
	B-PG-8-12	Glass	Sand Coated	#8	12	Top
	B-HG-8-12	Glass	Sand and Wrapped	#8	12	Top
	B-S1-8-12b	Steel	Deformed	#8	12	Bottom
	B-HG-8-12b	Glass	Sand and Wrapped	#8	12	Bottom
	B-PG-8-12b	Glass	Sand Coated	#8	12	Bottom
	B-S-5-24	Steel	Deformed	#5	24	Top
IV	B-HC1-5-24	Carbon	Fabric Texture	#5	24	Top
	B-PC2-5-24	Carbon	Uncoated	#5	24	Top
	B-PC1-5-24	Carbon	Sand Coated	#5	24	Top
	B-HG3-5-24	Glass	Uncoated	#5	24	Top
	B-HG1-5-24	Glass	Sand and Wrapped	#5	24	Top
	B-HG2-5-24	Glass	Fabric Texture	#5	24	Top
	B-PG2-5-24	Glass	Uncoated	#5	24	Top
	B-PG1-5-24	Glass	Sand Coated	#5	24	Top
	B-HG1-5-24b	Glass	Sand and Wrapped	#5	24	Bottom
	B-PG1-5-24b	Glass	Sand Coated	#5	24	Bottom

Table 2.3 Specimen Details (Phase II) (continued)

Series	Specimens	Bar Type	Deformation	Bar Size	L_s (in.)	Cast
V	B-HG1-5-12	Glass	Sand and Wrapped	#5	12	Top
	B-PG1-5-12	Glass	Sand Coated	#5	12	Top
	B-HG-8-24	Glass	Sand and Wrapped	#8	24	Top
	B-HG-8-54	Glass	Sand and Wrapped	#8	54	Top
	B-HG1-5-54	Glass	Sand and Wrapped	#5	54	Top
	B-PG1-5-54	Glass	Sand Coated	#5	54	Top
	B-HC1-5-54	Carbon	Fabric Texture	#5	54	Top
	B-HG1-5-12b	Glass	Sand and Wrapped	#5	12	Bottom
	B-PG1-5-12b	Glass	Sand Coated	#5	12	Bottom
	B-HG-8-24b	Glass	Sand and Wrapped	#8	24	Bottom

2.3.1 Test Variables

The variables tested in the experimental program included the modulus of elasticity, bar size, splice length, axial stiffness, surface deformation, and casting position of the lapped reinforcement. The same concrete mix design was used throughout the experimental program to maintain the concrete strength constant. Although the concrete strength was not a primary variable, it varied from 3,900 psi to 5,500 psi. Concrete cover and spacing of the reinforcing bars were maintained constant throughout the experimental program, and no transverse reinforcement was provided in the constant moment region. The key variables investigated in this program are described in the following sections.

2.3.1.1 Modulus of Elasticity

The effect of modulus of elasticity of the reinforcement was investigated among the specimens having the same surface deformation and bar size. The modulus of elasticity of the bars varied from 5,700 ksi to 21,000 ksi for the reinforcement possessing similar surface deformations. Both glass and carbon bars were tested (Figure 2.3).

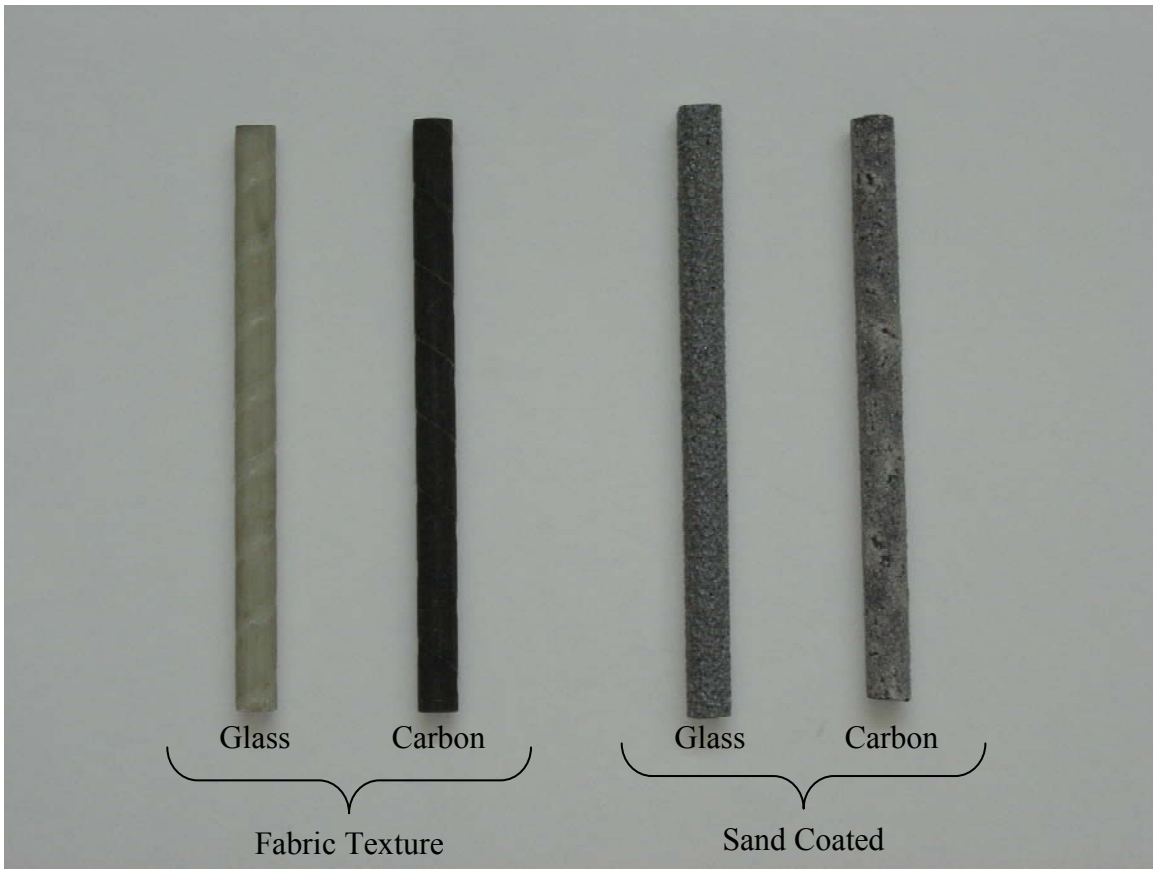

Figure 2.3 Reinforcement Tested to Examine the Effect of Modulus of Elasticity

2.3.1.2 Bar Size

Two bar sizes, #5 and #8, were used to examine the effect of bar size on the bond strength (Figure 2.4). In this study, #5 bars were investigated since they are commonly used in bridge deck and slab systems. Because the modulus of elasticity of FRP bars is significantly lower than that of conventional steel bars, the amount of FRP reinforcement required is typically higher than the amount of steel reinforcement required for the same section. The amount can be increased either using larger size bars or decreasing the spacing of the reinforcement. Consequently, larger bars sizes are also used in FRP reinforced concrete to provide increased stiffness. For this reason, #8 bars were also investigated.

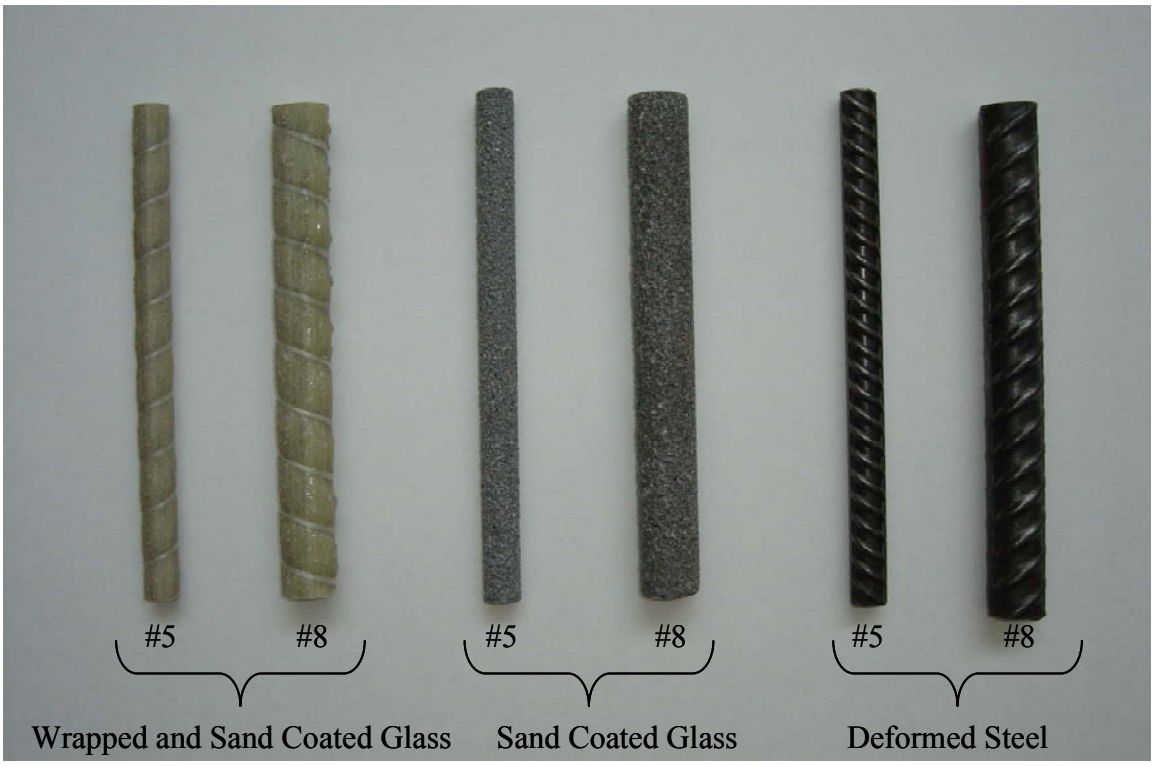

Figure 2.4 Reinforcement Tested to Examine the Effect of Bar Size

2.3.1.3 Splice Length

Splice length was selected to evaluate its effect on splice strength. The splice length of the bars was varied from 12 to 54 in. that resulted in splice lengths of 12 to 54 times the bar diameter for #8 bars and 19 to 86 times the bar diameter for #5 bars.

The effect of yielding on bond strength was also examined by testing a steel reinforced specimen that was designed such that the reinforcement yielded prior to the failure.

2.3.1.4 Axial Stiffness

Axial stiffness (AE) is a function of the cross-sectional area and the modulus of elasticity of the reinforcement. The effect of axial stiffness was evaluated by two different approaches. The first method varied the cross-sectional area while maintaining the modulus of elasticity constant. The area of the reinforcing bar can be changed either

by varying the bar size or using a hollow bar instead of a solid bar. Therefore, a 1 in. solid rod, 1 in. extra strong pipe, #8 solid reinforcing bar, and #8 hollow reinforcing bar were used to investigate the effect of axial stiffness without changing the bar size (Figure 2.5). The hollow #8 bar consisted of a #8 rebar in which a ½ in. hole was drilled along its length to provide a reduction in the cross sectional area of the bar. These specimens allowed evaluation of the splice strength without changing the bar size, the reinforcement type, or surface deformation. The second method varied the modulus of elasticity while maintaining the cross-sectional area constant. Therefore, #5 carbon and glass FRP bars with similar surface deformations (Figure 2.3) were also tested to investigate the effect of the modulus of elasticity, thus the axial stiffness.

Figure 2.5 Reinforcement Tested to Examine the Effect of Axial Stiffness

2.3.1.5 Surface Deformation

Uncoated, wrapped and sand coated, sand coated, and fabric texture coated glass FRP bars were compared so that the effect of surface deformation was evaluated. As all the reinforcement were #5 glass FRP, the modulus of elasticity was held constant.

Uncoated, sand coated, and fabric texture coated carbon FRP bars were also tested to evaluate their bond performance as their moduli of elasticity are approximately identical. Figure 2.6 shows the bars tested to investigate the effect of surface deformation on bond strength.

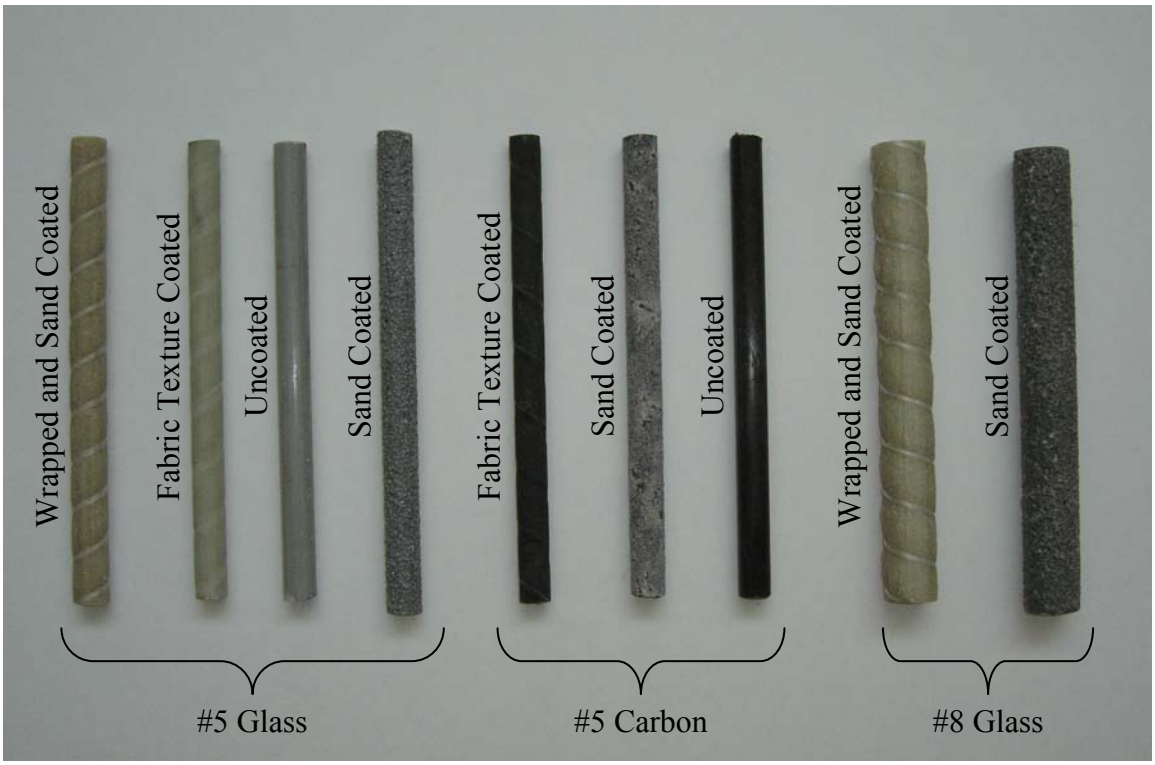

Figure 2.6 Reinforcement Tested to Examine the Effect of Surface Deformation

2.3.1.6 Casting Position

The effect of casting position on the splice strength of steel reinforced specimens has been studied by many researchers. These studies have shown that bottom cast bars provide higher splice strengths than top cast bars (Abrams (1913), Chinn, Ferguson, and Thompson (1955), Ferguson and Thompson (1962), Hadje-Ghaffari et al. (1994)). Consequently, both the ACI 318 design provisions and the ACI 440 design guidelines (ACI 440.1R-03) require that the splice length should be increased 30% for top cast specimens (> 12 in. fresh concrete cast below reinforcement). To evaluate the current design equations and the applicability of this requirement to spliced FRP reinforced sections, the effect of casting position was investigated. Spliced reinforcing bars in

thirty-eight of the specimens are considered top cast bars as defined by ACI 318 while the bars in eight of the specimens are considered bottom cast bars.

2.4 Materials

2.4.1 Reinforcement

Both FRP and steel reinforcement were considered in this study. FRP reinforcement included glass and carbon bars with different sizes and surface deformations. Steel reinforcement consisted of both deformed and plain bars.

2.4.1.1 Steel Reinforcement

Deformed and plain steel reinforcement were used in the experimental program as longitudinal reinforcement. Reinforcing bars were obtained from local suppliers. The steel reinforcement and their designation are presented in Table 2.4. The steel reinforcing bars used in this study are illustrated in Figure 2.7.

Table 2.4 Steel Bars used in the Experimental Program

Bar Size	Bar Type	Surface Deformation	Bar Designation	
			Phase I	Phase II
#5	Solid Bar	Deformed	S	S
#8	Solid Bar	Deformed	S	S1
#8	Hollow Bar	Deformed	-	S2
1"	Solid Bar	Plain	-	S3
3/4" SCH 80	Pipe	Plain	-	S4

Deformed steel reinforcement consisted of #5 and #8 bars, meeting ASTM A 615, Grade 60. Plain bars consisted of a 1 in. diameter steel rod (AISI 1018) and 0.75 in. nominal diameter, Schedule 80 steel pipe. To evaluate the effect of axial stiffness on the bond strength of deformed bars, a #8 hollow reinforcing bar was also used. A 0.5 in. diameter hole was drilled through a 16 in. length of the deformed bars to reduce the cross

sectional area in the splice region. The hollow steel section was then welded to a solid #8 steel bar per ANSI/AWS D1.4 to provide continuity along the reinforcing bar.

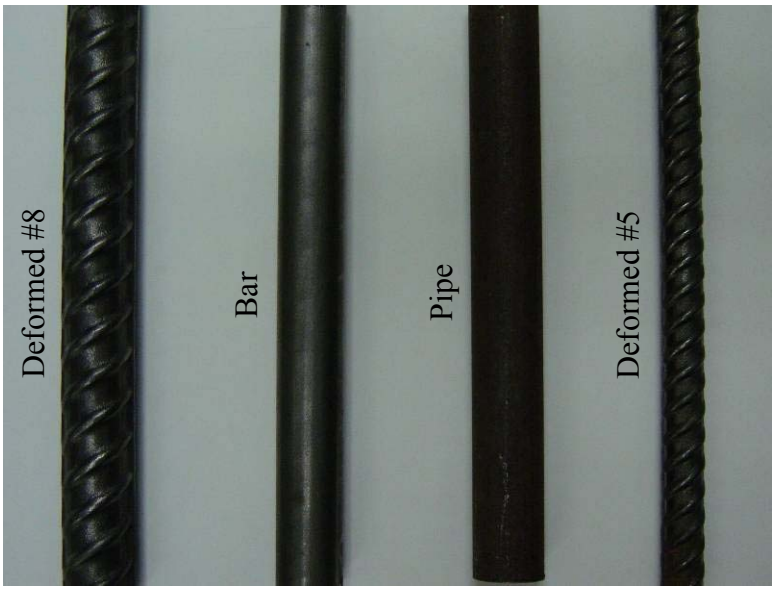

Figure 2.7 Steel Reinforcement Bars

Bars from each size were from same heat to insure consistent material properties of the reinforcement in each phase. Three steel coupons were tested in tension for each reinforcing bar type in a 120 kip Baldwin universal testing machine. Table 2.5 presents the mechanical and physical properties of reinforcing bars. Stress-strain curves for each of the steel reinforcing bars are presented in Appendix A.

Table 2.5 Mechanical Properties of Steel Bars

Phase	Bar Size	Bar Type	Designation	σ_y (ksi)	σ_u (ksi)	E (ksi)
I	#5	Deformed	S	75	95	27,350
	#8	Deformed	S	77	101	28,400
II	#5	Deformed	S	60	100	27,000
	#8	Deformed	S1	76	97	27,200
	#8	Hollow Deformed	S2	76	97	27,200
	1"	Solid Bar	S3	-*	95	30,500
	3/4" SCH 80	Pipe	S4	40	60	29,600

* Not Yielded

2.4.1.2 FRP Reinforcement

Glass and carbon FRP bars were provided by Hughes Bros Inc. and Pultrall Inc. FRP bars are manufactured using the pultrusion process. In this process, continuous fibers in rovings are held in constant tension and are drawn through a resin bath where the fibers are completely saturated with a thermosetting resin mixture using a continuous pulling device. The coated fibers are pulled through a series of dies, a sizing die and a curing die, to obtain the desired shape. Heat in the curing die activates the catalyst in the resin mix and cures the resin. Surface deformations are induced before the thermosetting resin hardens. Finally, the bars are cut to the desired length.

Tensile tests on representative coupons were performed for each type of reinforcement to determine their mechanical properties. Coupons for FRP bars were tested considering the requirements of ACI 440 (ACI 440.3R-04). The ends of the bars were encased in a 1.5 in. Schedule 80 steel pipe to attach the coupon sample to the testing machine. Sikadur 33, a smooth-paste epoxy adhesive, was used to attach the bars to the steel pipe. Stoppers were provided at the ends of the pipe to center the bar inside the pipe. This type of gripping system is needed to ensure that failure does not occur at the gripped ends before reaching the ultimate tensile strength of the FRP bar. Three coupons were tested for each reinforcing bar type. The details of the test coupon are shown in Figure 2.8 while details for each type of FRP reinforcement are provided in Table 2.6.

A 120 kip Baldwin universal testing machine was used to test the FRP coupons as shown in Figure 2.9. The loads were measured from the test machine, and strains were measured using an extensometer with a 2 in. gage length. The extensometer was removed from the specimen at a load which corresponded to approximately 70 % of the manufacturer's reported tensile strength of the bar. The measured modulus of elasticity, E_r, and ultimate strength of the FRP bars are provided in Table 2.7. The bar stress was calculated by dividing the measured load with the nominal bar cross-sectional area. The modulus of elasticity was computed from a straight line best-fit of the stress-strain curve. The rupture strain was not measured since the extensometer was detached prior to failure. Stress-strain curves for each type of reinforcement are provided in Appendix A.

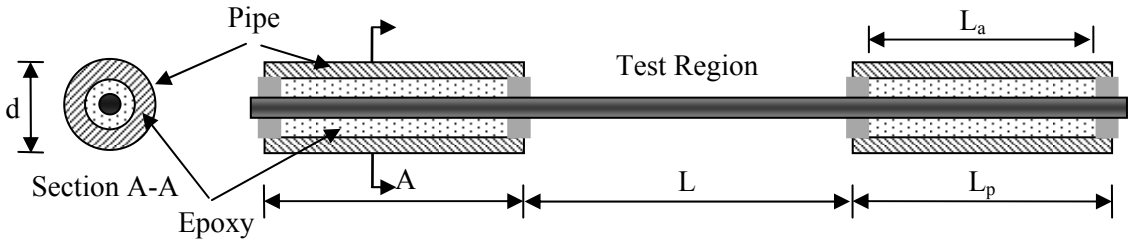

Figure 2.8 Test Coupon Details for FRP Reinforcement

Table 2.6 Details of Test Coupon

Bar Type	Bar Size	Outside Diameter, d (in.)	Pipe Wall Thickness, t (in.)	Anchor Length, L_a (in.)	Pipe Length, L_p (in.)	Free Length, L (in.)
Glass	#5	1.90	0.2	15	17	25
	#8	1.90	0.2	18	20	40
Carbon	#5	1.90	0.2	27	29	25

(a) 120 Kip Universal Testing Machine

(b) Coupon Test – Carbon FRP (HC1)

Figure 2.9 Test Setup for Coupon Tests

Table 2.7 Properties of Reinforcing Bars

Bar Type	Producer	Bar Size	E_r (ksi)	σ_u (ksi)	Surface Deformation
Glass	Hughes Bros	#5	5800	71	Sand and Wrapped
			6400	98	Sand and Wrapped
			7300*	115*	Fabric Texture
			7000	-§	Uncoated
		#8	5700	76	Sand and Wrapped
	Pultrall	#5	6400	89	Sand
			6500	-§	Uncoated
		#8	6200	76	Sand
Carbon	Hughes Bros	#5	18500	129	Fabric Texture
	Pultrall	#5	21700	-Ψ	Sand
			22500	-§	Uncoated

** Obtained from one coupon test*
§ *Pullout failure at anchor*
Ψ *Coating of the bar peeled at anchor at 100 ksi*

2.4.1.2.1 Glass FRP

No. 5 and No. 8 glass FRP bars were obtained from Pultrall Inc. and Hughes Brothers Inc. The glass FRP bars used in the study as well as their designations are listed in Table 2.8 and are shown in Figure 2.10. The glass bars from both companies are produced from E-Glass fibers and vinyl ester resin. Bars from Hughes Brothers Inc., commercially named Aslan 100, are composed of fibers which constitute at least 70% of the bar volume per ASTM D2584. Bars from Pultrall Inc, commercially named as ISOROD® GFRP, are composed of 25% resin matrix and 75% glass fibers by volume. Aslan 100 bars have a surface deformation of surface indentations and sand coating whereas ISOROD® GFRP bars have a sand coating.

In addition to the commercially available reinforcing bars that have specific surface characteristics, bars were specifically produced for this test program to evaluate the effect of the bar surface. The bars supplied by each company are summarized as follows and categorized based on their size and surface deformation.

Hughes Brothers Inc. (Aslan 100)

#5 Bars: 1 - Uncoated

2 - Wrapped and sand coated

3 - Fabric texture

#8 Bars: 1 - Wrapped and sand coated

Pultrall Inc. (ISOROD)

#8 Bars: 1 - Sand coated

#5 Bars: 1 - Uncoated

2 - Sand coated

The No. 5 Aslan 100 glass FRP bars, wrapped and sand coated, were obtained from two different batches. Bars from the first batch (HO) were received in 1999 for tests conducted by Mosley (2000). The bars were later stored in the Kettelhut Structural Engineering Laboratory at Purdue University. The bars from the second batch (HN aka HG1) were received in 2002 for this study. The composition of both materials was identical; however, there was a slight difference in the indentations of the bars. The bars from the first batch had higher indentations than the second, and the bars from the first batch had "resin puddles" at the bottom of the bars that formed during the curing process Both bars from Hughes Brothers Inc. were tested to investigate the effect of the production quality on the bond behavior.

Table 2.8 Glass FRP Bars used in the Experimental Program

Bar Size	Producer	Surface Deformation	Bar Designation	
			Phase I	Phase II
#5	Hughes Bros.	Sand and Wrapped	HO	-
		Sand and Wrapped	HN	HG1
		Fabric Texture	-	HG2
		Uncoated	-	HG3
	Pultrall	Sand	P	PG1
		Uncoated	-	PG2
#8	Hughes Bros.	Sand and Wrapped	H	HG
	Pultrall	Sand	H	PG

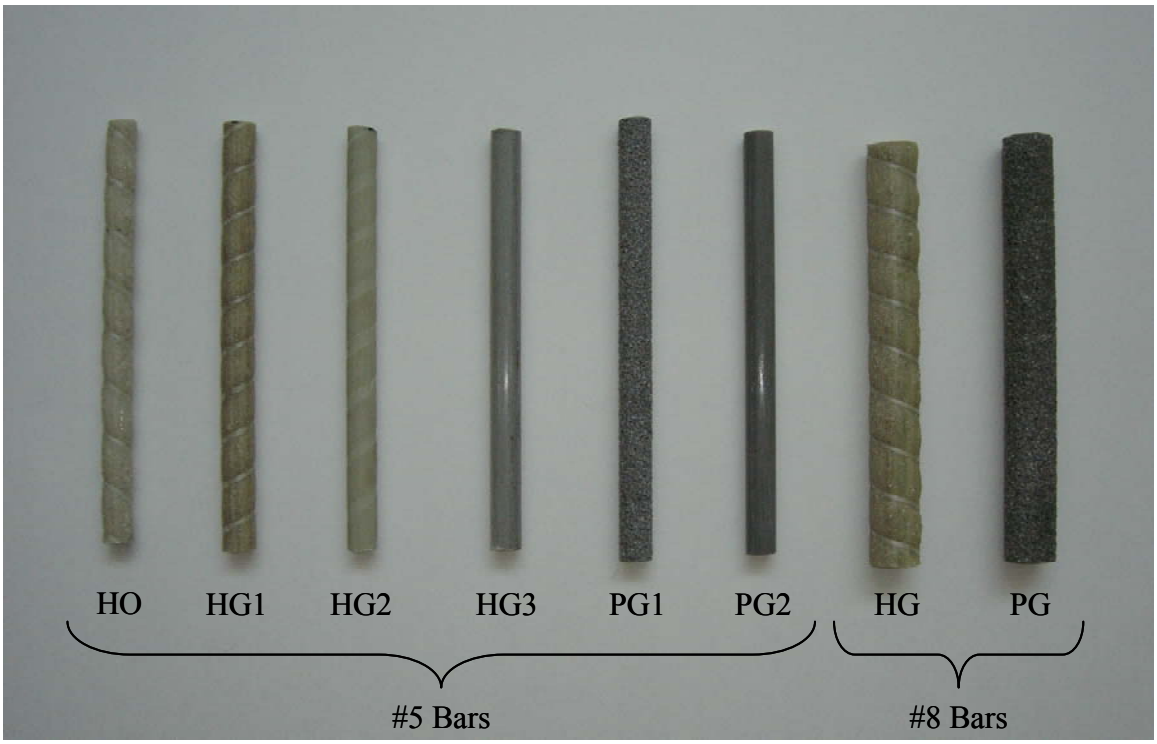

Figure 2.10 Glass FRP Bars

2.4.1.2.2 Carbon FRP

Bars with three different types of surface deformations were evaluated; uncoated, sand coated, and fabric texture coated bars. The carbon FRP bars used in this study as well as their designation are listed in Table 2.9 and shown in Figure 2.11. The bars were composed of carbon fibers and vinyl ester resin and produced by the pultrusion process. The reinforcing bars contained fibers which constitute at least 70% of the volume of the bar. Supplied bars can be summarized as follows:

Hughes Brothers Inc.

#5 Bars: 1 - Fabric texture

Pultrall Inc.

#5 Bars: 1 - Uncoated

2 - Sand coated

Table 2.9 Carbon FRP Bars used in the Experimental Program

Bar Size	Producer	Surface Deformation	Bar Designation	
			Phase I	Phase II
#5	Hughes Bros.	Fabric Texture	C	HC1
	Pultrall	Sand	-	PC1
		Uncoated	-	PC2

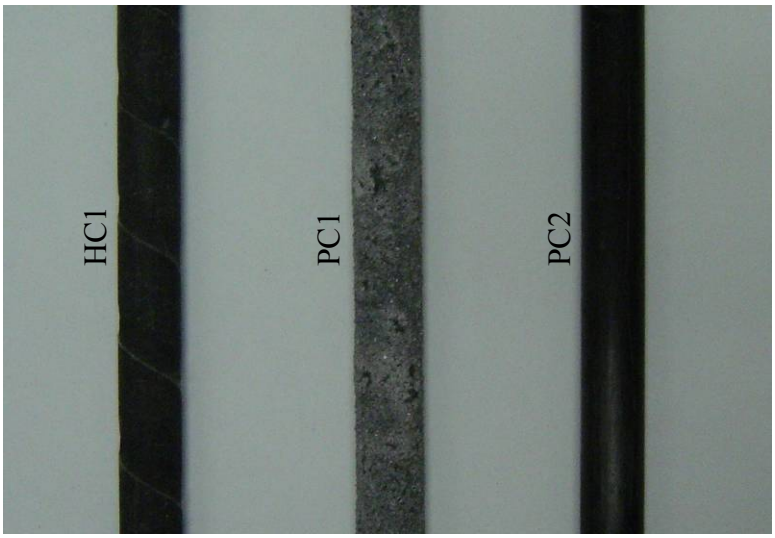

Figure 2.11 Carbon FRP Bars

2.4.2 Concrete

The beams were cast using a 3,500 psi nominal strength non air-entrained concrete that was obtained from Irving Materials Inc., a ready-mix concrete supplier in West Lafayette, Indiana. The same batch of concrete was used to cast the specimens in each series. In all series, the coarse aggregate consisted of river gravel with a 3/4 in. maximum aggregate size. The mix design and the actual slump measurement before casting for each batch are provided in Table 2.10.

The compressive and splitting tensile strength of the concrete was estimated from tests of 6x12 in. cylinders. In the second phase, in addition to the 6x12 in. cylinders, 4x8 in. cylinders were tested to obtain the compressive strength for comparison purposes. Load was applied using a 600 kip Forney testing machine at a rate of 35 psi/sec for

compressive tests and 16 kips/min for splitting tensile tests. The compressive strength gain curves obtained from 6x12 in. cylinders for each phase are shown in Figure 2.12 and Figure 2.13.

The same mix designs were ordered for each phase of the study. Because the cement supplier changed their cement production process, the specimens in the second phase resulted in a lower compressive strength than in the first phase. Concrete compressive and splitting tensile strengths obtained from 6x12 in. cylinders for each series are provided in Table 2.11.

Table 2.10 Mix Design per Cubic Yard

Material	Series I	Series II	Series III	Series IV	Series V
Type I Cement (lbs.)	425	430	429	430	428
Fine Aggregate (lbs.)	1651	1591	1611	1550	1609
Coarse Aggregate (lbs.)	1847	1849	1842	1850	1842
Water (lbs.)	163	145	196	240	184
Air (oz.)	1.1	1.1	0	0	0
Water Reducer (oz.)	8.7	7.8	6.5	1.5	6.4
Fly Ash (lb.)	None	None	None	None	None
Slump	4 in.	5 in.	5.5 in.	3 in.	4.5 in.

Table 2.11 Average Concrete Strength

Series	Age (days)	f_c (psi)	f_t (psi)
I	28	5090	614
	32	5270	592
	38	5410	571
II	28	5500	503
	35	5510	522
	43	5480	525
III	28	3660	-
	109	4120	381
	132	4000	376
	142	3930	385
IV	28	4040	-
	131	4670	430
	151	4610	462
	157	4650	435
V	28	3650	-
	156	4110	399
	167	3890	460
	183	4100	432

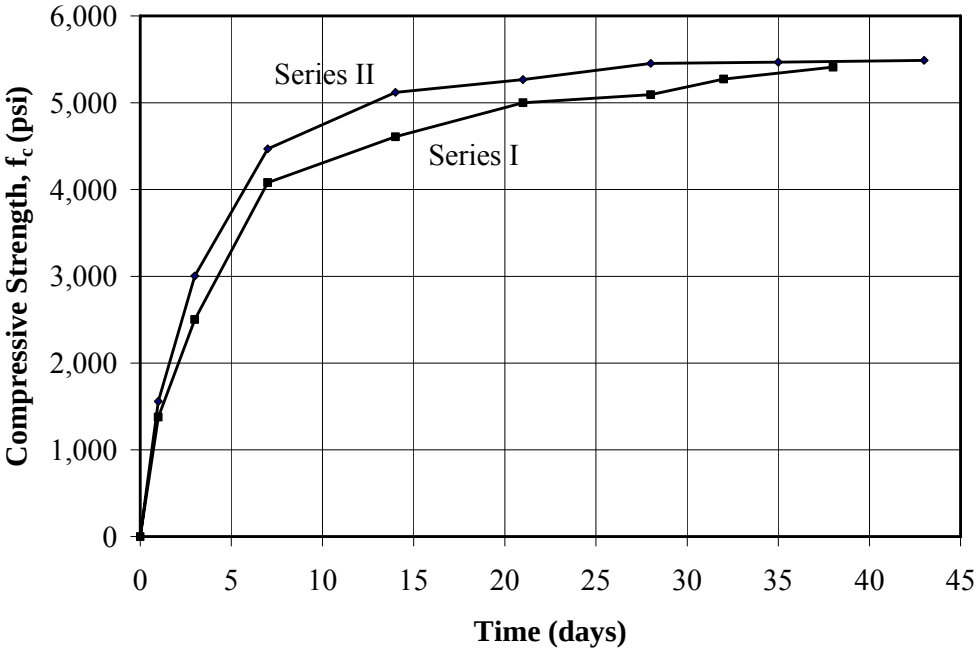

Figure 2.12 Concrete Compressive Strength, Phase I

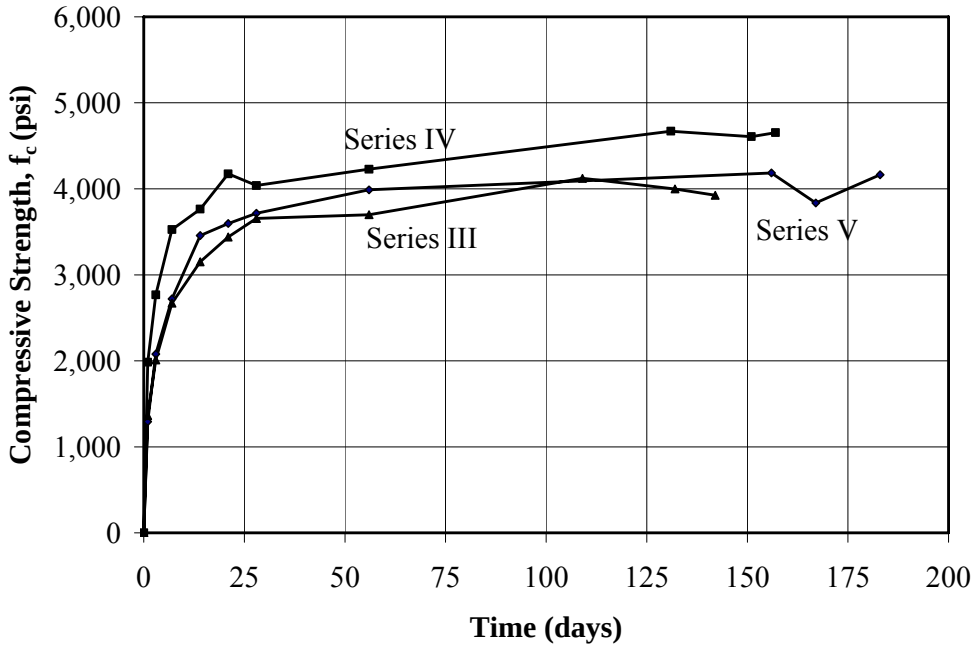

Figure 2.13 Concrete Compressive Strength, Phase II

2.5 Specimen Construction

2.5.1 Fabrication of Formwork

Wooden forms were designed and constructed to allow two specimens to be cast side-by-side. The assembled formwork for the specimens in Series I are shown in Figure 2.14. The same type of formwork was used throughout the experimental program. In the first phase, four sets of forms were constructed so that eight specimens were cast in each series. In the second phase, five sets of forms were constructed to cast ten beams in each series. The base of the formwork, containing 3/4 in. plywood and 2x4 in. lumber, was made wide enough to accommodate the varying width of the specimens. The side forms were also made from 3/4 in. plywood and 2x4 in. lumber. A ladder type structure was constructed by connecting 10 ft long 2x4 in. base and top plates with 12 in. long 2x4 in. studs. Plywood sheathing was attached to the face of the structure to complete the side forms. The center and side forms were secured to the base using wood screws. The end blocks were secured to the base, center form, and side form with wood screws. The inside of the forms were oiled before the reinforcement cage was placed into the forms. Each set of forms were braced at the top from two points to prevent bulging of the side and center forms due to the pressure of the fresh concrete.

2.5.2 Construction of Reinforcement Cages

The reinforcement cage contained longitudinal reinforcement both in the tension and compression sides and hoops in the shear span (Figure 2.15). Bars were spliced only in the constant moment region of the tension side of the beam. Transverse reinforcement was needed in the shear region to prevent shear failure prior to bond failure; therefore, two #3 steel bars were provided in the compression zone to assist in fabrication of the cage. The hoops were attached to the longitudinal bars with plastic ties to maintain the spacing of the bars. The cages were placed in the forms using 1.5 in. chairs to maintain a 1.5 in. concrete cover thickness. Steel chairs were spaced at 16 in. for the top cast specimens. For the bottom cast specimens, steel chairs were placed 9 in. away from the end of the splice. No chairs were provided in the splice region (Figure 2.16(a)). The

cages were secured transversely using plastic spacer wheels in the shear span. They were further secured by tying the cages to nails that were attached to the side and center forms (Figure 2.16(c)). The top cover was maintained at 1.5 in. by hanging longitudinal reinforcement from the top brace with steel ties (Figure 2.16(b)).

Figure 2.14 Assembled Formwork (Series I)

Figure 2.15 Assembled Reinforcing Cage (Series I)

(a) Bottom Cast Bars in Splice Region

(b) Top Cast Bars in Splice Region

(c) Details of the Reinforcing Bar in Shear Span

Figure 2.16 Reinforcing Cage Inside Forms

2.6 Casting, Curing, and Storage

Specimens in each series were cast at the same time from the same batch of concrete. With an exception of Series V, a bucket and overhead crane were used to transport the concrete from the ready-mix truck. In Series V, the concrete was placed in the form directly from the truck. The concrete was placed in the forms in two layers and each layer was vibrated using mechanical vibrators. The beams were screeded, and the surface was floated with a magnesium float.

The beams were covered with wet burlap, and plastic sheets were placed on top of the burlap to prevent moisture loss before final set. The burlap was maintained wet during the curing period. At the end of curing, the forms were stripped, and the beams were stored in the laboratory until the time of testing. Specimens in the first phase (Series I-II) were cured for three days. In the second phase (Series III-V), specimens cast from the first batch (Series III) were cured for three days while the remaining specimens were cured for seven days. This change in curing duration was provided because the initial compressive strength in Series III was lower than the strength observed in Phase I. Therefore, to reach the desired strength, the specimens in Series IV and V were cured longer.

For each series, cylinders were cast in plastic molds simultaneously with the beams. The cylinders were consolidated, cured, and stored in the same manner as the test specimens. In the first phase, the first specimen in each series was tested at 28 days while the remaining specimens were tested within 15 days after the first specimen was tested. In the second phase, however, the first specimens were tested at 109, 131, and 156 days in Series III, Series IV, and Series V, respectively. The remaining specimens were tested within a month after the first specimen was tested.

2.7 Test Setup and Procedure

The testing setup is shown in Figure 2.17 and Figure 2.18 for Phase I and Phase II, respectively. Beams were placed on two supports, and two equal, concentrated loads were applied at the end of the cantilever with hydraulic rams, creating a constant moment region between the supports. The rams were connected to a single hydraulic hand pump

to obtain equal pressure in each ram. At the loading points, a 1 in. diameter roller placed between two 1x4x12 in. steel bearing plates was used to transfer the load to the beam from the ram. Steel bearing plates were attached to the test specimen using hydrostone. At the supports, the load was transferred using a 1.5 in. diameter roller placed between two steel plates. The roller support was obtained by placing the roller between two 1.25x6x36 in. flat steel plates. The pin support was obtained by placing the rod between a 1.5x6x36 in. grooved and 1.25x6x36 in. flat steel plate.

Load was applied through 50 ton hydraulic rams with a 6 in. stroke capacity using increments of 1 kip for the 11 in. wide specimens (#8 bars) and 0.5 kip for the 8.75 in. wide specimens (#5 Bars). At each load stage, the crack pattern was carefully mapped and crack widths were measured on the beam top surface using an Edmund Direct Measuring microscope. Cracks were mapped and measured up to a critical load beyond which it was considered unsafe to approach the beam. In Phase II, the steel reaction frame was supported with a 4x6 in. and 2x4 in. wooden frame to prevent lateral movement of the reaction frame (Figure 2.18).

Figure 2.17 Test Setup (Phase I)

Figure 2.18 Test Setup (Phase II)

2.7.1 Instrumentation Layout

The instrumentation layout for a typical specimen in Phase I and Phase II is shown in Figure 2.19 and Figure 2.20, respectively. Eight linear voltage displacement transducers (LVDT) were used to measure the deflections in Phase I while ten were used in Phase II. LVDT's were attached to the following locations; two at each end, two in the middle, and one or two at each support. Applied loads were monitored using two Lebow load cells (50 kip and 100 kip capacity) placed between the ram and the beam of the loading frame (Figure 2.17). In some of the specimens, strain in the reinforcing bars was measured with strain gages attached to the reinforcing bars.

The LVDT's attached to the support points were used to measure the support settlements. The measured values were used to correct the measurements made at the end and middle of the beam. One LVDT was located at each support at Phase I; however, two were attached at each support in Phase II with the exception of Specimens B-HG-8-12 and B-PG-8-12.

In Phase I, three strain gages were placed on the reinforcing bars at the ends of the splice region (Figure 2.21). Two were attached to the middle reinforcing bars, and one was attached to the outer reinforcing bar. The strains measured with strain gages and strains calculated based on flexural theory agreed well in the first phase; therefore, no strain gages were installed on the FRP reinforcing bars in Phase II. However, strain gages were installed on the steel reinforced specimens where there was a possibility of yielding of the reinforcement. Details of the strain gage instrumentation for these specimens is shown in Figure 2.21(b-d).

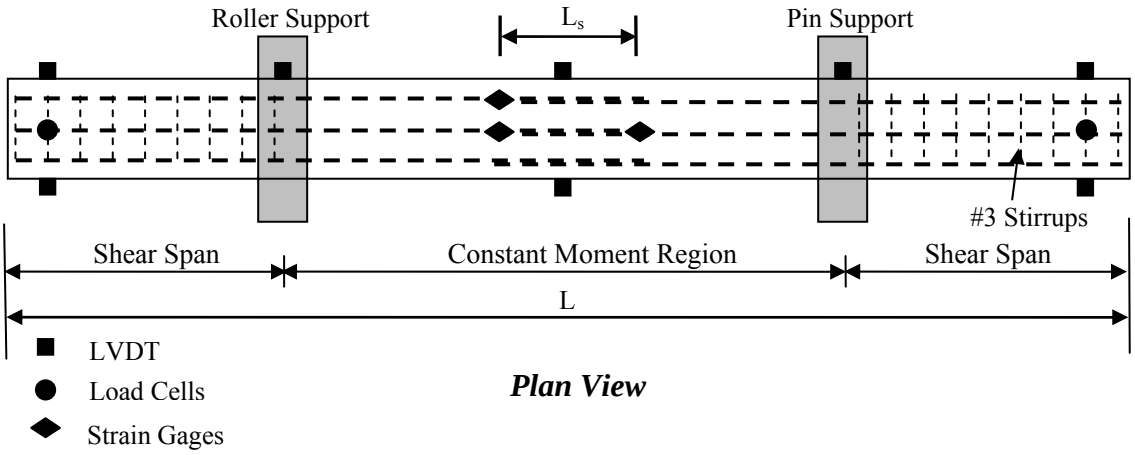

Figure 2.19 Plan View of Instrumentation Layout (Phase I)

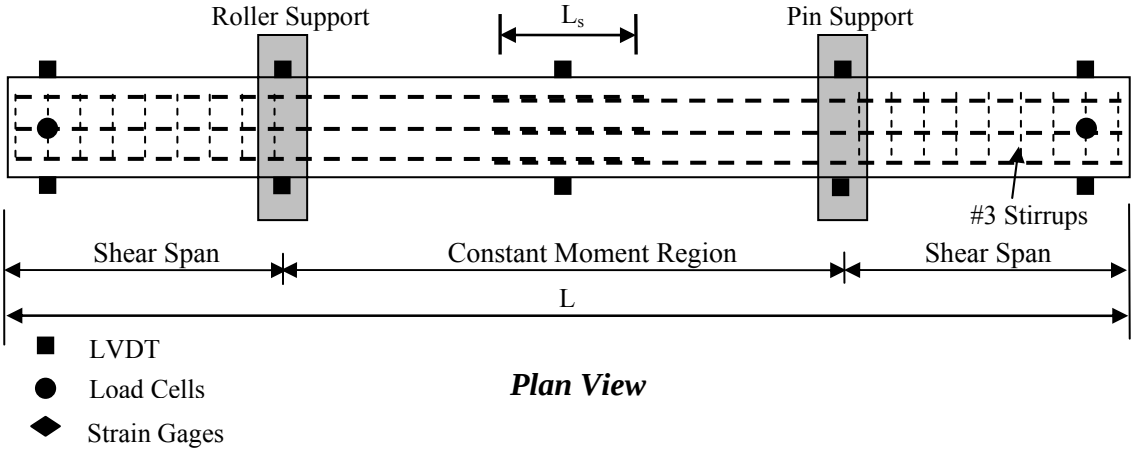

Figure 2.20 Plan View of Instrumentation Layout (Phase II)

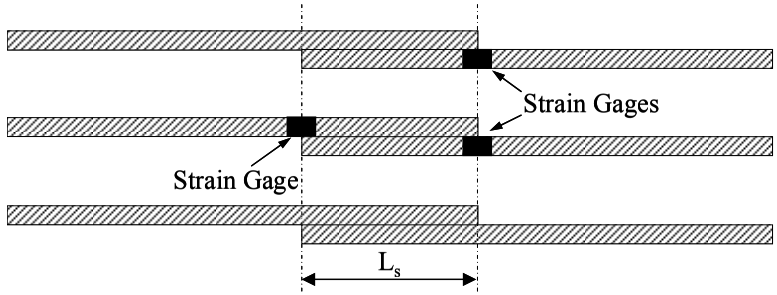

(a) Specimens in Phase I

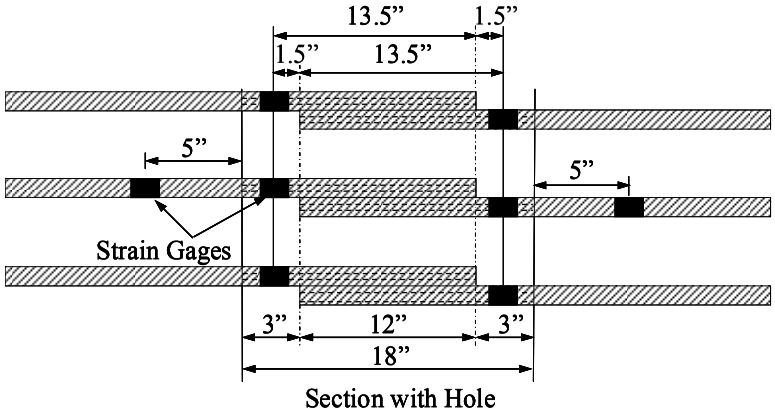

(b) Specimen B-S2-8-12

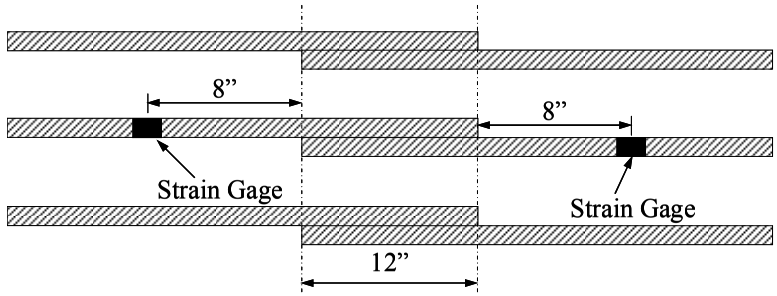

(c) Specimens B-S3-8-12 and B-S4-8-12

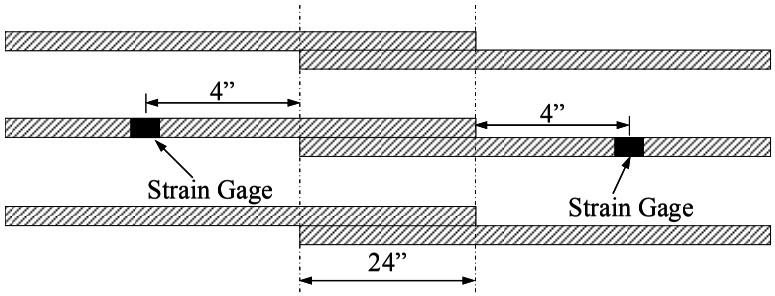

(d) Specimens B-S-5-24

Figure 2.21 Strain Gage Layout

CHAPTER 3

EXPERIMENTAL RESULTS

3.1 Introduction

The experimental results of each test are presented to evaluate the effect of the variables discussed in Section 2.3.1 on the behavior of the specimens and the development strength of the reinforcement. In this chapter, the general behavior of the specimens is explained with an emphasis on failure modes and cracking patterns. Load, deflection, crack width measurements, and crack patterns are presented. Complete crack width measurements and crack drawings for each specimen are presented in Appendix C, and strain gage data is provided in Appendix D.

3.2 General Behavior

3.2.1 Loading and Cracking of the Specimen

3.2.1.1 Specimens Reinforced with Bars Having Surface Deformations

Specimens with the same width and shear span in a given series cracked at approximately the same load. Cracking was observed from the load-deflection curve by a distinct reduction in the stiffness of the specimen. The stiffness of the specimens was approximately the same up to the cracking load while it reduced after the section was cracked.

Flexural cracks usually first occurred either in the shear span or simultaneously in the shear span and constant moment region. The first flexural crack in the shear span generally occurred either over the support or near the support where the first stirrup was located. The highest moment was generated over the supports due to the loading condition and the self-weight of the beam; therefore, it is reasonable that the first crack

was observed over or near the supports. As loading increased, further cracks formed within the length of the constant moment region, shear span, and the splice length. The cracking pattern for specimens reinforced with three different types of reinforcement is presented in Figure 3.1-Figure 3.3.

Figure 3.1 Cracking Pattern of Steel Reinforced Specimen Prior to Failure (Specimen B-S-5-24)

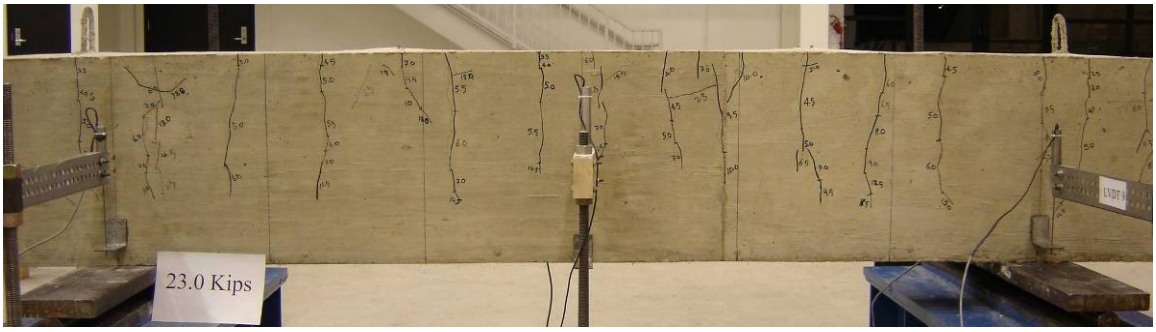

Figure 3.2 Cracking Pattern of Carbon FRP Reinforced Specimen Prior to Failure (Specimen B-PC1-5-24)

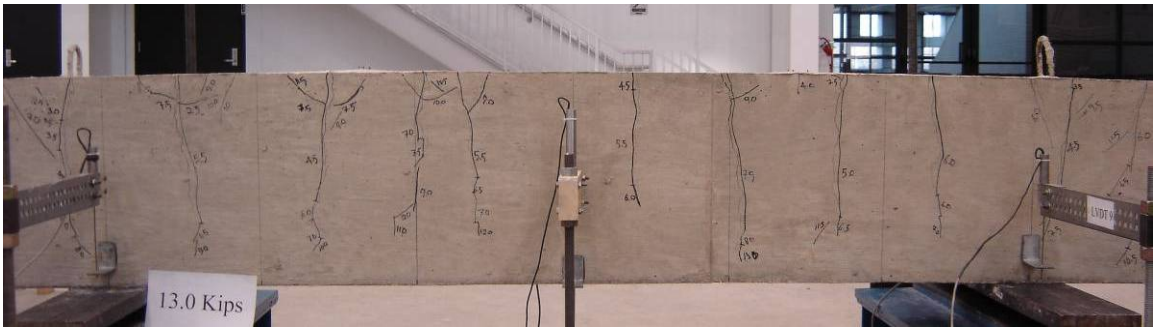

Figure 3.3 Cracking Pattern of Glass FRP Reinforced Specimen Prior to Failure (Specimen B-HG1-5-24)

These photographs were taken one load step before failure of the specimens. In general, the flexural cracks located in the constant moment region were approximately perpendicular to the axis of the beam. The cracks formed in the splice region did not penetrate as deep into the section as the cracks outside the splice region.

As the load was increased, cracks formed parallel to the reinforcing bars in some specimens. Most of these cracks occurred in the constant moment region either on the tension face or the side faces of the specimen. In some specimens, these cracks were also observed on the tension face of the shear span. Horizontal cracks that formed along the beam axis were considered the initial indication of splitting of concrete. Another observation regarding cracking is that the flexural cracks which occurred at the end of the splice region usually branched diagonally near the reinforcement level in several of the specimens (Figure 3.4(a)). This was generally observed on specimens reinforced with glass and carbon FRP bars. In spite of reaching higher reinforcement stresses, branching from the principal flexural cracks was not observed in the steel specimens (Figure 3.4(b)).

For the specimens that displayed crack branching, it was observed that the formation of these branches and their location was arbitrary. The flexural cracking pattern was generally symmetric with respect to the centerline of the beam. However, the branching of the cracks, mainly located at the end of the splice, was randomly distributed in the beams, if present. For example, branching of the flexural crack can be observed on one side of the specimen and splitting cracks can be observed on the other side (Figure 3.5).

In the shear span, the cracks were vertical during the early stages of loading and propagated by inclining towards to the supports as the load increased. Shear failure was prevented by providing stirrups in the shear span.

At a given load, the cracks in the carbon FRP reinforced specimens penetrated deeper into the section than that of the steel reinforced specimen. Cracks of the carbon FRP specimens, however, were shallower that that of the glass FRP reinforced specimens. The crack widths observed in steel reinforced specimens were always smaller than the comparable FRP reinforced specimens. It was observed that the crack widths

measured at a given load was always larger in the glass FRP reinforced specimens than the companion carbon FRP reinforced specimens. Figure 3.6 shows the constant moment region of specimens reinforced with steel, carbon FRP, and glass FPR bars at an applied loading of 13 kips. Crack width observations are discussed further in Section 3.6.

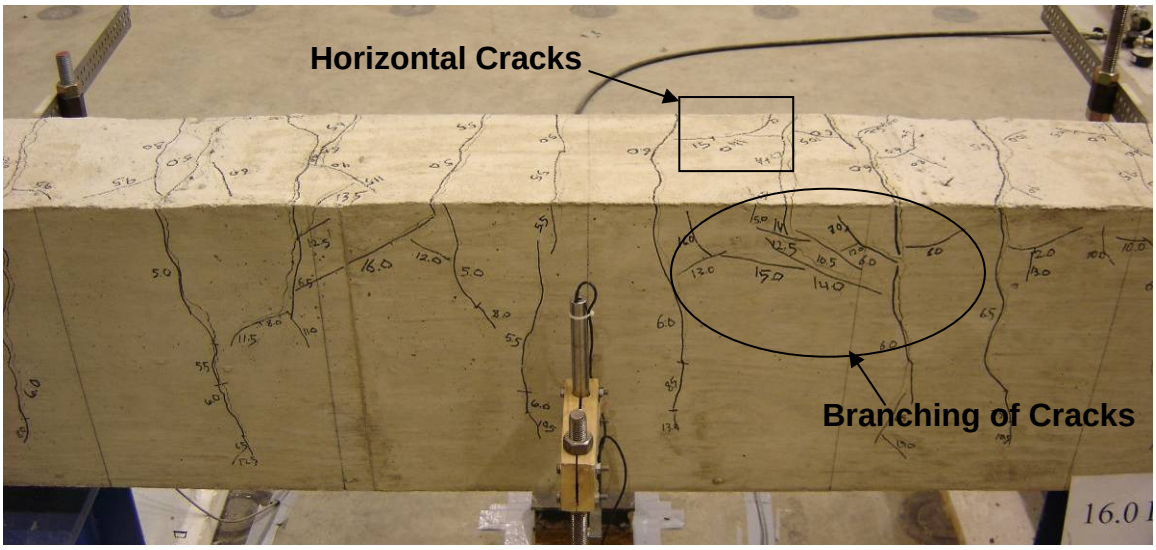

(a) Specimen B-PG1-5-24 at 45 ksi

(b) Specimen B-S-5-24 at 70 ksi

Figure 3.4 Comparison of Cracking in the Splice Region

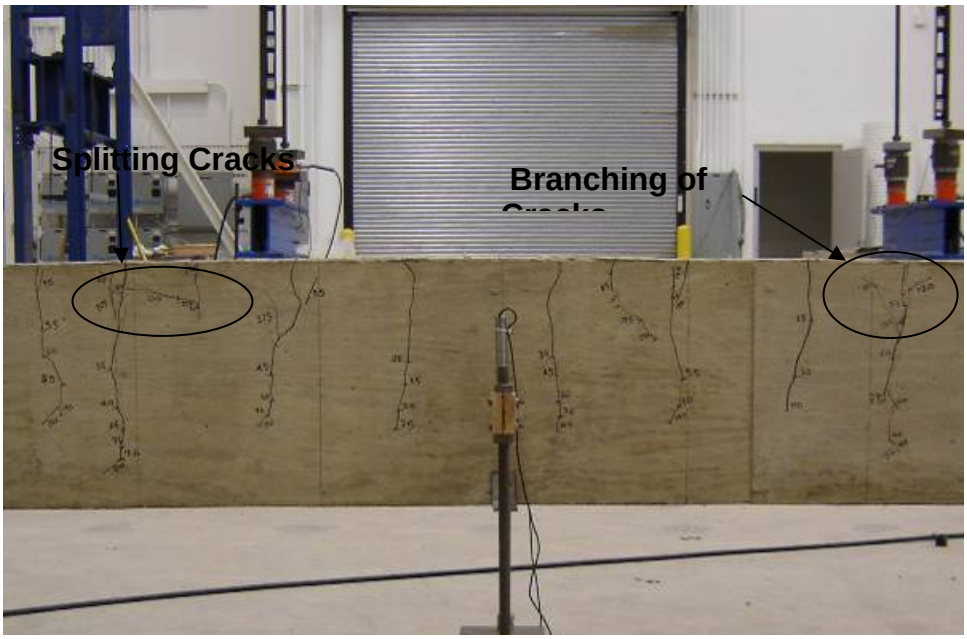

(a) East Side of Specimen, Splice Region

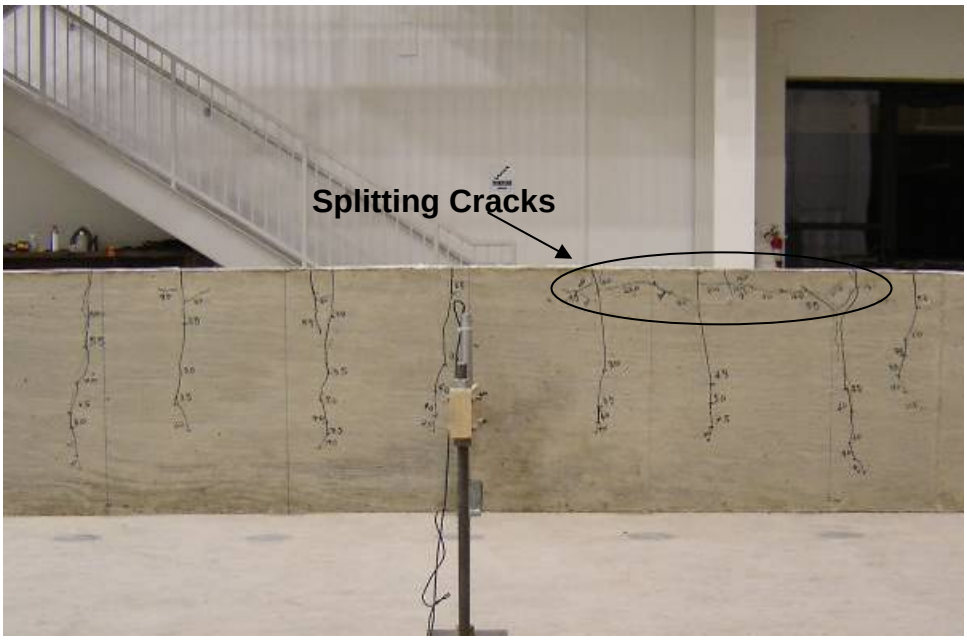

(b) West Side of Specimen, Splice Region

Figure 3.5 Comparison of Cracking on Both Sides of the Specimen B-HC1-5-54

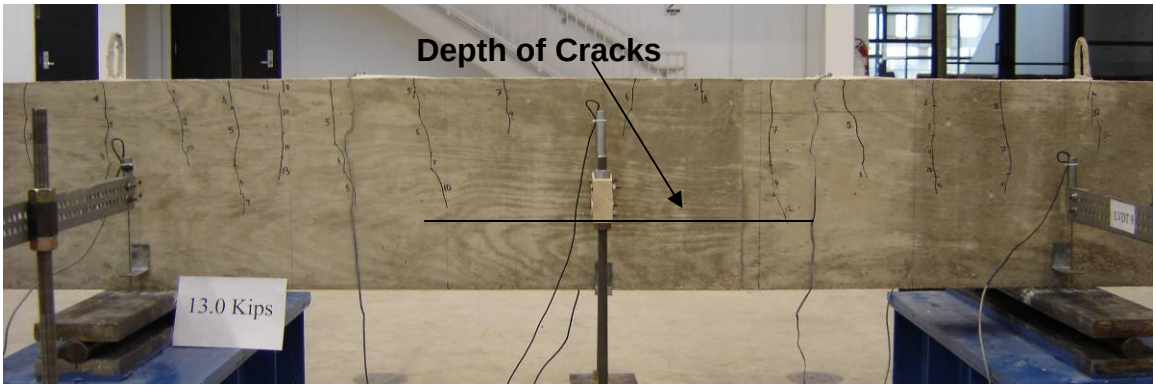

(a) Steel Reinforced Specimen at 13 Kips (Specimen B-S-5-24)

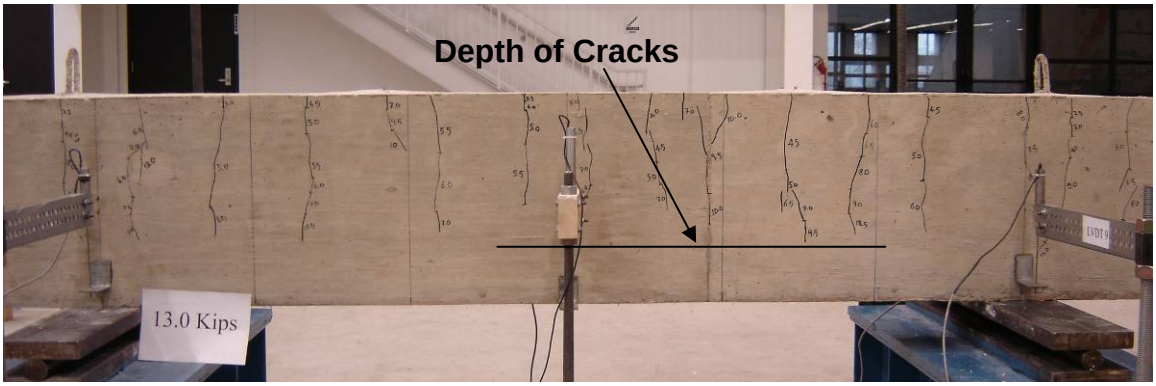

(b) Carbon FRP Reinforced Specimen at 13 Kips (Specimen B-PC1-5-24)

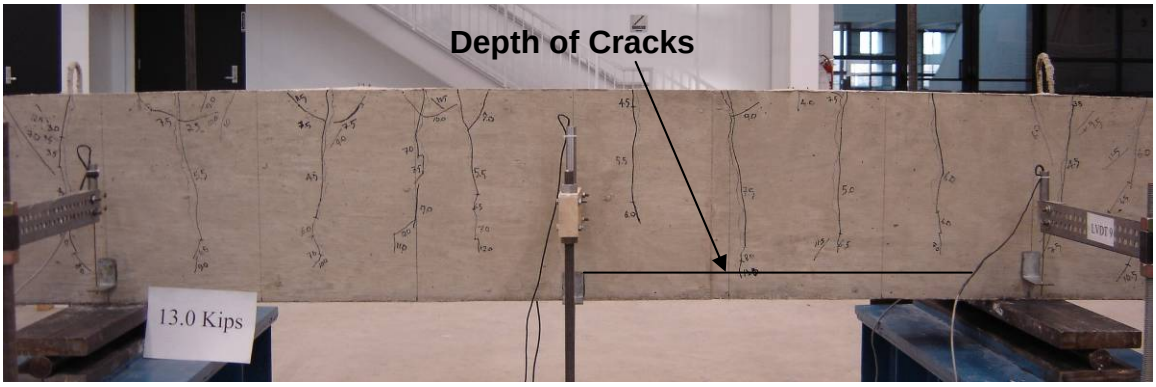

(c) Glass FRP Reinforced Specimen at 13 Kips (B-HG1-5-24)

Figure 3.6 Comparison of Crack Propagation in Specimens with 24 in. Splices

3.2.1.2 Specimens Reinforced with Plain Bars

3.2.1.2.1 Steel Reinforced Specimens

Specimens reinforced with plain steel bars cracked at approximately the same load with the companion specimens reinforced with bars having surface deformations. First flexural cracks occurred over the supports and several cracks formed along the constant moment region as the load increased. The load dropped slightly at the time of failure, and the specimen sustained the load as the deflection increased. No splitting cracks were observed in any of these specimens. The specimens failed in pullout in the splice region, and the failure was initiated by the flexural cracks that occurred in the constant moment region. Specimen B-S3-8-12 immediately prior to failure is shown in Figure 3.7.

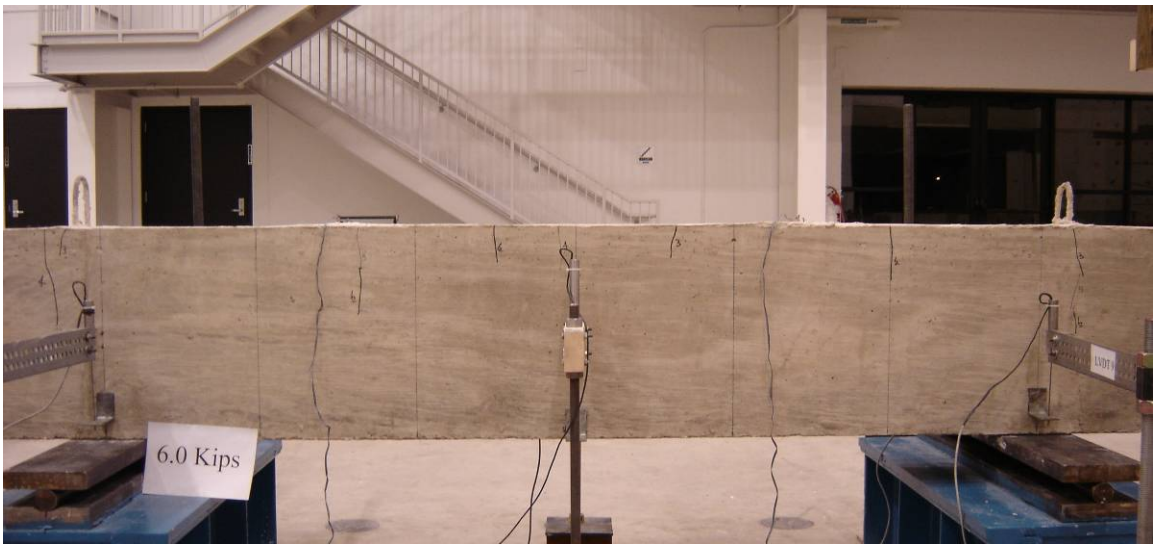

Figure 3.7 Cracking Pattern of Specimen B-S3-8-12 at 6 kips.

3.2.1.2.2 FRP Reinforced Specimens

All specimens reinforced with plain FRP bars cracked at approximately the same load. The cracking load, however, was slightly lower than those of the companion specimens reinforced with bars having surface deformations. Flexural cracks first formed over the supports. As loading increased, the flexural cracks widened as bar slippage occur. Failure occurred due to a bond failure by pullout. A sudden drop in the applied load was observed at failure as evident in the load-deflection response. As loading

increased after slippage, one additional crack formed in the constant moment region of B-PC2-5-24. Flexural cracks over the supports initiated the failure. The constant moment region of the Specimen B-PC2-5-24 prior to failure is shown in Figure 3.8.

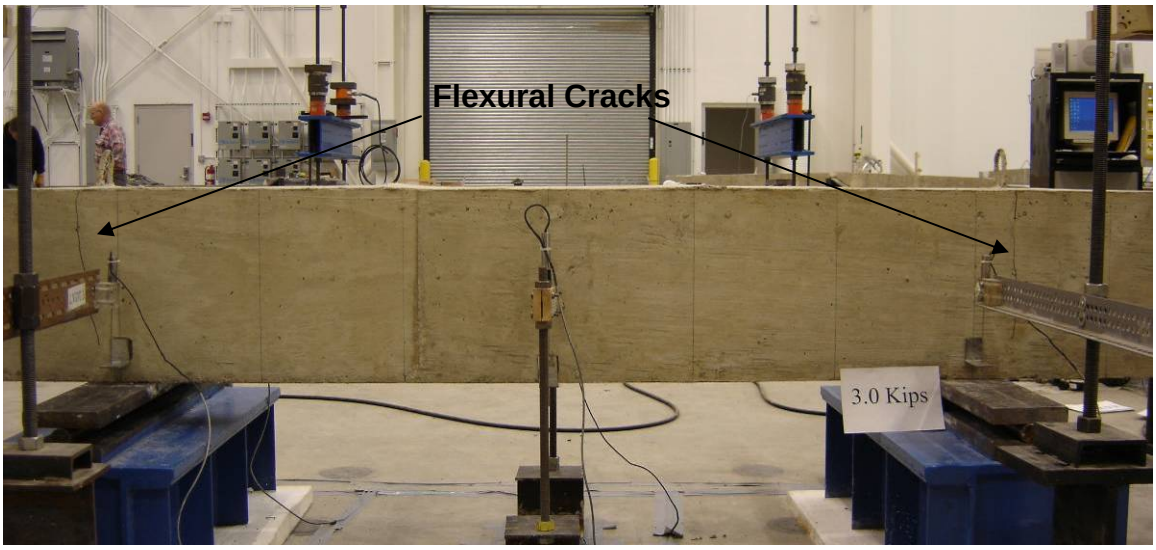

Figure 3.8 Cracking Pattern of Specimen B-PC2-5-24 at 3 kips.

3.3 Failure

3.3.1 Bond Tests with Bars Having Surface Deformation

All specimens reinforced with bars having surface deformations failed by splitting of the concrete in the splice region. The specimens failed in a brittle manner by splitting of the cover in a "side splitting" mode. The failures were sudden, brittle, and unexpected as the energy was released from the splice at the time of failure. Two different types of side splitting were observed during failure. In the first type, the concrete cover in the splice region exploded. In the second case, the failure was not explosive and the cover was still intact with the reinforcement. Photographs captured at the time of failure illustrating the failure types are shown in Figure 3.9 and Figure 3.10. It was observed that the splitting cracks penetrated along the reinforcing bars at the time of the failure. No obvious signs of warning were observed prior to failure in any of the tests. The splitting plane observed after the failure indicated that failure typically initiated from the splitting cracks present on the side face.

Following failure, the splice region was investigated and the findings were documented. The exact bar locations were measured after removing the concrete cover, and those dimensions were compared with the dimensions measured before casting concrete. No damage to the surface deformations was observed in any of the reinforcing bars.

(a) Specimen at the Time of Failure

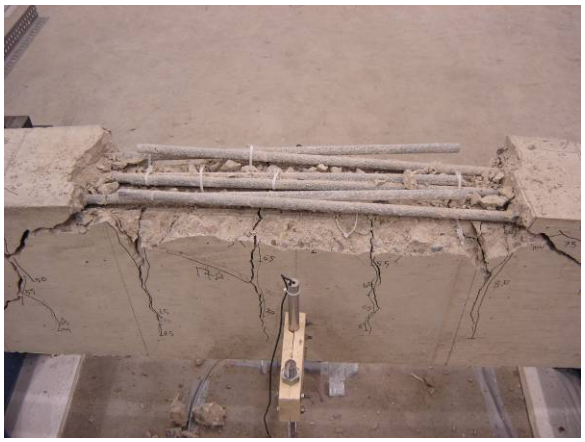

(b) Splice Region after Failure

Figure 3.9 Explosive Splitting Failure of B-PG1-5-24b

(a) Specimen After Failure

(b) Splice Region After Cover is Removed

Figure 3.10 Splitting Failure of B-HC1-5-24

3.3.2 Bond Tests with Plain Bars

Specimens reinforced with plain reinforcing bars failed in pullout. The bars pulled out from the shear span for the FRP reinforced specimens and from the splice

region for the steel reinforced specimens. No splitting cracks were evident in any of the specimens. A sudden drop in the load was observed at the time of failure. The specimens were further loaded after the pullout failure to determine the section where the slip failure occurred. As deflections were increased, the specimen was capable of sustaining a reduced load. At the same time, the width of the flexural crack which initiated the failure increased considerably with respect to the other flexural cracks present in the section (Figure 3.11).

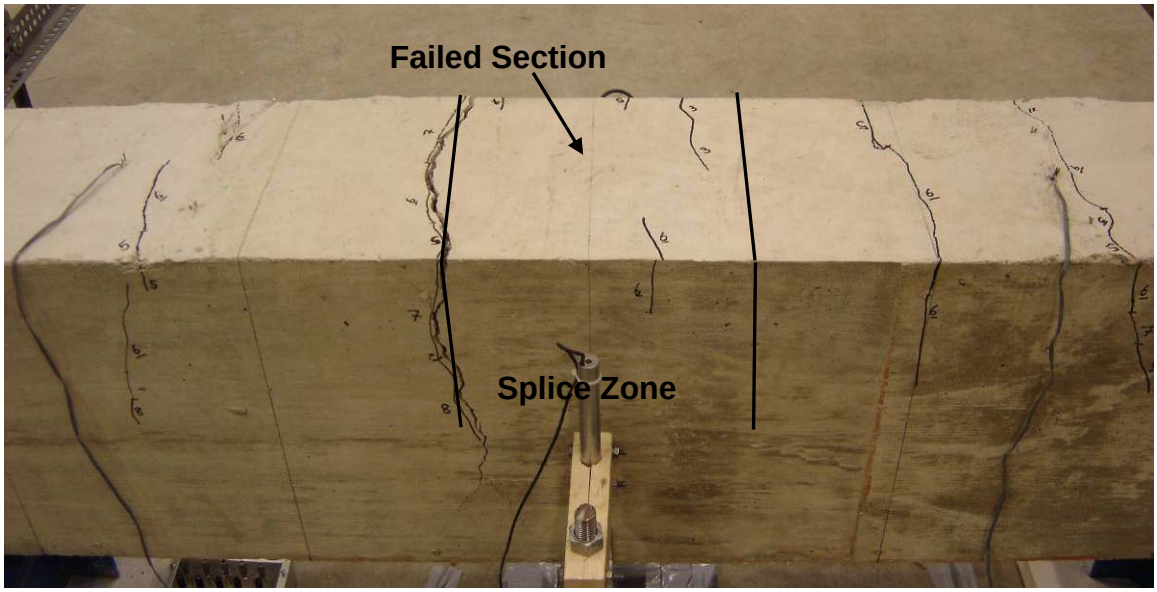

(a) Specimen B-S4-5-12 (Steel Reinforced)

(b) Specimen B-PG2-5-24 (FRP Reinforced)

Figure 3.11 Pullout Failure

3.4 Bond Strength

Load at failure (P_{ult}), moment at failure (M_{ult}), computed reinforcement stresses reached at failure ($_{bs}$), computed average bond stress along the splice ($_{avg}$), and age of the specimens at the time of testing are presented for Phase I and Phase II in Table 3.1 and Table 3.2, respectively. Specimens in this experimental program failed in two modes. Specimens that were reinforced with deformed bars failed by horizontal splitting extending through the width of the beam at the level of the bars. Specimens that were reinforced with smooth bars, however, failed in a pullout failure mode. The reinforcement stress at failure was calculated using both cracked section analysis and moment curvature analysis. For moment curvature analysis, the Hognestad stress-strain curve was used for concrete in compression and the tensile strength of the concrete was neglected. Values from both analyses were approximately the same; therefore, stresses from the crack section analysis are presented in this section.

Table 3.1 Bond Test Results (Phase I)

Series	Specimen ID	Age (days)	P_{ult} (kips)	M_{ult} (ft-kip)	$_{bs}$ (ksi)	$_{avg}$ (psi)
I	B-S-8-18	28	33.0	99.0	41.4	570
	B-P-8-18	29	24.1	72.3	28.3	390
	B-H-8-18	31	20.5	61.6	24.0	332
	B-H2-5-18	32	14.2	42.6	41.1	357
	B-H1-5-18	35	11.5	34.6	33.3	289
	B-P-5-18	36	16.5	49.6	48.1	415
	B-S-5-18	37	24.1	72.3	71.4	633
	B-C-5-18	38	19.9	59.7	59.5	515
II	B-C-5-12	28	15.1	45.2	44.9	585
	B-S-8-36	31	37.1	139.1	58.3	400
	B-P-8-36	32	19.9	74.9	29.3	202
	B-H-8-36	34	21.0	78.9	30.8	212
	B-H2-5-36	35	12.4	46.4	44.8	194
	B-H1-5-36	38	13.3	49.9	48.3	208
	B-P-5-36	40	13.9	52.3	50.6	219
	B-C-5-36	42	22.9	86.0	85.8	371

Table 3.2 Bond Test Results (Phase II)

Series	Specimen ID	Age (days)	P_{ult} (kips)	M_{ult} (ft-kip)	$_{bs}$ (ksi)	$_{avg}$ (psi)
III	B-S2-8-12	133	18.1	54.4	29.7	465
	B-S1-8-12	130	21.9	65.8	27.3	571
	B-S4-8-12	137	9.0	27.0	20.0[+]	228[+]
	B-S3-8-12	140	7.0	21.1	8.8[+]	185[+]
	B-PG-8-12	104	17.1	51.4	20.0	418
	B-HG-8-12	106	14.0	42.0	16.3	341
	B-S1-8-12b	111	21.2	63.5	26.3	551
	B-HG-8-12b	124	14.5	43.6	16.9	354
	B-PG-8-12b	126	15.8	47.3	18.4	385
	B-S-5-24	129	23.5	70.6	70.9[*]	467*
IV	B-HC1-5-24	132	21.9	65.6	64.7	426
	B-PC2-5-24	138	5.1	15.2	15.1[+]	58[+]
	B-PC1-5-24	139	24.1	72.3	71.8	472
	B-HG3-5-24	141	5.6	16.8	16.1[+]	62[+]
	B-HG1-5-24	142	13.6	40.8	39.0	256
	B-HG2-5-24	148	16.5	49.6	47.6	313
	B-PG2-5-24	152	4.3	12.9	12.3[+]	47[+]
	B-PG1-5-24	153	16.7	50.2	48.0	316
	B-HG1-5-24b	155	14.7	44.1	42.2	277
	B-PG1-5-24b	161	17.7	53.2	50.8	334
V	B-HG1-5-12	156	9.5	28.6	27.4	361
	B-PG1-5-12	160	10.6	31.7	30.4	400
	B-HG-8-24	161	20.8	62.3	24.1	253
	B-HG1-5-12b	162	12.1	36.4	34.8	458
	B-PG1-5-12b	164	13.6	40.8	39.0	514
	B-HG-8-24b	169	23.0	69.1	26.7	280
	B-HG-8-54	175	22.8	85.4	33.0	154
	B-HG1-5-54	177	14.1	52.7	50.4	148
	B-PG1-5-54	181	14.1	52.9	50.6	148
	B-HC1-5-54	183	22.9	86.0	85.0	249

[*] Yielded

[+] Pullout

The average bond stress was calculated assuming that the tension force in the bar is resisted by a uniform distribution of stress along the surface of the splice. Nominal cross-sectional dimensions were used in all calculations. The average bond stress for the specimens that failed in pullout was calculated using the actual length from where the bar

pulled out. Because the plain steel reinforcement pulled out from the splice region and the crack which initiated failure formed at the end of the splice, the actual splice length, 12 in., was used for calculating the average bond strength for Specimens B-S3-8-12 and B-S4-8-12. For the plain FRP reinforced specimens, pullout failure occurred in the shear span. The length of the failure section for Specimens B-PC2-5-24, B-HG3-5-24, and B-PG2-5-24 was measured as 41 in. in all three specimens since the flexural crack which initiated failure formed over the support for these specimens. Therefore, the average bond strength for the plain FRP reinforced section was calculated over a length of 41 in. It should be noted that the steel reinforcement in Specimen B-S-5-24 yielded prior to splitting failure.

3.5 Load-Deflection Response

3.5.1 Load-Deflection Curves

Deflections were measured with linear voltage displacement transducers (LVDT), and loads were monitored with two load cells. The applied load versus end deflection curves for Phase I (Series I and II specimens) are presented in Figure 3.12 and Figure 3.13, respectively. The applied load presented in the vertical axis is the average load applied to each end of the specimen. The LVDT readings which were measured at the loading points and at midspan were corrected based on the LVDT readings at the support locations. The end deflection presented in the horizontal axis is the average of the corrected deflections at each end of the specimen. The curves obtained from specimens with the same width and shear span are presented on the same graph for each series for comparative purposes.

As stated earlier, the beams reinforced with bars having surface deformations failed in a splitting mode, while plain bar reinforced specimens failed by slippage of the bar inside the concrete.

3.5.1.1 Specimens with Bars Having Surface Deformation

Behavior of the specimens can be described by three distinct stages in the load-deflection plot. In the first stage, before flexural cracking, the load-deflection curves are

linear and the slopes of the curves are approximately identical, indicating that before cracking, the stiffness of the specimens is primarily controlled by the concrete. In this stage, the behavior of all beams is elastic. In the second stage, after flexural cracking, the slope reduces; however, the response remains essentially linear up to failure. It can be seen that all specimens in a given series cracked at approximately the same load. In this stages, the stiffness is a function of the axial stiffness of the reinforcing bars which is a function of the modulus of elasticity and cross-sectional area of the bars. Because the area of the reinforcement in each graph is the same, the axial stiffness is only a function of the modulus of elasticity of the bars for these tests. Bars having a lower modulus of elasticity resulted in a lower beam stiffness in this stage of response. In general, beams reinforced with steel bars had the highest stiffness followed by beams reinforced with carbon and glass FRP bars. Beams reinforced with different types of glass FRP bars have approximately the same stiffness due to their similar moduli of elasticity. In the last stage, failure, all specimens failed suddenly by splitting of the concrete in the splice region.

In each series, among the specimens with the same cross-sectional dimensions and shear span length, steel reinforced specimens reached the highest load followed by carbon FRP and then glass FRP reinforced specimens. However in both series, specimens reinforced with glass FRP deflected most, followed by carbon FRP and steel reinforced specimens. Based on the observations, the modulus elasticity of the reinforcing bar was directly proportional to the failure load and inversely proportional to the deflection at the time of failure.

The same observations were made for the specimens tested in the second phase (Series III-V). Load versus deflection plots for all specimens tested in both phases are presented in Appendix E.

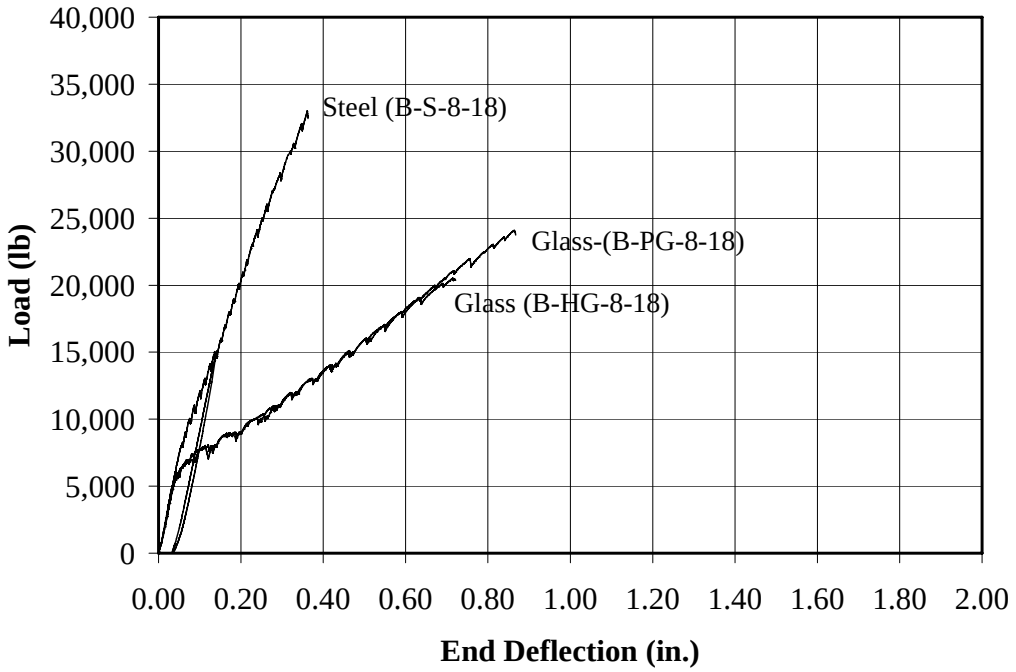

(a) Specimens Reinforced with #8 Bars

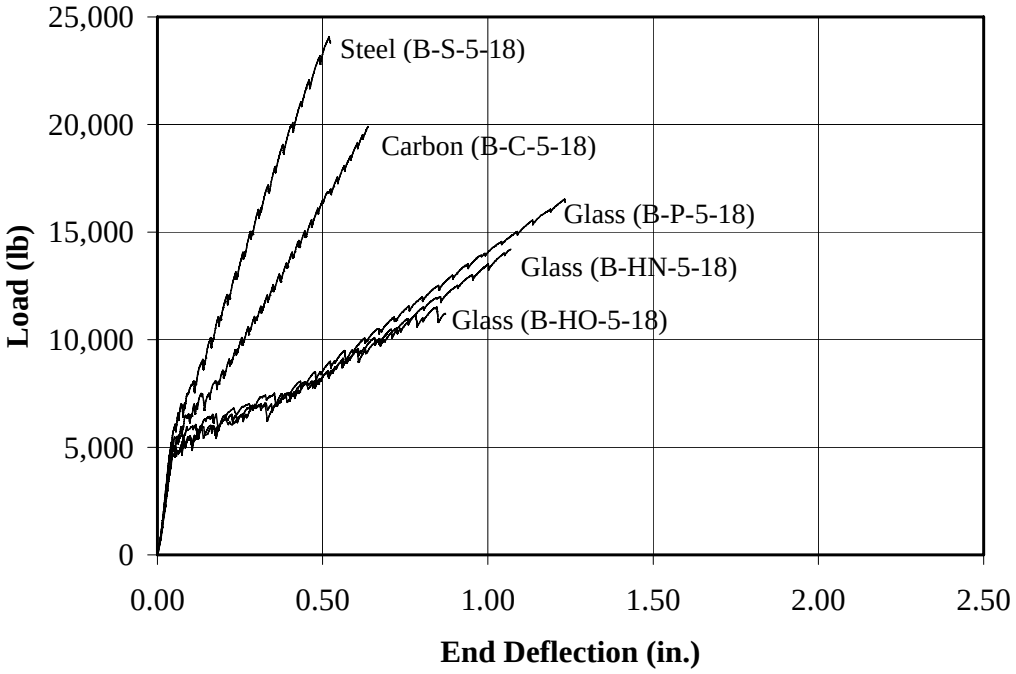

(b) Specimens Reinforced with #5 Bars

Figure 3.12 Load-Deflection for Specimens in Series I

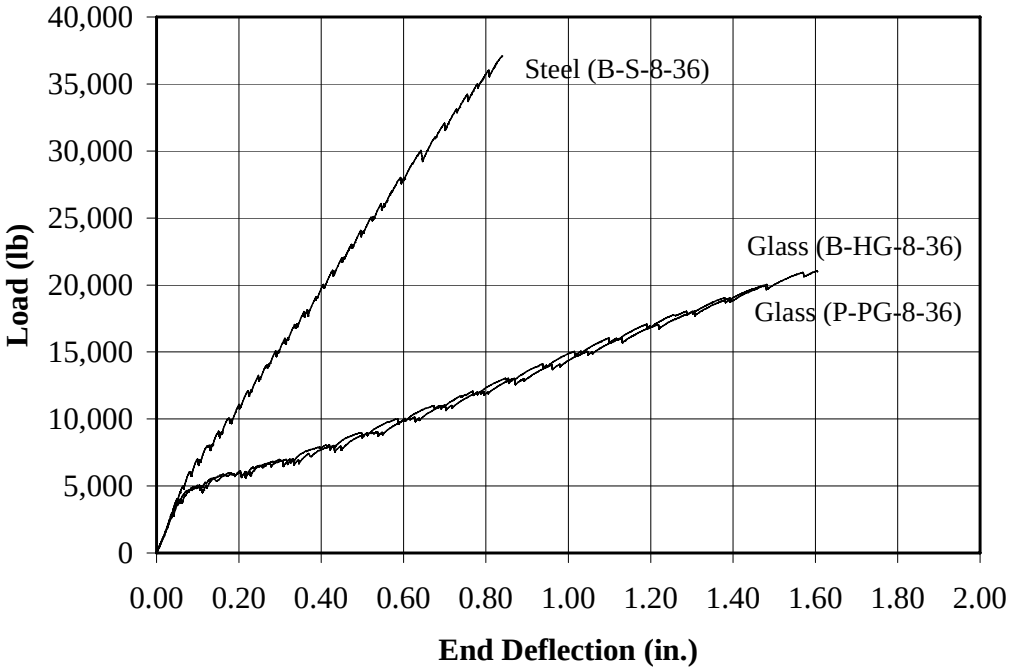

(a) Specimens Reinforced with #8 Bars

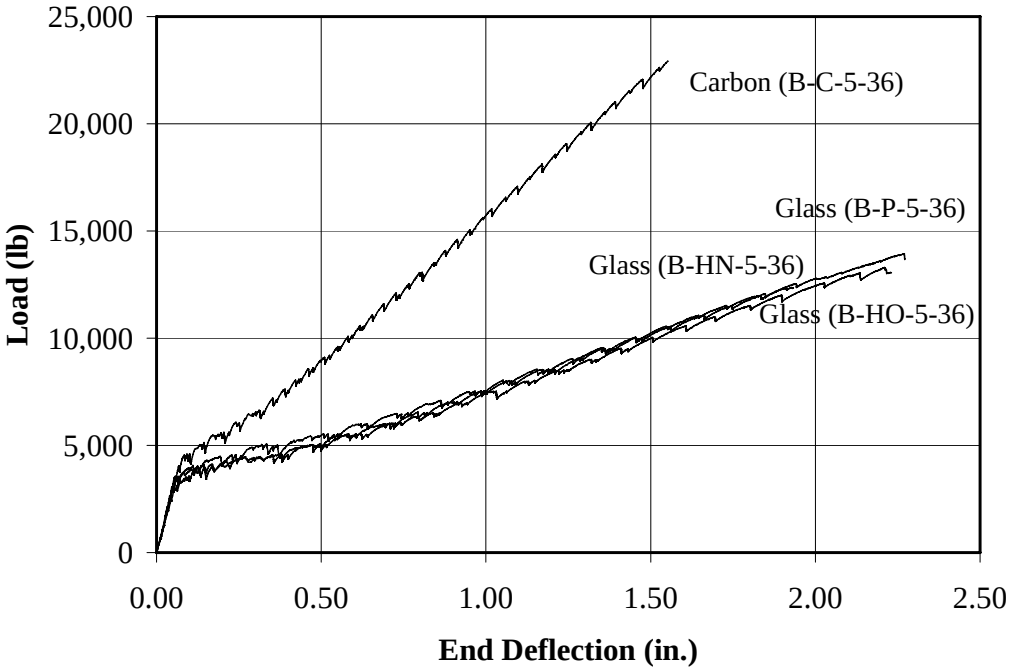

(b) Specimens reinforced with #5 Bars

Figure 3.13 Load-Deflection for Specimens in Series II

3.5.1.2 Bond Tests with Plain Bars

The load-deflection curves for plain bar reinforced specimens are presented in Figure 3.14. As evident in the load-deflection curves, the behavior of the plain bar reinforced specimens was quite different than the specimens reinforced with bars having surface deformations due to the failure mechanisms. The behavior of the plain steel reinforced specimens (Figure 3.14) can be described by three distinct stages in the load-deflection plot. The observed behavior in the first and the second stages was similar to that observed for the specimens reinforced with deformed bars (Figure 3.12 and Figure 3.13). In the first stage, the load increased linearly up to the cracking load. The behavior of the beam was elastic in this range. In the second stage, the beam stiffness dropped due to cracking of the specimen; however, the curve remained linear until the failure. In the last stage, failure, the load dropped approximately 3 kips. The specimen subsequently sustained this reduced load as the deflection increased.

Although the same type of failure was observed in both FRP and steel reinforced specimens, the load-deflection curves for the plain FRP reinforced specimens were remarkably different than for the plain steel reinforced specimens. The main difference was that the plain FRP reinforced specimens did not exhibit the same behavior in the second stage of loading. There was a sudden drop in the load when the first flexural crack formed. The drop in the applied load indicated slippage of the bar inside the concrete. The plain FRP reinforced specimens cracked 2 kips prior to the cracking load of the companion specimens with bars having surface deformations (Figure 3.12 and Figure 3.13). The specimens were capable of sustaining additional load as the deflection increased due to friction between the concrete and the reinforcement.

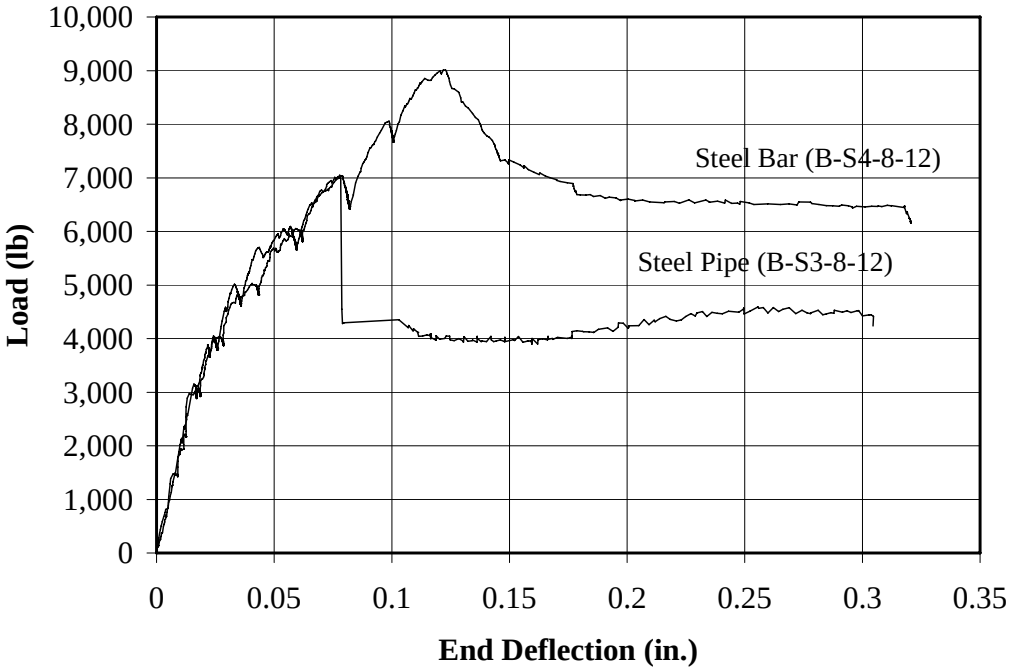

(a) Specimens Reinforced with Plain Steel Bars

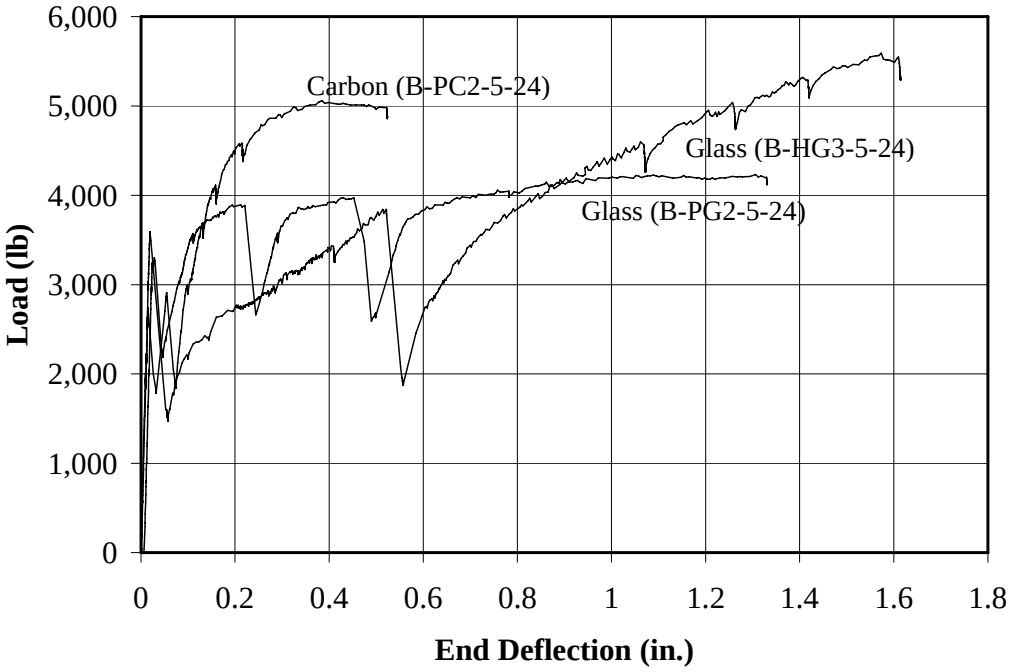

(b) Specimens Reinforced with Plain FRP Bars

Figure 3.14 Load-Deflection for Specimens Reinforced with Plain Bars

3.6 Crack Widths

Cracks were monitored throughout the experimental program for each specimen. Cracks and the corresponding loads were marked on the beam during the course of loading. Cracks widths were measured on the top surface of the beam using an Edmund Direct Measuring microscope with a 0.001 in. resolution. Crack widths were measured at 0.5 kip intervals for specimens reinforced with #5 bars and 1 kip intervals for specimens reinforced with #8 bars. Photographs were taken and mapped cracks were sketched on paper. Cracks widths were measured at the same location of each crack, and the location of the reading was recorded on the sketch. Cracks were measured up to a critical point at which it was considered unsafe to approach the beam.

Crack widths were only measured in the constant moment region of the specimen. Because the bar stress within this region was assumed to be constant for a given load, the calculated stresses were also assumed to be the stresses at the crack locations. Average and maximum crack width values were plotted against the calculated reinforcement stress in the constant moment region. These curves are grouped according to the size and type of reinforcement used in the specimens and presented in Figure 3.15 and Figure 3.16. For comparison purposes, the plots are drawn to the same scale. Crack widths measured in the splice region and over the supports are not included in these plots. The crack widths that were measured in the splice region were significantly smaller than those measured outside the splice region because of the increased amount of reinforcement in this region.

The reinforcement stress was calculated using both cracked section analysis and moment curvature analysis. Because values from both analyses were approximately the same, the values obtained from the cracked section analysis are presented in this section. The reinforcement stress was calculated based on the design dimensions of the cross section.

The curves for specimens reinforced with #8 and #5 bars are grouped according to bar type. The curves obtained from specimens with different types of reinforcement are remarkably different. At a given stress level, the crack widths measured in the glass FRP

specimens were significantly larger than those observed in the companion steel and carbon FRP reinforced specimens (Figure 3.15 and Figure 3.16).

The glass FRP reinforced specimens reached an average crack width of 0.016 in. at stress levels as low as 15 ksi. However, carbon FRP reinforced specimens reached a 0.016 in. crack width at approximately 40 ksi. At 15 ksi, the average crack width in the steel specimens was about 0.003 in. and increased to 0.010 in. when stress in the reinforcement reached to 40 ksi. Based on the available data, it can be concluded that at a given stress level, specimens reinforced with glass FRP bars achieved the highest crack widths followed by the carbon FRP specimens and the steel specimens.

Although the deformation pattern varies among the reinforcing bars, thus the stress-slip relationship, one trend is apparent that the slope of the stress versus crack width curves for steel reinforced specimens are the steepest followed by the carbon FRP reinforced specimens and the glass FRP reinforced specimens. In other words, the rate at which the crack width increases with the bar stress is primarily a function of the stiffness of the reinforcing bar assuming that the stress-slip relationship of the reinforcement is similar. The same behavior was observed from the load-deflection curves as well.

As seen from the reinforcement stress versus crack width graphs, the slope of the curve changes with the type of flexural reinforcement used in the specimens indicating that the stress alone is not the correct indicator for crack width calculations. Crack widths at the tension face of the beam are a function of the reinforcement strain, crack spacing, concrete cover, and the slip relationship between the concrete and the reinforcement. The spacing of the cracks is also a function of the slip characteristics of the flexural reinforcement embedded in concrete.

It is evident from Figure 3.15 and Figure 3.16 that the glass FRP reinforced specimens have more scatter in the average crack width data than the steel and the carbon reinforced specimens. This may be attributed in part due to variations in splice length and in particular variations in surface deformations. Therefore, the effect of the splice length and surface deformations on crack width were further investigated as shown in Figure 3.17 and Figure 3.18 for #5 and #8 bars. The specimens in each graph were cast from the same concrete batch to eliminate the influence of the concrete strength.

Furthermore, the modulus of elasticity of the reinforcement plotted in each graphs was approximately the same.

At a given stress, the crack widths in the specimens reinforced with #5 sand coated bars resulted in smaller crack widths than those observed in the specimens reinforced with the #5 sand wrapped bars for all splice lengths. However, for #8 bars reinforced specimens, the crack widths were approximately the same at a given stress. Therefore, based on the observed data, it is difficult to make any generalization on the slip performance of the reinforcing bars.

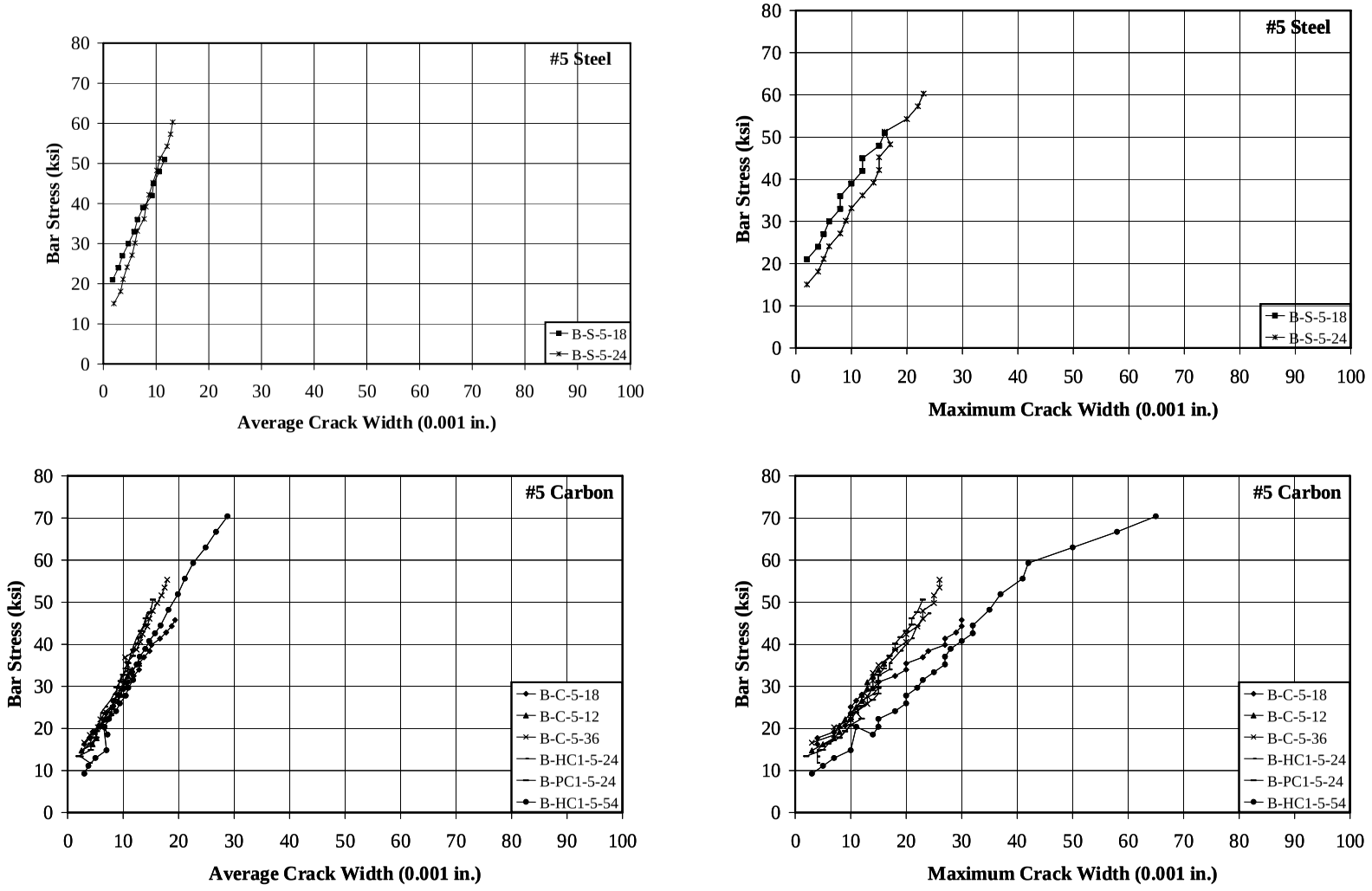

Figure 3.15 Reinforcement Stress versus Crack Widths for Specimens Reinforced with #5 Bars

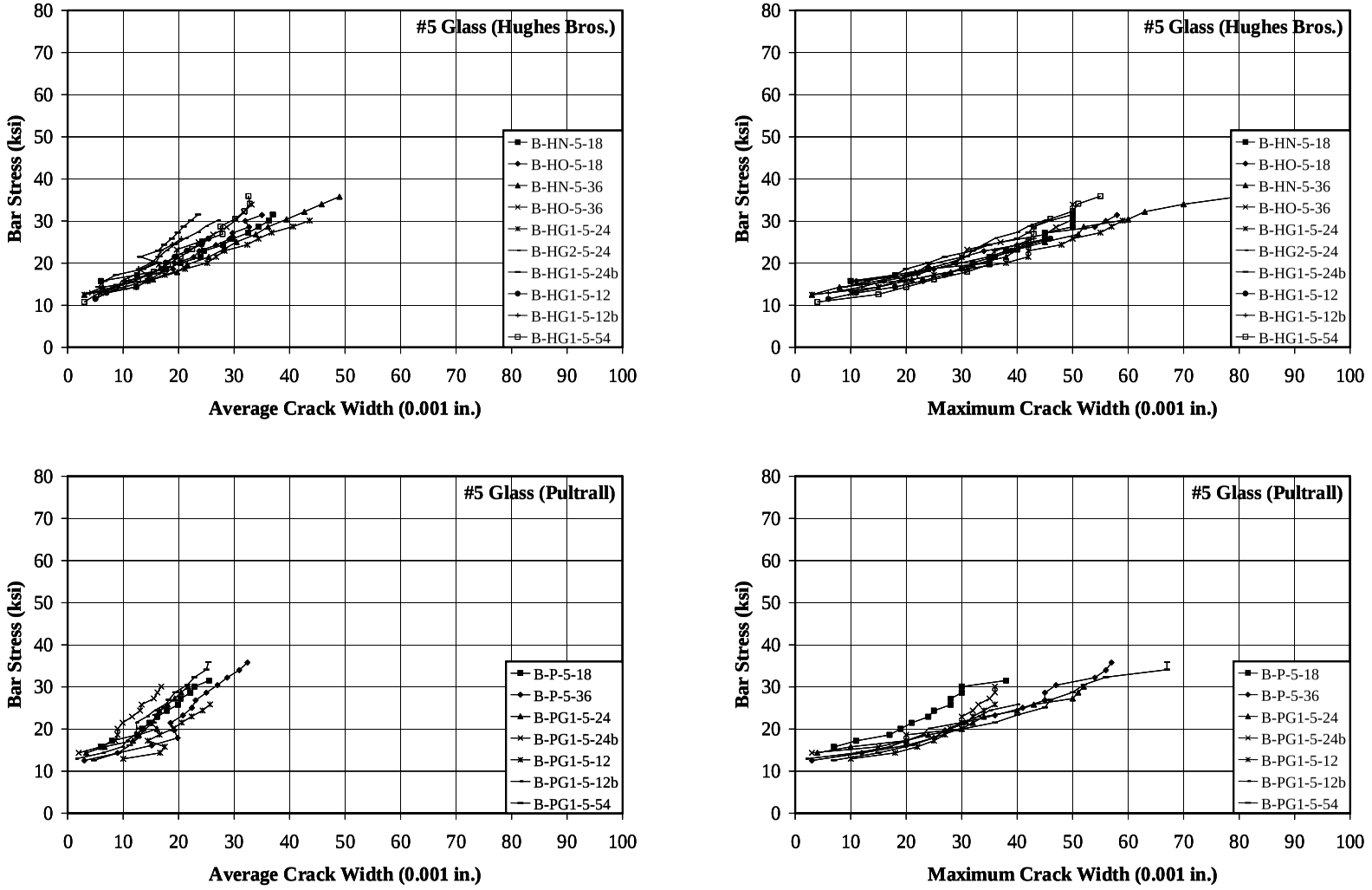

Figure 3.15 Reinforcement Stress versus Crack Widths for Specimens Reinforced with #5 Bars (continued)

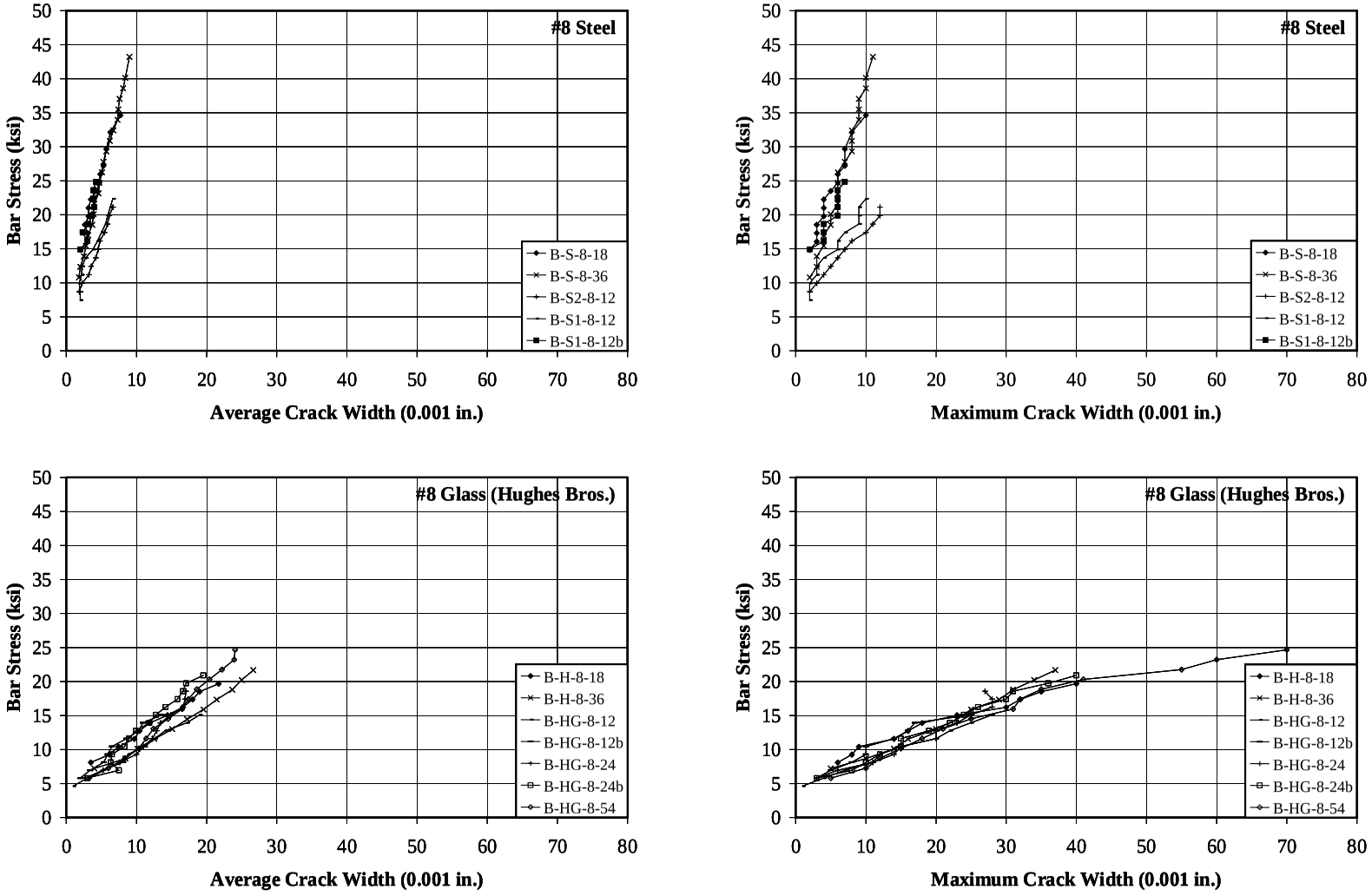

Figure 3.16 Reinforcement Stress versus Crack Widths for Specimens Reinforced with #8 Bars

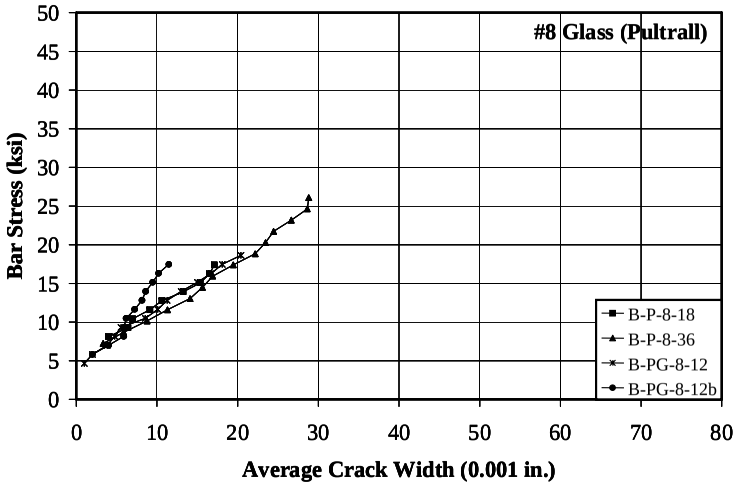

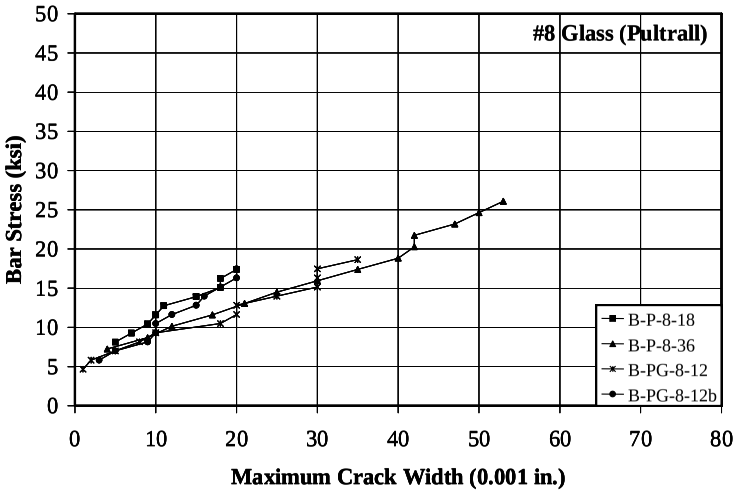

Figure 3.16 Reinforcement Stress versus Crack Widths for Specimens Reinforced with #8 Bars (continued)

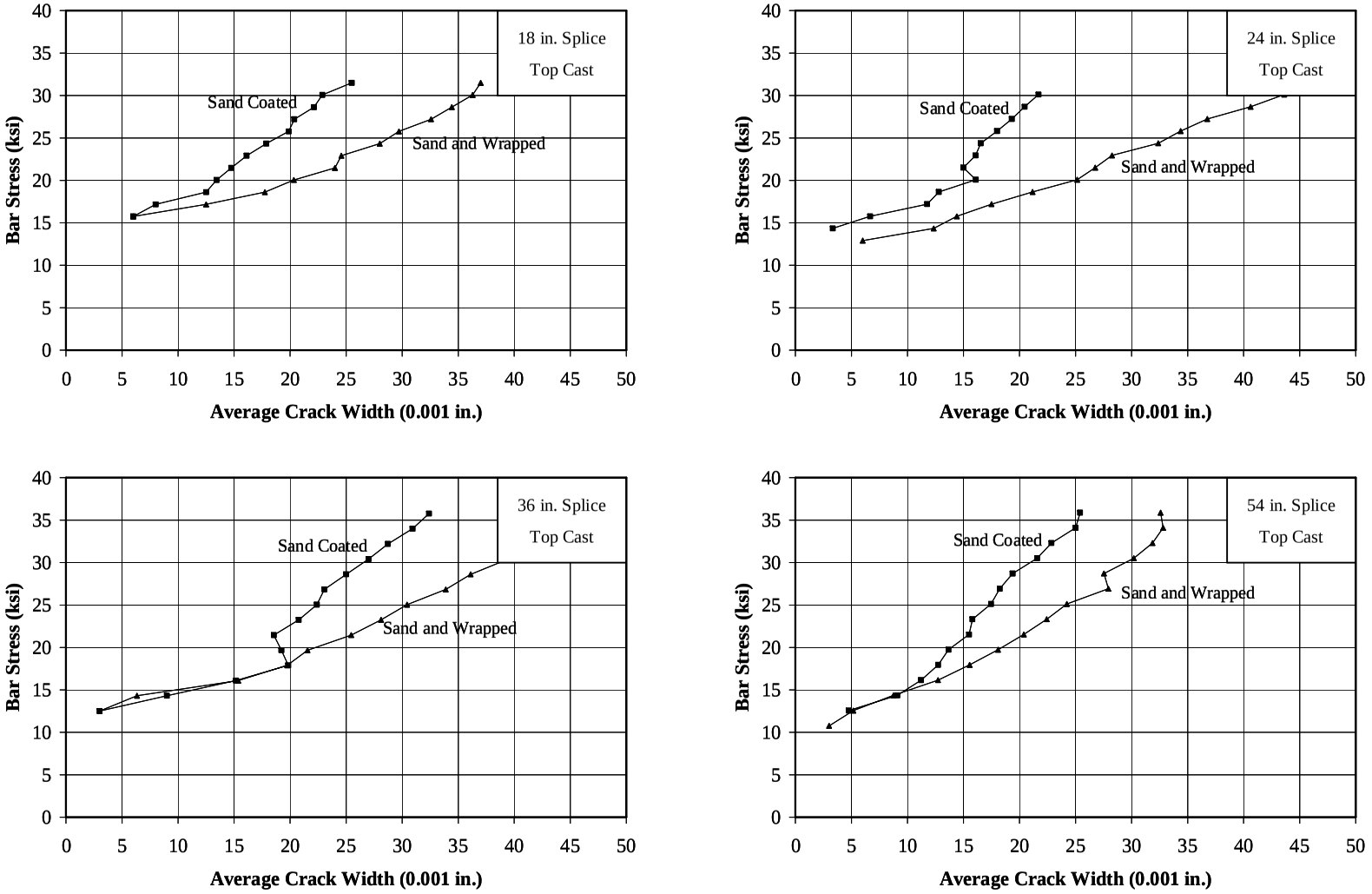

Figure 3.17 Effect of Surface Deformation on Crack Widths, #5 Bars

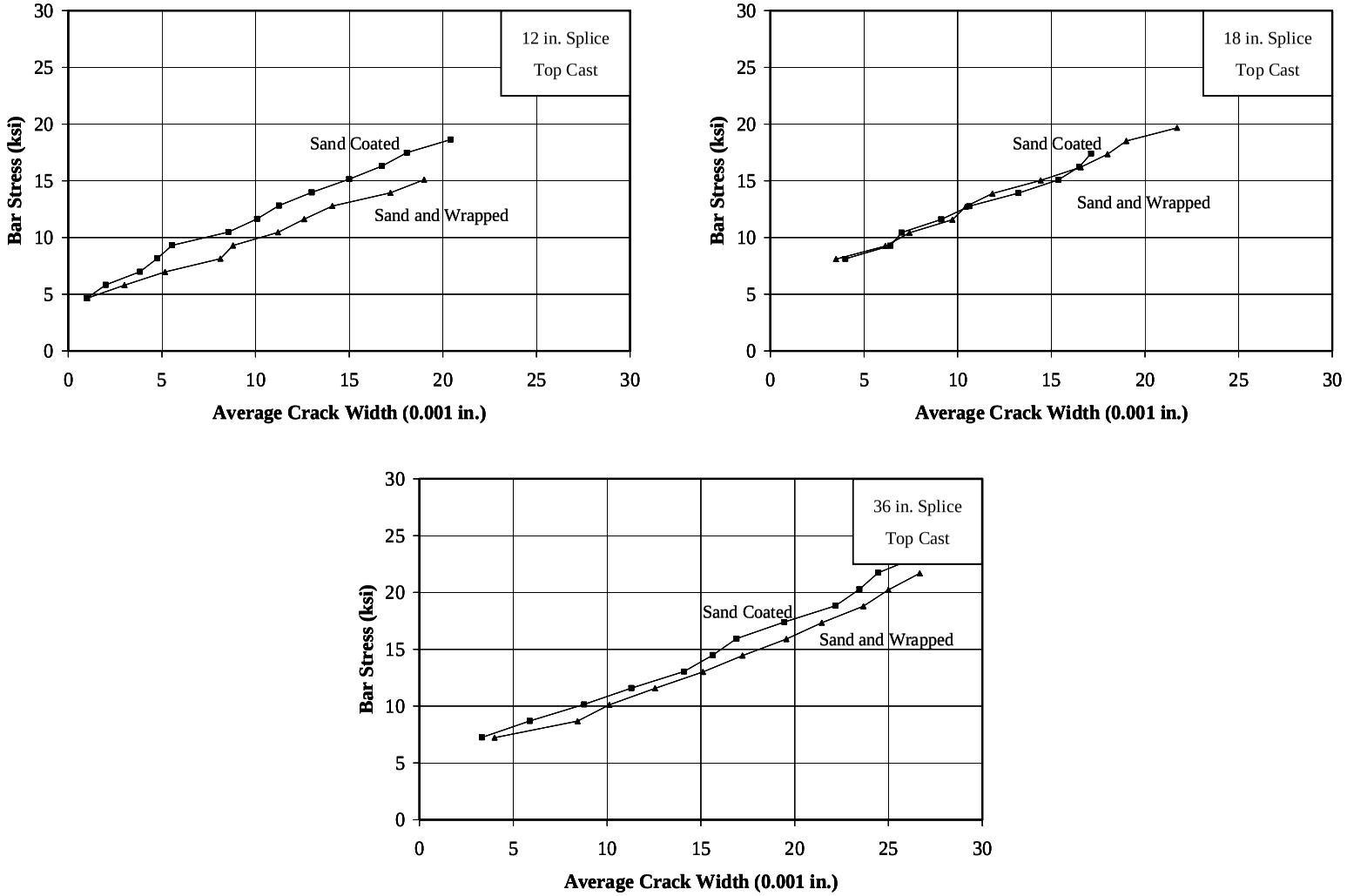

Figure 3.18 Effect of Surface Deformation on Crack Widths, #8 Bars

CHAPTER 4

DATA ANALYSIS AND DISCUSSION

4.1 Introduction

To evaluate the bond strength of the FRP and steel reinforced specimens, the data was analyzed on the basis of current design recommendations. The bond strength of the test specimens that failed in a splitting mode were computed using the ACI 318-05 Building Code Requirements for Structural Concrete, ACI Committee 408 Recommendations, AASHTO LRFD Bridge Design Specifications, and ACI Committee 440 Recommendations. The calculated reinforcement stresses at failure were compared with the experimental results. The test results of the plain reinforced specimens were not evaluated with these expressions because they were derived for specimens reinforced with deformed bars and are not considered applicable.

In addition, the crack width design expression provided by ACI Committee 440 was evaluated. The calculated crack widths are compared with the measured crack widths. The effect of surface deformations on the maximum crack width measurement is also discussed.

4.2 Bond Strength

4.2.1 ACI 318-05 Building Code

The design provisions in ACI 318-05 for development and splices of deformed bars in tension are based on the expression developed by Orangun, Jirsa, and Breen (1975, 1977). Orangun et al. derived the equation which reflects the effect of length, cover, bar diameter, concrete strength, and transverse reinforcement on the strength of anchored bars by performing a nonlinear regression analysis on the test results of 116

beam splice tests. The expression, a measure of an average bond stress over the splice length, is shown in the following equation:

$$\frac{u}{\sqrt{f_c'}} = 1.2 + \frac{3C}{d_b} + \frac{50d_b}{l_d} + \frac{A_{tr}f_{yt}}{500sd_b} \tag{4-1}$$

where:

A_{tr} = *area of transverse reinforcement normal to the plane of splitting through the anchored bars, in.*^{2}

C = *smaller of the clear cover* c_b*, or half the clear spacing* c_s *between the next adjacent bar, in.*

d_b = *diameter of reinforcing bars, in.*

f_c' = *concrete cylinder strength, psi*

f_{yt} = *yield strength of transverse reinforcement, psi*

l_d = *development length, in.*

s = *spacing of transverse reinforcement, in.*

u = *average bond strength, psi*

The expression may be written in terms of force in the bar by replacing the average bond stress u with $A_{bs}f_s/\pi d_b l_d$ and considering that $A_{bs} = \frac{\pi d_b^{\,2}}{4}$

$$\frac{A_{bs}f_s}{\sqrt{f_c'}} = 3\pi l_d(C + 0.4d_b) + 200A_b + \frac{\pi l_d A_{tr}}{500s}f_{yt} \tag{4-2}$$

where:

A_b = *area of developed/spliced bar, in.*^{2}

f_s = *stress in the reinforcing bar, psi*

Solving Equation (4-2) for the ratio of the development length l_d to the diameter of the bar d_b gives:

$$\frac{l_d}{d_b} = \frac{\frac{f_s}{\sqrt{f_c'}} - 200}{12\left(\frac{C + 0.4d_b + K_{tr}}{d_b}\right)} \tag{4-3}$$

where $K_{tr} = \dfrac{A_{tr} f_{yt}}{1500sn}$

The development length equation used in the ACI 318-05 building code is obtained by replacing $c = C+0.4d_b$ with $c = C+0.5d_b$, removing 200 from the numerator, and replacing 1/12 (0.083) with 3/40 (0.075). In Equation (4-3), l_d is the development length required to develop a stress of f_s in the reinforcement. In ACI 318-05, f_s is replaced with the nominal value f_y, which is the specified yield strength of the reinforcing bar. The ACI 318-05 equation is as follows:

$$\frac{\ell_d}{d_b} = \frac{3}{40}\frac{f_y}{\sqrt{f_c'}}\frac{\psi_t \psi_e \psi_s \lambda}{\frac{c_b + K_{tr}}{d_b}} \tag{4-4}$$

where:

A_{tr}= total cross-sectional area of all transverse reinforcement within spacing, s, that crosses the potential plane of splitting through the reinforcement being developed, in.^{2}

c_b = smaller of (a) the distance from center of a bar to nearest concrete surface, and (b) one-half the center-to-center spacing of bars being developed, in.

d_b = nominal diameter of reinforcing bars, in.

f_c' = specified compressive strength of concrete, psi

f_y = specified yield strength of reinforcement, psi

f_{yt} = specified yield strength of transverse reinforcement, psi

K_{tr} = *transverse reinforcement index,* $K_{tr} = \left(A_{tr}\, f_{yt}\right)/\left(1500\, s\, n\right)$

ℓ_d = *development length in tension of deformed bar, in.*

n = number of bars being spliced or developed along the plane of splitting

s = spacing of transverse reinforcement, in.

ψ_t = *reinforcement location factor*

ψ_e = *coating factor*

ψ_s = *reinforcement size factor*

λ = *lightweight aggregate concrete factor*

To limit the probability of a pullout failure, ACI 318-02 requires that the term $(c+K_{tr})/d_b$ not be taken greater than 2.5. The value of $\sqrt{f_c'}$ is limited to a maximum value of 100 psi mainly due to a lack of data on specimens with concrete compressive stress in excess of 10,000 psi.

The modification factors for reinforcement location, coating, reinforcement size, and lightweight aggregate concrete is presented as follows:

ψ_t = reinforcement location factor (1.3 for reinforcement placed so that more than 12 in. of fresh concrete is cast below the development length or splice; 1.0 for other reinforcement)

ψ_e= coating factor (1.5 for epoxy-coated reinforcement with cover less than $3d_b$ or clear spacing less than $6d_b$; 1.2 for other epoxy-coated reinforcement; 1.0 for uncoated reinforcement); with $\psi_t\, \psi_e \leq 1.7$

Ψ_s = reinforcement size factor (0.8 for No. 6 and smaller bars; 1.0 for No. 7 and larger bars

λ = lightweight concrete factor (1.3 for lightweight concrete; 1.0 for normal weight concrete; $6\sqrt{f_c'}\,\big/\, f_{ct} \geq 1.0$ for lightweight concrete with split cylinder strength f_{ct} specified)

The surface deformation and modulus of elasticity of FRP bars are considerably different than that of steel; therefore, it is expected that the bond performance of these materials will be different. Studies have shown that the bond strength of FRP bars is lower than that of steel bars (Tighiouart, Benmokrine, and Mukhopadhyaya (1999), Larralde, Silvia-Rodriquez (1993)). The ACI development length equation was developed from a database including only steel reinforced specimens; therefore, satisfactory bond strength calculations for FRP reinforced specimens should not be expected from this equation. However, the data obtained from the FRP reinforced specimens were analyzed with this equation for comparative purposes.

The ratio of experimental to calculated bar stresses at failure are shown in Figure 4.1 through Figure 4.3. The calculated values presented were obtained by solving Equation (4.4) for the reinforcement stress. The values l_d and c_b were based on the design dimensions and nominal bar diameter. For all specimens in each series, the average concrete compressive strength was used. The calculated stresses were solved by using the modification factors as well as without using the modification factors.

Because ACI 318-05 implements a bar size modification factor in its simplified equation, the modification factor for bar size (Ψ_s*=0.8 for #6 and smaller bars)* specified in ACI 318-05 were used in the calculations for specimens reinforced with #5 bars.

Table 4.1 summarizes the ratio of the experimental to calculated reinforcement stresses obtained by Equation (4.4). The modulus of elasticity of the reinforcing bar (E_{bar}), average concrete compressive strength of concrete (f_c), average splitting tensile strength (f_t), reinforcement stress at the time of failure (f_{test}) are also presented in Table 4.1. M_F represents the product of the various modification factors.

Based on the comparison of the experimental and calculated results, the following observations were made. The development length equation yielded conservative bond strengths for the steel reinforced specimens (Figure 4.1). The ratio of experimental to calculated values ranges from 1.75 to 3.80 when the modification factors (M_F) were included in the calculations. In the case of CFRP reinforced specimens, the equation yielded conservative results for the shorter spliced lengths (Figure 4.2). As the splice length of the specimens increased, the equation resulted with unconservative results even

though the modification factors were used. For GFRP reinforced specimens, the ratio of experimental to calculated values ranges from 0.55 to 2.55. Unconservative results were observed in specimens with 24, 36, and 54 in splices (Figure 4.3). It should be noted that Equation (4-4) yielded unconservative results for Specimen B-HO-5-18 which had an 18 in. splice.

Two apparent trends were observed from analysis of Figure 4.1 through Figure 4.3. The first trend is that as the splice length increases, the ratio of experimental results to calculated values decreases regardless of the reinforcement type indicating that stress achieved in the reinforcement does not vary linearly with the splice length. The other trend is that among the same size bar, the bond strength of steel is higher than that of CFRP bars, followed by GFRP bars.

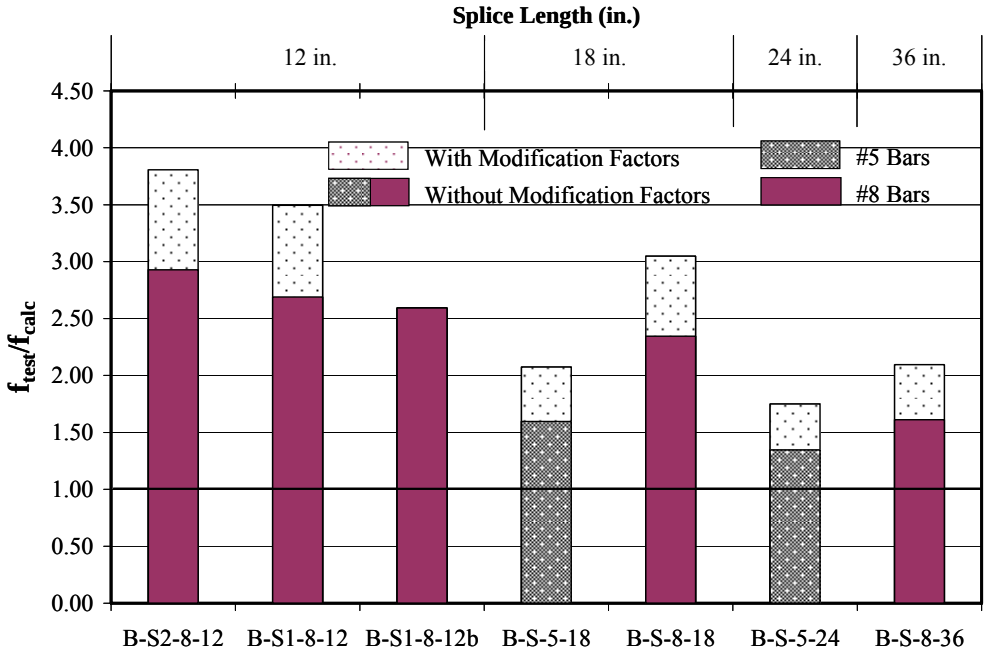

Figure 4.1 Comparison of Strength Calculations of Steel Reinforcement by ACI 318-05 (Equation (4-4))

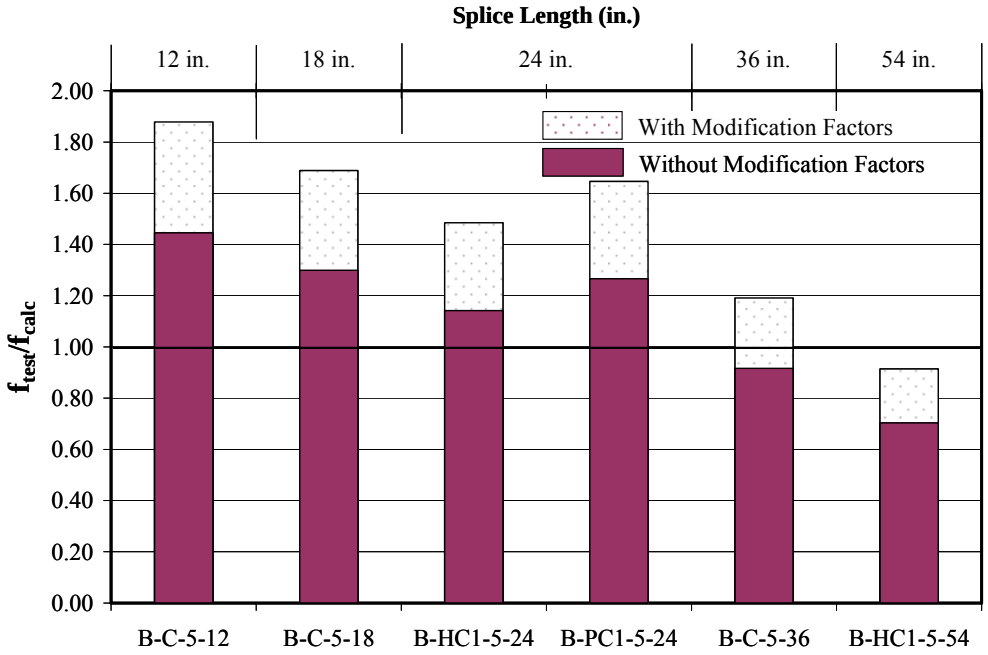

Figure 4.2 Comparison of Strength Calculations of CFRP Reinforcement by ACI 318-05 (Equation (4-4))

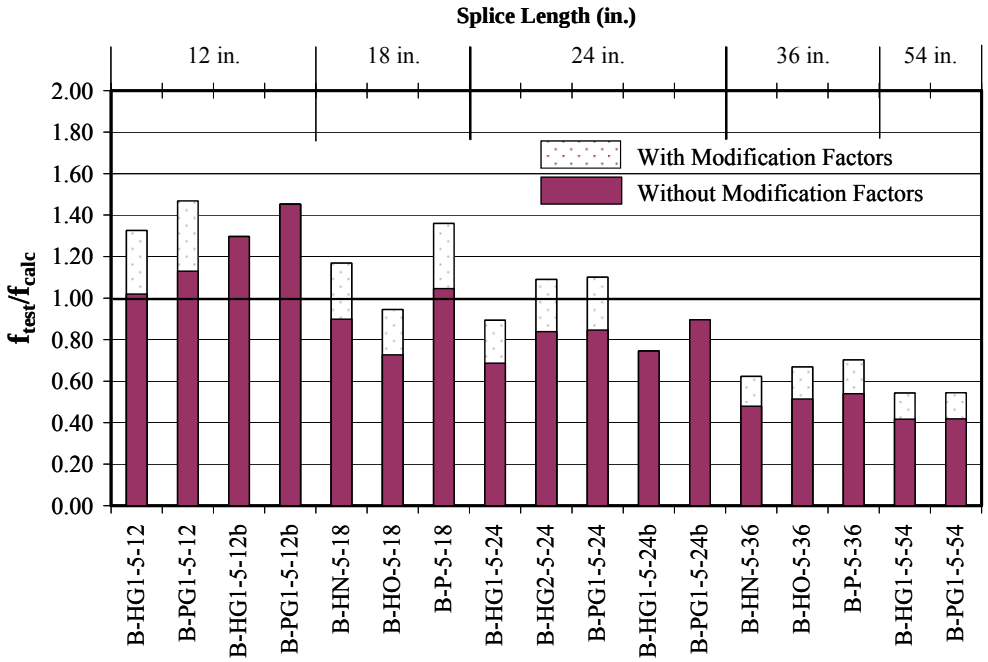

#5 Glass FRP Bars

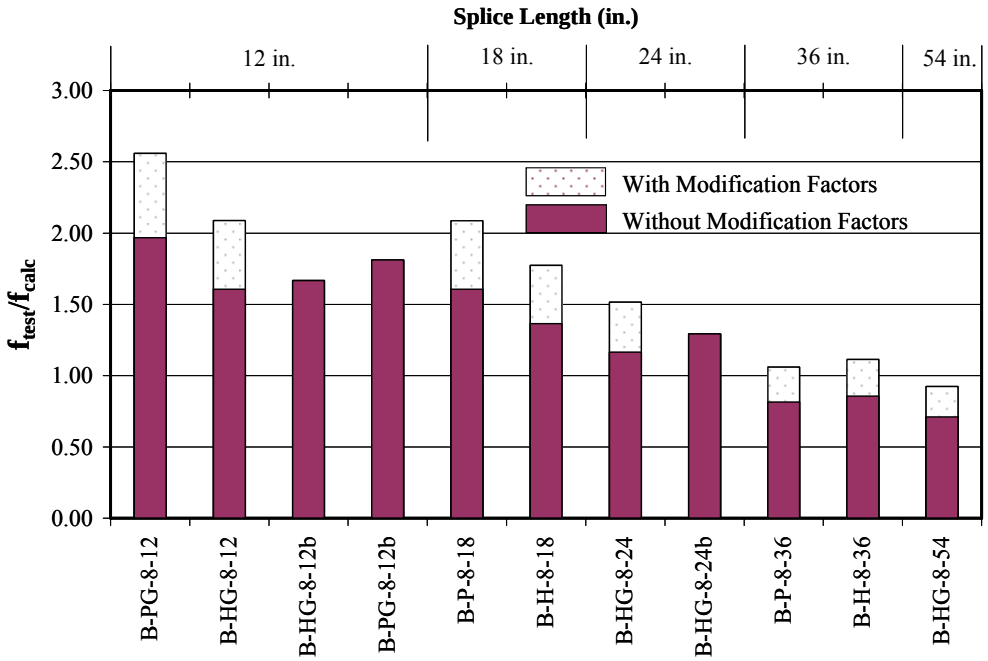

#8 Glass FRP Bars

Figure 4.3 Comparison of Strength Calculations of GFRP Reinforcement by ACI 318-05 (Equation (4-4))

The ACI 318-05 equation consistently produces conservative results for steel reinforced concrete members; however, the level of conservatism varies with the splice length. Because the equation was derived by a regression analysis with a limited amount of data, it is important to note that the equation may not reflect actual bond behavior. Furthermore, the equation was obtained from data which contained only steel reinforced specimens; therefore, it was not intended and does not account for FRP reinforced specimens. From this analysis, it was found that the ACI design equation is not suitable for the development length calculation of FRP reinforced specimens.

Table 4.1 Comparison of Experimental to Calculated Strength Ratios (ACI 318-05 and ACI 408R-03)									
Series	**Specimen**	**E_{bar} (ksi)**	**f_c (psi)**	**f_t (psi)**	**f_{test} (ksi)**	**ACI 318-05 (Eq. (4-4))**		**ACI 408R-03 (Eq. (4-5))**	
						w/o M_F	***with M_F***	***w/o M_F***	***with M_F***
						$\frac{f_{test}}{f_{calc}}$	$\frac{f_{test}}{f_{calc}}$	$\frac{f_{test}}{f_{calc}}$	$\frac{f_{test}}{f_{calc}}$
I	B-S-8-18	28400	5260	544	40.8	2.34	3.05	1.15	1.28
	B-P-8-18	6200	5260	544	27.9	1.61	2.09	0.79	0.87
	B-H-8-18	5700	5260	544	23.7	1.36	1.77	0.67	0.74
	B-HN-5-18	6400	5260	544	40.7	0.90	1.17	0.77	0.90
	B-HO-5-18	5800	5260	544	32.9	0.73	0.95	0.62	0.73
	B-P-5-18	6401	5260	544	47.3	1.05	1.36	0.90	1.04
	B-S-5-18	27350	5260	544	72.2	1.60	2.07	1.37	1.59
	B-C-5-18	18500	5260	544	58.8	1.30	1.69	1.11	1.30
II	B-C-5-12	18500	5470	555	44.5	1.45	1.88	1.05	1.19
	B-S-8-36	28400	5470	555	57.2	1.61	2.10	1.13	1.31
	B-P-8-36	6200	5470	555	28.9	0.81	1.06	0.57	0.66
	B-H-8-36	5700	5470	555	30.4	0.86	1.11	0.60	0.70
	B-HN-5-36	6400	5470	555	44.3	0.48	0.62	0.52	0.63
	B-HO-5-36	5800	5470	555	47.5	0.51	0.67	0.55	0.67
	B-P-5-36	6401	5470	555	49.9	0.54	0.70	0.58	0.71
	B-C-5-36	18500	5470	555	84.6	0.92	1.19	0.99	1.20
III	B-S2-8-12	27200	4010	475	29.7	2.93	3.81	1.04	1.13
	B-S1-8-12	27200	4010	475	27.3	2.69	3.50	0.96	1.04
	B-S4-8-12	29600	4010	475	20.0	Pullout Failure (Plain Bar)			
	B-S3-8-12	30500	4010	475	8.8	Pullout Failure (Plain Bar)			
	B-PG-8-12	6200	4010	475	20.0	1.97	2.56	0.70	0.76
	B-HG-8-12	5700	4010	475	16.3	1.61	2.09	0.57	0.62
	B-S1-8-12b	27200	4010	475	26.3	2.59	2.59	0.92	0.92

Table 4.1 continued

Series	Specimen	E_{bar} (ksi)	f_c (psi)	f_t (psi)	f_{test} (ksi)	ACI 318-05 (Eq. (4-4))		ACI 408R-03 (Eq. (4-5))	
						w/o M_F	*with* M_F	*w/o* M_F	*with* M_F
						$\frac{f_{test}}{f_{calc}}$	$\frac{f_{test}}{f_{calc}}$	$\frac{f_{test}}{f_{calc}}$	$\frac{f_{test}}{f_{calc}}$
III	B-HG-8-12b	5700	4010	475	16.9	1.67	1.67	0.59	0.59
	B-PG-8-12b	6200	4010	475	18.4	1.81	1.81	0.65	0.65
	B-S-5-24	27350	4010	475	70.9	1.35	1.75	1.20	1.42
IV	B-HC1-5-24	18500	4640	511	64.7	1.14	1.48	1.05	1.25
	B-PC2-5-24	22500	4640	511	15.1	Pullout Failure (Plain Bar)			
	B-PC1-5-24	21700	4640	511	71.8	1.27	1.65	1.17	1.38
	B-HG3-5-24	7000	4640	511	16.1	Pullout Failure (Plain Bar)			
	B-HG1-5-24	6400	4640	511	39.0	0.69	0.89	0.63	0.75
	B-HG2-5-24	7300	4640	511	47.6	0.84	1.09	0.77	0.92
	B-PG2-5-24	6500	4640	511	12.3	Pullout Failure (Plain Bar)			
	B-PG1-5-24	6401	4640	511	48.0	0.85	1.10	0.78	0.92
	B-HG1-5-24b	6400	4640	511	42.2	0.74	0.74	0.69	0.69
	B-PG1-5-24b	6401	4640	511	50.8	0.90	0.90	0.83	0.83
V	B-HG1-5-12	6400	4170	485	27.4	1.02	1.33	0.69	0.78
	B-PG1-5-12	6401	4170	485	30.4	1.13	1.47	0.77	0.87
	B-HG-8-24	5700	4170	485	24.1	1.17	1.52	0.63	0.71
	B-HG1-5-12b	6400	4170	485	34.8	1.30	1.30	0.88	0.88
	B-PG1-5-12b	6401	4170	485	39.0	1.45	1.45	0.98	0.98
	B-HG-8-24b	5700	4170	485	26.7	1.29	1.29	0.70	0.70
	B-HG-8-54	5700	4170	485	33.0	0.71	0.92	0.54	0.64
	B-HG1-5-54	6400	4170	485	50.4	0.42	0.54	0.46	0.56
	B-PG1-5-54	6401	4170	485	50.6	0.42	0.54	0.46	0.57
	B-HC1-5-54	18500	4170	485	85.0	0.70	0.91	0.77	0.95

4.2.2 ACI Committee 408

The ACI Committee 408 (ACI 408R-03) recommendation for splice and development length criteria is based on the work by Zuo and Darwin (1998, 2000). Zuo and Darwin (1998, 2000) expanded the work of Darwin, Zuo, Tholen, and Idun (1996) by increasing the number of specimens in the database being evaluated. Zuo and Darwin's equation is based on 171 unconfined and 196 confined splice tests reinforced with deformed steel bars. All bars were bottom cast and the database included specimens having high strength concrete ($f_c' > 8000$ psi).

The Orangun, Jirsa, and Breen (1975, 1977) study provided the basis for Zuo and Darwin (1998, 2000). Zuo and Darwin (1998, 2000) incorporated the effect of the ratio of c_{max}/c_{min}, relative rib area, and, the fourth root of the concrete compressive strength, $\sqrt[4]{f_c'}$, to the Orangun et al. (1975, 1977) equation. Darwin et al. (1996) and Zuo and Darin (1998, 2000) concluded that for unconfined splice tests, $\sqrt[4]{f_c'}$ provides a better representation than the traditional $\sqrt{f_c'}$ for the contribution of concrete strength to bond strength. Canbay and Frosch (2005) also observed the same phenomenon in their study.

An ACI Committee 408 recommendation has updated the Zuo and Darwin (1998, 2000) equation by using ACI 408 Database 10-2001 (ACI 408R-03). The recommendation includes ϕ factors to ensure a realistically low probability of failure for two different load factor combinations (1.2D + 1.6L and 1.4D + 1.7L). A ϕ factor of 0.82 is recommended for the load factors included in Chapter 9 of ACI 318-05 (1.2D + 1.6L) while 0.92 is recommended for the load factors included in Appendix C of ACI 318-05 (1.4D + 1.7L). The recommended equation including $\phi = 0.92$ is as follows:

$$\frac{\ell_d}{d_b} = \frac{\left(\frac{f_y}{\sqrt[4]{f_c'}} - 2200\,\omega\right)\alpha\,\beta\,\lambda}{70\left(\frac{c\,\omega + K_{tr}}{d_b}\right)} \qquad (4\text{-}5)$$

where:

$$c = c_{min} + 0.5\, d_b$$

$$\omega = 0.1\frac{c_{max}}{c_{min}} + 0.9 \quad \leq \quad 1.25$$

$$K_{tr} = \left(\frac{0.52\, t_r\, t_d\, A_{tr}}{s\, n}\right)\sqrt{f_c'}$$

$$t_r = 9.6\, R_r + 0.28 \quad \leq \quad 1.72$$

$$t_d = 0.78\, d_b + 0.22$$

where:

A_{tr}= total cross-sectional area of all transverse reinforcement within spacing, s that crosses the potential plane of splitting through the reinforcement being developed, in.^{2}

c_b = bottom cover, in.

c_{min}, c_{max} = minimum or maximum value of c_s or c_b, in.

c_s = min(c_{si} + 0.25, c_{so})

c_{si} = half of the clear spacing between bars, in.

c_{so} = clear side cover of reinforcing bars, in.

d_b = nominal diameter of reinforcing bars, in.

f_c' = specified compressive strength of concrete, psi

f_y = specified yield strength of reinforcement, psi

f_{yt} = specified yield strength of transverse reinforcement, psi

ℓ_d = development length in tension of deformed bar, in.

R_r = relative rib area of the reinforcement (for conventional reinforcement, an average R_r value of 0.0727 can be used)

t_d = term representing the effect of bar size on the steel contribution to total bond force

t_r = term representing the effect of relative rib area on the steel contribution to total bond force

α = reinforcement location factor (1.3 for reinforcement placed so that more than 12 in. of fresh concrete is cast below the development length or splice; 1.0 for other reinforcement)

β= coating factor (1.5 for epoxy-coated reinforcement with cover less than $3d_b$ or clear spacing less than $6d_b$; 1.2 for other epoxy-coated reinforcement; 1.0 for uncoated reinforcement); with $\alpha\,\beta \leq 1.7$

λ = lightweight concrete factor (1.3 for lightweight concrete; 1.0 for normal weight concrete; $6\sqrt{f_c'}\,/\,f_{ct} \geq 1.0$ for lightweight concrete with split cylinder strength, f_{ct}, specified)

The equation which incorporates a ϕ factor of 0.82 is not evaluated in this section because it yields more conservative results that those of Equation (4-5) (ϕ = 0.92). Furthermore, the development length equation in ACI-318-05 was not modified when the load factor combinations in Chapter 9 of ACI 318-05 were changed from 1.4D + 1.7L to 1.2D + 1.6L; therefore, the results obtained from Equation (4-5) can be compared directly with the results obtained from the ACI 318-05 development length equation (Equation (4-4)).

Comparison of the experimental results to calculated values for each type of reinforcement are illustrated in Figure 4.4 through Figure 4.6. Experimental results and the ratio of the experimental to calculated bond strengths are tabulated in Table 4.1. As shown in Figure 4.4, Equation (4-5) performs reasonably well for specimens with steel reinforcement The calculated bond strengths according to Equation (4-5) is conservative for underestimates the experimental results except for Specimens B-S1-8-12 and B-S1-8-12b if the modification factors are not included in the analysis. However, if the modification factors are included, Equation (4.5) only overestimates the experimental result of Specimen B-S1-8-12b. The equation also provides results which are more consistent than the ACI-318-05 equation.

As shown in Figure 4.5, the equation underestimates the bond strength of CFRP bars and is within 20% of the experimental results for the shorter splice lengths yielding

conservative results. However, as the splice length increased, the equation was unconservative for the CFRP. In the case of GFRP reinforced specimens, Equation (4-5) provided unconservative results for essentially all specimens. As shown in Figure 4.6, the ratio of the experimental to calculated bond strength ranges from 0.5 to 0.95 for the glass FRP reinforcement.

Overall, Equation (4-5) compares reasonably well with experimental data obtained from steel specimens. The level of conservatism of Equation (4-5) for steel specimens is within 20% of the experimental results and is more consistent than Equation (4-4) (ACI 318-05). Because Equation (4-5) was derived from a database including only steel reinforced specimens, however, the equation is insensitive to the type of reinforcement and should not be used to evaluate FRP reinforced specimens in its current form.

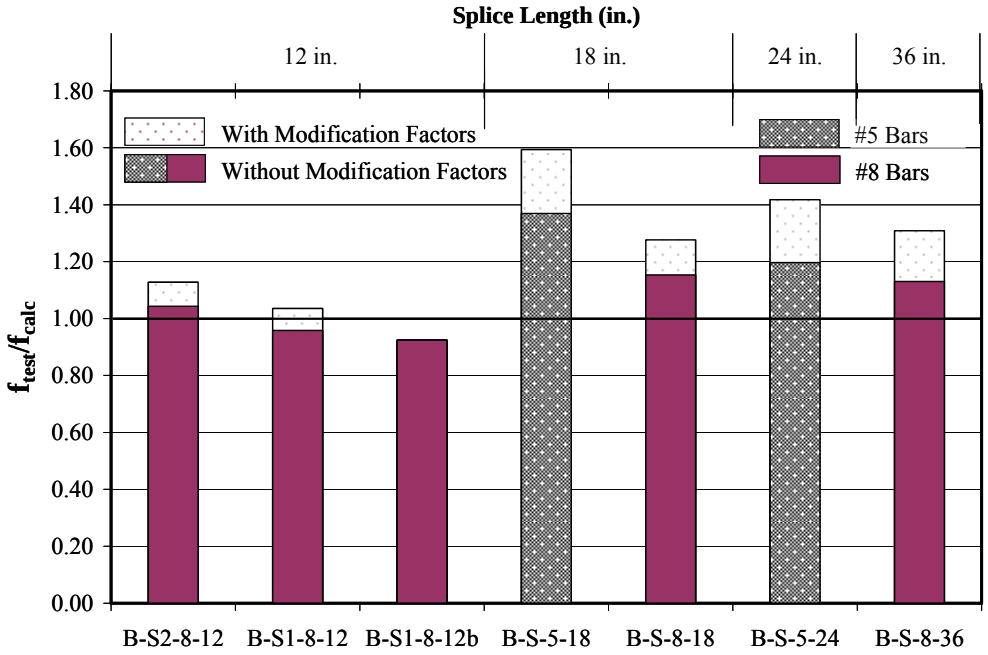

Figure 4.4 Comparison of Strength Calculations of Steel Reinforcement by ACI 408-03 (Equation (4-5))

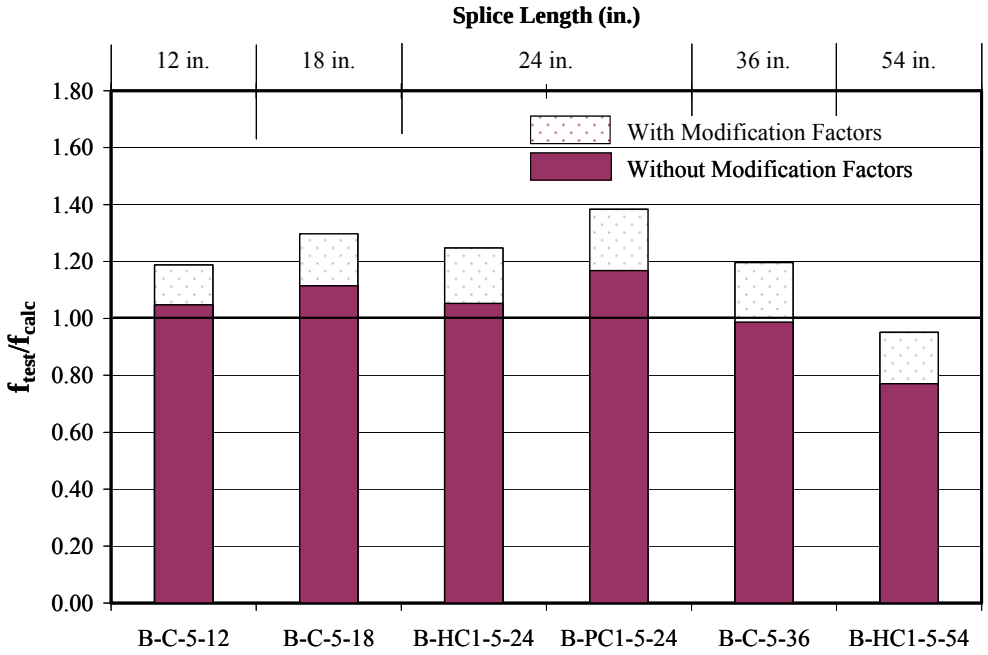

Figure 4.5 Comparison of Strength Calculations of CFRP Reinforcement by ACI 408-03 (Equation (4-5))

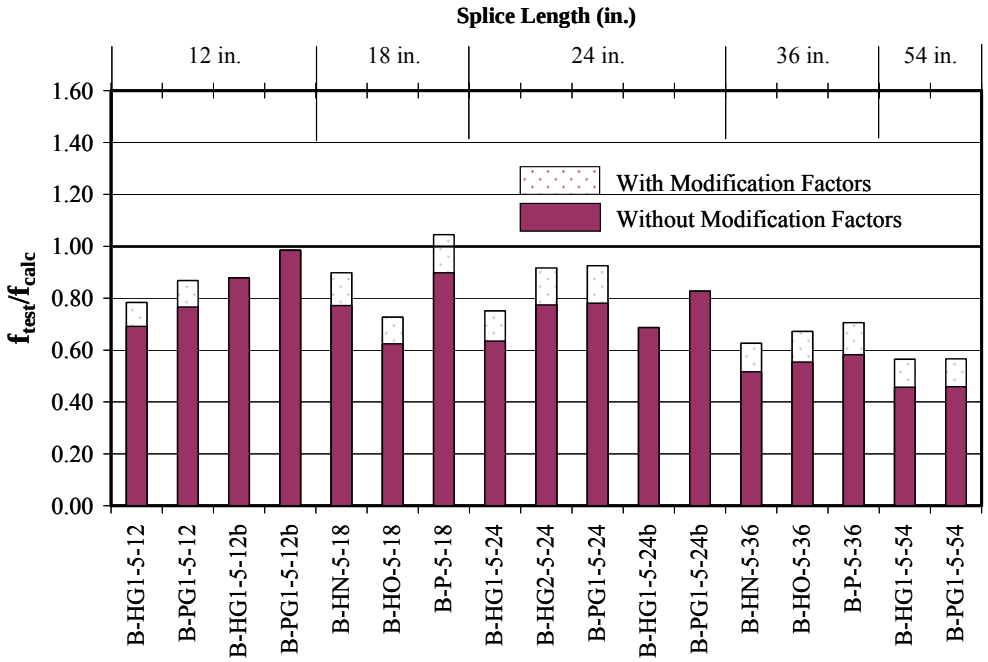

#5 Glass FRP Bars

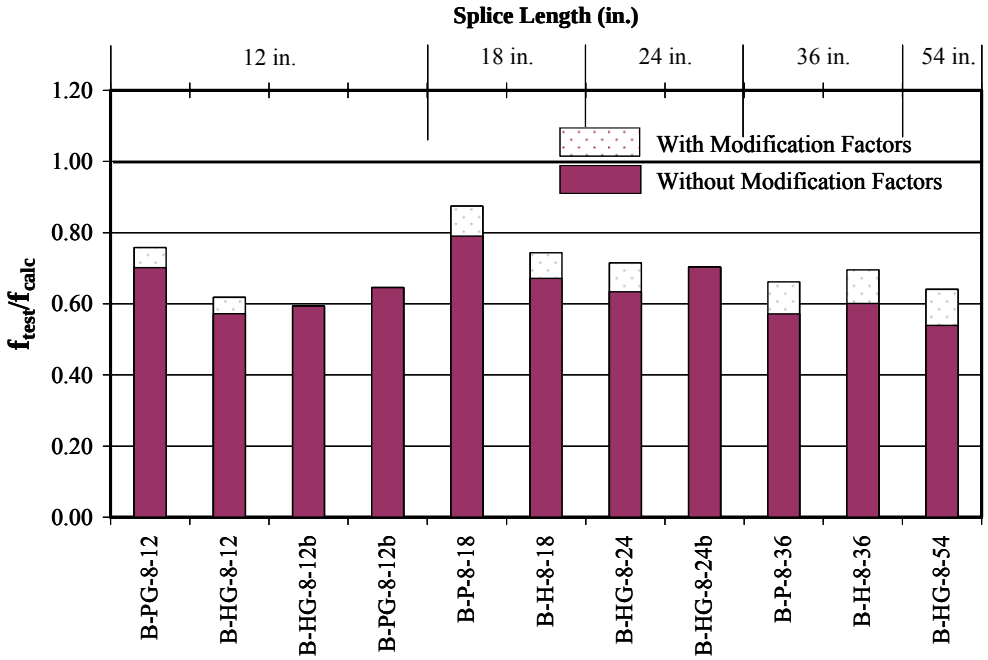

#8 Glass FRP Bars

Figure 4.6 Comparison of Strength Calculations of GFRP Reinforcement by ACI 408-03 (Equation (4-5))

4.2.3 ACI Committee 440

ACI Committee 440 (ACI 440.1R-03) has published a guideline for the design and construction of concrete members reinforced with FRP bars. The basic development length proposed by the committee is given by:

$$l_{bf} = K_2 \frac{d_b^{\,2} f_{fu}}{\sqrt{f_c'}} \tag{4-6}$$

where:

d_b=*diameter of reinforcing bar, in.*

f_c' = *specified compressive strength of concrete, psi*

f_{fu}=*design tensile strength of FRP, considering reductions for service environment, psi* ($f_{fu}=C_E f_{fu}^*$)

f_{fu}^* = *guaranteed tensile strength of an FRP bar, defined as the mean tensile strength of a sample of test specimens minus three times the standard deviation* ($f_{fu}^* = f_{fu,ave} - 3\sigma$), *psi*

C_E = *environmental reduction factor for various fiber type and exposure conditions*

K_2= *constant determined from experimental results*

l_{bf} = *basic development length of an FRP bar, in.*

To prevent splitting of concrete, ACI Committee 440 suggests modification factors to the basic development length computed by Equation (4-6). Two types of modification factors are provided, namely, a bar location modification factor and a concrete cover modification factor. A modification factor of 1.3 is recommended for specimens with top cast FRP bars. The concrete cover modification factor is as follows:

$$k_m = \begin{cases} 1.0 \text{ if } c > 2d_b \\ \dfrac{4d_b - c}{2d_b} \text{ if } d_b \le c \le 2d_b \end{cases}$$

The calculated development length is a function of the bar diameter, concrete strength, stress developed in the reinforcement, and a constant K_2. ACI Committee 440

has not specifically assigned a value to K_2, but the values obtained by several researchers are reported in the document (ACI 440.1R-03). The K_2 factors presented in the document, the test method, and reinforcement types are shown in Table 4.2.

Table 4.2 Documented K_2 factors for Equation (4-6)

Researcher(s)	$1/K_2$	Type of Test	Material
Pleimann (1987,1991)	19.4	Pullout	GFRP
Pleimann (1987,1991)	18.0	Pullout	AFRP
Faza and GangaRao (1990)	16.7	Beam-end	GFRP
Ehsani, Saadatmanesh, and Tao (1996a)	21.3	Beam-end Pullout	GFRP
Tighiouart, Benmokrane, and Gao (1998)	15.6	Beam Anchorage	GFRP

To evaluate the efficiency of the proposed equation in estimating bond strength, $1/K_2$ values were obtained for each specimen by solving Equation (4-6) for the $1/K_2$ factor by substituting development length, reinforcement stress at failure, bar diameter, and concrete strength. The $1/K_2$ factors were calculated for the specimens tested in the experimental program to compare the results with the $1/K_2$ factors proposed by several researchers. The calculated $1/K_2$ values for the specimens reinforced with bars having surface deformations are presented in Figure 4.7 through Figure 4.9. The values were calculated with and without using modification factors, and the results are presented in Table 4.3.

It should be noted that as the value of $1/K_2$ increases, the development length required to achieve a desired reinforcement stress decreases. In other words, for specimens with the same splice length, a bar with higher $1/K_2$ values reaches higher reinforcement stresses at failure. The $1/K_2$ values provided in ACI 440 (ACI 440.1R-03) were calculated without using the modification factors; therefore, the discussions in the following paragraphs are based on evaluation of the equation without using the modification factors as the use of modification factors during evaluation yields unconservative results.

As illustrated in Figure 4.7 through Figure 4.9, the $1/K_2$ factors range from approximately 18 to 39 for steel, 9 to 20 for CFRP bars, 6 to 20 for #5 GFRP bars, and 9

to 25 for #8 GFRP bars. This indicates that the K_2 factor does not have a constant value for each reinforcement type considering the current form of Equation (4-6). The scatter in the calculated values can be observed from the graphs. It is also observed that the equation generally produces lower $1/K_2$ values as the splice length increases for all of the specimens considered in the study.

Although ACI Committee 440 has not assigned a value to K_2, the lowest $1/K_2$ value ($1/K_2 = 15.6$) reported in the ACI 440 document (ACI 440.1R-03) was used to evaluate the performance of Equation (4-6) as it should provide conservative estimates. Equation (4-6) resulted in $1/K_2$ values lower than 15.6 for most of the specimens reinforced with FRP reinforcement yielding unconservative results. The level of unconservatism increases with the increasing splice length. Even with the use of modification factors, the $1/K_2$ values obtained from 24 in. and higher spliced #5 GFRP bars are lower than the lowest provided by ACI 440, 15.6.

Based on this analysis, it was concluded that K_2 is not constant. Significant variation in K_2 is evident with varying splice length and reinforcement type. Therefore, the use of Equation (4-6) in its current form is not suitable for the evaluation of specimens with spliced reinforcement.

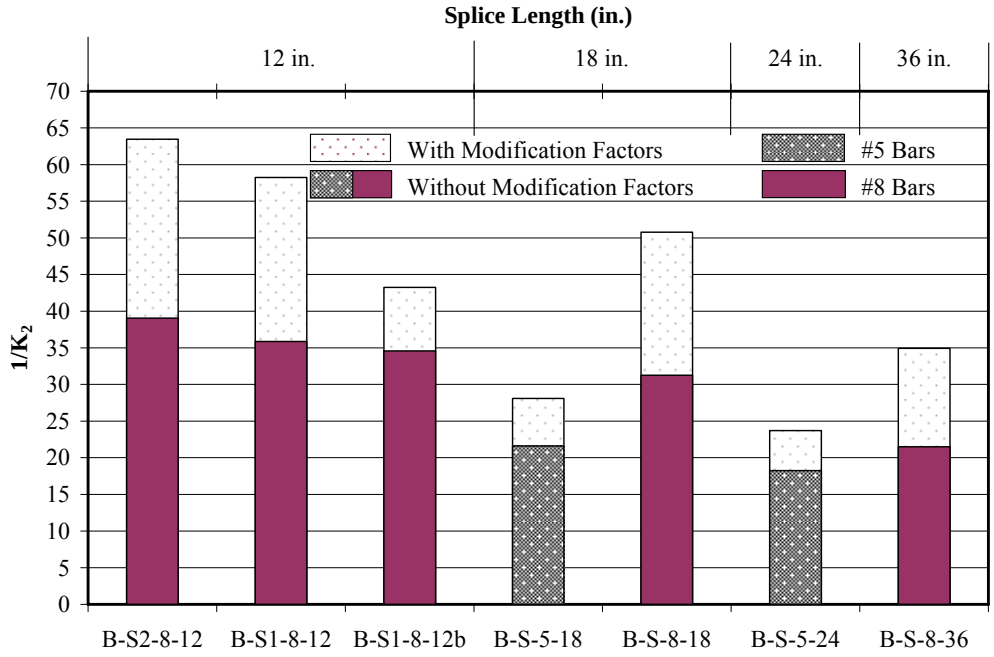

Figure 4.7 Comparison of Strength Calculations of Steel Reinforcement by ACI 440.1R-03 (Equation (4-6))

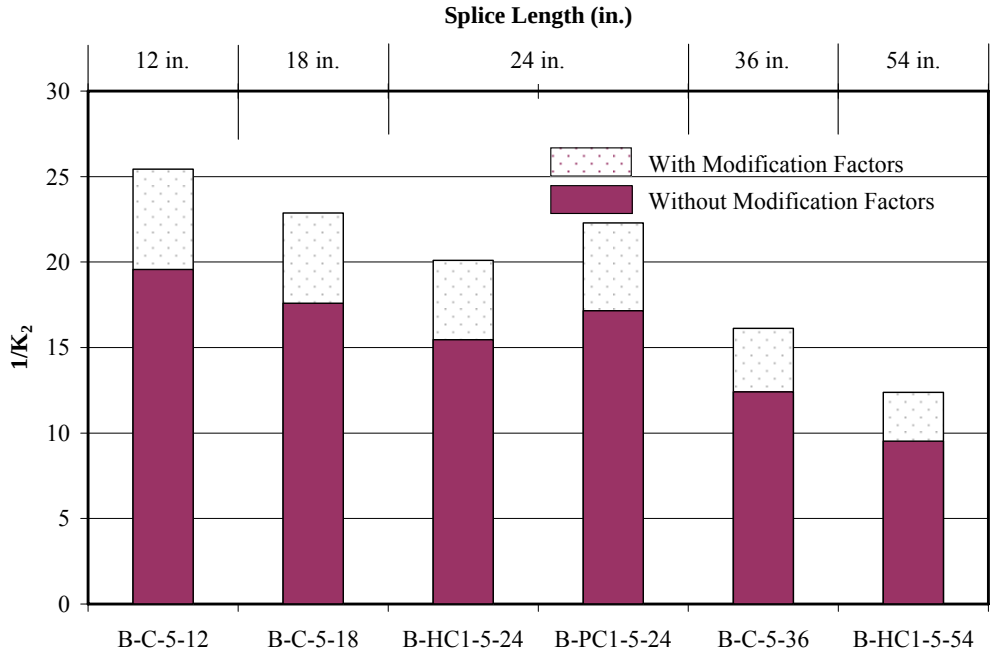

Figure 4.8 Comparison of Strength Calculations of CFRP Reinforcement by ACI 440.1R-03 (Equation (4-6))

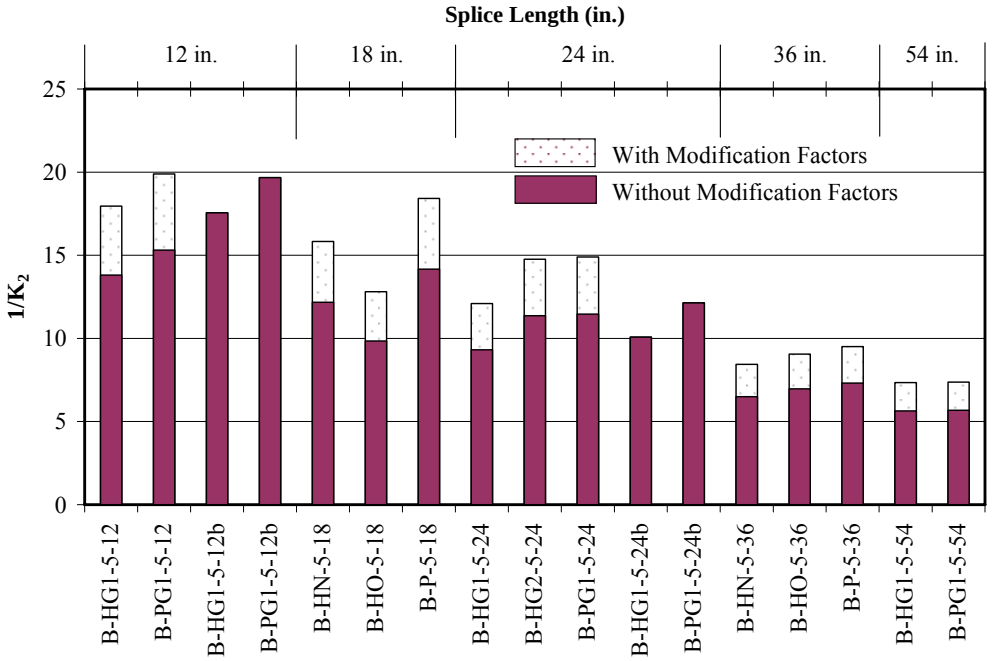

#5 Glass FRP Bars

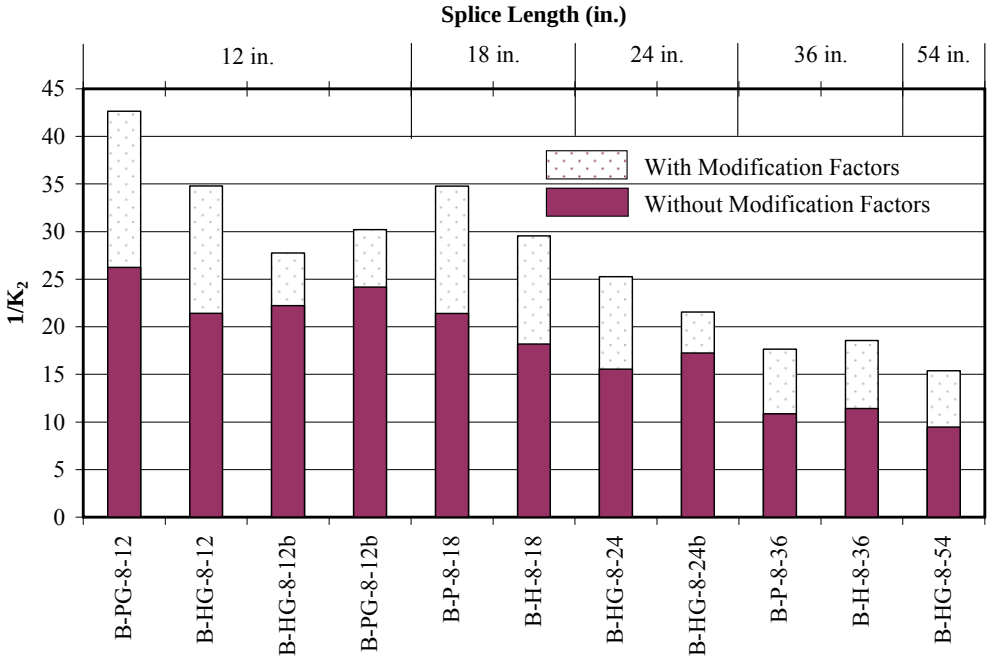

#8 Glass FRP Bars

Figure 4.9 Comparison of Strength Calculations of GFRP Reinforcement by ACI 440.1R-03 (Equation (4-6))

Table 4.3 Comparison of Experimental to Calculated Strength Ratios (ACI 440.1R-03 and ACI 440.1R-XX)											
Series	**Specimen**	**E_{bar} (ksi)**	**f_c (psi)**	**f_t (psi)**	**f_{test} (ksi)**	**440.1R-03 (Eq 4-6)**		**440.1R-03 (Eq 4-7)**		**440.1R-05 (Eq 4-9)**	
						w/o M_F	***with M_F***	***w/o M_F***	***with M_F***	***w/o M_F***	***with M_F***
						$\frac{1}{K_2}$	$\frac{1}{K_2}$	$\frac{f_{test}}{f_{calc}}$	$\frac{f_{test}}{f_{calc}}$	$\frac{f_{test}}{f_{calc}}$	$\frac{f_{test}}{f_{calc}}$
I	B-S-8-18	28400	5260	544	40.8	31.3	50.8	0.84	1.36	0.93	1.40
	B-P-8-18	6200	5260	544	27.9	21.4	34.8	0.57	0.93	0.64	0.96
	B-H-8-18	5700	5260	544	23.7	18.2	29.6	0.49	0.79	0.54	0.81
	B-HN-5-18	6400	5260	544	40.7	12.2	15.8	0.52	0.68	0.73	1.09
	B-HO-5-18	5800	5260	544	32.9	9.8	12.8	0.42	0.55	0.59	0.88
	B-P-5-18	6401	5260	544	47.3	14.2	18.4	0.61	0.79	0.85	1.27
	B-S-5-18	27350	5260	544	72.2	21.6	28.1	0.93	1.21	1.29	1.94
	B-C-5-18	18500	5260	544	58.8	17.6	22.9	0.76	0.98	1.05	1.58
II	B-C-5-12	18500	5470	555	44.5	19.6	25.4	0.86	1.12	0.96	1.44
	B-S-8-36	28400	5470	555	57.2	21.5	34.9	0.59	0.96	0.89	1.34
	B-P-8-36	6200	5470	555	28.9	10.9	17.7	0.30	0.48	0.45	0.68
	B-H-8-36	5700	5470	555	30.4	11.4	18.6	0.31	0.51	0.47	0.71
	B-HN-5-36	6400	5470	555	44.3	6.5	8.4	0.28	0.37	0.50	0.75
	B-HO-5-36	5800	5470	555	47.5	7.0	9.1	0.31	0.40	0.54	0.80
	B-P-5-36	6401	5470	555	49.9	7.3	9.5	0.32	0.42	0.56	0.84
	B-C-5-36	18500	5470	555	84.6	12.4	16.1	0.54	0.71	0.95	1.43
III	B-S2-8-12	27200	4010	475	29.7	39.1	63.5	0.92	1.49	0.91	1.36
	B-S1-8-12	27200	4010	475	27.3	35.9	58.3	0.84	1.37	0.84	1.25
	B-S4-8-12	29600	4010	475	20.0	Pullout Failure (Plain Bar)					
	B-S3-8-12	30500	4010	475	8.8	Pullout Failure (Plain Bar)					
	B-PG-8-12	6200	4010	475	20.0	26.2	42.7	0.62	1.00	0.61	0.92
	B-HG-8-12	5700	4010	475	16.3	21.4	34.8	0.50	0.82	0.50	0.75
	B-S1-8-12b	27200	4010	475	26.3	34.6	43.2	0.81	1.01	0.81	0.81

Table 4.3 continued

Series	Specimen	E_{bar} (ksi)	f_c (psi)	f_t (psi)	f_{test} (ksi)	440.1R-03 (Eq 4-6)		440.1R-03 (Eq 4-7)		440.1R-05 (Eq 4-9)	
						w/o M_F	*with* M_F	*w/o* M_F	*with* M_F	*w/o* M_F	*with* M_F
						$\frac{1}{K_2}$	$\frac{1}{K_2}$	$\frac{f_{test}}{f_{calc}}$	$\frac{f_{test}}{f_{calc}}$	$\frac{f_{test}}{f_{calc}}$	$\frac{f_{test}}{f_{calc}}$
III	B-HG-8-12b	5700	4010	475	16.9	22.2	27.8	0.52	0.65	0.52	0.52
	B-PG-8-12b	6200	4010	475	18.4	24.2	30.2	0.57	0.71	0.56	0.56
	B-S-5-24	27350	4010	475	70.9	18.2	23.7	0.68	0.89	1.23	1.84
IV	B-HC1-5-24	18500	4640	511	64.7	15.5	20.1	0.62	0.81	1.04	1.56
	B-PC2-5-24	22500	4640	511	15.1	Pullout Failure (Plain Bar)					
	B-PC1-5-24	21700	4640	511	71.8	17.1	22.3	0.69	0.90	1.15	1.73
	B-HG3-5-24	7000	4640	511	16.1	Pullout Failure (Plain Bar)					
	B-HG1-5-24	6400	4640	511	39.0	9.3	12.1	0.38	0.49	0.63	0.94
	B-HG2-5-24	7300	4640	511	47.6	11.4	14.8	0.46	0.60	0.77	1.15
	B-PG2-5-24	6500	4640	511	12.3	Pullout Failure (Plain Bar)					
	B-PG1-5-24	6401	4640	511	48.0	11.5	14.9	0.46	0.60	0.77	1.16
	B-HG1-5-24b	6400	4640	511	42.2	10.1	10.1	0.41	0.41	0.68	0.68
	B-PG1-5-24b	6401	4640	511	50.8	12.1	12.1	0.49	0.49	0.82	0.82
V	B-HG1-5-12	6400	4170	485	27.4	13.8	18.0	0.53	0.69	0.68	1.02
	B-PG1-5-12	6401	4170	485	30.4	15.3	19.9	0.59	0.76	0.75	1.13
	B-HG-8-24	5700	4170	485	24.1	15.5	25.3	0.37	0.60	0.54	0.81
	B-HG1-5-12b	6400	4170	485	34.8	17.6	17.6	0.67	0.67	0.86	0.86
	B-PG1-5-12b	6401	4170	485	39.0	19.7	19.7	0.75	0.75	0.96	0.96
	B-HG-8-24b	5700	4170	485	26.7	17.2	21.6	0.41	0.52	0.60	0.60
	B-HG-8-54	5700	4170	485	33.0	9.5	15.4	0.23	0.37	0.45	0.68
	B-HG1-5-54	6400	4170	485	50.4	5.6	7.3	0.22	0.28	0.48	0.72
	B-PG1-5-54	6401	4170	485	50.6	5.7	7.4	0.22	0.28	0.48	0.72
	B-HC1-5-54	18500	4170	485	85.0	9.5	12.4	0.36	0.47	0.81	1.21

ACI Committee 440 (440.1R-03) has also proposed an equation for pullout controlled failure based on studies conducted by Ehsani, Saadatmanesh, and Tao (1996) and Gao, Benmokrene, and Tighiouart (1998).

$$l_{bf} = \frac{d_b f_{fu}}{2700} \tag{4-7}$$

The value in the denominator was selected as 2700 instead of the value obtained by the researchers (2850) with the goal of providing conservative results. The variables of the equation are the same as defined in Equation (4-6). It is stated in the ACI 440 report that splitting of the concrete is prevented by imposing modification factors to the basic development length computed by Equation (4-7). The modification factors required for Equation (4-7) are identical to those described for Equation (4-6).

It should be noted that the development length equation is a function of the bar diameter and reinforcement stress. The equation is insensitive to the concrete compressive strength and the type of reinforcement. While this equation is meant only for the calculation of development length of FRP bar reinforced structures, the test results obtained from the steel reinforced specimens were also analyzed with this equation for comparison purposes.

The ratio of the experimental to calculated stresses are presented in Table 4.3 for each specimen. A comparison of the ratio of the experimental to calculated values for each type of reinforcement are shown in Figure 4.10 through Figure 4.12. As shown, the equation yields unconservative results regardless of reinforcement type. The level of unconservatisim increases as the splice length of the specimen increases. Because the equation was derived and verified from the results of pull-out specimens and the modification factors only account for the cover dimension and bar location, the equation yields very unconservative results for the specimens that failed in a side-splitting mode even though the modification factors were implemented in the equation.

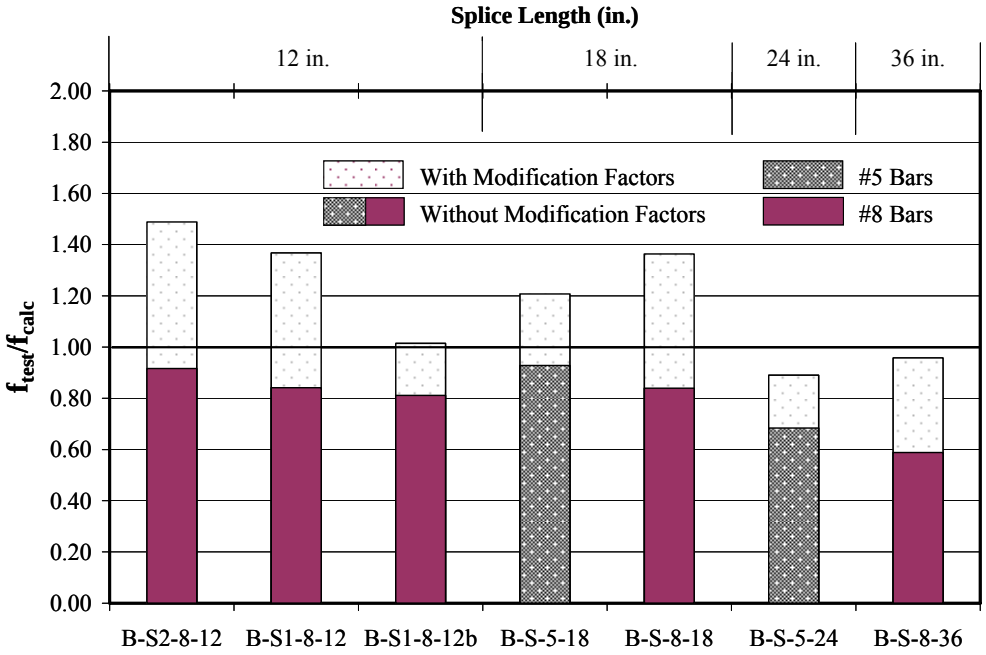

Figure 4.10 Comparison of Strength Calculations of Steel Reinforcement by ACI 440-03 (Equation (4-7))

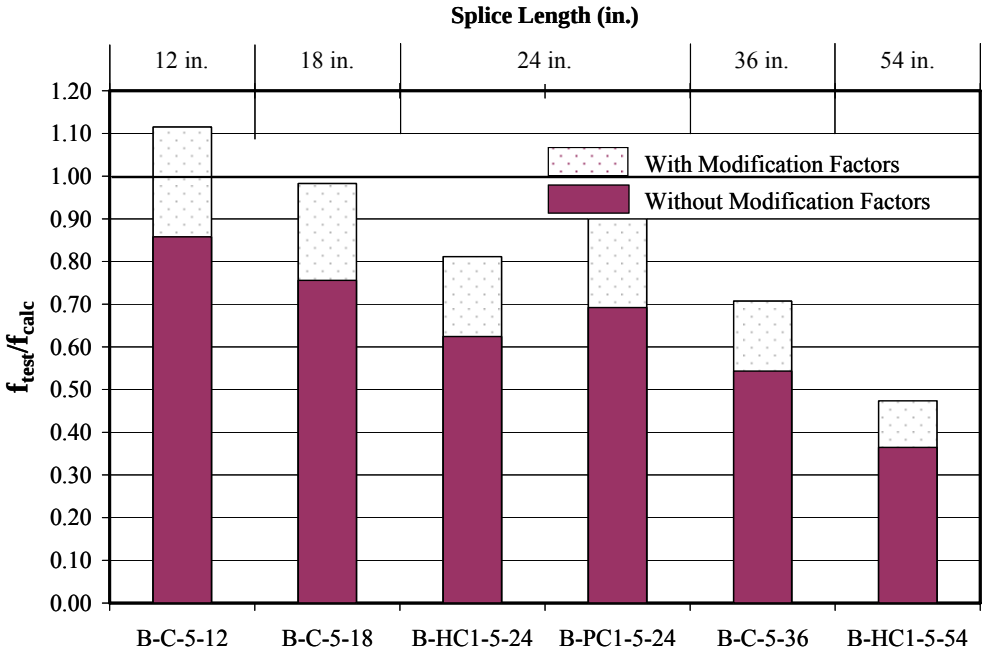

Figure 4.11 Comparison of Strength Calculations of CFRP Reinforcement by ACI 440-03 (Equation (4-7))

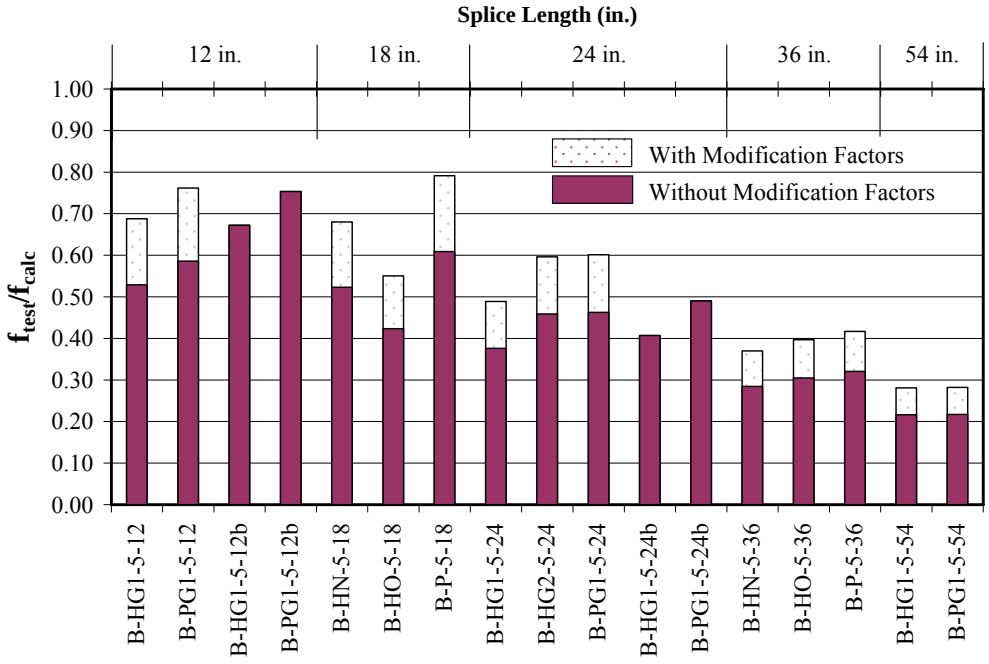

#5 Glass FRP Bars

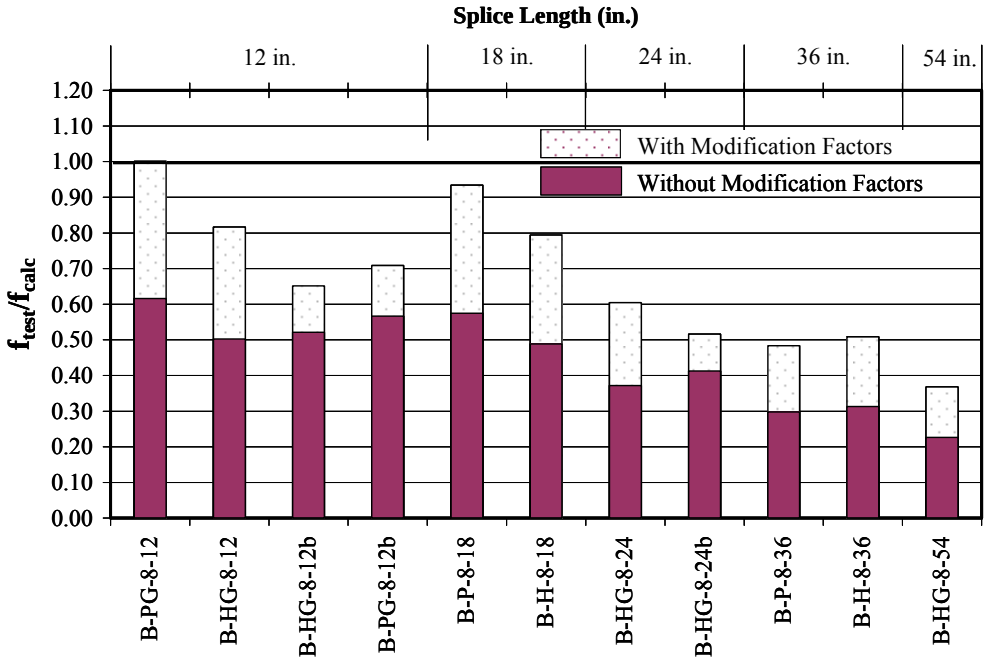

#8 Glass FRP Bars

Figure 4.12 Comparison of Strength Calculations of GFRP Reinforcement by ACI 440-03 (Equation (4-7))

Based on the evaluation of Equations (4-6) and (4-7) using the specimens investigated in the experimental program, it can be seen that the ACI Committee 440 recommendations (440.1R-03) produce unconservative results for FRP reinforced specimens. Therefore, the use of the development length provisions provided in the report for FRP reinforced concrete (440.1R-03) are not recommended.

4.2.3.1 Recent Changes in ACI Committee 440 (ACI 440.1R-XX) Development Length Equation

ACI Committee 440 has developed a new equation that is planned to replace Equations (4-6) and (4-7) in a future edition of the document (440.1R-XX). The proposed change has been balloted and accepted by the committee in 2005. Subsequently, the document was submitted for approval by the ACI Technical Activities Committee (TAC) and publication by Institute.

The new equation is based on the Orangun et al. (1977) equation and was adapted from a study performed by Wambeke (2003) for Glass FRP reinforced beam specimens (Equation (4-8)).

$$\frac{u}{\sqrt{f_c'}} = 4.0 + 0.3\frac{C}{d_b} + 100\frac{d_b}{l_e} \tag{4-8}$$

where

C = the lesser of the cover to the center of the bar or one half of the center to center spacing of the bars present.

Wambeke (2003) used a database which included 269 beam specimens, 82 of which failed in splitting. The database was limited to beam-end tests, notch-beam tests, and splice tests. Linear regression analysis of the normalized average bond strength versus the normalized cover and embedment length were performed on the specimens that failed in splitting to obtain Equation (4-8).

Both confined and unconfined splices were included in the study; however, the parameter considered by Orangun et al. (1977) for confinement was not considered

during the evaluation of Equation (4-8). Darwin et al. (1996a) found that the effect of the transverse reinforcement on bond strength of high relative rib area reinforced steel is more beneficial than that of moderate rib area. Based on this finding by Darwin et al. (1996a), Wambeke (2003) concluded that because glass FRP bars have very low relative rib area, the presence of confinement is not likely to increase the average bond stress. Therefore, Equation (4-8) was derived using a database containing both confined and unconfined splices. It should be noted that if the presence of transverse reinforcement in the splice region does increase the splice strength of FRP bars, Equation (4-8) may yield unconservative results for unconfined specimens.

Figure 4.13 illustrates the normalized average bond strength versus the ratio of embedment length to diameter of the bar for the database used by Wambeke (2003) including only bottom cast bars. Separate equations derived for confined and unconfined splices as well as Equation (4-8) are presented in the graph. While separate equations were derived, Equation (4-8) was proposed.

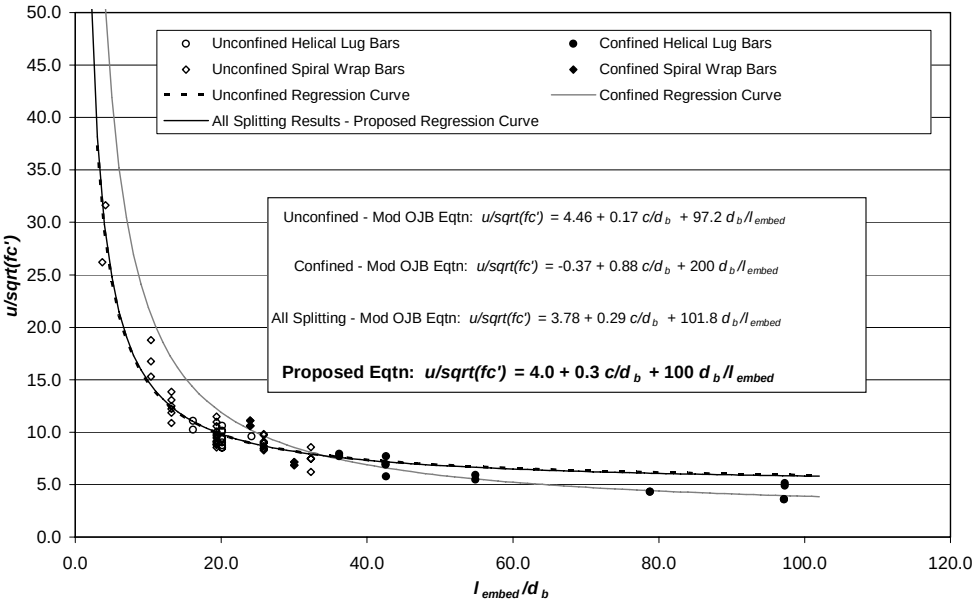

Figure 1: Consolidated Plot of Average Bond Stress vs. Normalized Embedment Length for 71 Beam Tests with Splitting Failures - OJB Approach

Figure 4.13 Normalized Bond Strength versus Normalized Embedment Length (Database of Wambeke (2003))

Equation (4-8) can be solved for the achievable bar stress given the existing embedment length, cover, and spacing dimensions. The resulting expression which incorporates a factor of safety of 1.15 is:

$$f_{fe} = \frac{\sqrt{f'_c}}{\alpha}\left(13.6\frac{l_e}{d_e} + \frac{C}{d_b}\frac{l_e}{d_b} + 340\right) \le f_{fu} \qquad (4\text{-}9)$$

where:

C= smaller of (a) the distance from center of a bar to nearest concrete surface, and (b) one-half the center-to-center spacing of bars being developed, in.

d_b= diameter of reinforcing bar, in.

f_c'= specified compressive strength of concrete, psi

l_e= embedded length of reinforcing bar, in.

α= top bar modification factor (1.5 for reinforcement placed so that more than 12 in. of fresh concrete is cast below the development length or splice; 1.0 for other reinforcement)

The term C/d_b should not be taken larger than 3.5. For the specimens tested in the experimental program conducted here, C/d_b is always less than 3.5 and does not control.

The ratio of the experimental to calculated stress using Equation (4-9) along with the reinforcement stress at failure are presented in Table 4.3 The ratio of the experimental to calculated stresses for each reinforcement type are also illustrated in Figure 4.14 through Figure 4.16. The equation was evaluated with and without the modification factor. The bar location factor, α, was the only modification factor used for this equation. Because the equation was derived using a database containing specimens with bottom cast bars, unconservative estimates may be expected from the equation for specimens with top cast bars. It should be noted that although the recommendations of ACI 440 are provided for FRP reinforced specimens, Equation (4-9) was also evaluated with the test results of steel reinforced specimens for comparative purposes.

In the case of the steel reinforced specimens, Figure 4.14 illustrates that when the modification factor was not used, the equation provides conservative results for the #5

bars but unconservative results for the #8 bars. With the recommended modification factor, the equation provided conservative results for the steel reinforced specimens with the exception of one specimen (B-S1-8-12b) in which the bars were bottom cast.

As shown in Figure 4.15, for the CFRP reinforced specimens, the ratio of the experimental to calculated stress ranges from 0.8 to 1.15 when the modification factor is not considered. With the modification factor, the equation provided conservative results. The conservatism decreases, however, as the splice length increases.

Although the equation was derived from a database including glass and aramid FRP bars, Figure 4.16 illustrates that the equation provides unconservative results for the glass FRP reinforced specimens in this investigation even with the inclusion of modification factor. The unconservatism increases as the splice length increases from 12 to 54 in. In the case of bottom cast specimens, the experimental results were as low as 52% of the calculated values for #8 bars.

Based on the comparision of the experimental and calculated results, it is found that even with the recommended modification factor of 1.5, the proposed recommendations of ACI Committee 440 (440.1R-XX) produce unconservative results for the Glass FRP bar reinforced specimens tested in this experimental program. The level of unconservatisim varies with the splice length, the reinforcement location, bar size, and bar type. In general, it is also observed that the ratio of experimental to calculated results decreases as the splice length increases. It should be noted that the proposed equation is not sensitive to reinforcement type.

Equation (4-9) was derived from a database in which the c/d_b ratio was greater than 2.0 except one specimen which had a c/d_b ratio of 1.0. In this experimental program, the governing c/d_b ratio is 1.0 for specimens with #8 bars and 1.3 for specimens with #5 bars according to the c/d_b definition Equation (4-9). This difference likely explains the unconservative results for the specimens with lower c/d_b (< 2.0).

As Equation (4-9) resulted in unconservative results for the glass FRP reinforced specimens, the proposed ACI 440 recommendations are not recommended for design use. The recommendations should be reevaluated.

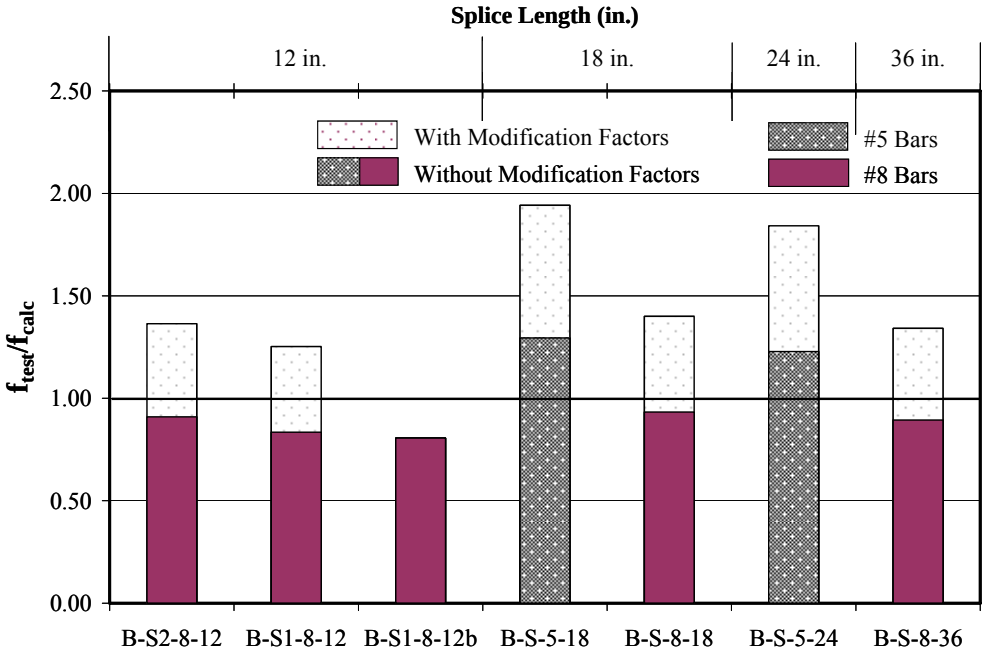

Figure 4.14 Comparison of Strength Calculations of Steel Reinforcement by ACI 440.1R-XX (Equation (4-9))

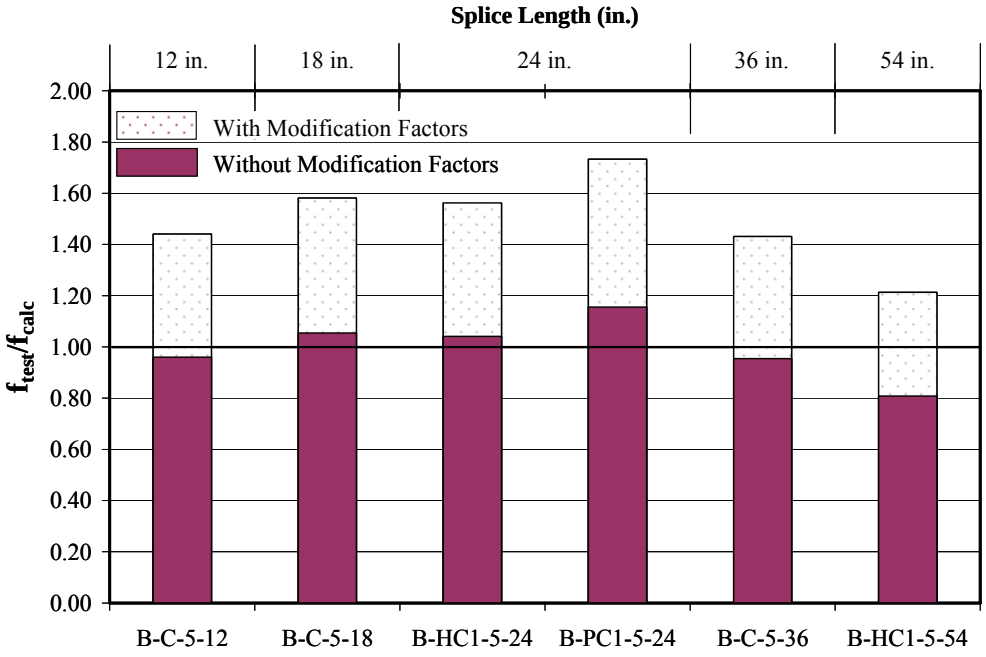

Figure 4.15 Comparison of Strength Calculations of CFRP Reinforcement by ACI 440.1R-XX (Equation (4-9))

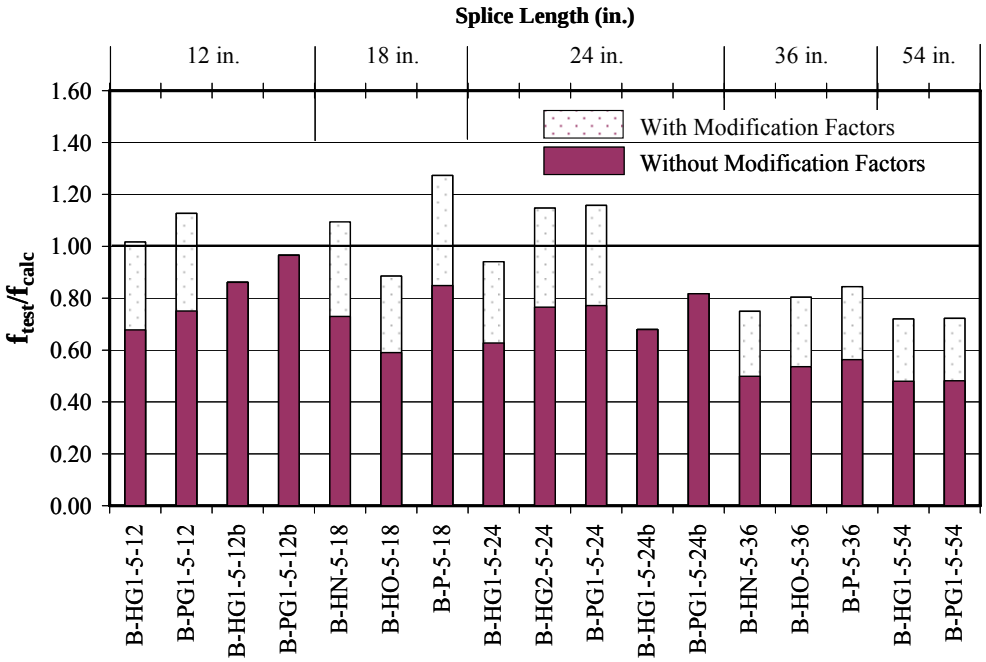

#5 Glass FRP Bars

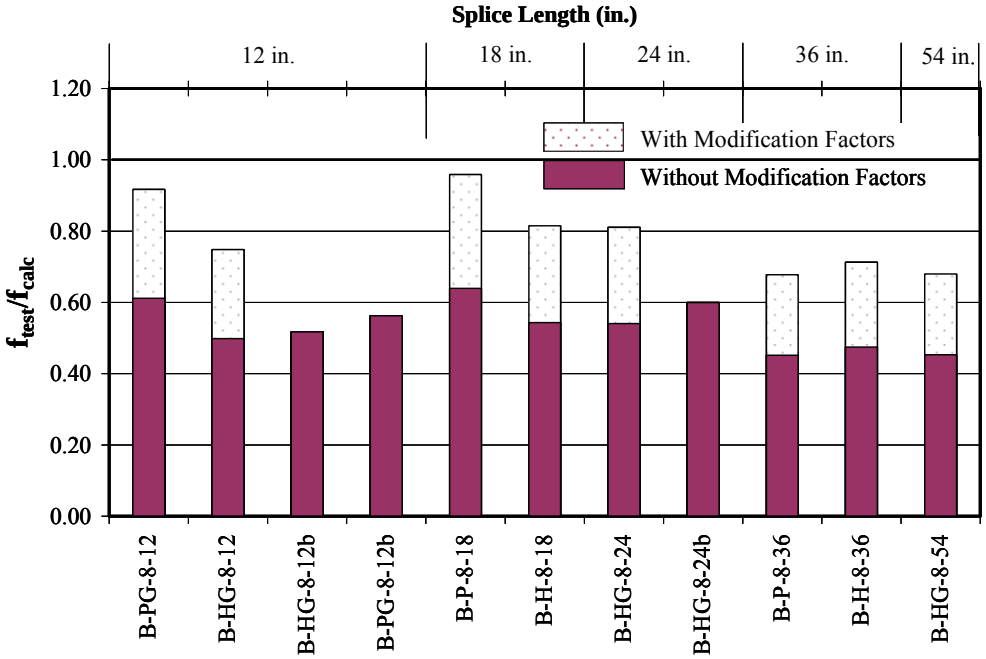

#8 Glass FRP Bars

Figure 4.16 Comparison of Strength Calculations of GFRP Reinforcement by ACI 440.1R-XX (Equation (4-9))

4.2.4 AASHTO Design Specifications

Design provisions for the design of highway bridges are provided by the American Association of State Highway and Transportation Officials through two documents: Standard Specifications for Highway Bridges and AASHTO LRFD Bridge Design Specifications. The development length provisions for AASHTO Standard Specifications (Seventeenth Edition) and the AASHTO LRFD Bridge Design Specifications are identical and are presented as follows:

$$l_{bf} = 0.04 \frac{A_b f_y}{\sqrt{f_c'}} \qquad (4\text{-}10)$$

$$l_{bf} > 0.0004 d_b f_y$$

where:

l_d = *development length of reinforcement, in.*

A_b = *cross sectional area of reinforcement*

Rearranging Equation (4-10) in terms of the diameter of the reinforcing bar results in the following equation.

$$l_{bf} = \frac{{d_b}^2 f_y}{31.8\sqrt{f_c'}} \qquad (4\text{-}11)$$

The AASHTO development length equation has the same form as ACI Committee 440 (440.1R-03) Equation (4-6) with a $1/K_2$ factor of 31.8. This $1/K_2$ factor is significantly higher than that suggested by Committee 440 (15.6 - 21.3). Therefore, the AASHTO equation provides unconservative results for the FRP reinforced specimens. In addition, there are several other problems associated with the use of this design expression as demonstrated in the analysis of Equation (4-6). Consequently, the AASHTO design expression is not appropriate for FRP reinforced structures.

4.3 Crack Width Calculations

Crack widths in FRP reinforced concrete structures are expected to be larger than those of a comparable steel reinforced structure because most FRP bars have a lower modulus of elasticity than steel. Although FRP bars are corrosion resistant, controlling crack widths may be important due to aesthetic concerns.

ACI 440 Committee (440.1R-XX) has proposed an equation which is based on an equation developed by Frosch (1999). Because the equation considers the modulus of elasticity of the reinforcement and is based on a physical model, the equation is independent of the reinforcement type, and thus should be applicable to all types of reinforcing bars. However, due to differences in the slip characteristics between the concrete and reinforcement, it is important to evaluate if the different surface characteristics have any effect on crack widths.

Frosch (1999) derived the following equation for the calculation of the maximum crack width for uncoated steel reinforcement.

$$w_c = 2\frac{f_s}{E_s}\beta d^* \qquad (4\text{-}12)$$

where:

w_c= *crack width*

f_s= *reinforcing steel stress*

E_s= *reinforcing steel modulus of elasticity*

β= *ratio of the distance between the neutral axis and tension face to the distance between neutral axis and center of reinforcement,* $\beta = \frac{h-c}{d-c}$

d^*= *controlling cover distance (Figure 4.17)*

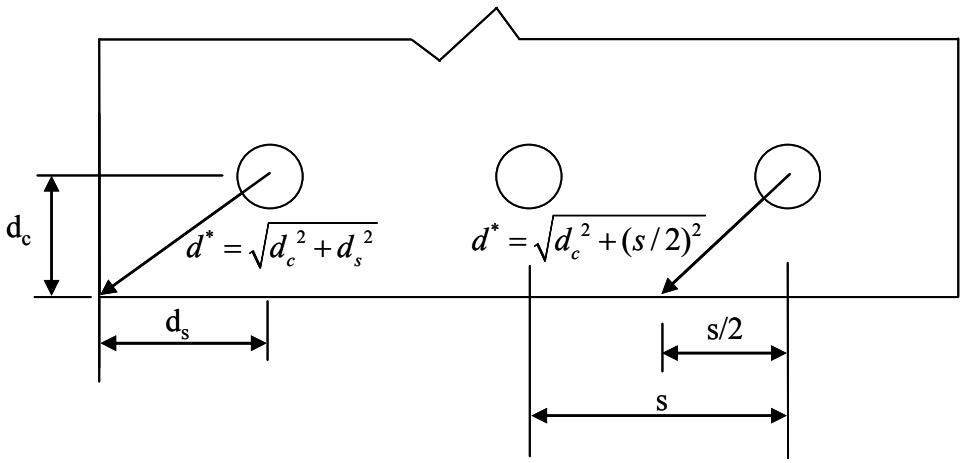

Figure 4.17 Controlling Cover Distance, d^*

The maximum crack widths on the tension face of the beam were calculated according to the Frosch (1999) equation. Nominal spacing and cover dimensions were used for the analysis. The calculated crack widths were divided by the measured widths to evaluate the accuracy of the model. The results for each reinforcement type are shown in Figure 4.18 through Figure 4.20.

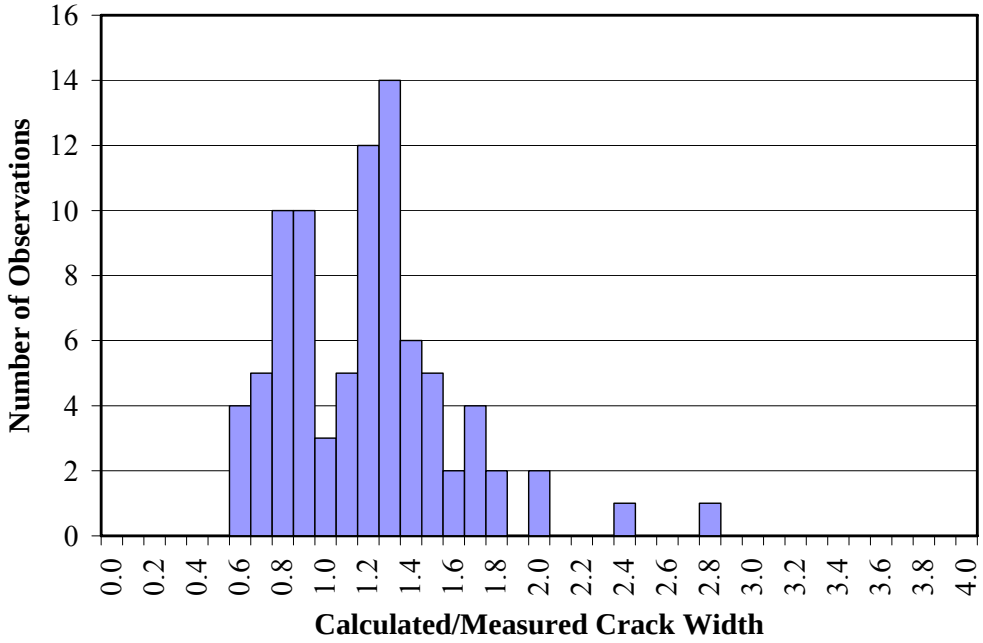

Figure 4.18 Maximum Crack Width Calculation for Steel Bar Reinforced Specimens with Equation (4-12)

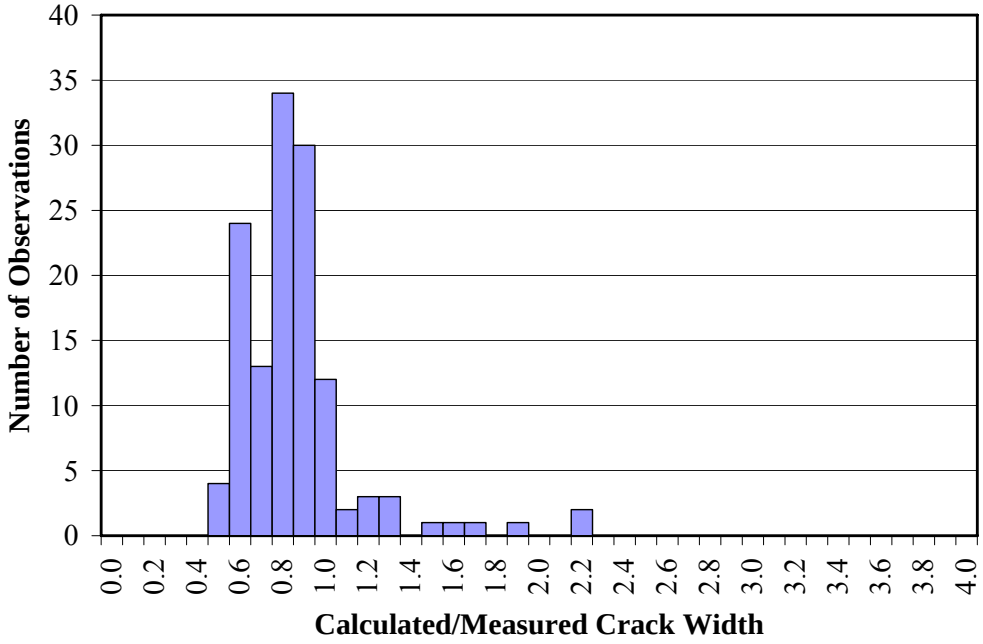

Figure 4.19 Maximum Crack Width Calculation for CFRP Bar Reinforced Specimens with Equation (4-12)

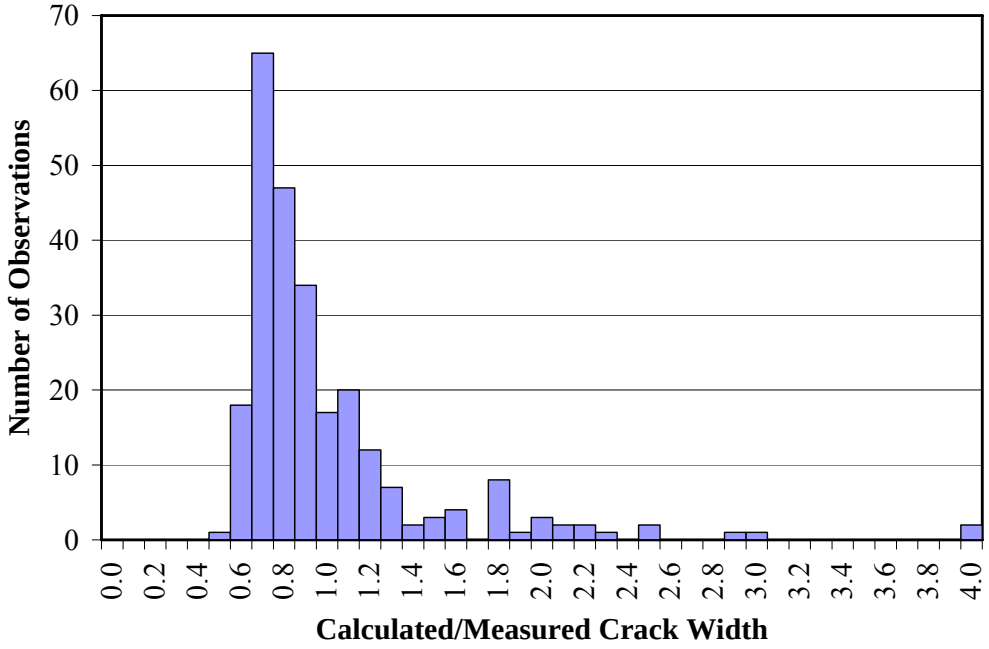

Figure 4.20 Maximum Crack Width Calculation for GFRP Bar Reinforced Specimens with Equation (4-12)

As shown in Figure 4.18, Equation (4-12) provides reasonable results for specimens reinforced with steel bars. It can be seen that the equation can also be used effectively to compute maximum crack width for both glass and carbon FRP reinforced specimens (Figure 4.19 and Figure 4.20). However, it can be seen that the majority of the FRP data is shifted slightly to the left of a calculated to measured ratio of 1.0. The mode of the CFRP data is 0.8 while the mode of the GFRP data is 0.7; therefore, the equation can be adjusted to provide improved results by implementing a factor for each reinforcement type so that the mode of the data for each reinforcement is 1.0. The calculated material factors based on this study are 1.25 for CFRP reinforced specimens and 1.4 for GFRP reinforced specimens.

To further investigate the effect of the bar surface deformation on crack width calculations, the specimens reinforced with glass FRP bars are presented in Figure 4.21 according to their surface deformation. As can be seen, the specimens with a sand coating surface deformation as well as the sand and wrapped coating behaved similarly.

The mode was still approximately 0.7. It can be concluded that same material factor is appropriate for bars having a sand and a sand and wrapped coating.

Based on these observations, a material factor should be implemented into the equation for maximum crack width calculations for FRP bar reinforced specimens. A material factor of 1.4 is recommended for both glass and carbon FRP bar reinforced specimens to obtain satisfactory crack width calculations with the proposed equation (Equation (4-12)). A material factor of 1.4 is suggested instead of 1.25 for carbon FRP bar reinforced specimens to provide one constant material factor for FRP bar reinforced specimens. In addition, the equation with a material factor of 1.4 will yield 12% larger crack width than that of the equation with a material factor of 1.25 yielding a more conservative estimate.

ACI Committee 440 (440.1R-XX) has suggested a coefficient (k_b) of 1.4 which can be implemented into Equation (4-12) for FRP bars to accounts for the degree of bond between the FRP bar and surrounding concrete. The committee analyzed crack width data which included a variety of cross-sections and FRP bar manufacturers, fiber types, resin formulations and surface treatments. It was found that average k_b values ranges from 0.60 to 1.72 with a mean of 1.10. They concluded that a conservative value of 1.4 should be assumed for the cases where k_b is not known from the experimental data. This result is consistent with the results of this study.

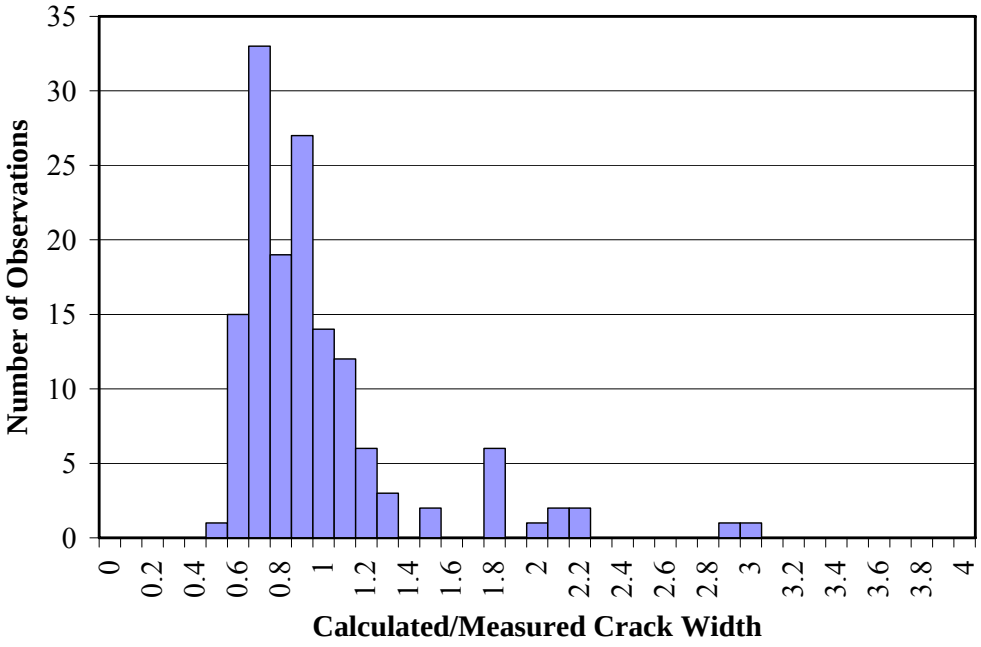

(a) Sand and Wrapped Coated Reinforcement (Hughes Bros Inc.)

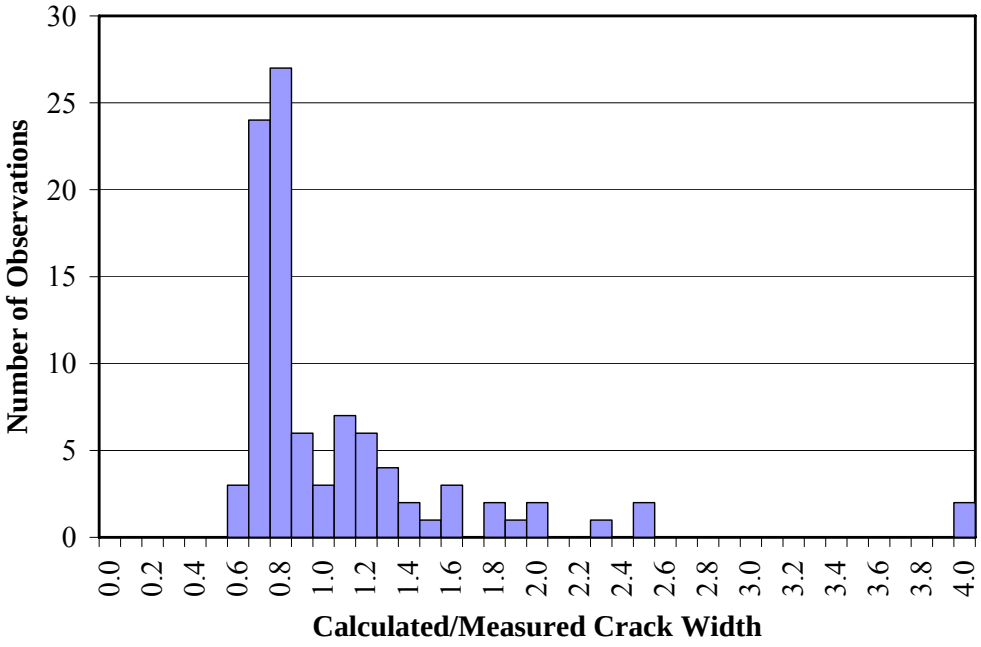

(b) Sand Coated Reinforcement (Pultrall Inc.)

Figure 4.21 Effect of Surface Deformation on Maximum Crack Width

CHAPTER 5

ANALYSIS AND DESIGN METHODS

5.1 Introduction

In Chapter 4, the beams tested in the experimental program were analyzed using several available design methods. The design methods for steel reinforced specimens yielded satisfactory results; however, the methods for FRP reinforced sections were not capable of calculating the splice strength of FRP reinforced section adequately. In addition, a design method does not exist that addresses the splice strength of both FRP and steel bar reinforced beams. In this chapter, the effects of parameters investigated in the experimental program are analyzed, and the results of these analyses are presented. Furthermore, an analysis method is developed to calculate the splice strength of both steel and FRP bar reinforced concrete beams. Finally, a simple design method is proposed to calculate the splice strength of reinforced concrete beams regardless of the reinforcement type.

5.2 Influence of Investigated Parameters

The variables investigated in the experimental program are described in detail in Chapter 2. The variables tested in the experimental program included the modulus of elasticity, bar size, splice length, axial stiffness, surface deformation, and casting position of the lapped reinforcement. The same mix design was used throughout the experimental program with the intent of keeping the concrete strength constant. The concrete compressive strength, however, varied from 3,900 to 5,500 psi which differed from the desired value of 4,000 psi. It has been shown in ACI 408R-03 and Canbay and Frosch (2005) that the net effect of the concrete strength on bond strength is proportional to the

fourth root of the concrete compressive strength, $\sqrt[4]{f_c'}$. Therefore, specimens with different concrete compressive strengths can be normalized using the fourth root of the concrete compressive strength for comparison purposes. The effect of the compressive strength of the concrete on the normalization is minimal because of the small variation in the concrete compressive strength. The stresses and forces presented in this section were normalized to 4,000 psi concrete as follows:

$$f_{test(f_c'=4000\,psi)} = f_{test(f_c')} \cdot \sqrt[4]{4000/f_c'}$$

$$F_{test(f_c'=4000\,psi)} = F_{test(f_c')} \cdot \sqrt[4]{4000/f_c'}$$

where:

f_c' = *concrete cylinder strength, psi*

F_{test}= *bar force at failure, kips*

f_{test} = *bar stress at failure, ksi*

5.2.1 Additional Splice Specimens Reinforced with FRP

In addition to the specimens tested in the experimental program, 12 splice specimens tested by Mosley (2000) are added to the database to evaluate the effect of the investigated parameters. Mosley (2000) tested specimens reinforced with #5 glass, aramid, and steel bars. Two types of glass FRP bars were investigated with different surface deformations: the first was wrapped and sand coated while the second had helical lugs. The aramid bars had a spiral wrap surface deformation. All the specimens were cast with top bars as defined by ACI 318-05. Eight of the specimens which failed in side splitting had the same cross sectional dimensions as the companion specimens tested in the experimental program conducted here (Figure 5.1 (a)). Four of the specimens failed in face splitting. Their section depth and face cover dimensions were identical; however, they had a clear spacing of 4.75 in. and a side cover of 2.4 in (Figure 5.1 (b)). Table 5.1 summarizes the test results of the specimens conducted as part of the current study and those conducted by Mosley (2000) along with the bar size, splice length, concrete

compressive strength, bar modulus of elasticity, bar axial stiffness, and cover and spacing dimensions.

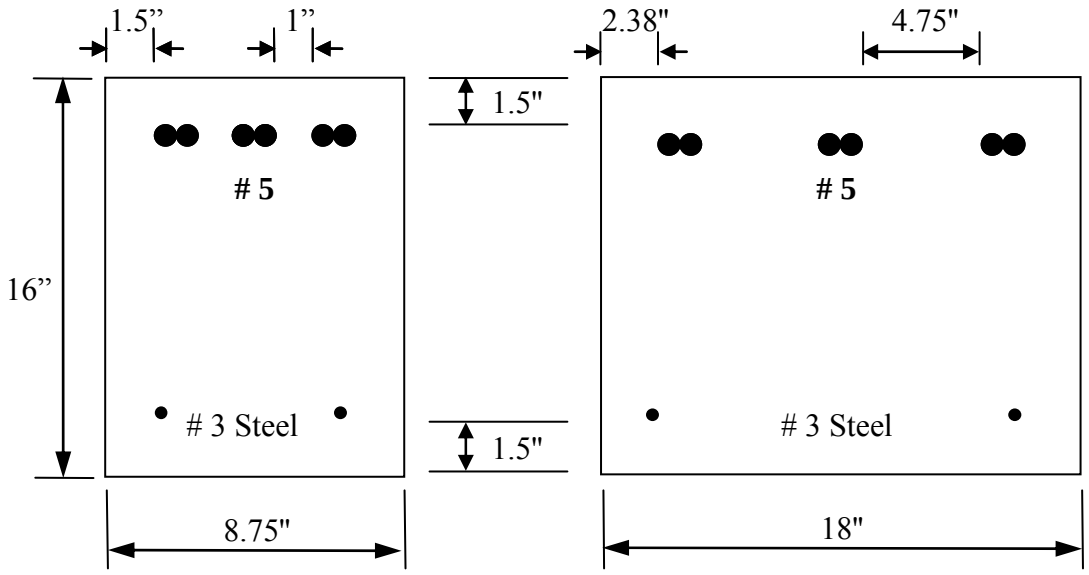

(a) Side Splitting (b) Face Splitting

Figure 5.1 Cross Section Detail at Splice Region (Tests by Mosley (2000))

Table 5.1 Summary of Test Results

	Specimen	Surface Deformation	Bar Size	L_s (in.)	Casting Position	f_c' (psi)	E_{bar} (ksi)	AE (kips)	c_{so} (in.)	c_{si} (in.)	c_b (in.)	f_{test} (ksi)	$f_{test(4000)}$ (ksi)	$F_{test(4000)}$ (kips)
Series I	B-S-8-18	Deformed	#8	18	Top	5260	28400	22436	1.5	0.5	1.5	40.8	38.1	30.1
	B-P-8-18	Sand Coated	#8	18	Top	5260	6200	4898	1.5	0.5	1.5	27.9	26.1	20.6
	B-H-8-18	Wrapped and Sand	#8	18	Top	5260	5700	4503	1.5	0.5	1.5	23.7	22.2	17.5
	B-HN-5-18	Wrapped and Sand	#5	18	Top	5260	6400	1984	1.5	0.5	1.5	40.7	38.0	11.8
	B-HO-5-18	Wrapped and Sand	#5	18	Top	5260	5800	1798	1.5	0.5	1.5	32.9	30.7	9.5
	B-P-5-18	Sand Coated	#5	18	Top	5260	6401	1984	1.5	0.5	1.5	47.3	44.2	13.7
	B-S-5-18	Deformed	#5	18	Top	5260	27350	8478	1.5	0.5	1.5	72.2	67.4	20.9
	B-C-5-18	Fabric Texture	#5	18	Top	5260	18500	5735	1.5	0.5	1.5	58.8	54.9	17.0
Series II	B-C-5-12	Fabric Texture	#5	12	Top	5470	18500	5735	1.5	0.5	1.5	44.5	41.1	12.8
	B-S-8-36	Deformed	#8	36	Top	5470	28400	22436	1.5	0.5	1.5	57.2	52.9	41.8
	B-P-8-36	Sand Coated	#8	36	Top	5470	6200	4898	1.5	0.5	1.5	28.9	26.8	21.1
	B-H-8-36	Wrapped and Sand	#8	36	Top	5470	5700	4503	1.5	0.5	1.5	30.4	28.1	22.2
	B-HN-5-36	Wrapped and Sand	#5	36	Top	5470	6400	1984	1.5	0.5	1.5	44.3	40.9	12.7
	B-HO-5-36	Wrapped and Sand	#5	36	Top	5470	5800	1798	1.5	0.5	1.5	47.5	43.9	13.6
	B-P-5-36	Sand Coated	#5	36	Top	5470	6401	1984	1.5	0.5	1.5	49.9	46.1	14.3
	B-C-5-36	Fabric Texture	#5	36	Top	5470	18500	5735	1.5	0.5	1.5	84.6	78.2	24.2
Series III	B-S2-8-12	Deformed	#8	12	Top	4010	27200	16048	1.5	0.5	1.5	29.7	29.7	17.5
	B-S1-8-12	Deformed	#8	12	Top	4010	27200	21488	1.5	0.5	1.5	27.3	27.2	21.5
	B-S4-8-12	Plain	1 in.	12	Top	4010	29600	12728	1.5	0.5	1.5	20.0	20.0	8.6
	B-S3-8-12	Plain	1 in.	12	Top	4010	30500	24095	1.5	0.5	1.5	8.8	8.8	7.0
	B-PG-8-12	Sand Coated	#8	12	Top	4010	6200	4898	1.5	0.5	1.5	20.0	19.9	15.8
	B-HG-8-12	Wrapped and Sand	#8	12	Top	4010	5700	4503	1.5	0.5	1.5	16.3	16.3	12.9
	B-S1-8-12b	Deformed	#8	12	Bottom	4010	27200	21488	1.5	0.5	1.5	26.3	26.3	20.8
	B-HG-8-12b	Wrapped and Sand	#8	12	Bottom	4010	5700	4503	1.5	0.5	1.5	16.9	16.9	13.3
	B-PG-8-12b	Sand Coated	#8	12	Bottom	4010	6200	4898	1.5	0.5	1.5	18.4	18.4	14.5
	B-S-5-24	Deformed	#5	24	Top	4010	27350	8478	1.5	0.5	1.5	70.9	70.9	22.0

Table 5.1 Summary of Test Results (continued)

	Specimen	Surface Deformation	Bar Size	L_s (in.)	Casting Position	f_c' (psi)	E_{bar} (ksi)	AE (kips)	c_{so} (in.)	c_{si} (in.)	c_b (in.)	f_{test} (ksi)	$f_{test(4000)}$ (ksi)	$F_{test(4000)}$ (kips)
Series IV	B-HC1-5-24	Fabric Texture	#5	24	Top	4640	18500	5735	1.5	0.5	1.5	64.7	62.4	19.3
	B-PC2-5-24	Uncoated	#5	24	Top	4640	22500	6975	1.5	0.5	1.5	15.1	14.6	4.5
	B-PC1-5-24	Sand Coated	#5	24	Top	4640	21700	6727	1.5	0.5	1.5	71.8	69.2	21.4
	B-HG3-5-24	Uncoated	#5	24	Top	4640	7000	2170	1.5	0.5	1.5	16.1	15.5	4.8
	B-HG1-5-24	Wrapped and Sand	#5	24	Top	4640	6400	1984	1.5	0.5	1.5	39.0	37.6	11.6
	B-HG2-5-24	Fabric Texture	#5	24	Top	4640	7300	2263	1.5	0.5	1.5	47.6	45.8	14.2
	B-PG2-5-24	Uncoated	#5	24	Top	4640	6500	2015	1.5	0.5	1.5	12.3	11.9	3.7
	B-PG1-5-24	Sand Coated	#5	24	Top	4640	6401	1984	1.5	0.5	1.5	48.0	46.2	14.3
	B-HG1-5-24b	Wrapped and Sand	#5	24	Bottom	4640	6400	1984	1.5	0.5	1.5	42.2	40.6	12.6
	B-PG1-5-24b	Sand Coated	#5	24	Bottom	4640	6401	1984	1.5	0.5	1.5	50.8	49.0	15.2
Series V	B-HG1-5-12	Wrapped and Sand	#5	12	Top	4170	6400	1984	1.5	0.5	1.5	27.4	27.1	8.4
	B-PG1-5-12	Sand Coated	#5	12	Top	4170	6401	1984	1.5	0.5	1.5	30.4	30.0	9.3
	B-HG-8-24	Wrapped and Sand	#8	24	Top	4170	5700	4503	1.5	0.5	1.5	24.1	23.8	18.8
	B-HG1-5-12b	Wrapped and Sand	#5	12	Bottom	4170	6400	1984	1.5	0.5	1.5	34.8	34.5	10.7
	B-PG1-5-12b	Sand Coated	#5	12	Bottom	4170	6401	1984	1.5	0.5	1.5	39.0	38.6	12.0
	B-HG-8-24b	Wrapped and Sand	#8	24	Bottom	4170	5700	4503	1.5	0.5	1.5	26.7	26.4	20.9
	B-HG-8-54	Wrapped and Sand	#8	54	Top	4170	5700	4503	1.5	0.5	1.5	33.0	32.7	25.8
	B-HG1-5-54	Wrapped and Sand	#5	54	Top	4170	6400	1984	1.5	0.5	1.5	50.4	49.9	15.5
	B-PG1-5-54	Sand Coated	#5	54	Top	4170	6401	1984	1.5	0.5	1.5	50.6	50.1	15.5
	B-HC1-5-54	Fabric Texture	#5	54	Top	4170	18500	5735	1.5	0.5	1.5	85.0	84.1	26.1

Table 5.1 Summary of Test Results (continued)

	Specimen	Surface Deformation	Bar Size	L_s (in.)	Casting Position	f_c' (psi)	E_{bar} (ksi)	AE (kips)	c_{so} (in.)	c_{si} (in.)	c_b (in.)	f_{test} (ksi)	$f_{test(4000)}$ (ksi)	$F_{test(4000)}$ (kips)
Mosley (2000)	B-S-1	Deformed	#5	18	Top	5600	29000	8990	1.5	0.5	1.5	73.2	67.3	20.9
	B-G1-1	Wrapped and Sand	#5	18	Top	5600	5900	1829	1.5	0.5	1.5	38.3	35.2	10.9
	B-G2-1	Helical Lugs	#5	18	Top	5600	5900	1829	1.5	0.5	1.5	32.6	29.9	9.3
	B-A-1	Spiral Wrap	#5	18	Top	5600	6800	2108	1.5	0.5	1.5	40.4	37.1	11.5
	B-S-2	Deformed	#5	12	Top	4100	29000	8990	1.5	0.5	1.5	55.6	55.2	17.1
	B-G1-2	Wrapped and Sand	#5	12	Top	4100	5900	1829	1.5	0.5	1.5	28.9	28.8	8.9
	B-G2-2	Helical Lugs	#5	12	Top	4100	5900	1829	1.5	0.5	1.5	29.5	29.3	9.1
	B-A-2	Spiral wrap	#5	12	Top	4100	6800	2108	1.5	0.5	1.5	31.1	30.9	9.6
	B-S-3	Deformed	#5	12	Top	5900	29000	8990	2.69	2.375	1.5	75.6	68.6	21.3
	B-G1-3	Wrapped and Sand	#5	12	Top	5900	5900	1829	2.69	2.375	1.5	49.3	44.7	13.9
	B-G2-3	Helical Lugs	#5	12	Top	5900	5900	1829	2.69	2.375	1.5	46.8	42.4	13.2
	B-A-3	Spiral Wrap	#5	12	Top	5900	6800	2108	2.69	2.375	1.5	51.7	46.9	14.5

c_b = face cover

c_{si} = half of the clear spacing between bars

c_{so} = clear side cover of reinforcing bars

5.2.2 Modulus of Elasticity

The effect of the modulus of elasticity of the reinforcement was investigated among the specimens having the same surface deformation and bar size. As shown in Figure 5.2, the normalized bar stress is plotted versus the modulus of elasticity. Both glass and carbon bars (#5) having surface deformations of sand coating and fabric texture are presented in the graph. Although, there is a little scatter among the glass FRP data, the graph clearly shows a trend between the modulus of elasticity and the ultimate strength reached by the bar at failure. It is important to note that, although the surface deformations of the two carbon FRP bars are different, the data points follow the trend as the modulus of elasticity increases.

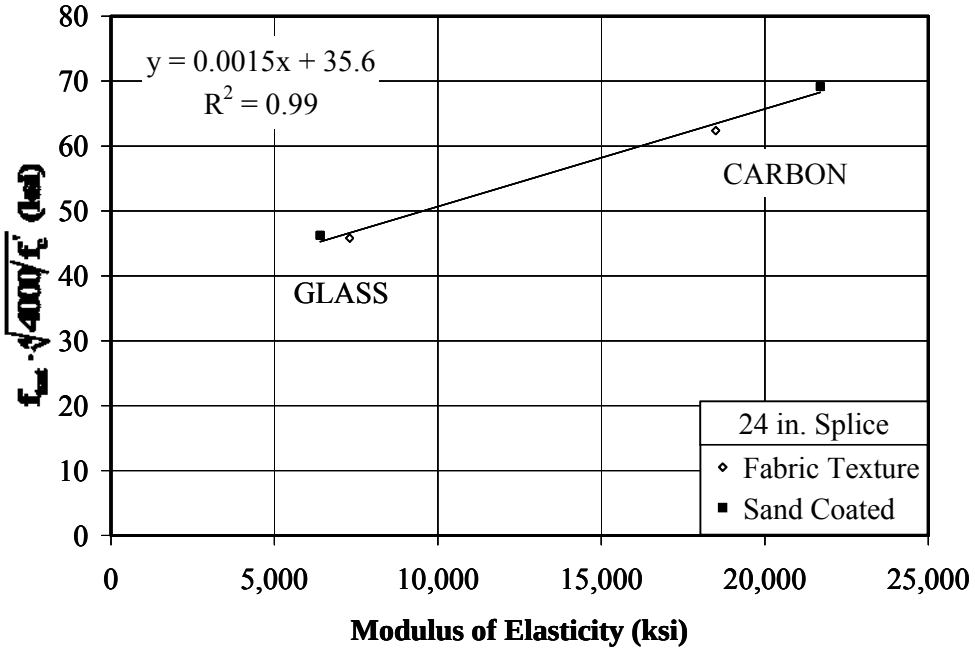

Figure 5.2 Effect of Modulus of Elasticity on Bond Strength

5.2.3 Bar Size

Two bar sizes, #5 and #8, were used to examine the effect of the bar size on the splice strength. The effect of bar size was evaluated by plotting the bar size versus the normalized bar force reached at failure (Figure 5.3). For the same bar type, as the diameter of bar increases from #5 to #8 (0.625 in.-1.0 in.), the force obtained by the bar increases.

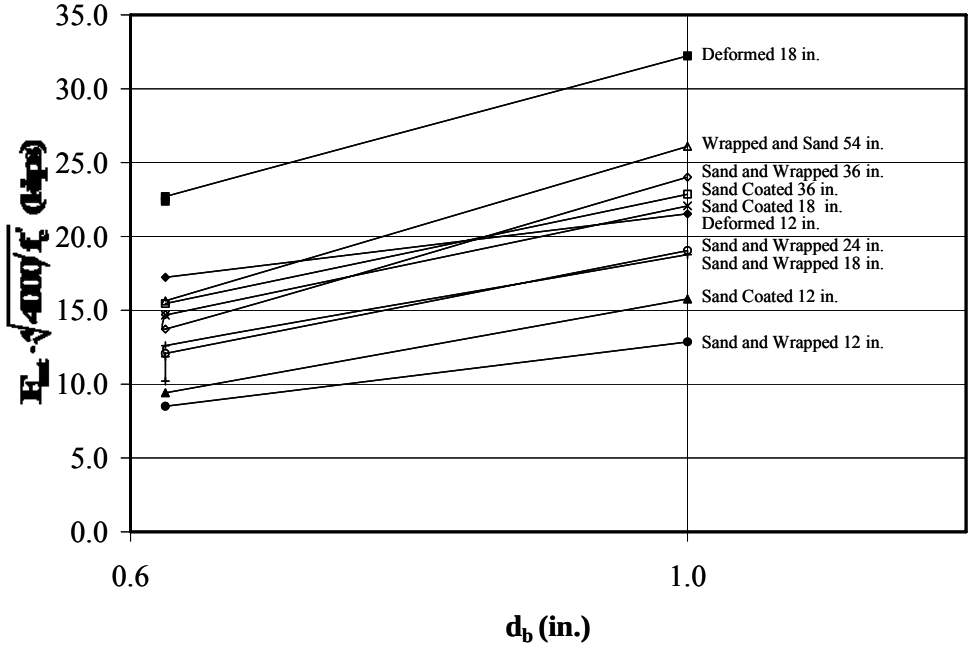

Figure 5.3 Effect of Bar Size on Bond Strength

5.2.4 Splice Length

The effect of splice length on developed bar stress for #5 and #8 reinforced beams is illustrated in Figure 5.4 and Figure 5.5, respectively. Table 5.2 provides a summary of the stress increase achieved by increasing the splice length from 12 in. to 54 in. for bars with different surface deformation and size.

As shown in Figure 5.4 and Figure 5.5, bar stresses reached at failure increase as the splice length increases. However, the effectiveness of the splice decreases with the increase in splice length. As a result, the strength gain reduces. In addition, the strength gain as the splice length increases is different for each reinforcement type. The strength

gain for the steel and carbon bars as the splice length increases is greater than for the glass bars. For example, doubling the splice length of the #5 sand coated glass bars, wrapped and sand coated glass bars, and fabric texture carbon bars from 18 in. to 36 in., increased the stress by 1.9 ksi (4%), 7.8 ksi (22%), and 23.3 ksi (43%), respectively. The specimens reinforced with #8 sand coated GFRP, wrapped and sand coated GFRP, and deformed steel bars gained 0.7 ksi (3%), 5.9 ksi (27%), and 14.8 ksi (39%), respectively as the splice length was doubled from 18 in. to 36 in.

From these results, it appears that the effect of splice length on the ultimate stress reached by the reinforcement is a function of the modulus of the elasticity of the reinforcement. The impact of an increase in splice length decreases as the modulus of elasticity is decreased. As previously discussed in Section 5.2.2, for a given splice length and bar size, the bar force at failure increases as the modulus of elasticity increases. Although the #5 sand coated and wrapped and the sand coated glass FRP bars have a similar modulus of elasticity, the sand coated bars slightly reached higher bar forces than the wrapped and sand coated bars. Regardless, the trend regarding the effect of splice length is similar as shown in Figure 5.4. The effect of surface deformation on bond strength is further discussed in Section 5.2.6.

Table 5.2 Summary of Test Results for Splice Length Comparison

Bar Size	Bar Type	Surface Type	12”	18”	24”	36”	54”
			$f_{test(4000)}$ (ksi)				
#5	Glass	Wrapped and Sand	27.9[+]	34.6[§]	37.6	42.4[+]	49.9
	Glass	Sand Coated	30.0	44.2	46.2	46.1	50.1
	Carbon	Fabric Texture	41.1	54.9	62.4	78.2	84.1
	Steel	Deformed	55.2	67.4[+]	70.9[*]	-	-
#8	Glass	Wrapped and Sand	16.3	22.2	23.8	28.1	32.7
	Glass	Sand Coated	19.9	26.1	-	26.8	-
	Steel	Deformed	27.2	38.1	-	52.9	-

[+] Average of two specimens

[§] Average of three specimens

[*] Yielded

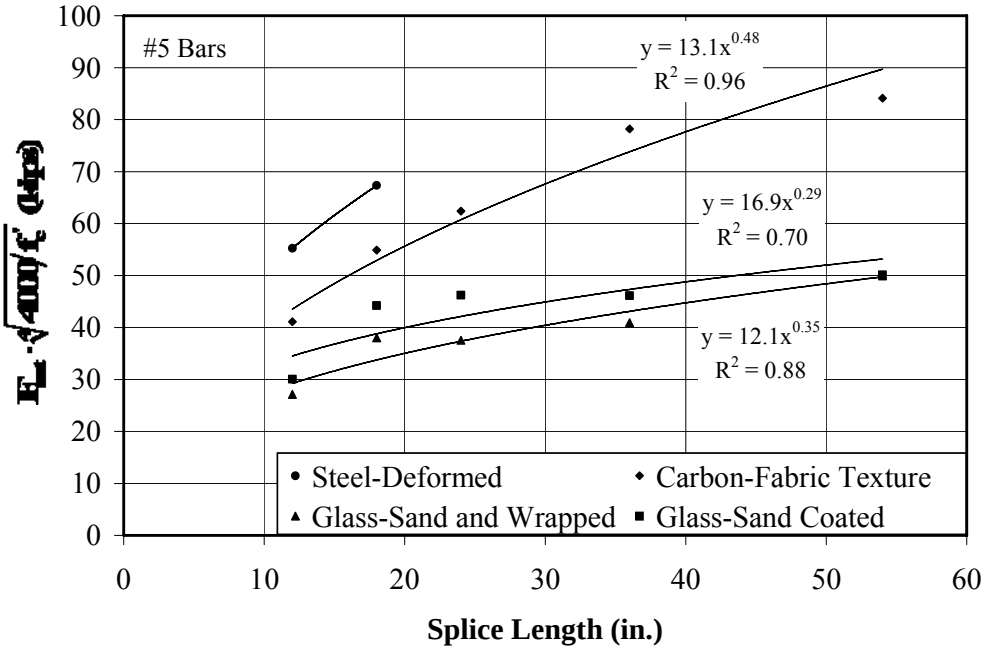

Figure 5.4 Effect of Splice Length on Bond Strength for #5 Bars

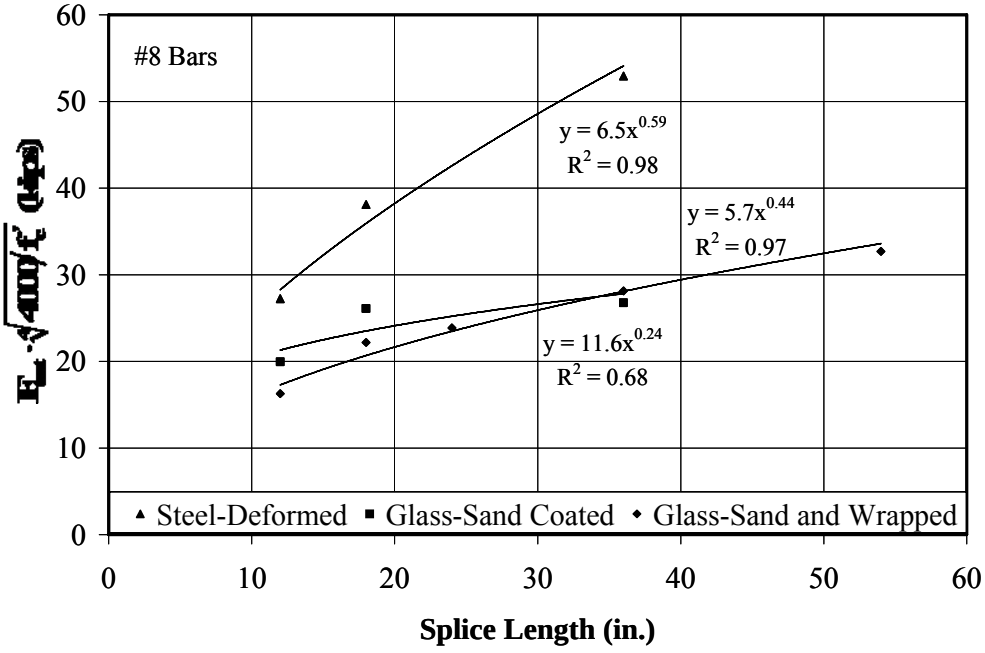

Figure 5.5 Effect of Splice Length on Bond Strength for #8 Bars

5.2.5 Axial Stiffness

Axial stiffness of the bar is calculated by multiplying the nominal cross-sectional area of the bar and the modulus of the elasticity of the reinforcement (AE). The effect of axial stiffness for #5 and #8 bars is illustrated in Figure 5.6 and Figure 5.7, respectively where the normalized bar force at failure is plotted versus the axial stiffness (AE). As shown, more scatter is apparent for the glass FRP bars than for the steel and carbon FRP reinforcement. This scatter can be explained as follows. First, a variety of surface deformations were tested for the glass FRP bars. The scatter resulting from the surface deformation is discussed in Section 5.2.6. Second, while the specimens were constructed and tested in the same manner, there is the potential for variability in construction and testing of the specimens. Finally, there are fewer tests that are presented for the carbon and steel reinforcement. Although, there is scatter among the glass FRP data, a trend is evident between the axial stiffness and the ultimate strength reached by the bar at failure.

Figure 5.8 illustrates the relationship between axial stiffness and the force developed in the reinforcement for #8 bars with 12 in. splices. As shown, the specimen reinforced with the hollow steel bar failed at a lower load than the specimen reinforced with the solid steel bar. The hollow bar which had the same modulus of elasticity as the solid bar reached a lower bar force than that of the solid bar indicating the importance of axial stiffness on splice strength. It should be noted that the surface deformations of both bars were identical.

Based on these results, it is concluded that a major factor influencing splice strength is the axial stiffness of the reinforcement rather than the modulus of elasticity of the reinforcement alone.

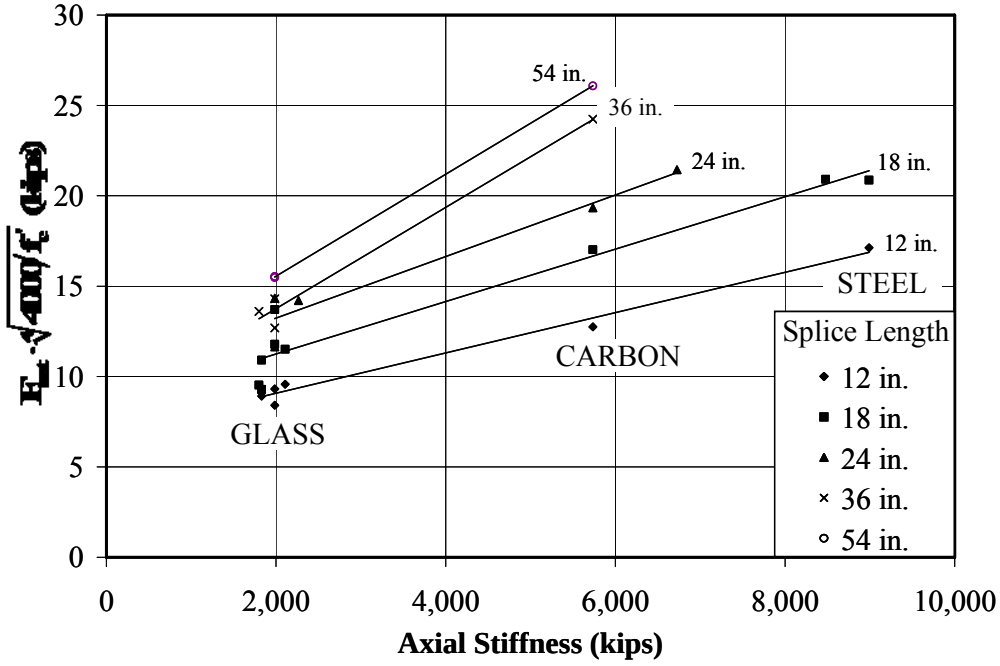

Figure 5.6 Effect of Axial Stiffness on Bond Strength for #5 Bars

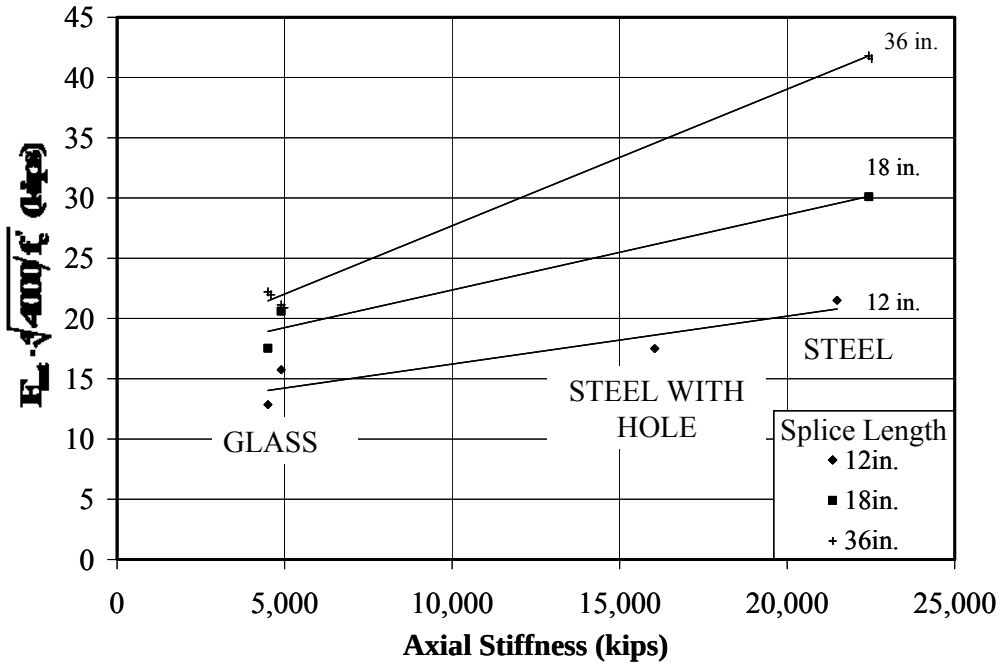

Figure 5.7 Effect of Axial Stiffness on Bond Strength for #8 Bars

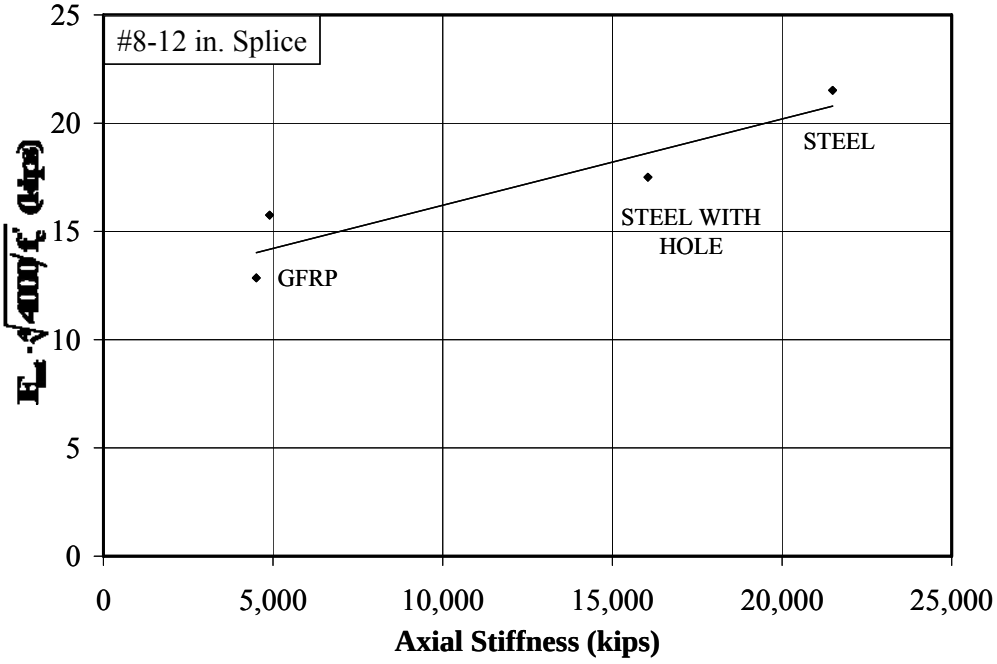

Figure 5.8 Effect of Axial Stiffness on Bond Strength for 12 in. Spliced #8 Bars

5.2.6 Surface Deformation

Four types of surface deformations induced on glass FRP bars were tested to evaluate the effect of surface deformation on splice strength. The deformations included uncoated, wrapped and sand coated, sand coated, and fabric texture coated. Table 5.3 summarizes the experimental results based on their surface deformation. Sand coated as well as wrapped and sand coated glass FRP bars are commercially available from Hughes Brothers Inc. and Pultrall Inc., respectively. Therefore, a complete set of specimens for various splice lengths were tested considering both sand coated bars and wrapped and sand coated bars.

The bar stress reached at failure versus splice length for #5 and #8 Glass FRP bars are plotted in Figure 5.9 and Figure 5.10, respectively. These figures compare the effect of the sand coated bar and the wrapped and sand coated bar on bond strength for various splice lengths. For #5 specimens, the sand coated bars reached higher bond stresses than the wrapped and sand coated bars except for the 54 in. splice specimens which failed at approximately the same load (Figure 5.9). Among the #8 bar reinforced specimens, the

same trend is also apparent; however, among the 36 in. splice specimens, the wrapped and sand coated bar reached a higher bond stress than the sand coated bar.

Table 5.3 Summary of Test Results for Bars with Different Surface Deformations

Bar Size	Specimen	Surface Deformation	L_s (in.)	E_{bar} (ksi)	f_c' (psi)	f_{test} (ksi)	$f_{test(4000)}$ (ksi)
#5	B-G1-2	Wrapped and Sand	12	5900	4100	28.9	28.8
	B-G2-2	Helical Lugs	12	5900	4100	29.5	29.3
	B-HG1-5-12	Wrapped and Sand	12	6400	4170	27.4	27.1
	B-PG1-5-12	Sand Coated	12	6400	4170	30.4	30.0
	B-HO-5-18	Wrapped and Sand	18	5800	5260	32.9	30.7
	B-G1-1	Wrapped and Sand	18	5900	5600	38.3	35.2
	B-G2-1	Helical Lugs	18	5900	5600	32.6	29.9
	B-HN-5-18	Wrapped and Sand	18	6400	5260	40.7	38.0
	B-P-5-18	Sand Coated	18	6400	5260	47.3	44.2
	B-HG1-5-24	Wrapped and Sand	24	6400	4640	39.0	37.6
	B-PG1-5-24	Sand Coated	24	6400	4640	48.0	46.2
	B-HG2-5-24	Fabric Texture	24	7300	4640	47.6	45.8
	B-HO-5-36	Wrapped and Sand	36	5800	5470	47.5	43.9
	B-HN-5-36	Wrapped and Sand	36	6400	5470	44.3	40.9
	B-P-5-36	Sand Coated	36	6400	5470	49.9	46.1
	B-HG1-5-54	Wrapped and Sand	54	6400	4170	50.4	49.9
	B-PG1-5-54	Sand Coated	54	6400	4170	50.6	50.1
#8	B-HG-8-12	Wrapped and Sand	12	5700	4010	16.3	16.3
	B-PG-8-12	Sand Coated	12	6200	4010	20.0	19.9
	B-H-8-18	Wrapped and Sand	18	5700	5260	23.7	22.2
	B-P-8-18	Sand Coated	18	6200	5260	27.9	26.1
	B-H-8-36	Wrapped and Sand	36	5700	5470	30.4	28.1
	B-P-8-36	Sand Coated	36	6200	5470	28.9	26.8

In addition to the commercially available reinforcing bars that have specific surface characteristics, bars were specifically produced for this test program to evaluate the effect of the bar surface. As presented in Table 5.3, the 24 in. spliced #5 fabric texture coated Glass FRP bar (B-HG2-5-24) reached stresses as high as the companion sand coated Glass FRP bar (B-PG1-5-24). Therefore, Glass FRP bars having a fabric surface texture that appears essentially smooth are capable of reaching stresses as high as the sand coated glass FRP bar. This result is surprising if surface texture is considered

alone. As illustrated in Table 5.3, the modulus also varies slightly among the glass FRP bars. Therefore, it is not easy to differentiate the differences based on surface deformation among the different types of bars because other factors such as modulus of elasticity also affect bond behavior. However, it is observed that, the sand coated glass FRP bars in general reached the highest stresses among the deformation types tested in the experimental program.

The bars reinforced with uncoated FRP and plain steel bars failed in pullout instead of a splitting failure in the early stages of loading. Table 5.4 summarizes the test results of these specimens. The bars in the specimens reinforced with plain and uncoated reinforcement reached stresses at failure that were about one third of the companion specimen having a surface deformation. The results from this study clearly indicate the importance of having some level of surface deformation. Once a surface deformation was provided, however, little difference was observed with varying surface deformations. Therefore, the type of bar surface deformation will not be considered in further evaluation of the data and the development of analysis methods.

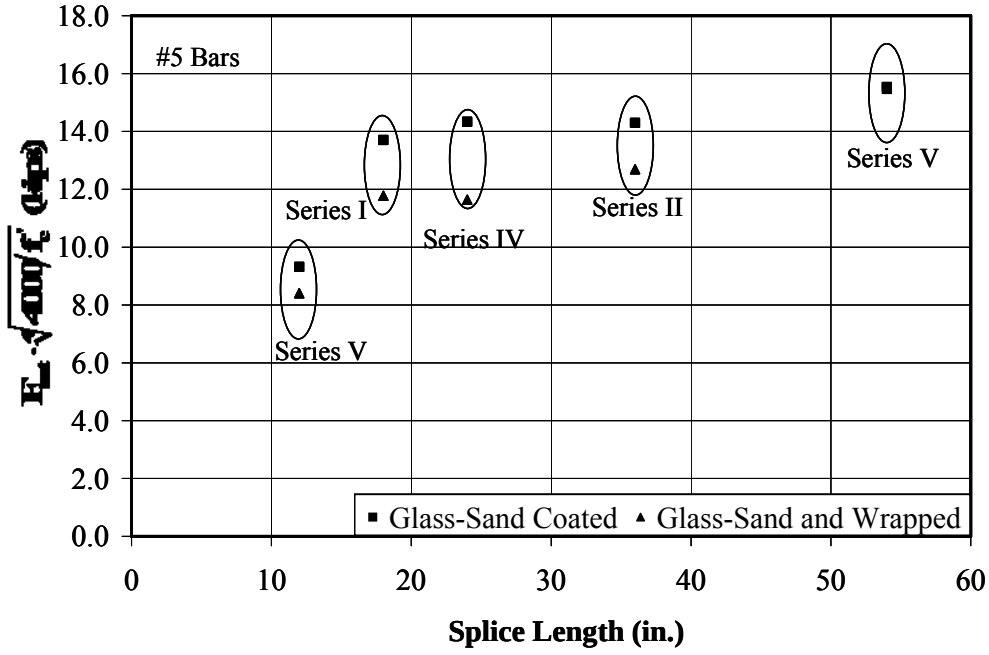

Figure 5.9 Effect of Surface Deformation on Bond Strength for #5 Bars

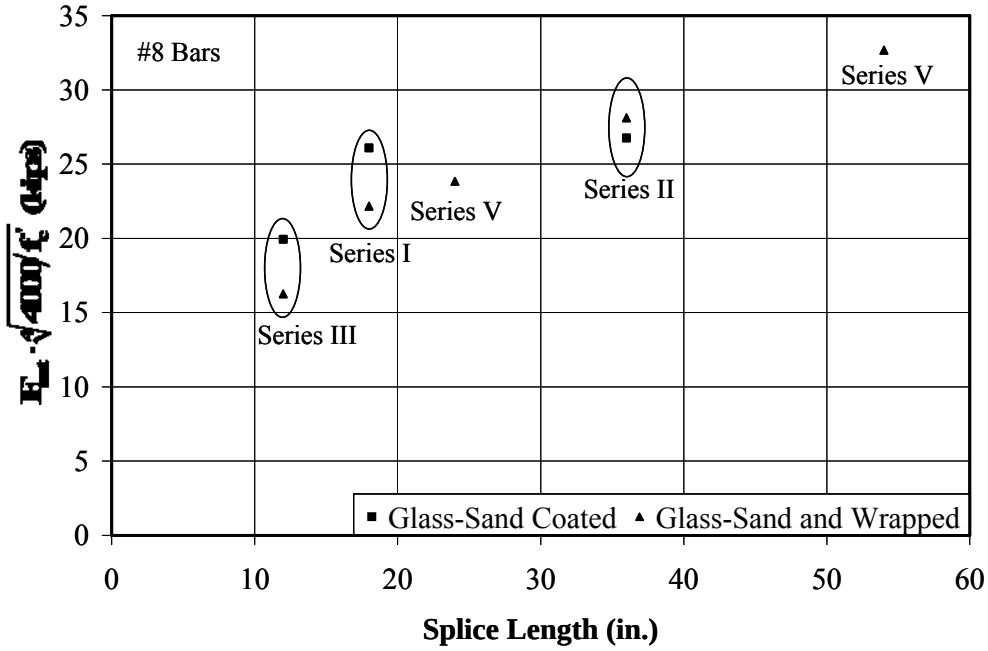

Figure 5.10 Effect of Surface Deformation on Bond Strength for #8 Bars

Table 5.4 Summary of Test Results for Plain Bars

Bar Size	Specimen	L_s (in.)	E_{bar} (ksi)	AE (kips)	f_c' (psi)	f_{test} (ksi)	$f_{test(4000)}$ (ksi)	$F_{test(4000)}$ (kips)
1 in.	B-S4-8-12	12	29600	12728	4010	20.0	20.0	8.60
	B-S3-8-12	12	30500	24095	4010	8.8	8.8	6.95
#5	B-PG2-5-24	24	6500	2015	4640	12.3	11.9	3.68
	B-PC2-5-24	24	22500	6975	4640	15.1	14.6	4.51
	B-HG3-5-24	24	7000	2170	4640	16.1	15.5	4.80

5.2.7 Casting Position

Eight bottom cast specimens were tested along with eight companion top cast specimens to determine the effect of casting position on the behavior of specimens with lap spliced reinforcement. Research by Ferguson and Thompson (1962), Jirsa et al. (1982), and DeVries, Moehle, and Hester (1991) showed that the influence of casting position on bond strength is mainly affected by concrete slump and bleeding of concrete. Table 5.5 presents the experimental values along with water-cement ratio and concrete slump of the concrete batch for each series. In Table 5.5, the bar stress ratio represents the ratio of the stress at failure for the top cast to bottom cast specimens for the companion specimens.

Based on the test results, it is found that the bond strength of top cast specimens is generally lower than that of the bottom cast specimens. However, it should be noted that the reinforcement in two of the top cast specimens in Series III reached higher bar stresses than the companion bottom cast specimens even though the slump of the concrete in Series III was the highest. The bars in the top cast specimens in Series V reached approximately 10% to 22% lower stresses than the bottom cast specimens. Although, the water-cement ratio of Series III and Series V were about the same and the slump of the concrete in Series V was lower than Series III, the top cast specimens in Series V resulted in lower stress ratios than in Series III. The only difference the specimens faced among the series was the curing period. The specimens in Series III were wet cured for three days while the specimens in Series IV and V were cured for seven days. It should be noted that in six of the companion top and bottom cast specimens, the difference in stresses at failure are within 10%.

Based on the observations and test results, it is found that the bottom cast FRP specimens tend to yield higher ultimate bar stresses than top cast specimens. However, the effect of bleeding and concrete slump on bond strength could not be identified for specimens tested in the experimental program.

The effect of casting position on bond strength will not be considered as a parameter for the development of the analysis method for FRP reinforced specimens. Although top cast specimens tend to yield lower bond stresses; difference in bar stresses

at failure between top and bottom cast specimens are within ±10% and are not considered significant. In addition, methods developed considering results from top cast specimens will generally be conservative for bottom cast specimens as they tend to yield lower bond stresses.

Table 5.5 Summary of Bottom and Top Cast Specimens

Series	Specimen	Surface Deformation	Bar Size	L_s (in.)	Casting Position	w/c	Slump (in.)	f'_c (psi)	$f_{test(4000)}$ (ksi)	Stress Ratio
III	B-S1-8-12b	Deformed	#8	12	Bottom	0.46	5.5	4010	26.3	1.00
	B-HG-8-12	Deformed	#8	12	Top				27.2	1.03
	B-PG-8-12b	Sand Coated	#8	12	Bottom				18.4	1.00
	B-PG-8-12	Sand Coated	#8	12	Top				19.9	1.08
	B-HG-8-12b	Wrapped and Sand	#8	12	Bottom				16.9	1.00
	B-HG-8-12	Wrapped and Sand	#8	12	Top				16.3	0.96
IV	B-HG1-5-24b	Wrapped and Sand	#5	24	Bottom	0.56	3.0	4640	40.6	1.00
	B-HG1-5-24	Wrapped and Sand	#5	24	Top				37.6	0.93
	B-PG1-5-24b	Sand Coated	#5	24	Bottom				49.0	1.00
	B-PG1-5-24	Sand Coated	#5	24	Top				46.2	0.94
V	B-PG1-5-12b	Sand Coated	#5	12	Bottom	0.43	4.5	4170	38.6	1.00
	B-PG1-5-12	Sand Coated	#5	12	Top				30.0	0.78
	B-HG1-5-12b	Wrapped and Sand	#5	12	Bottom				34.5	1.00
	B-HG1-5-12	Wrapped and Sand	#5	12	Top				27.1	0.79
	B-HG-8-24b	Wrapped and Sand	#8	24	Bottom				26.4	1.00
	B-HG-8-24	Wrapped and Sand	#8	24	Top				23.8	0.90

5.3 Analysis Methods for Bond Strength

In this section, an analysis method which can be used effectively to evaluate the bond strength of spliced reinforced beams without confinement in the splice region will be developed. The validity of the method will be assessed using both steel and FRP bar reinforced concrete splice beam tests. A steel reinforced beam database was compiled by Canbay and Frosch (2005) which is based on ACI 408 Database 10-2001 (ACI 408R-03) while a FRP reinforced beam database was developed that includes the specimen tested in the experimental program as well as the specimens tested by Mosley (2000) as summarized in Table 5.1.

5.3.1 Steel Reinforced Beam Database

The steel database was developed by Canbay and Frosch (2005) and includes 190 unconfined, uncoated, bottom cast, steel reinforced specimens which failed in splitting. The database is consistent with the ACI 408 Database 10-2001 (ACI 408R-03). However, it also includes 14 additional bottom cast specimens found in the literature. All beams were loaded with two concentrated loads to create a constant moment region throughout the splice length.

The database was investigated to identify specimens where yielding of the bars occurred before bond failure. In twenty six of the specimens the reinforcement yielded before bond failure. These specimens were separately considered.

The steel reinforced beam tests used in the database are summarized in Table 5.6. The references from where the test data was obtained, the range of variables (L_s, d_b, f_c', and c), and the number of test specimens considered from each reference are listed. The concrete cover c listed in Table 5.6 is defined as the smaller of the concrete clear cover or half the spacing of the reinforcement. Detailed information regarding each specimen including section properties, yield stress of the reinforcement, and ultimate bar stresses at failure are presented in Appendix G.

Table 5.6 Summary of the Steel Beam Database

Reference	Total Number of Tests	Yielded Bars	Splice Length L_s, (in.)	Bar Diameter d_b, (in.)	f_c' (ksi)	Concrete Cover c, in.
Chinn, Ferguson, and Thompson (1955)	32	2	0.5 to 24.0	0.375 to 0.750	3.16 to 7.48	0.50 to 2.94
Chamberlin (1958)	2	-	6.0	0.500	4.37 to 4.45	0.50 to 2.50
Ferguson and Breen (1965)	26	8	18.0 to 82.5	1.000 to 1.410	2.61 to 4.65	1.31 to 4.70
Ferguson and Krishnaswamy (1971)	4	-	15.0 to 98.0	0.625 to 2.257	2.71 to 3.22	0.83 to 4.61
Thompson et al. (1975)	11	-	12.0 to 60.0	0.750 to 1.693	2.87 to 4.71	2.00 to 4.00
Treece and Jirsa (1989)	2	-	18.0 to 36.0	1.410	4.29 to 9.60	2.00 to 2.01
Cleary and Ramirez (1991)*	4	2	10.0 to 16.0	0.750	3.99 to 8.20	2.00 to 3.25
Choi et al. (1991)	8	1	12.0 to 24.0	0.625 to 1.410	5.36 to 6.01	1.00 to 2.00
Hester et al. (1993)	7	-	16.0 to 22.8	1.000	5.24 to 6.45	1.50 to 4.00
Rezansoff, Akanni, and Sparling (1993)	4	-	29.5 to 44.3	0.990 to 1.180	3.73 to 4.03	0.99 to 2.01
Hwang, Lee, and Lee, (1994)*	4	-	11.8	1.130	9.24 to 12.18	1.13 to 1.14
Darwin et al. (1996)	12	-	16.0 to 40.0	0.625 to 1.410	3.83 to 5.25	1.02 to 3.06
Hamad and Mansour (1996)*	3	-	11.8 to 13.8	0.551 to 0.787	2.90 to 3.35	0.79 to 4.69
Hamad and Itani (1998)	8	-	12.0	0.984	7.59 to 11.12	1.50 to 1.58
Hamad and Machaka (1999)*	3	-	12.0	0.984	6.77 to 13.46	1.02 to 1.10
Azizinamini et al. (1999)	32	12	10.0 to 80.0	1.000 to 1.410	5.08 to 15.59	1.00 to 3.36
Zuo and Darwin (2000)	28	1	16.5 to 40.0	0.625 to 1.410	4.25 to 15.65	0.51 to 4.05
Total	190	26	5.5-98.0	0.375 to 2.257	2.61 to 15.65	0.50 to 4.70

* Added to the ACI 408 Database 10-2001 (ACI 408-2003)

The characteristics of the database were examined by evaluating the distribution of the available data because the applicability of the conclusions derived from use of the database depends on the frequency distribution of the parameters which influence bond strength. The frequency distribution of f_c', d_b, and L_s/d_b are illustrated in Figure 5.11 through Figure 5.13. It can be seen from the graphs that there are concentrations of data within certain ranges for all three variables (f_c', d_b, and L_s/d_b) that affect bond strength. First, the majority of the tests in the database have concrete compressive strengths in the range of 3,000 psi to 6,000 psi, the range which is usually considered normal strength concrete. However, it is also important to note that the database includes 51 specimens (26% of the data) which have concrete compressive strengths higher than 10,000 psi. Therefore, the conclusions derived from the analysis should also be applicable for specimens with high strength concrete. Second, eighty-nine percent of the specimens were reinforced with #6, #8, or #11 bars. Finally, the data is also concentrated in the range of L_s/d_b ratios from 10 to 40. Because a splitting failure is the desired failure mechanism for splice tests, this range of L_s/d_b ratios is reasonable to promote splitting failure in unconfined concrete. The spacing and cover dimensions which are also important factors influencing bond strength will be discussed in the following sections.

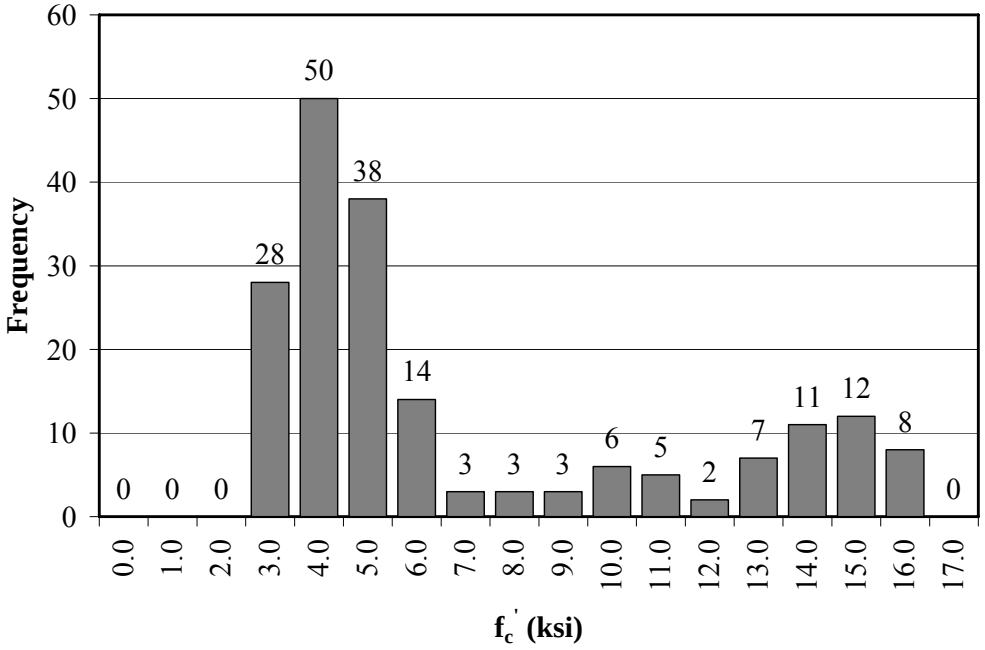

Figure 5.11 Frequency Distribution of Concrete Strength (Steel Database)

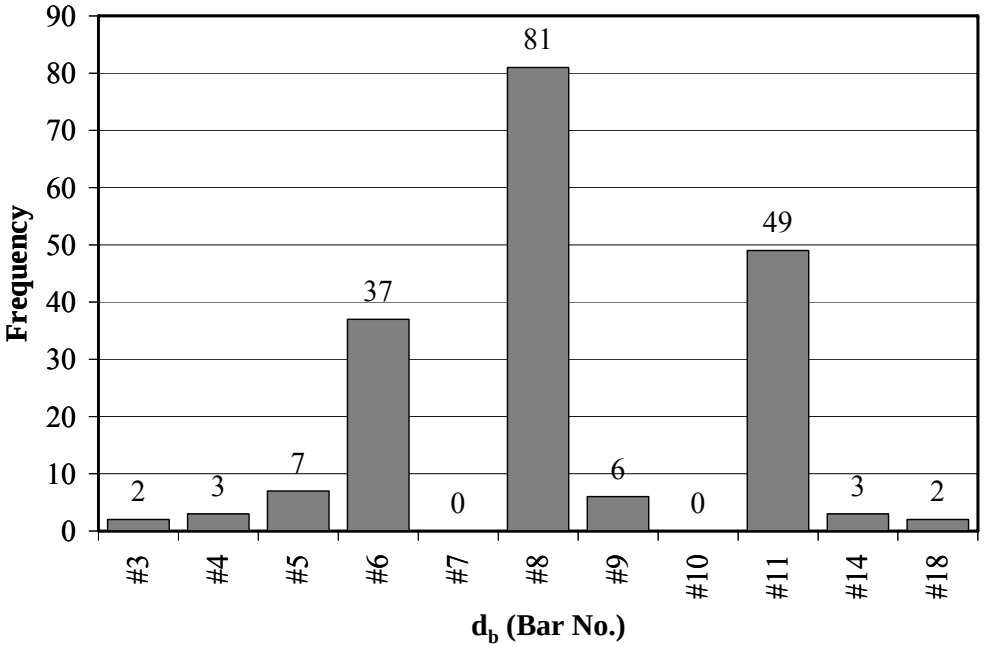

Figure 5.12 Frequency Distribution of Bar Diameter (Steel Database)

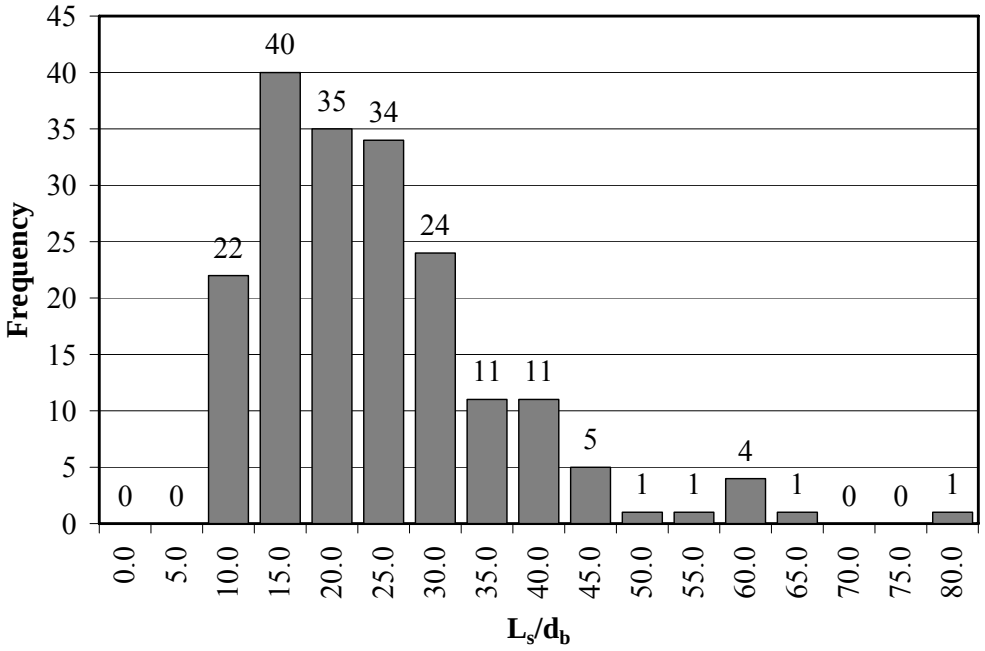

Figure 5.13 Frequency Distribution of L_s/d_b ratio (Steel Database)

Scatter in the database was also investigated by evaluating specimens with the same bar size, cover and spacing dimensions, and cross sectional properties, as well as similar concrete strengths. Specimens found in the database with similar properties are grouped and presented in Table 5.7. The ratio shown in the table presents the ratio of the bar stress at failure to the lowest bar stress in each group. As presented, the ratio of highest to lowest stress in each group varies from 1 to 1.46. The highest ratio was obtained in Group 3, followed by Group 2, and then Group 8. It is interesting that for Group 2 and 3, the specimens were tested to evaluate the effect of silica fume on bond strength where for Group 8, the effect of aggregate type was investigated. It is important to keep in mind that the database does not specify the aggregate type and concrete mix design proportions for specimens as these variables are typically not considered during the design of lap splice and development length. Furthermore, significant scatter was only observed for the specimens with concrete strengths higher than 10,000 psi.

Considering only the concrete strengths lower than 10,000 psi, a maximum scatter of approximately 6% was demonstrated.

Table 5.7 Specimens in the Database Grouped with Similar Properties

Group	Specimen	Ls (in.)	d_b (in.)	c_{so} (in.)	c_{si} (in)	c_b (in.)	f_c' (psi)	f_{test} (ksi)	Ratio
1	S33-N-U	11.8	1.13	1.13	1.14	1.13	10310	40.17	-
	P28-N-M	11.8	1.13	1.13	1.14	1.13	10237	43.21	1.08
2	C0S16	12.0	0.98	1.02	1.10	1.02	12415	40.42	-
	C0S8	12.0	0.98	1.02	1.10	1.02	13459	52.48	1.29
3	SC-20-B-SP4	12.0	0.98	1.50	1.57	1.50	11081	38.66	-
	SC-10-B-SP2	12.0	0.98	1.50	1.57	1.50	11124	51.64	1.34
	SC-05-B-SP2	12.0	0.98	1.50	1.57	1.50	11124	56.69	1.46
4	18	19.0	1.00	2.00	2.00	2.00	15591	66.96	-
	19	19.0	1.00	2.00	2.00	2.00	15591	67.33	1.01
5	4-11C0-24-0-U	24.0	1.41	2.00	2.00	2.00	5850	37.82	-
	4-11S0-24-0-U	24.0	1.41	2.00	2.00	2.00	5850	40.22	1.06
6	38.2-B-S-U	26.0	1.00	2.13	1.84	2.08	5080	60.13	-
	36.3-B-S-U	26.0	1.00	2.02	1.84	2.00	5060	62.34	1.00
7	2a	29.5	0.99	1.83	0.99	2.01	3958	58.56	-
	2b	29.5	0.99	1.83	0.99	2.01	3799	58.63	1.00
8	28.5-B-S-U	30.0	1.41	1.98	4.03	2.0	12610	51.2	-
	30.5-B-S-U	30.0	1.41	2.06	4.02	1.96	13220	67.3	1.31
9	4	32.0	1.00	1.00	1.50	1.00	15591	67.28	-
	3	32.0	1.00	1.00	1.50	1.00	15591	69.08	1.03
10	40	36.0	1.41	1.41	1.68	1.41	14550	57.21	-
	42	36.0	1.41	1.41	1.68	1.41	14550	57.47	1.00
11	16.2	40.0	1.41	3.02	2.97	1.90	5180	52.38	-
	15.5	40.0	1.41	3.06	2.98	1.91	5250	54.12	1.03

5.3.2 FRP Beam Database

The FRP database includes 43 splice specimens reinforced with FRP bars having some level of surface deformation. The database were composed from 34 specimens tested in the experimental program and 9 specimens tested by Mosley (2000). All of the specimens failed in splitting. Thirty-two specimens were reinforced with #5 bars while the remaining 11 were reinforced with #8 bars. Detailed information regarding each specimen including section properties, type of surface deformation, and ultimate bar stresses at failure are presented in Appendix H.

The database consists of 36 top cast specimens and 7 bottom cast specimens. The frequency distribution of the bar type, f_c', and L_s/d_b are illustrated in Figure 5.14 through Figure 5.16. As shown, the majority of the specimens in the database were reinforced with glass FRP bars. The database includes 3 aramid FRP reinforced specimens and 6 carbon FRP reinforced specimens in addition to the 34 glass FRP reinforced specimens. Tests in the database have concrete compressive strengths in the range of 4,000 psi to 6,000 psi, the range which is usually considered normal strength concrete. L_s/d_b ratios vary from 12 to 86; however, the data is concentrated in the range of L_s/d_b ratios from 10 to 40, similar to the steel database.

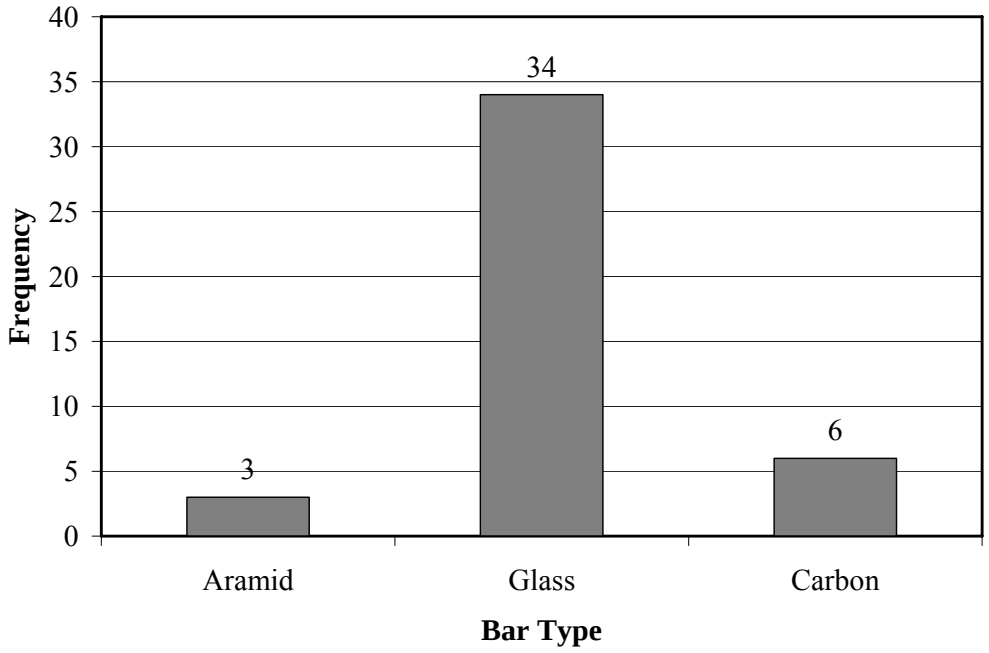

Figure 5.14 Frequency Distribution of Bar Type (FRP Database)

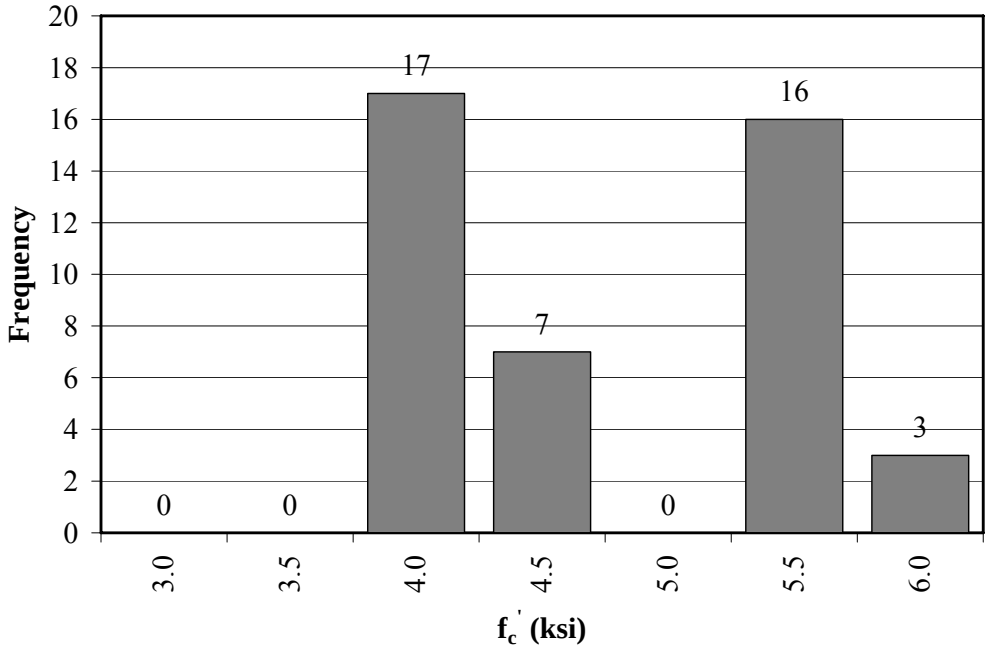

Figure 5.15 Frequency Distribution of Concrete Strength (FRP Database)

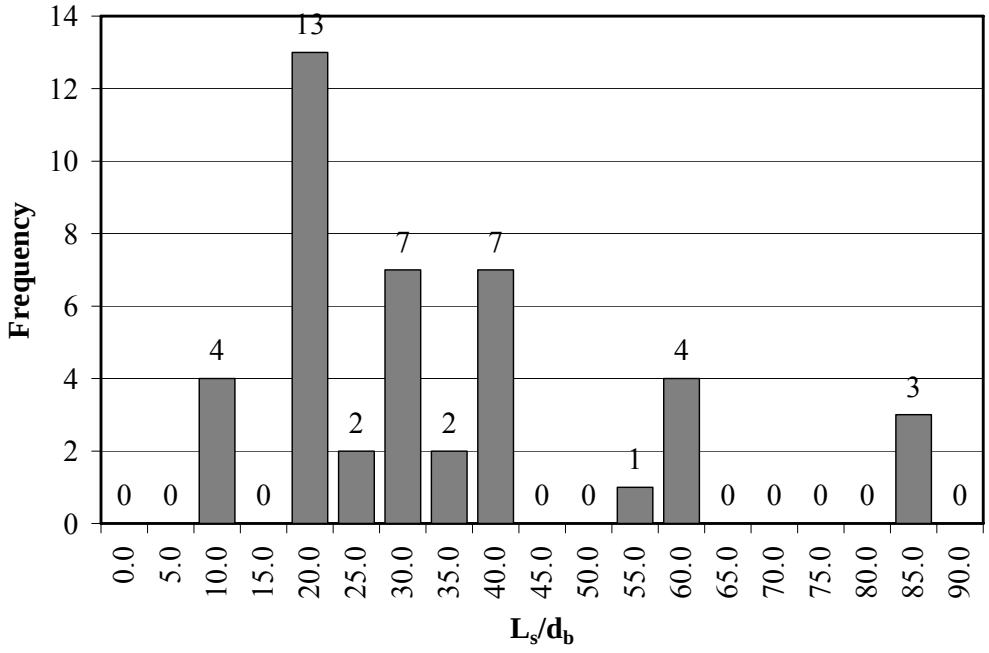

Figure 5.16 Frequency Distribution of L_s/d_b Ratio (FRP Database)

5.3.3 Descriptive Equations

The most commonly used modeling approaches for the calculation of bond stresses are those by Orangun, Jirsa, and Breen (1977) and Zuo and Darwin (2000). In addition to those equations, an expression developed by Canbay and Frosch (2005) are provided in this section for comparison purposes. The various analysis tools will be used as a basis of comparison for analytical models developed as part of this study.

The development length equation in ACI 318 is based on the equation developed by Orangun, Jirsa, and Breen (1977). The Orangun, Jirsa, and Breen equation was previously discussed in Section 4.2.1 and was presented as Equation (4-1).

The ACI Committee 408 design provisions are based on a study conducted by Zuo and Darwin (2000). Zuo and Darwin investigated the effects of concrete strength, coarse aggregate quantity and type, and reinforcing bar geometry on splice strength. Their expression is based on regression analysis of both unconfined and confined test data. The expression for unconfined specimens is shown in the following equation:

$$\frac{A_b f_s}{\sqrt[4]{f_c'}} = \left[59.8 l_s \left(c_{\min} + 0.5 d_b\right) + 2350 A_b\right]\left(0.1\frac{c_{\max}}{c_{\min}} + 0.9\right) \qquad (5\text{-}1)$$

where:

$$0.1\frac{c_{\max}}{c_{\min}} + 0.9 \quad \leq \quad 1.25$$

A_b = *area of spliced reinforcement, in*^{2}.

c_b = *bottom cover, in.*

c_{min}, c_{max} = *minimum or maximum value of* c_s *or* c_b, *in.*

c_s = *min*(c_{si} + 0.25, c_{so})

c_{si} = *half of the clear spacing between bars, in.*

c_{so} = *clear side cover of reinforcing bars, in.*

d_b = *nominal diameter of reinforcing bars, in.*

f_c' = *specified compressive strength of concrete, psi*

f_s = bar stress at failure, psi

ℓ_s =splice or development length in tension of deformed bar, in.

Canbay and Frosch (2005) developed an expression based on a physical model of tension cracking of concrete in the lapped splice region. The equation is a function of cover and spacing dimensions, concrete compressive strength, bar diameter, splice length, and number of spliced bars. The expression is presented as follows:

Side Split Failure:

$$F_{splitting} = \ell_s^* \cdot \left[2 \cdot c_{so}^* + (N_b - 1) \cdot 2 \cdot c_{si}^*\right] \cdot 6\sqrt{f_c'}$$

Face Split Failure:

$$F_{splitting} = \ell_s^* \cdot \left[2 \cdot c_b^* \cdot \left(0.1 \cdot \frac{c_{so}}{c_b} + 0.9\right) + 2 \cdot c_b^* \cdot (N_b - 1) \cdot \left(0.1 \cdot \frac{c_{si}}{c_b} + 0.9\right)\right] \cdot 6\sqrt{f_c'}$$

$$f_b = \frac{F_{splitting}}{\tan\beta \cdot N_b \cdot A_b} \qquad (5\text{-}2)$$

where:

$$\ell_s^* = \ell_s \cdot \frac{33}{\sqrt{\frac{\ell_s}{d_b}} \cdot \sqrt[4]{f_c'}}$$

$$c_b^* = c_b \cdot \frac{0.8}{\sqrt{\frac{c_b}{d_b}}} \quad , \qquad c_{so}^* = c_{so} \cdot \frac{0.8}{\sqrt{\frac{c_{so}}{d_b}}} \quad , \qquad c_{si}^* = c_{si} \cdot \frac{0.8}{\sqrt{\frac{c_{si}}{d_b}}}$$

The following restrictions apply to the equation.

$$\frac{0.8}{\sqrt{\frac{c}{d_b}}} \le 1.0 \ , \qquad \frac{33}{\sqrt{\frac{\ell_s}{d_b}} \cdot \sqrt[4]{f_c'}} \le 1.0 \ , \qquad \left(0.1\frac{c_s}{c_b} + 0.9\right) \ge 1.0$$

A_b = *area of spliced reinforcement, in*^{2}.

c_b = *bottom cover, in.*

c_s = *min*(c_{si} + 0.25, c_{so})

c_{si} = *half of the clear spacing between bars, in.*

c_{so} = *clear side cover of reinforcing bars, in.*

d_b = *nominal diameter of reinforcing bars, in.*

f'_c = *specified compressive strength of concrete, psi*

f_b = *bar stress at failure, psi*

ℓ_s =*splice or development length in tension of deformed bar, in.*

N_b = *number of spliced bars*

β = *20 degrees*

The basic form of Equation (5-2) can be obtained without using the modification factors for the cover and bar spacing. The expressions for both the side and face splitting failure modes for the basic form are presented as follows:

Side Split Failure (Basic Equation):

$$F_{splitting} = \ell_s \cdot \left[2 \cdot c_{so} + \left(N_b - 1 \right) \cdot 2 \cdot c_{si} \right] \cdot 6\sqrt{f'_c}$$

Face Split Failure (Basic Equation):

$$F_{splitting} = \ell_s \cdot \left[2 \cdot c_b + 2 \cdot c_b \cdot \left(N_b - 1 \right) \right] \cdot 6\sqrt{f'_c}$$

5.3.4 Analysis Method

Several observations made in Section 5.2 provide the basis for the development of an analytical model:

1. As the axial stiffness of the reinforcing bar increases, the bar force obtained at failure increases.
2. The effect of splice length on ultimate stress reached by the reinforcement is a function of the axial stiffness of the reinforcement.

As the effect of splice length on the ultimate bar force is different for bars with different axial stiffness, splice length by itself is not the appropriate measure of bond strength. Therefore, the definition of equivalent splice length, L_{eq}, which is a function of the axial stiffness of the reinforcing bar, is introduced in this section. L_{eq} is defined as follows:

$$L_{eq} = L_s \frac{E_b A_b}{E_{ref} A_{ref}} \tag{5-3}$$

where:

A_b = *area of spliced reinforcement, in.*^{2}

A_{ref} = *area of reference reinforcement, in.*^{2}

E_b = *modulus of elasticity of the spliced reinforcement, ksi*

E_{ref} = *modulus of elasticity of reference reinforcement, ksi*

L_{eq} = *equivalent splice length, in.*

L_s = *splice length, in.*

In other words, L_{eq} is the splice length required for the reference reinforcement (E_{ref}, A_{ref}) to reach the same bar force as the reinforcement (E_b, A_b) having a splice length of L_s.

The reference reinforcement in this study was chosen as the #5 wrapped and sand coated glass FRP bar which had the lowest axial stiffness tested in the experimental program. Although (EA) in the denominator can be assumed any value, by choosing the

glass FRP bar, the evaluation of the data will be more meaningful considering the FRP reinforced specimens tested in the experimental program.

Equation (5-3) may be written in terms of the cross-sectional area and modulus of elasticity of the reinforcement by substituting the properties of the reference reinforcement into the equation.

A_{ref} = 0.31 in.^{2} (area of a #5 bar)

E_{ref} = 5,800 ksi (modulus of elasticity of wrapped and sand coated Glass FRP)

$$L_{eq} = \frac{L_s E_b A_b}{1800} \tag{5-4}$$

In Figure 5.17, bar force at failure normalized at a concrete compressive strength of 4,000 psi versus the equivalent splice length, L_{eq}, is presented for steel reinforced specimens contained in the database. Yielded specimens were not included in this analysis. The range of splice length and normalized bar force are adjusted in Figure 5.18 so that the scatter in the data can be better observed.

A trend line was obtained using regression analysis, and the equation as well as the trend line are shown in Figure 5.17. It is observed that there is good correlation between the equivalent splice length and the normalized bar force at failure even though the cover and spacing parameters were not included in the analysis. Eligehausen, Popov, and Bertero (1983) investigated the effect of bar spacing on bond strength and concluded that increasing the bar spacing from one bar diameter to four times the bar diameter resulted in an increase in the bond resistance of approximately 20%. Therefore, the cover and bar spacing may account for some of the variation observed in Figure 5.17 and Figure 5.18. The effect of cover and spacing will be discussed further in a later section.

The resulting equation from a best fit curve for the steel database is as follows:

$$F_b \cdot \sqrt[4]{4000 / f_c'} = 1.39 \cdot L_{eq}^{\ 0.59} \tag{5-5}$$

where:

$$L_{eq} = \frac{L_s E_b A_b}{1800}$$

A_b = *area of spliced reinforcement, in.*^{2}

E_b = *modulus of elasticity of the spliced reinforcement, ksi*

F_b = *bar force at failure, kips*

L_s = *splice length, in.*

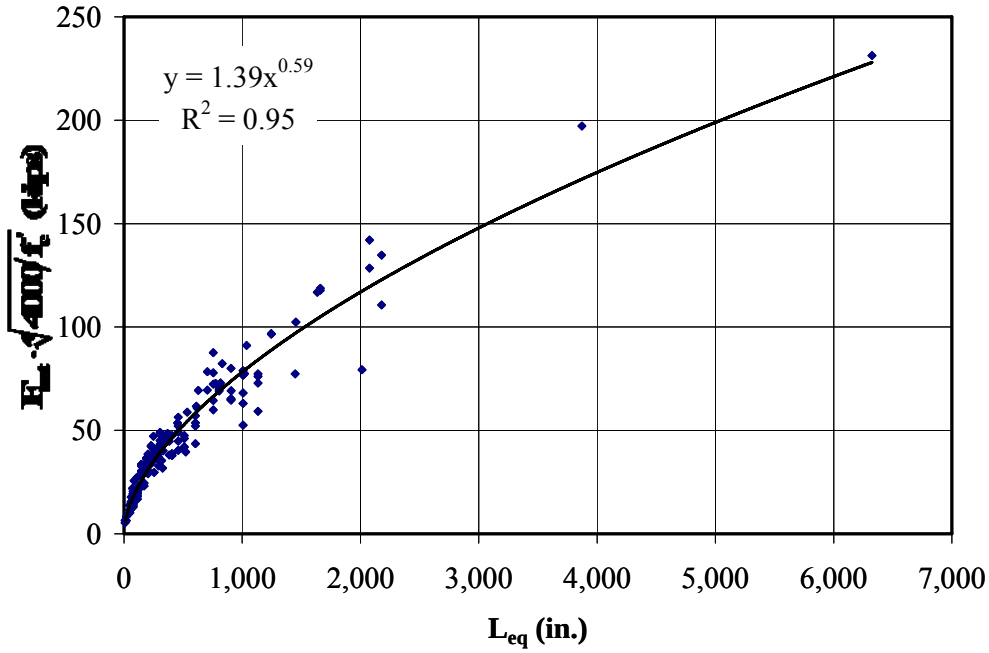

Figure 5.17 Normalized Bar Force versus Effective Splice Length (Steel Database)

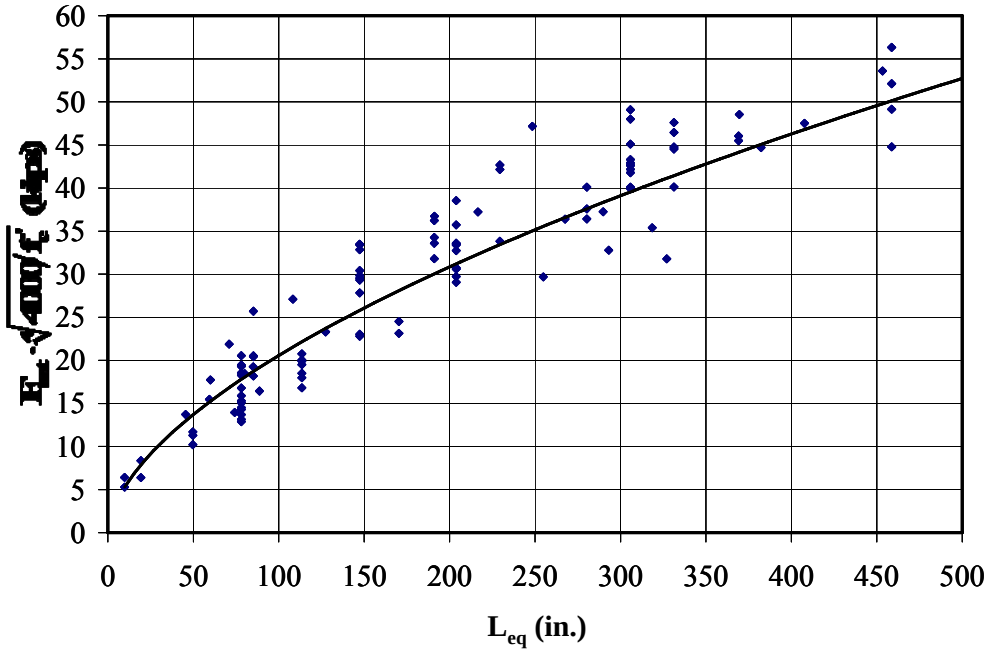

Figure 5.18 Normalized Bar Force versus Effective Splice Length, Zoomed (Steel Database)

Equation (5-5) was derived from the database without considering the effect of cover and spacing dimensions. The calculated bar stress obtained using the derived equation is compared with results obtained by the basic equation proposed by Canbay and Frosch (2005) and the Orangun, Jirsa, and Breen (1977) equation for the steel database. It is important to note that the ACI building code equations were not used to evaluate the performance of the derived expression because the equations in the code are design expressions and are not appropriate for predicting behavior. Figure 5.19 presents the comparison of the proposed equations by Canbay and Frosch (2005), Orangun, Jirsa, and Breen (1977), and Equation (5-5). The horizontal axis in Figure 5.19 shows the ratio of the measured to calculated reinforcement stress while the vertical axis presents the frequency of the test specimens between particular f_{test}/f_{calc} ratios. As can be seen in Figure 5.19, Equation (5-5) provides very reasonable results and provides estimates with similar accuracy as the Canbay and Frosch (2005) basic equation and the Orangun, Jirsa,

and Breen (1977) equation. In addition, the scatter of the ratio of experimental to calculated stress obtained from Equation (5-5) is less than the other methods.

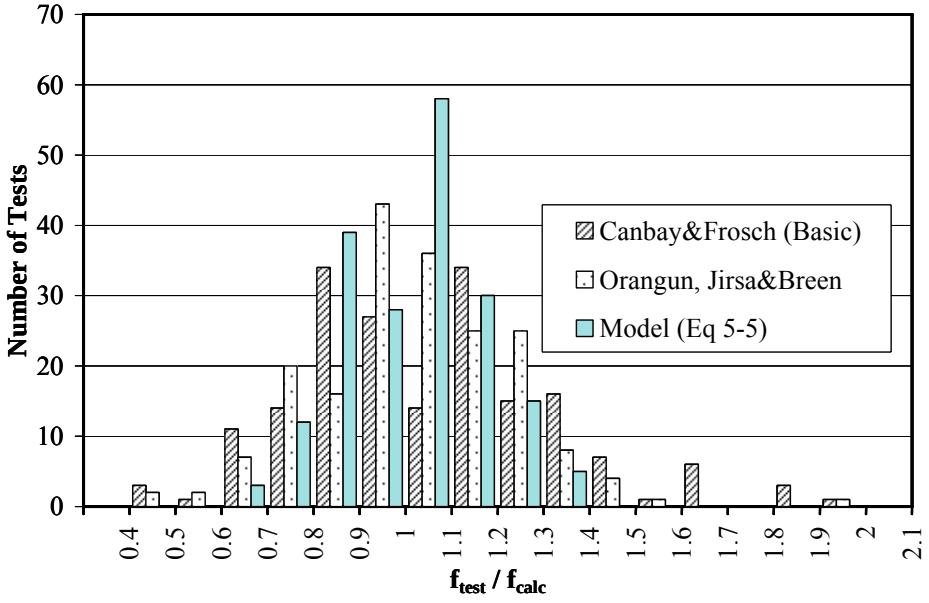

Figure 5.19 Comparison of Canbay and Frosch (2005), Orangun, Jirsa, and Breen (1977), and Equation (5-5) (Steel Database)

5.3.4.1 Effect of Concrete Strength

The effect of the concrete compressive strength on splice strength was further investigated to determine the appropriateness of the fourth root normalized bar forces and stresses. Using the results from the steel database, an analysis was performed to evaluate the optimum power of the concrete compressive strength used to normalize the bar force. It was found that a power of 0.243 resulted in the highest correlation coefficient. It has generally been accepted that the effect of concrete compressive strength on bond strength is represented using the square root of concrete compressive strength, $\sqrt{f_c'}$. Therefore, for comparison purposes, the bar force normalized by the square root of the concrete compressive strength versus equivalent splice length is plotted in Figure 5.20. From a

comparison of Figure 5.17 and Figure 5.20, it is evident that the fourth root of concrete compressive strength represents the data better than the square root. Furthermore, the correlation coefficient (R^2) for the data normalized with the fourth root is higher than that for the data normalized with the square root. Therefore, test results were normalized with the fourth root of the concrete compressive strength for all further investigations including those investigating the effects of the concrete cover and the equivalent splice strength.

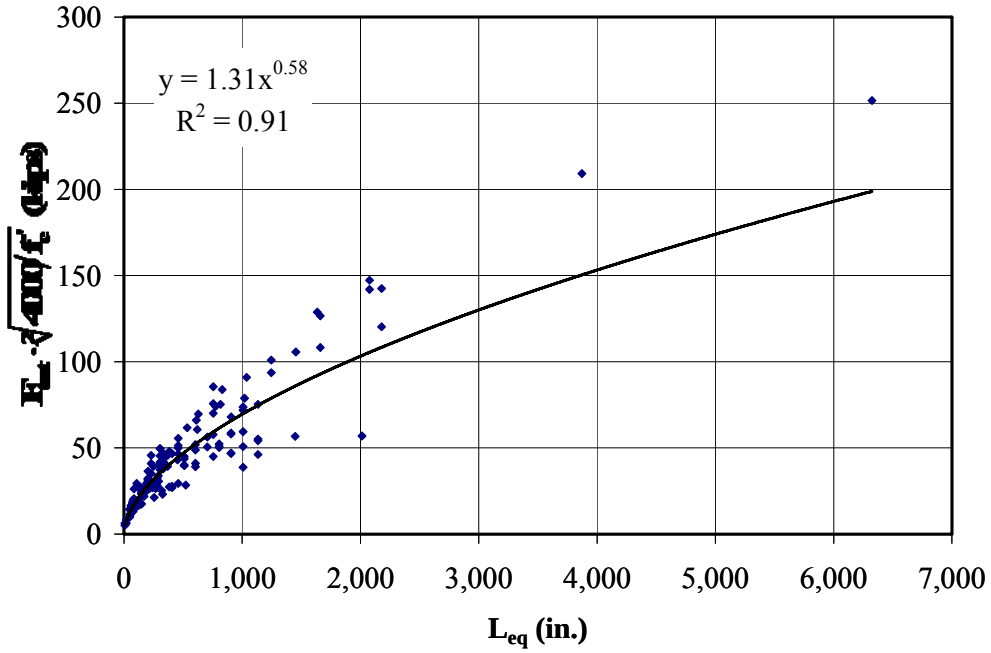

Figure 5.20 Bar Force Normalized with $\sqrt[4]{f_c'}$ versus Effective Splice Length

5.3.4.2 Effect of Concrete Cover

The specimens in the database failed in either side or face splitting; however, to investigate the effect of concrete cover, the specimens need to be grouped according to their failure modes. Two splitting modes are presented in Figure 5.21. Side splitting occurs as a horizontal crack develops at the level of the bars while face splitting occurs when a vertical crack develops in the cover along the length of the splice region.

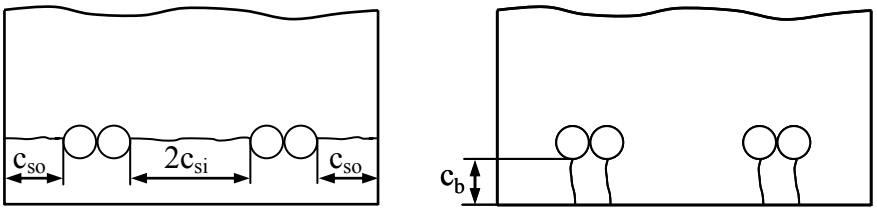

(a) Side Splitting **(b) Face Splitting**

Figure 5.21 Splitting Failure Types

It is generally assumed that a specimen fails in side splitting if the area of the side splitting plane (Eq. (5-6)) is lower than the area of the face splitting plane (Eq. (5-7)); otherwise, the specimen fails in face splitting.

The range of cover and cover to bar diameter in the database are presented in Table 5.8. It is important to note that the specimens included in the database have a minimum side cover to bar diameter (c_{so}/d_b) and spacing to bar diameter ratio ($2c_{si}/d_b$) of 1.00 and a face cover to bar diameter ratio (c_b/d_b) of 0.71. All specimens in the database satisfy the minimum spacing requirement for ACI 318-05 (d_b or 1 in.). Therefore, the conclusions drawn from this analysis are valid only for reinforced concrete specimens which satisfy the minimum spacing requirements of ACI 318-05.

Table 5.8 Range of Cover and Spacing Dimensions in the Steel Database

	c_{so} (in.)	$2c_{si}$ (in.)	c_b (in.)	c_{so}/d_b	$2c_{si}/d_b$	c_b/d_b
Minimum	0.50	1.00	0.56	1.00	1.02	0.71
Maximum	4.50	9.40	3.00	5.00	17.00	3.06

The effect of splice length is directly incorporated into Equation (5-5); therefore, only cover and spacing dimensions were used in this section to evaluate behavior. The equation implicitly includes the effect of minimum cover and spacing dimensions. The cover and bar spacing dimensions will be used to modify the expression to obtain improved estimations for specimens with cover and bar spacing dimensions other than minimum.

The specimens that failed in side and face splitting were grouped as follows:

Side Splitting Plane:

$$A_{side} = \left[2c_{so} + (N_b - 1) \cdot 2c_{si}\right] L_s \tag{5-6}$$

Face Splitting Plane:

$$A_{face} = 2N_b c_b L_s \tag{5-7}$$

where:

A_{face} = *area of face splitting plane, in.*^{2}

A_{side} = *area of side splitting plane, in.*^{2}

c_b = *bottom cover, in.*

c_{si} = *half of the clear spacing between bars, in.*

c_{so} = *clear side cover of reinforcing bars, in.*

L_s = *splice length, in.*

N_b = *number of spliced bars*

$$\textit{Failure Criteria} = \begin{cases} \textit{Side Splitting Failure} & \textit{if} \quad \dfrac{A_{side}}{A_{face}} < 0.95 \\ \textit{Undecided} & \textit{if} \quad 0.95 \le \dfrac{A_{side}}{A_{face}} \le 1.05 \\ \textit{Face Splitting Failure} & \textit{if} \quad \dfrac{A_{side}}{A_{face}} > 1.05 \end{cases}$$

It is important to note that reinforcing bars in 26 of the specimens yielded before failure; therefore, those data points were excluded for this analysis. It is assumed that if the area of the splitting planes are within 5% of each other, the failure of the specimens are considered undecided. Failure mode computed according to the failure criteria were shown to be consistent with those reported. Using the failure criteria outlined above, the remaining 164 specimens in the database were grouped according to their failure mode: 37 side splitting and 83 face splitting. Forty-four specimens were listed as undecided,

failing in either side or face splitting. These undecided specimens were excluded from the cover and spacing analysis.

For the specimens that failed in side splitting, the ratio of the experimental to calculated bar forces versus spacing ($2c_{si}$) and spacing to bar diameter ratio ($2c_{si}/d_b$) are presented in Figure 5.22. For specimens that failed in face splitting, the effect of twice the cover ($2c_b$) and twice the cover to bar diameter ratio ($2c_b/d_b$) on splice strength are illustrated in Figure 5.23. Equation (5-5) was used for the calculated bar force at failure. As shown in both Figure 5.22 and Figure 5.23, as the cover is increased, there is an increase in the F_{test}/F_{calc} ratio.

The trend of the data is plotted with a best fit line. The derived equations and r^2 values are also provided. Based on analysis of the data, it was found that that the cover to bar diameter ratio (c/d_b) reflects the trend of the data slightly better. Based on this analysis, modification factors can be derived to incorporate the effects of the cover and bar spacing.

$$M_{side} = 0.16\left(\frac{c_{si}}{d_b}\right) + 0.84 \tag{5-8}$$

$$M_{face} = 0.20\left(\frac{c_b}{d_b}\right) + 0.71 \tag{5-9}$$

The modification factors are incorporated in Equation (5-5) and give the following equations.

For side splitting failure:

$$F_b \cdot \sqrt[4]{4000/f_c'} = 1.39 \cdot L_{eq}{}^{0.59}\left(0.16\left(\frac{c_{si}}{d_b}\right) + 0.84\right)$$

For face splitting failure: (5-10)

$$F_b \cdot \sqrt[4]{4000/f_c'} = 1.39 \cdot L_{eq}{}^{0.59}\left(0.20\left(\frac{c_b}{d_b}\right) + 0.71\right)$$

where:

$$L_{eq} = \frac{L_s E_b A_b}{1800}$$

A_b = *area of spliced reinforcement, in.*^{2}

c_b = *bottom cover, in.*

c_{si} = *half of the clear spacing between bars, in.*

d_b = *bar diameter, in.*

E_b = *modulus of elasticity of the spliced reinforcement, ksi*

F_b = *bar force at failure, kips*

L_{eq} = *equivalent splice length, in.*

L_s = *splice length, in.*

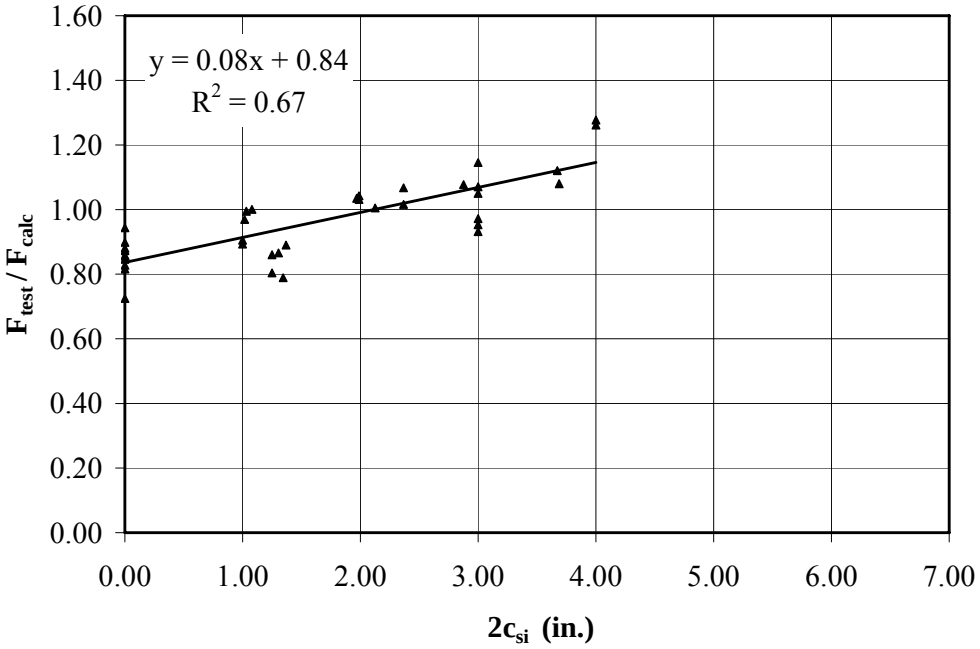

(a) Bar Spacing

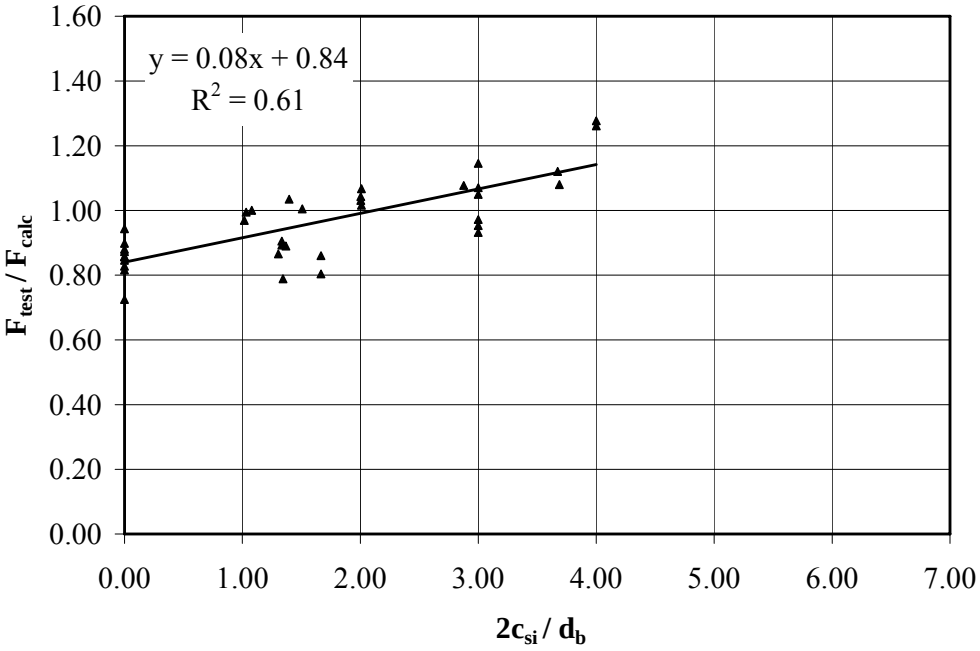

(b) Ratio of Spacing to Bar Diameter

Figure 5.22 Effect of Spacing on Splice Strength

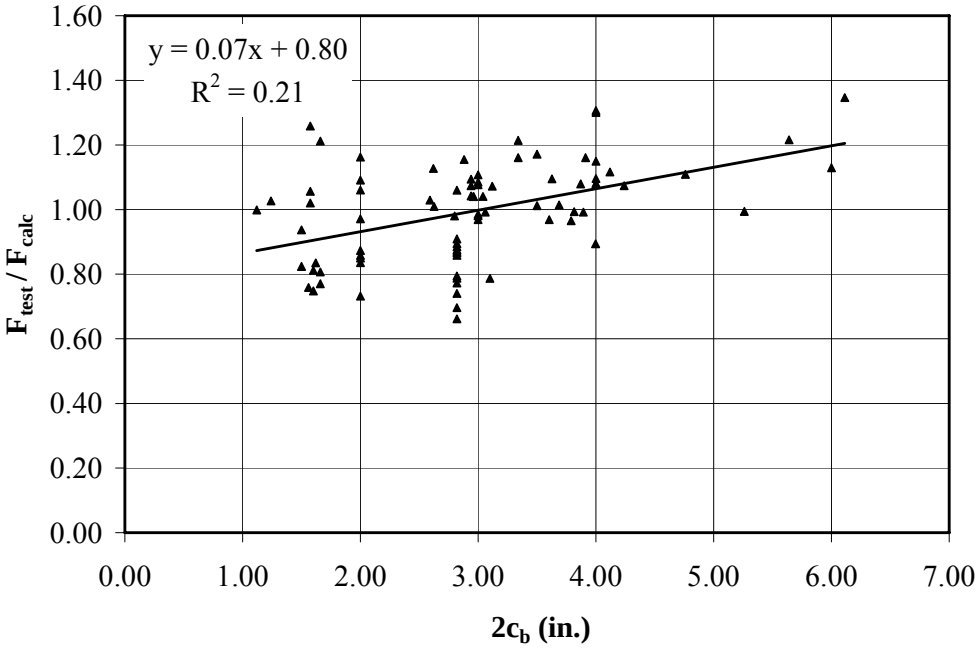

(a) Face Cover

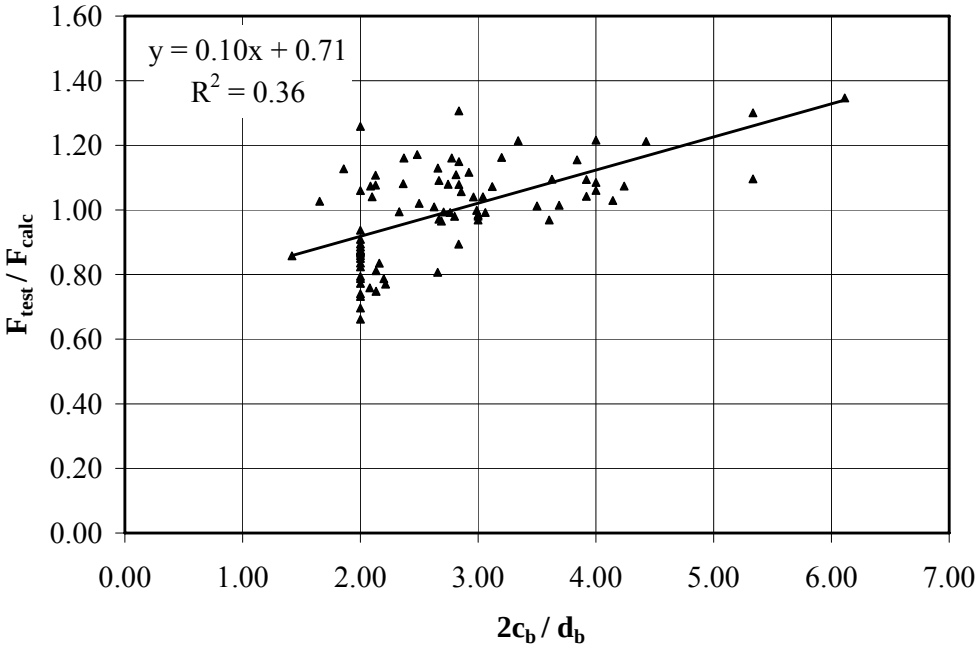

(b) Face Cover to Bar Diameter

Figure 5.23 Effect of Top Cover

5.3.5 Comparison of Analysis Equation with Descriptive Equations

Table 5.9 presents the comparisons of the ratio of the experimental to calculated values in terms of the mean (μ), standard deviation (σ), coefficient of variation (CV) and the product moment coefficient of correlation (r^2) for the expressions investigated. The product moment coefficient of correlation (r^2) indicates how closely the calculated values are related with the experimental values. The expression is more reliable when its r^2 is close to 1. The coefficient of variation measures the deviation of the variable from its mean (μ). The dispersion of the data is less with a low coefficient of variation.

Table 5.9 Statistical Comparison of Design Expressions (Steel Database)

Model	μ	σ	CV	r^2
Simple Model, Equation (5-5)	1.013	0.149	0.147	0.646
Modified Model, Equation (5-10)	1.032	0.135	0.131	0.757
Orangun, Jirsa, and Breen (1977) Eq. (4-1)	1.022	0.163	0.160	0.586
Zuo and Darwin (2000), Eq. (5-1)	1.012	0.128	0.126	0.799
Canbay and Frosch (2005), Eq. (5-2)	0.987	0.119	0.121	0.801

Equation (5-10) resulted in stronger correlation than Equation (5-5). Both methods resulted in similar average values. The standard deviation as well as the coefficient of variation for Equation (5-10) are lower than those obtained for Equation (5-5). This result was to be expected considering the improvement obtained from incorporation of the cover and bar spacing.

The expressions proposed by Zuo and Darwin (2000), Frosch and Canbay (2005), and Equation (5-10) resulted in a higher correlation (r^2) than the Orangun, Jirsa, and Breen expression (1977) as well as a lower coefficient of variation. All methods resulted in similar average values. When compared statistically, Canbay and Frosch (2005) performs the best among the expressions because it has a higher r^2 value and a lower coefficient of variation; however, these results are comparable to the ones obtained by Zuo and Darwin (2000) and Equation (5-10).

Figure 5.24 presents the ratio of the experimental to calculated bar stresses at failure versus the frequency of test specimens falling in a given range of f_{test}/f_{calc}. All of the methods follow approximately a normal distribution. The scatter of the experimental to calculated stress ratios using the Orangun, Jirsa, and Breen equation (1977) is the highest among the four methods. From Table 5.9 and Figure 5.24, it is concluded that Equation (5-10) provides reasonable estimates of splice strength for steel reinforcing bars.

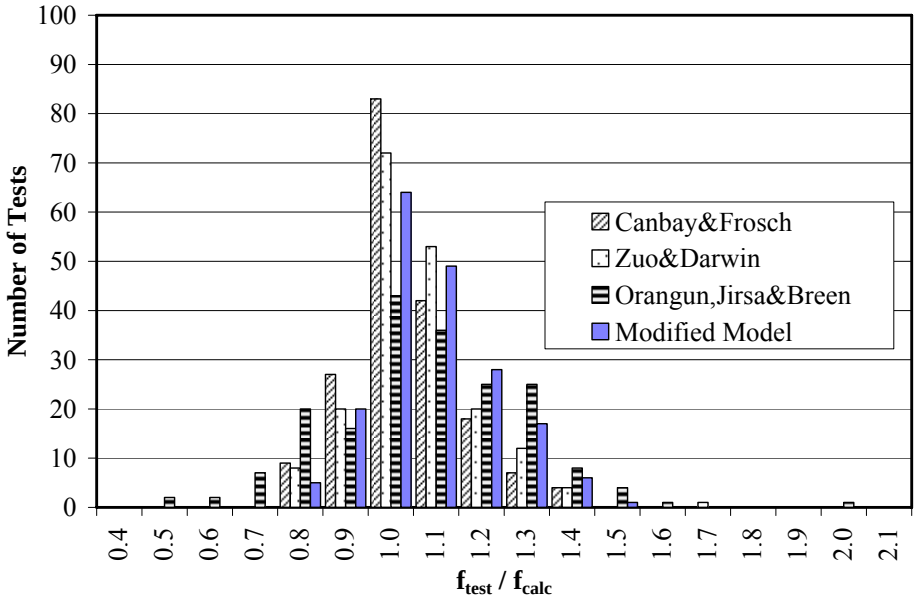

Figure 5.24 Comparison of Modified Model for Steel Database

Although Equations (5-5) and (5-10) were derived from a database with steel reinforced specimens, the equations incorporate the axial stiffness of the reinforcing bars; therefore, they may be used to calculate the splice strength of FRP reinforced specimens. These equations will be evaluated considering the FRP reinforced beam database in the following section.

5.3.6 Evaluation of the Test Results in the Experimental Program

To evaluate the performance of the expression developed from the steel database considering the FRP reinforced specimens, the specimens tested in the experimental program and by Mosley (2000) (FRP database) are plotted along with the data points from the steel database (Figure 5.25(a)). The trend-line obtained from Equation (5-5) is also shown in Figure 5.25(a).

It is observed that the bar force reached at failure for FRP reinforced specimens follows a similar trend as the steel reinforced specimens when the horizontal axis is plotted against L_{eq}. However, as shown in the zoomed view of Figure 5.25(b), the data points generally falls above the trend line which indicates that Equation (5-5) will yield conservative estimates for FRP reinforced specimens. Therefore, Equation (5-5) and (5-10) derived from steel specimens may be used to conservatively estimate the bond strength of FRP reinforced specimens.

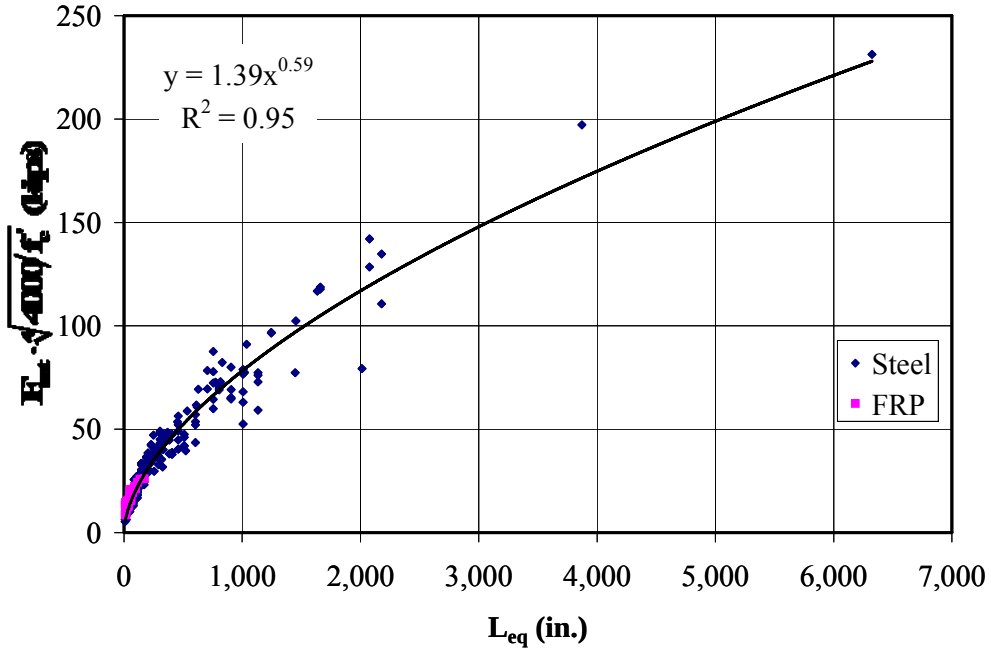

(a) General Trend

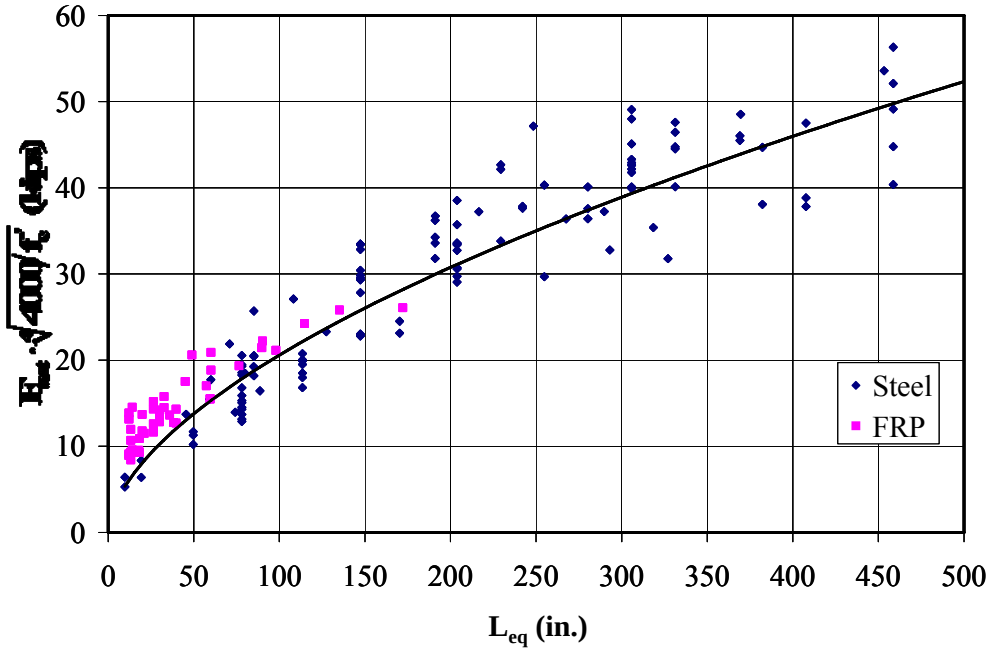

(b) General Trend (Zoomed)

Figure 5.25 Normalized Bar Force versus L_{eq} for FRP and Steel Database

Figure 5.26 presents how well the calculations with the modified equation (Eq. (5-10)) agree with the test results. The horizontal axis presents the bar force calculated using Equation (5-10) while the vertical axis presents the experimental results. As can be seen, Equation (5-10) yields conservative calculations for glass and aramid FRP reinforced specimens. For carbon FRP reinforced specimens, the expression yielded an unconservative estimate for only one data point. From this analysis, it is concluded that Equation (5-10) can be used to conservatively estimate the bond strength of both FRP and steel reinforced specimens.

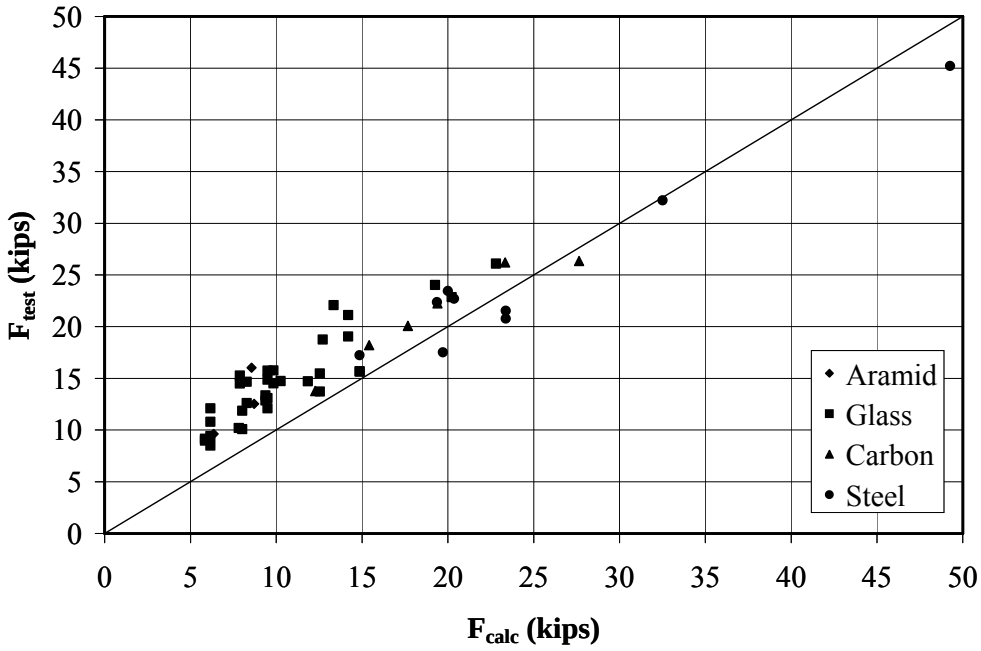

Figure 5.26 Experimental versus Calculated Bar Force (Equation (5-10))

Because Equation (5-10) was derived using only the steel database, it is reasonable that stresses calculated using this method will vary from the experimental results provided by the reinforcement. Therefore, improvement may be possible if the FRP results are directly considered. To investigate the effect of equivalent splice length L_{eq} on the bond strength of FRP reinforced specimens, the ratio of the experimental to calculated bar force versus L_{eq} is plotted in Figure 5.27.

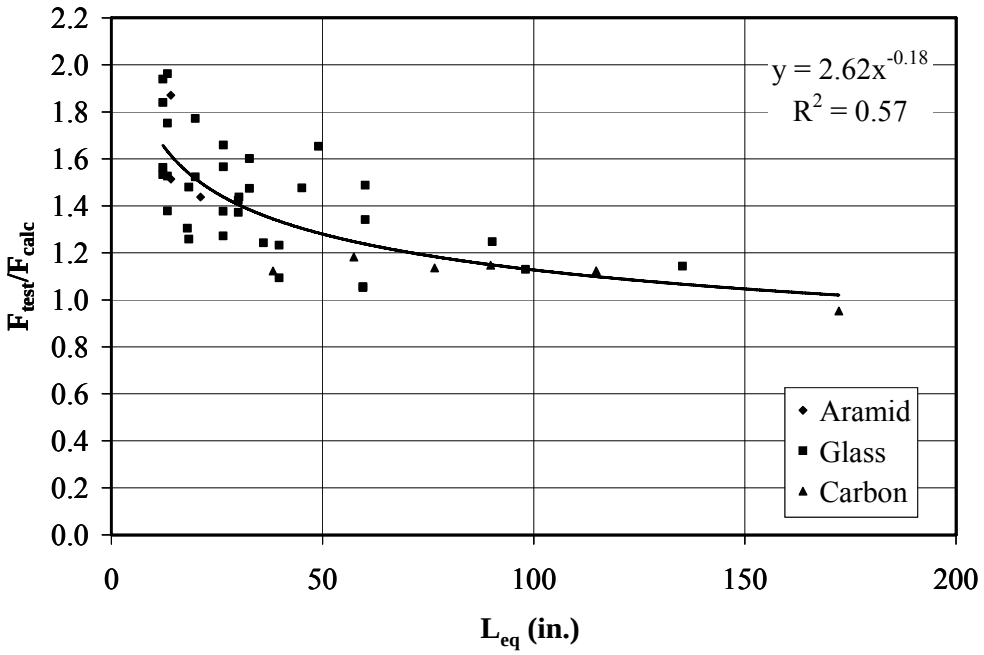

Figure 5.27 Ratio of Experimental to Calculated Bar Force versus L_{eq}

As shown in Figure 5.27, as the equivalent splice length increases, the ratio of the experimental to calculated values decreases and approaches a value of 1.00. For FRP reinforced specimens, the modification factor $\left(2.62L_{rel}^{-0.18}\right)$ which is the equation of the best fit curve can be used to modify the equations derived from the steel database. The equation modified for FRP reinforced specimens is presented as follows:

For side splitting failure:

$$F_b \cdot \sqrt[4]{4000/f_c'} = 3.64 \cdot L_{eq}^{0.41}\left(0.16\left(\frac{c_{si}}{d_b}\right)+0.84\right)$$

For face splitting failure: (5-11)

$$F_b \cdot \sqrt[4]{4000/f_c'} = 3.64 \cdot L_{eq}^{0.41}\left(0.20\left(\frac{c_b}{d_b}\right)+0.71\right)$$

Table 5.10 presents comparisons of the ratio of the experimental to calculated values obtained using Equations (5-10) and (5-11) for the FRP reinforced specimens in terms of the mean (μ), standard deviation (σ), coefficient of variation (CV) and the product moment coefficient of correlation (r^2). The maximum and minimum ratios of experimental to calculated stresses are also presented in Table 5.10.

Table 5.10 Statistical Comparison of Equation (5-10) and (5-11) (FRP Database)

	μ	σ	CV	r^2	f_{test}/f_{calc}	
					max.	**min.**
Equation (5-10)	1.411	0.255	0.180	0.881	1.963	0.953
Equation (5-11)	0.992	0.119	0.120	0.925	1.272	0.810

Equation (5-11) results in a stronger correlation and lower coefficient of variation indicating that dispersion using the equation is less than Equation (5-10). Furthermore, Equation (5-11) resulted in a lower average than Equation (5-10).

Figure 5.28 presents the frequency of test specimens falling in a given range of f_{test}/f_{calc} versus the ratio of the experimental to calculated bar stresses for FRP reinforced specimens. The scatter of the tested to calculated stress ratios using Equation (5-10) is higher than Equation (5-11). However, as already discussed, Equation (5-10) generally yields conservative estimates for FRP reinforced specimens. From Table 5.10 and Figure 5.28, it is concluded that Equation (5-11) provides reasonable estimates of splice strength of FRP reinforced specimens. However, this equation should only be used to estimate the splice strength of FRP reinforced specimens and is not applicable for steel reinforced specimens. Equation (5-10) on the other hand is suitable for calculating the splice strength of FRP and steel reinforced specimens. It should be noted, however, that Equation (5-10) yields very conservative results for FRP reinforced specimens.

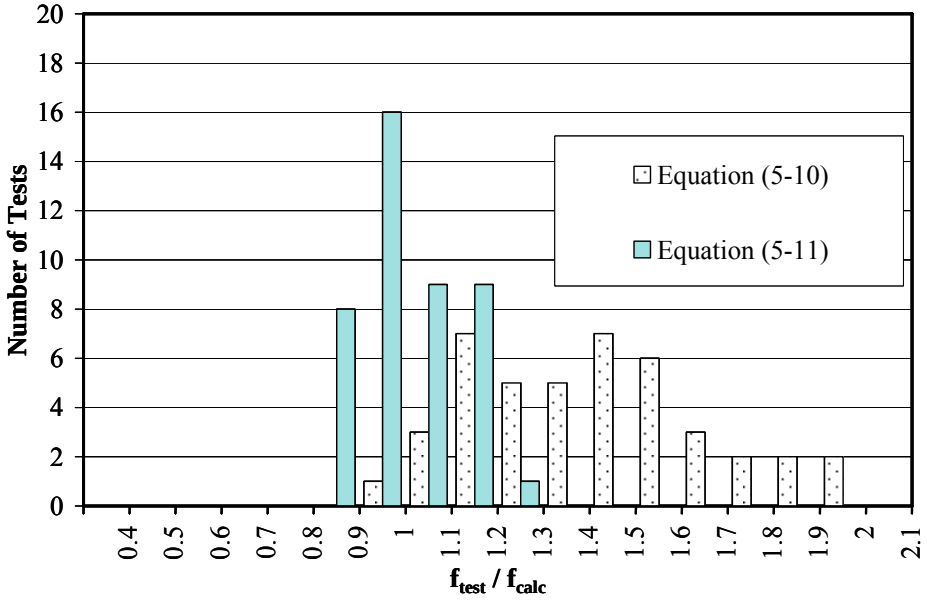

Figure 5.28 Comparison of Eq. (5-10) and Eq. (5-11) (FRP Database)

5.4 Simplified Design Equation

The use of an equivalent splice length L_{eq} provides the opportunity to relate the data obtained from FRP reinforced specimens to the data obtained from steel reinforced specimens. A unified design expression that may be used for the evaluation of the bond strength of both FRP and steel reinforced specimens is presented in this section. However, it should be noted that this expression is empirically derived considering a limited amount of data currently available for FRP and reinforced specimens.

A new database which includes specimens having both FRP and steel bar splices was formed by combining the steel and FRP databases. Normalized bar force versus equivalent splice length is plotted in Figure 5.29 for the combined database. A general trend-line of a best fit curve representing both the FRP and steel database was obtained and is presented in Figure 5.29.

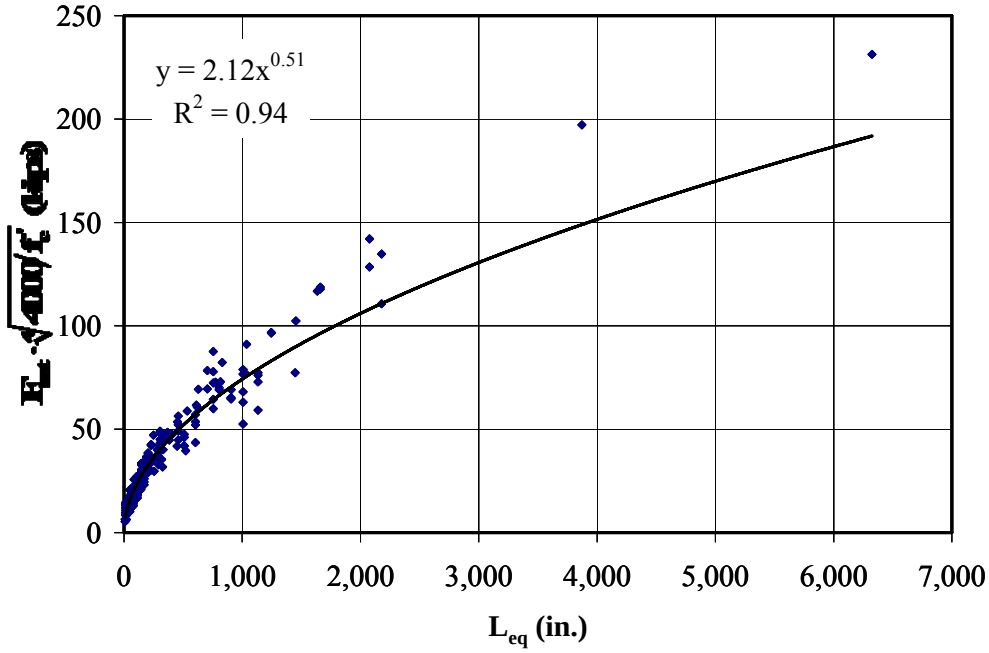

Figure 5.29 Normalized Bar Force versus L_{eq} for Combined FRP and Steel Database

The best fit equation for the FRP and steel database is:

$$F_b \cdot \sqrt[4]{4000/f_c'} = 2.1 \cdot L_{eq}^{0.50} \tag{5-12}$$

The effect of concrete cover was previously investigated in Section 5.3.4.2. Figure 5.30 plots the equations which account for the effect of the cover and spacing dimensions for face and side splitting failures. A more general equation which can be used for both face and side splitting failures is presented as follows:

$$M = 0.20\left(\frac{c}{d_b}\right) + 0.75$$

where:

c = minimum of c_{si} or c_b, in.

The expression which includes the effect of cover is presented in Equation (5-13).

$$F_b \cdot \sqrt[4]{4000/f_c'} = 2.1 \cdot L_{eq}^{0.50}\left(0.20\left(\frac{c}{d_b}\right) + 0.75\right) \tag{5-13}$$

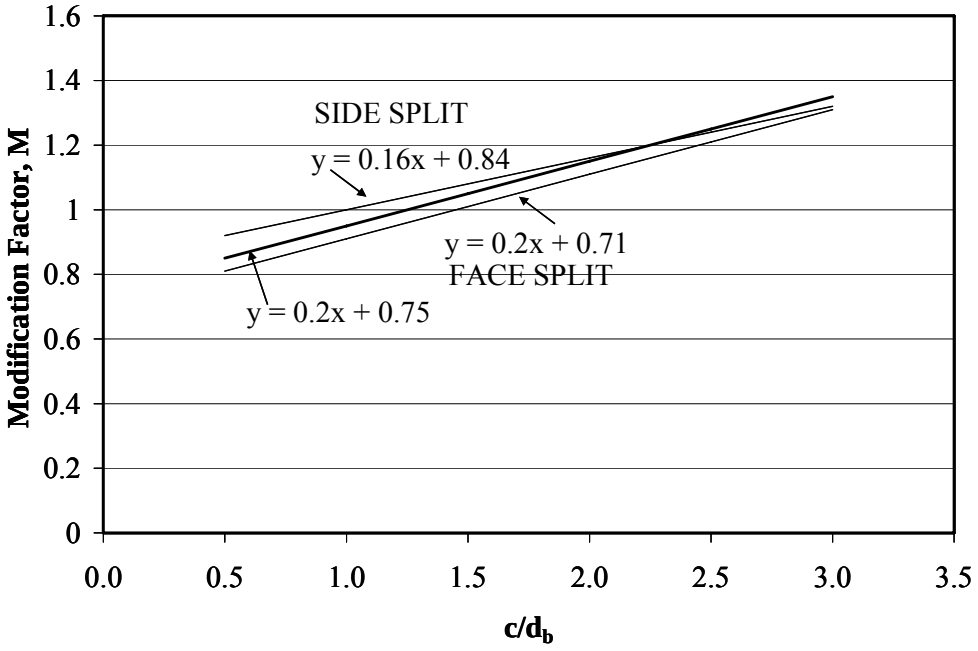

Figure 5.30 Modification for Cover and Spacing

Table 5.11and Table 5.12 present comparisons of the ratio of the experimental to calculated values obtained using Equations (5-12) and (5-13) on FRP reinforced specimens in terms of the mean (μ), standard deviation (σ), coefficient of variation (CV) and the product moment coefficient of correlation (r^2). Also presented in the tables are the maximum and minimum ratios of the experimental to calculated stresses. The equations are compared using the test results from the FRP and steel databases, separately.

Table 5.11 Statistical Comparison of Equation (5-12) and (5-13) (Steel Database)

	μ	σ	CV	r^2	f_{test}/f_{calc}	
					max.	min.
Equation (5-12)	1.092	0.185	0.169	0.531	1.520	0.690
Equation (5-13)	1.109	0.165	0.149	0.659	1.550	0.600

Table 5.12 Statistical Comparison of Equation (5-12) and (5-13) (FRP Database)

	μ	σ	CV	r^2	f_{test}/f_{calc}	
					max.	min.
Equation (5-12)	1.214	0.225	0.185	0.858	1.890	0.721
Equation (5-13)	1.321	0.174	0.131	0.921	1.721	1.040

In each database, the highest r^2 and lowest coefficient of variation is obtained by Equation (5-13) indicating that Equation (5-13) represents the behavior better than Equation (5-12). This result was expected because Equation (5-13) incorporates the effect of the cover and spacing dimensions. Figure 5.31 presents a histogram illustrating the frequency of test specimens within a given range of f_{test}/f_{calc} ratios for steel and FRP reinforced specimens. As shown, the number of unconservative data points decrease when Equation (5-13) is used to calculate bond strength for both the steel and FRP databases. In addition, Equation (5-13) consistently produces conservative results for the FRP reinforced specimens.

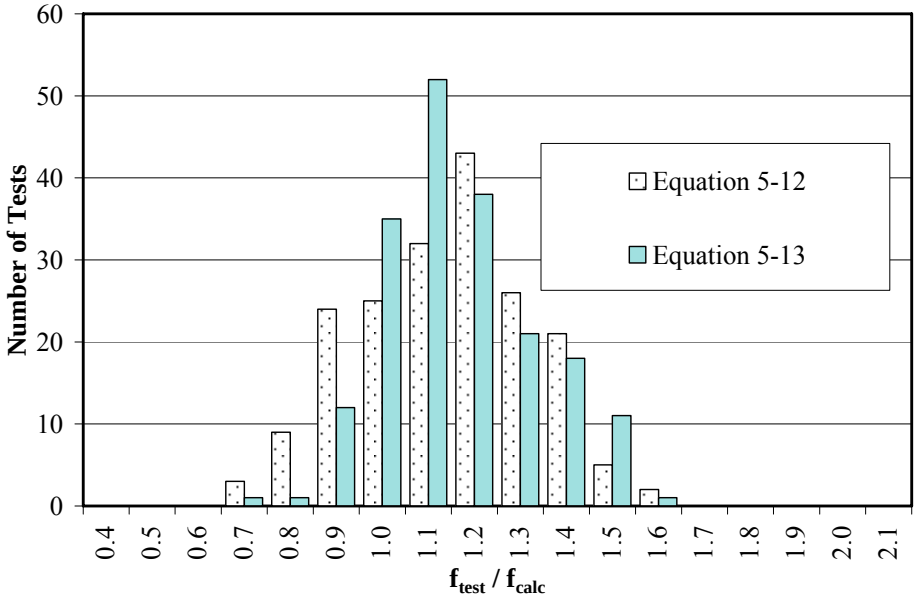

(a) Steel Reinforced Beam Database

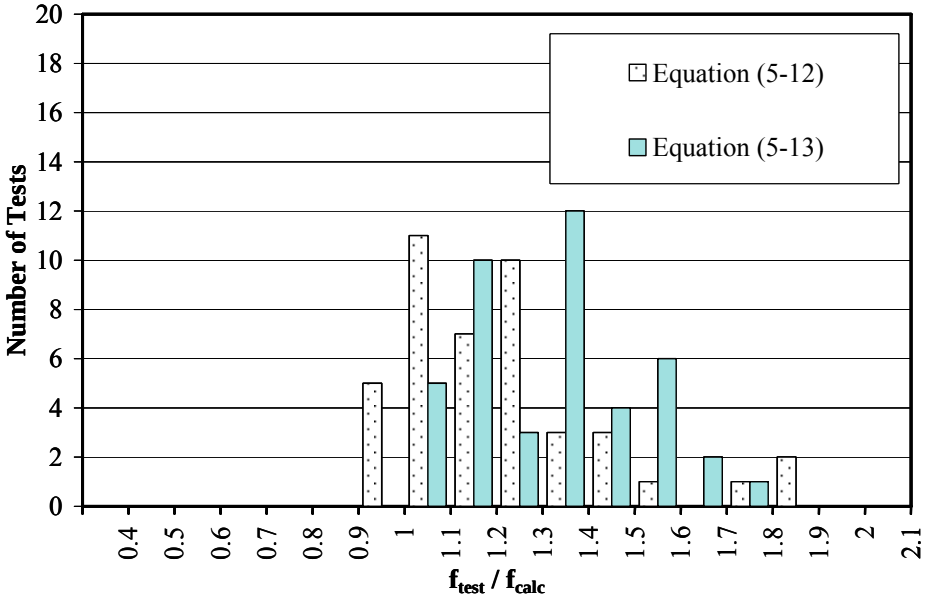

(a) FRP Bar Reinforced Beam Database

Figure 5.31 Comparison of Eq. (5-12) and Eq. (5-13)

The results of Equation (5-13) are compared with those provided by the ACI 318 and ACI 408 design expressions considering the steel test data. The ACI 318 and ACI 408 methods were previously presented in Section 4.2.1 and Section 4.2.2, respectively. The design equations were solved for bar stress for comparison purposes. Table 5.13 presents the statistical comparisons of the ratio of the experimental to calculated values obtained using these design expressions. Furthermore, Figure 5.32 shows the distribution of the ratio of the experimental to calculated stresses for the steel specimens.

This comparison demonstrates that the ACI 318 method exhibits considerably more scatter than that provided by Equation (5-13) and ACI 408. As shown in Table 5.13, the ACI 408 equation produced a lower coefficient of variation than Equation (5-13) and the ACI 318 design expression. Therefore, when compared statistically, the ACI 408 design expression provided better results than Equation (5-13) and the ACI 318 expression. However, the number of unconservative calculations ranges from 23% to 25% for all methods. Overall, Equation (5-13) produces results which are comparable with the ACI 408 design expression. Furthermore, Equation (5-13) can be used effectively to calculate the reinforcement stresses for FRP reinforced concrete.

Based on this evaluation, Equation (5-13) provides plausible estimates of splice strength for both FRP and steel reinforced beams. It should be noted that the concrete compressive strength is limited to a maximum value of 10,000 psi in ACI 318 design expression due to a lack of data on concrete compressive strength higher than 10,000 psi at the time that the equation was developed. Equation (5-13) was derived considering both normal and high strength concrete; therefore, it is also applicable for the specimens with high strength concrete (>10,000 psi).

Table 5.13 Statistical Comparison of Equation (5-12) and (5-13) for (Steel Database)

	μ	σ	CV	f_{test}/f_{calc}	
				max.	min.
ACI-318	1.217	0.324	0.266	2.724	0.508
ACI-408	1.091	0.137	0.125	1.733	0.781
Equation (5-13)	1.109	0.165	0.148	1.550	0.600

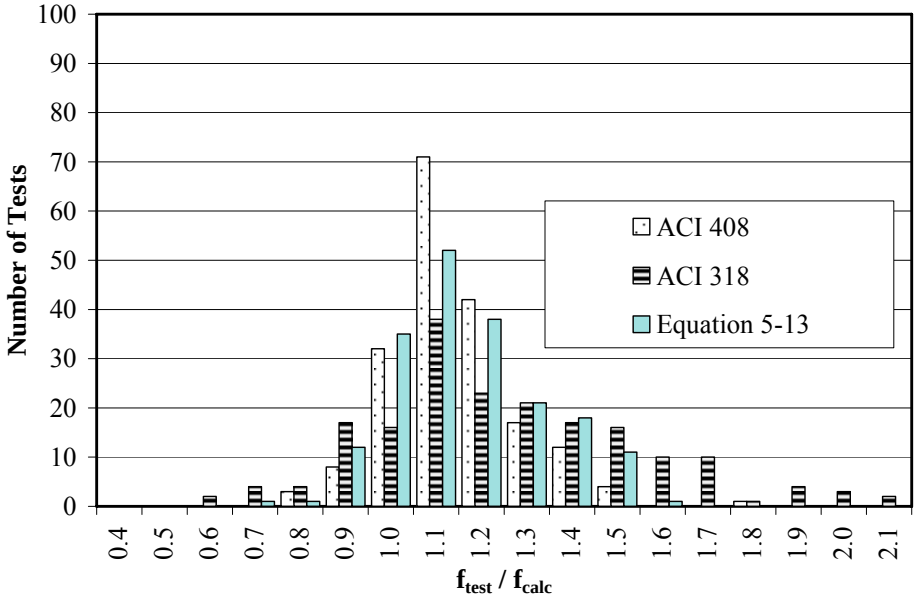

Figure 5.32 Comparison of Eq. (5-13) and Design Expressions (Steel Database)

The expression presented in Equation (5-12) can be written in terms of bar stress and the modulus of elasticity of the reinforcement for solid bars by substituting the following equations.

$$F_b = f_b A_b$$

$$L_{eq} = \frac{L_s E_b A_b}{1800}$$

$$A_b = \frac{\pi d_b^{\,2}}{4}$$

These substitutions yield the following equation:

$$f_b = \frac{\sqrt[4]{f_c'}\sqrt{L_s \cdot E_b}}{142 \cdot d_b} \tag{5-14}$$

The equation which incorporates the effect of concrete cover is as follows:

$$f_b = \frac{\sqrt[4]{f_c'}\sqrt{L_s \cdot E_b}}{142 \cdot d_b}\left(0.20\left(\frac{c}{d_b}\right)+0.75\right) \tag{5-15}$$

c = minimum of c_{si} or c_b, in.

c_b = bottom cover, in.

c_{si} = half of the clear spacing between bars, in.

d_b = bar diameter, in.

E_b = modulus of elasticity of the spliced reinforcement, ksi

f_b = bar stress at failure, ksi

f_c' = concrete cylinder strength, psi

L_s = splice length, in.

These equations can be rearranged and solved for L_s/d_b.

Without cover modification factor:

$$\frac{L_s}{d_b} = \frac{20,280}{E_b}\frac{f_b^{\,2} d_b}{\sqrt{f_c'}} \tag{5-16}$$

With cover modification factor:

$$\frac{L_s}{d_b} = \frac{20,280}{E_b} \frac{f_b^2 d_b}{\sqrt{f_c'}} \left(\frac{1}{\left(0.20 \left(\frac{c}{d_b} \right) + 0.75 \right)} \right)^2 \qquad (5\text{-}17)$$

Figure 5.33 provide a comparison of the proposed design equations (Eq. (5-16) and Eq. (5-17)) with the ACI 318 and ACI 408 design expressions for a case study which is summarized in the figure. The case study presented in Figure 5.33 was evaluated for minimum concrete cover and bar spacing as well as for f_y = 60 ksi and f_c' = 4000 psi. A minimum concrete cover of 1.5 in. which is specified for beams not exposed to weather by ACI 318-05 was considered for this study.

The ACI simplified equation provides conservative results for the bars smaller than No.11 when compared to the other expressions. For No.11 and smaller bars, Equation (5-16) and Equation (5-17) provide a lower bound while Equation (5-17), provides an upper bound for No.14 and No.18 bars.

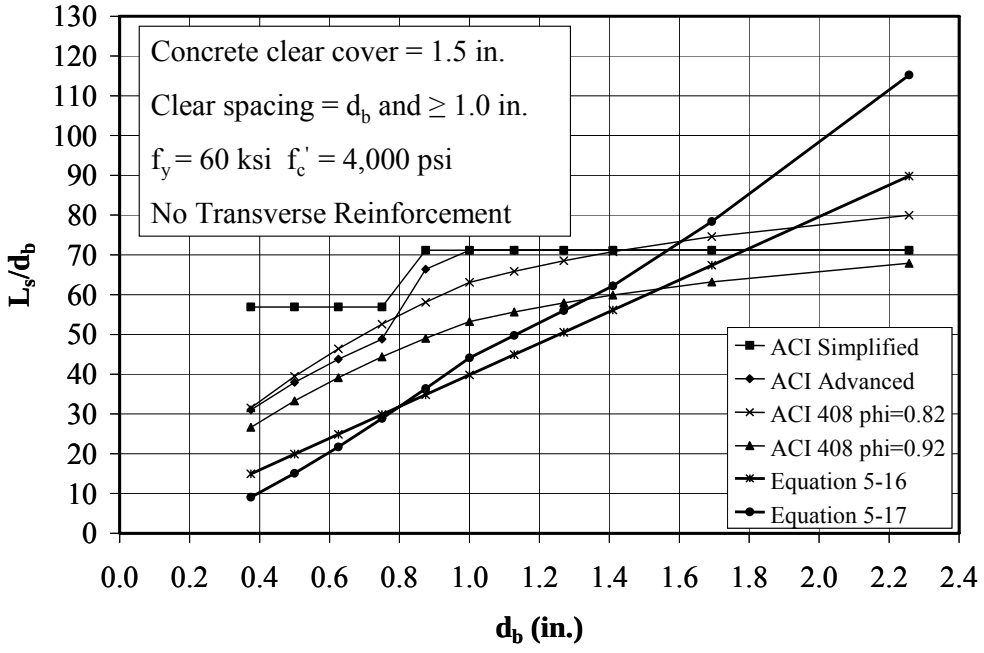

Figure 5.33 Comparison of Design Expressions and Eq. 5-16 and Eq. 5-17 (f_y = 60 ksi)

Figure 5.34 presents the ratio of the measured to calculated bar stress versus bar diameter for the design expressions and Equation (5-17) considering the steel database. As shown in Figure 5.34, the ACI 318 method exhibits more scatter than that provided by Equation (5-17) and ACI 408. However, the scatter observed from each method is consistent for varying bar diameter. It is important to note that eighty-nine percent of the specimens in the database were reinforced with #6, #8, or #11 bars. In general, the upper and lower boundaries for the measured to calculated bar stresses obtained from specimens reinforced with #6, #8 and #11 bars set the upper and lower f_{test}/f_{calc} values for the entire database. It is evident that each equation calculates bar stresses with approximately the same level of accuracy for the entire range of bar diameters.

To investigate the consistency of the estimated bar stresses, the ratio of the measured to calculated bar stresses is plotted against the calculated bar stress for the various design equations (Figure 5.35). The ACI 408 expression exhibits a slight decrease in f_{test}/f_{calc} as the calculated stress increases while Equation (5-17) calculates the bar stresses with approximately the same level of accuracy. Therefore, regardless of stress level, the equation provides reasonable results. However, an apparent trend is observed using the ACI 318 expression. As the calculated bar stress increases, the ratio of the experimental to calculated values decreases and approaches a value of 0.5. A trend line was obtained using regression analysis and is shown in Figure 5.36. The equation of the best fit curve is presented as follows:

$$\frac{f_{test}}{f_{calc}} = 8.15 \cdot f_{calc}^{-0.51}$$

Rearranging the equation gives:

$$f_{test} = 8.15 \cdot f_{calc}^{0.49}$$

The equation is simplified and presented as:

$$f_{test} = 8.15 \cdot \sqrt{f_{calc}} \qquad (5\text{-}18)$$

The ACI 318 development length equation (Equation (4-4)) is presented as follows:

$$\frac{\ell_d}{d_b} = \frac{3}{40}\frac{f_y}{\sqrt{f_c'}}\frac{\psi_t\psi_e\psi_s\,\lambda}{\frac{c_b + K_{tr}}{d_b}} \tag{4-4}$$

Parameters that are constant for the steel database are presented as follows:

K_{tr} = 0 (No Stirrup)

ψ_t =1.00 (Bottom Cast)

ψ_e = 1.00 (Black Bars)

ψ_s = 1.00 (Assume no modification factor for bar size)

λ = 1.00 (Normal weight concrete)

Solving Equation (4-4) for bar stress in ksi with the above parameters gives:

$$f_{calc} = \frac{l_d\sqrt{f_c'}}{d_b^{\,2}} \cdot \frac{40c_b}{3} \cdot \frac{1}{1000}\ \text{(ksi)} \tag{5-19}$$

Bar stress calculated according to Equation (5-19) can be substituted into Equation (5-18), yielding the following equation:

$$f_{test} = 0.94 \cdot \frac{\sqrt{l_d}\sqrt[4]{f_c'}\sqrt{c_b}}{d_b} \tag{5-20}$$

It is interesting that the form of Equation (5-20) is similar to the proposed equation developed in the study (Eq. (5-15)) except the modification factor for concrete cover.

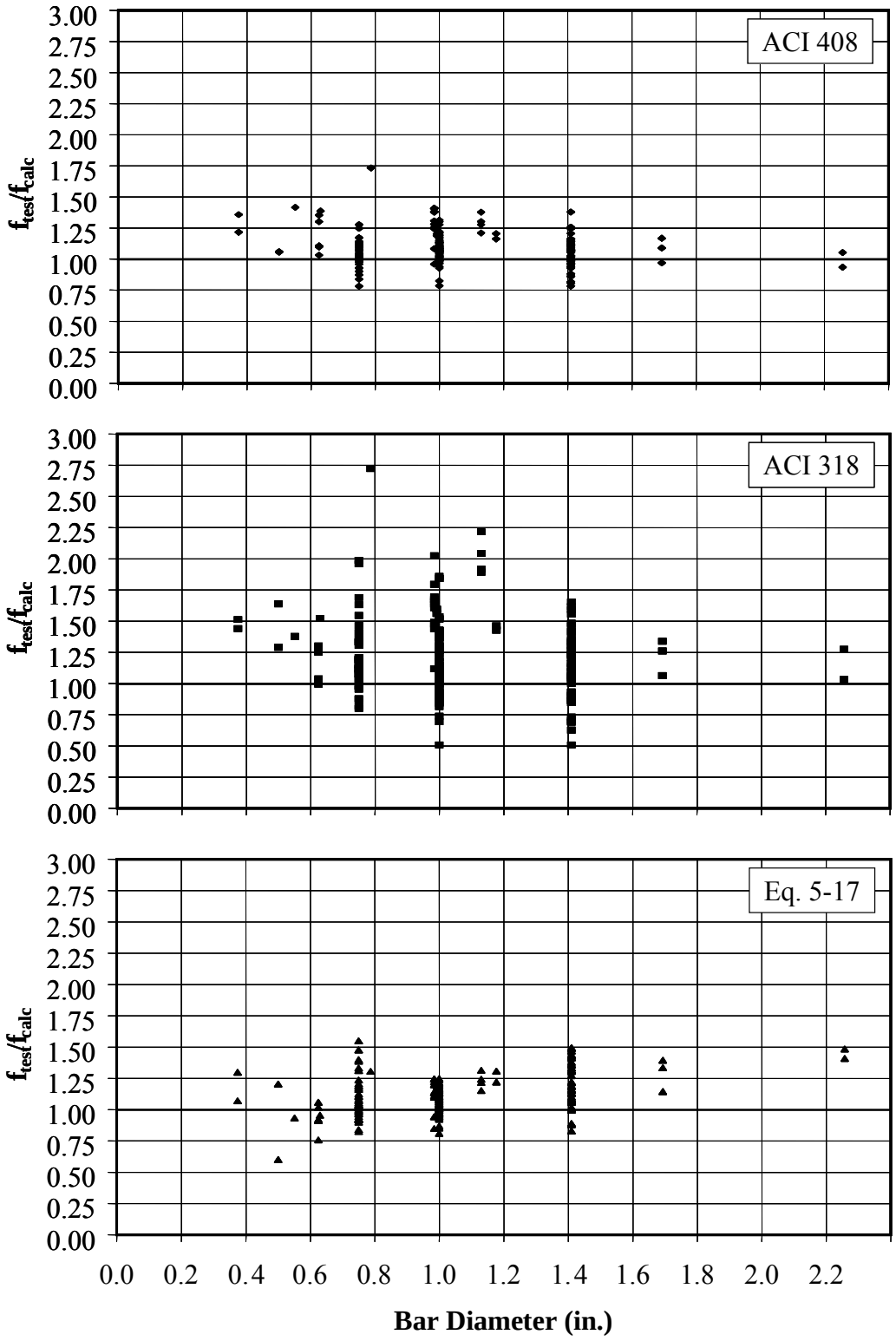

Figure 5.34 f_{test}/f_{calc} Ratios versus Varying Bar Diameter (Steel Database)

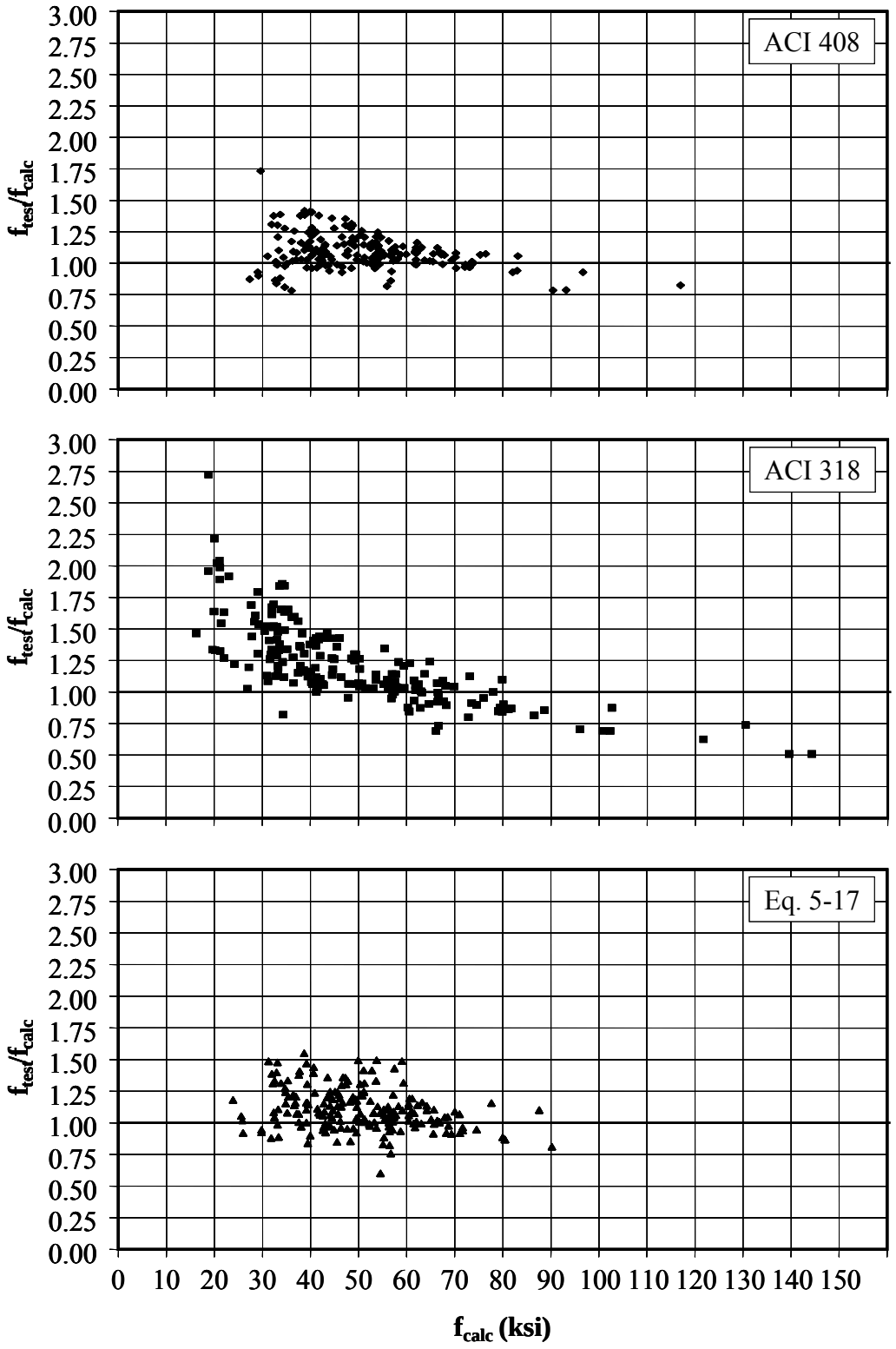

Figure 5.35 f_{test}/f_{calc} Ratios versus Calculated Bar Stress (f_{calc}) (Steel Database)

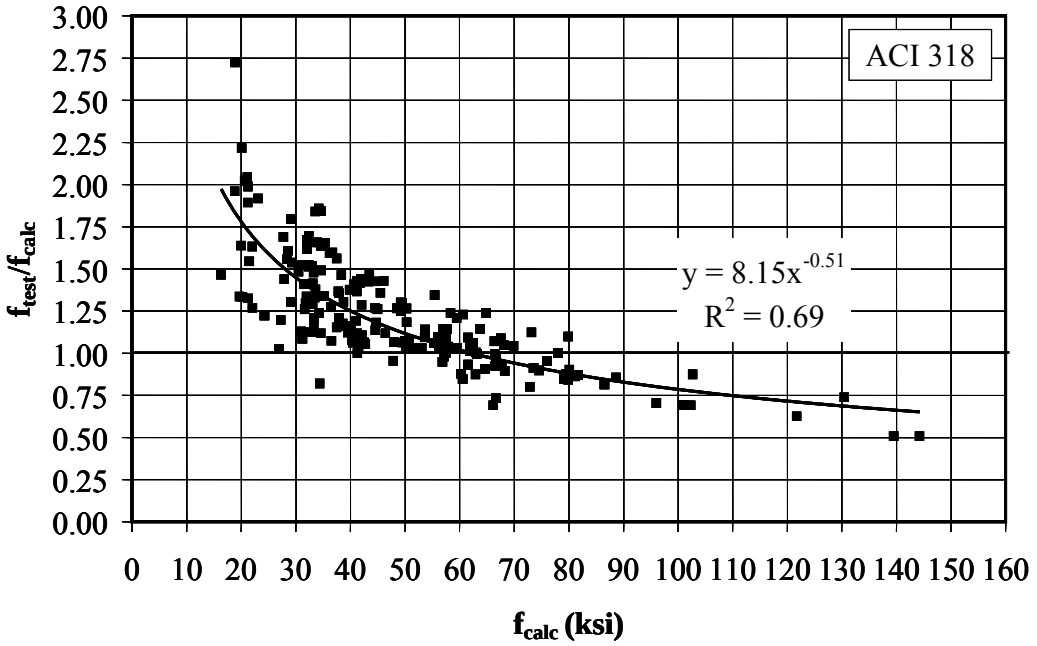

Figure 5.36 f_{test}/f_{calc} ratio versus Calculated Bar Stress (ACI 318) (Steel Database)

5.4.1 Safety Considerations

It is important to note that Equation (5-13) implicitly includes a factor of safety because the equation was derived using the combined FRP and steel database. The average ratio of the measured to calculated stress (f_{test}/f_{calc}) is approximately 1.1 for the steel database and 1.3 for the FRP database. The expression results in conservative calculations for all FRP bars while approximately 75% of the calculations are conservative for the steel bars.

Figure 5.37 presents the trend lines obtained from the steel, FRP, and combined database for calculated bar force versus the equivalent splice length to allow comparison of the curves. Also presented are the ranges of equivalent splice length available for the FRP and steel databases. As presented, Equation (5-13) which is the best fit curve for the combined database is conservative relative to the trend line obtained from the FRP database for the range of FRP bars and is conservative relative to the trend line from the steel database for the range of steel bars.

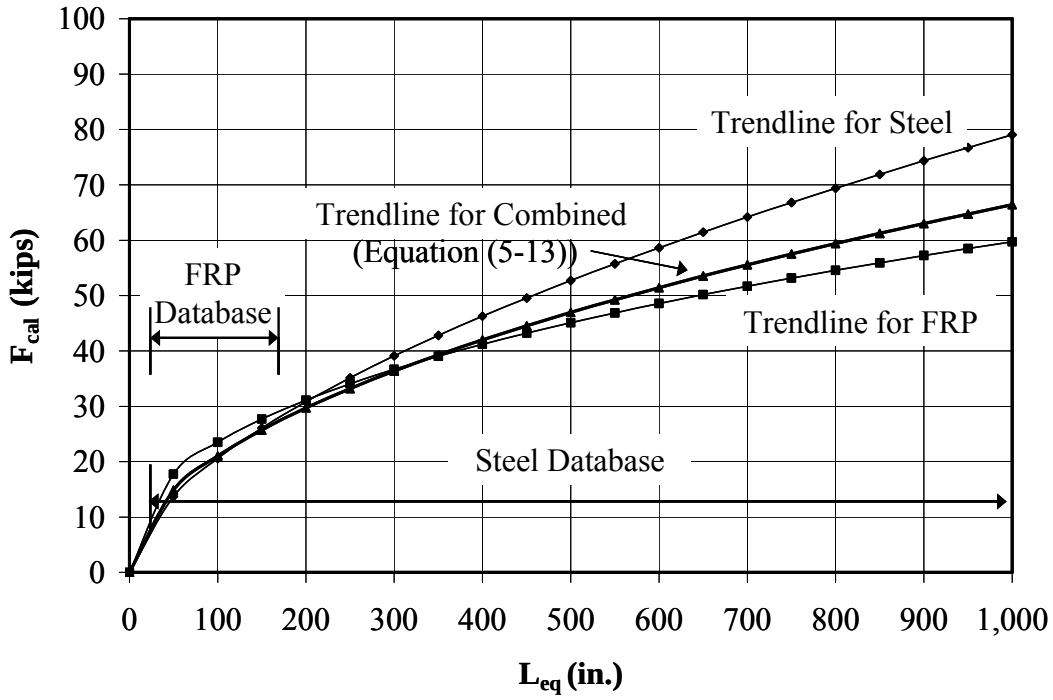

Figure 5.37 Comparison of Proposed Equations

Figure 5.38 presents a histogram of the ratio of the measured to calculated bar stresses for the steel database along with the normal distribution obtained using the statistical parameters for Equation (5-13). As shown, Equation (5-13) follows approximately the normal distribution; therefore, confidence intervals obtained from the normal distribution can be used to evaluate the database. Equation (5-13) can be modified for any desired factor of safety considering the confidence intervals obtained from the normal distribution curve. Considering the normal distribution, 68.3% of the data lie within one standard deviation of the average while 95.4% of the data lie within two standard deviation of the average. The 90% confidence interval can be obtained within 1.65 times the standard deviation of the average value.

As discussed previously, the number of unconservative calculations ranges from 23% to 25% for all design methods evaluated indicating that, the equation is comparible with the ACI 318 and ACI 408 design expressions in terms of level of safety. However, the number of unconservative data can be reduced to any desired level of safety for the

proposed model by multiplying the bar stress in Equation (5-17) with $1/(\mu - C\sigma)$ where C is a multiplier required to obtain the required level of safety.

The equation yields conservative results for 95% of the specimens if the bar stress in Equation (5-17) is multiplied by $1/(\mu - 1.65\sigma)$. Considering the steel database, μ=1.109 and σ = 0.165 for Equation (5-17). Therefore, the modifier for bar stress is calculated as 1.19. Replacing the bar stress in Equation (5-17) with 1.19 times the bar stress results the following equation:

$$\frac{L_s}{d_b} = \frac{28,720}{E_b}\frac{f_b^2 d_b}{\sqrt{f_c'}}\left(\frac{1}{\left(0.20\left(\frac{c}{d_b}\right)+0.75\right)}\right)^2 \qquad (5\text{-}21)$$

It is important to note that, Equation (5-21) yields conservative results for 97.5% of the steel database considered in the study. Using a stress multiplier of 1.19, 22.5% of the data moves to the conservative side. However, as discussed previously, the level of safety of the equation can be adjusted to any preferred levels by considering various multipliers.

Figure 5.39 provide a comparison of Equation (5-17) and Equation (5-21) with the ACI 318 and ACI 408 design expressions for a case study which is summarized in the figure. As shown, the ACI simplified equation provides conservative results for the bars smaller than No.10 when compared to the other expressions. As shown, Equation (5-17) provides a lower bound for specimens reinforced with No. 11 and smaller bars while Equation (5-21) provides upper bound for specimens reinforced with No. 10 and larger bars.

Figure 5.40 presents the ratio of the measured to calculated bar stress versus bar diameter for Equations (5-17) and (5-21) considering the steel database. As presented, the number of unconservative calculations decreases with Equation (5-21). It should be noted that only the steel database is considered in this section as Equation (5-17) yields

conservative results for FRP reinforced specimens. Equation (5-21) can also be used for specimens reinforced with FRP bars with an increased safety level.

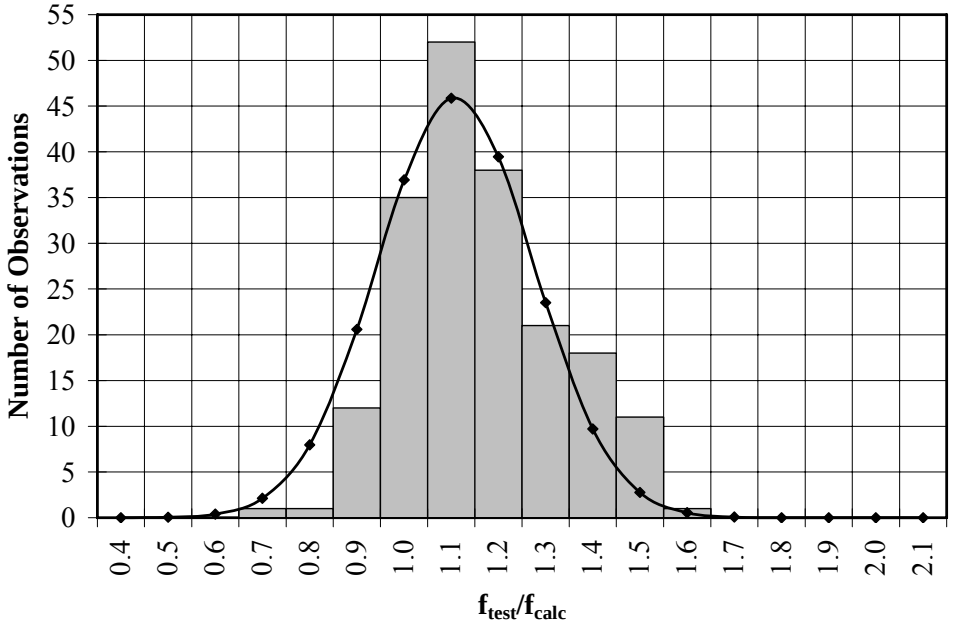

Figure 5.38 Comparison of Eq. (5-13) with Normal Distribution Curve (Steel Database)

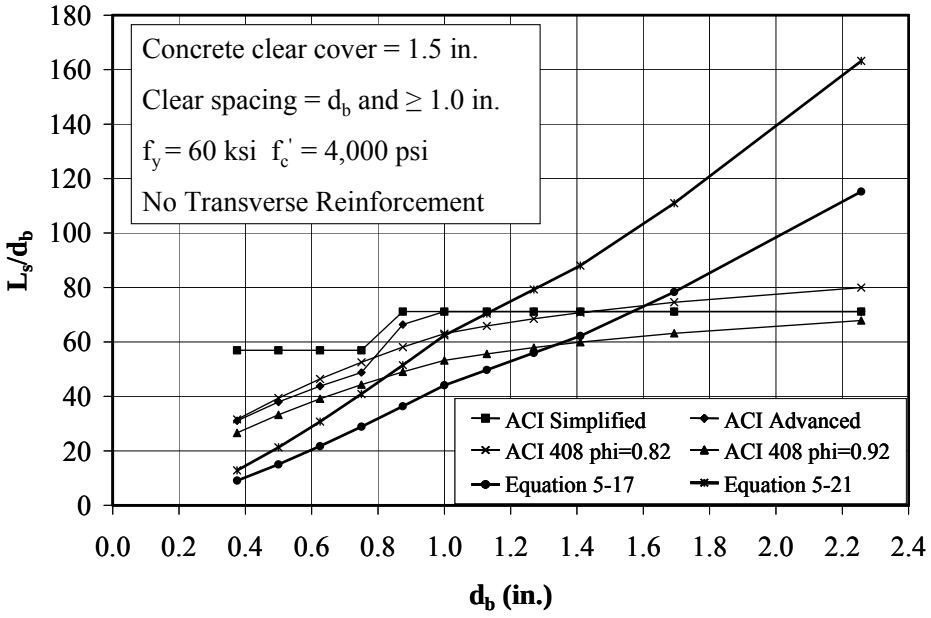

Figure 5.39 Comparison of Design Expressions and Eq. 5-17 and Eq. 5-21 (f_y = 60 ksi)

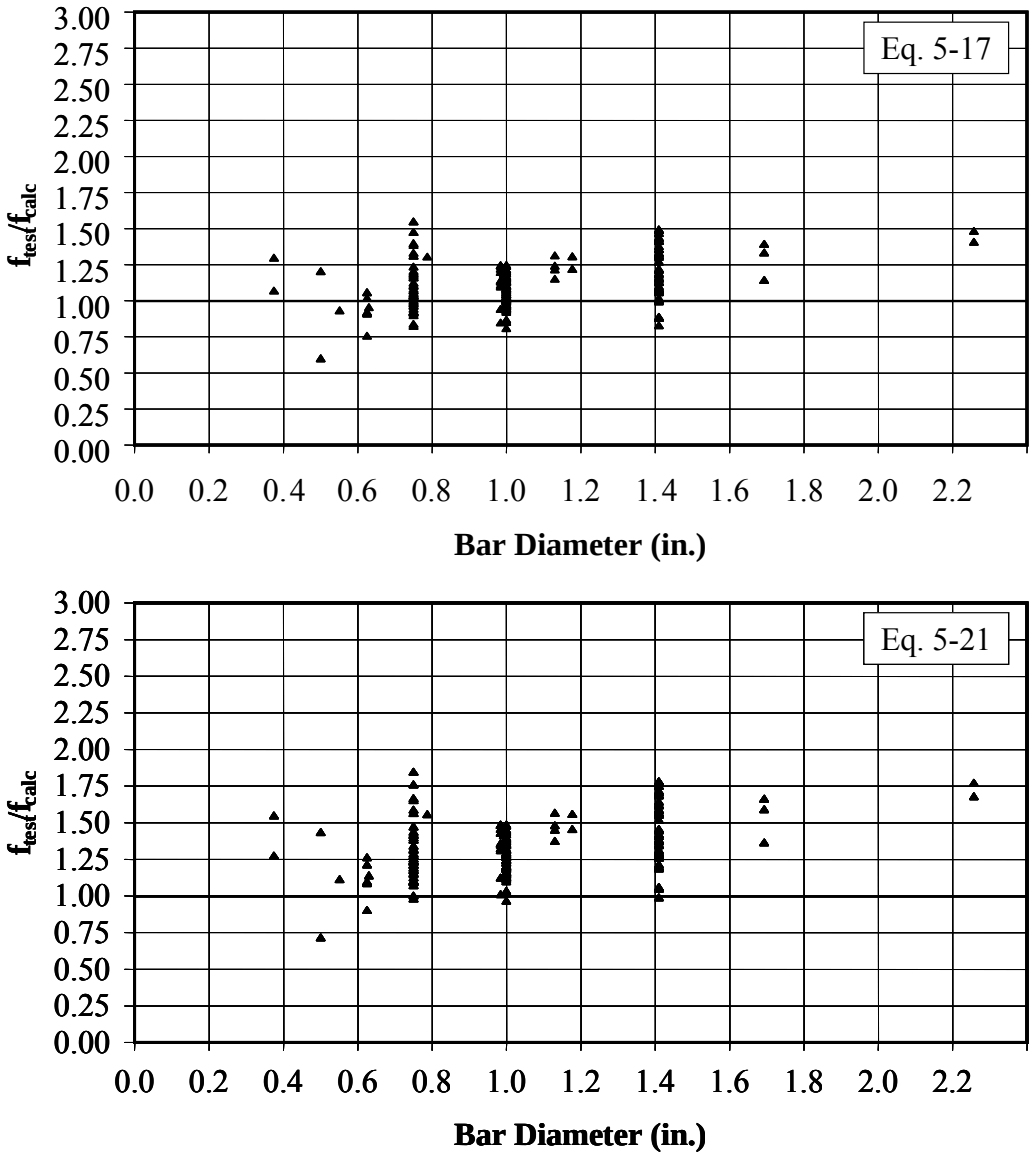

Figure 5.40 f_{test}/f_{calc} Ratios versus Varying Bar Diameter for Eq. (5-13) and Eq. (5-21) (Steel Specimens)

5.5 Design Recommendations

Based on the analysis conducted on the database of FRP and steel bar reinforced concrete specimens, the following design procedure is proposed for the design of FRP and steel reinforced concrete. It should be noted that the design expression was developed based on a minimum cover and bar spacing of one bar diameter. Therefore,

this expression should not be considered appropriate for cover and spacings below this minimum. In addition, the cover to bar diameter ratio was limited to 3.0 for the investigated database. For larger cover to bar diameter ratios, c/d_b should be taken as 3.0.

$$\frac{L_s}{d_b} = \frac{29,000}{E_b} \frac{f_b^2 d_b}{\sqrt{f_c'}} \left(\frac{1}{M} \right)^2 \tag{5-22}$$

where:

$$M = \left(0.20 \left(\frac{c}{d_b} \right) + 0.75 \right)$$

$$\frac{c}{d_b} \leq 3.0$$

c = *minimum of* c_{si} *or* c_b*, in.*

c_b = *bottom cover, in.*

c_{si} = *half of the clear spacing between bars, in.*

d_b = *bar diameter, in.*

E_b = *modulus of elasticity of the spliced reinforcement, ksi*

f_b = *bar stress at failure, ksi*

f_c' = *concrete cylinder strength, psi*

L_s = *splice length, in.*

The proposed design equation yields conservative results for 97.5% of the steel database. However, the constant in the equation can be adjusted so that the desired level of conservatism can be achieved. The same level of conservatism with ACI 318 and ACI 408 equations can be obtained by changing the constant from 29,000 to 20,000.

CHAPTER 6

SUMMARY AND CONCLUSIONS

6.1 Introduction

Because the physical and mechanical properties of FRP bars are different from those of steel reinforcement, especially the surface deformation and modulus of elasticity of the reinforcement, the bond behavior of FRP reinforced concrete specimens is expected to be quite different than of steel reinforced specimens. The objective of this research was to evaluate the effects of the axial stiffness, modulus of elasticity, reinforcement size, surface deformation, splice length, and casting position on the bond behavior of FRP and steel reinforcing bars spliced at tension, as well as to develop a plausible model for the bond strength of FRP and steel bars.

The goals of study were to address the following key questions:

- Is the effect of splice length on bond strength a function of the axial stiffness of the reinforcing bar?
- Is there a relationship between the axial stiffness of the bar and the bar stresses reached at failure?
- What is the effect of surface deformation on the bond strength of different types of reinforcement?
- What is the effect of casting position on splice strength of different types of reinforcing bar.
- Is it possible to develop a plausible model representing the bond behavior of FRP and steel reinforced structures?

The research was conducted in two phases which included an experimental and analytical investigation.

6.2 Experimental Investigation

The experimental program investigated the bond behavior of fiber reinforced polymer (FRP) and steel reinforced concrete beams with unconfined tension lap splices. The study included forty-six concrete beams reinforced with steel and FRP bars. FRP reinforcement included glass and carbon bars with different sizes and surface deformations. Steel reinforcement consisted of both deformed and plain bars. The concrete strength ranged from approximately 4,000 psi to 5,500 psi. Three reinforcing bars were spliced at the center of the constant moment region of the beam. All beams were rectangular in cross section with a total depth of 16 in. The width of the specimens was dictated by the minimum cover and spacing limitations and the size of the reinforcement. All specimens were designed with a clear spacing of 1 in. between the bars located in the splice region and a 1-1/2 in. side and top clear cover.

The objective of the experimental program was to evaluate the effect of the modulus of elasticity, surface deformation, axial rigidity, bar size, splice length, and casting position of the longitudinal reinforcement on splice strength.

6.2.1 Behavior of the Specimens

6.2.1.1 Specimens Reinforced with Bars Having Surface Deformation:

The specimens reinforced with bars having surface deformations failed by splitting of the concrete in the splice region. It was observed that, at a given load, the cracks in the carbon FRP reinforced specimens penetrated deeper into the section than those of the steel reinforced specimens. Cracks of the carbon FRP specimens, however, were shallower that those of the glass FRP reinforced specimens which correlated with the modulus of elasticity. All failures were sudden and brittle with no obvious warning evident prior to failure. Among the specimens with the same cross-sectional dimensions, shear span length, and concrete strength, steel reinforced specimens reached the highest

load followed by carbon FRP and then glass FRP reinforced specimens. The specimens reinforced with glass FRP, however, deflected most, followed by carbon FRP and steel reinforced specimens. The crack widths that were measured in the splice region were significantly smaller than those measured outside the splice region because of the increased amount of reinforcement in this region. At a given stress level, the crack widths measured in the glass FRP specimens were significantly larger than those observed in the companion steel and carbon FRP reinforced specimens.

6.2.1.2 Specimens Reinforced with Bars Without Surface Deformation:

The specimens reinforced with plain reinforcing bars failed in pullout. The bars pulled out from the shear span for the FRP reinforced specimens and from the splice region for the steel reinforced specimens. A sudden drop in load was observed at the time of failure for both FRP and steel reinforced specimens. Test results indicated that minimal deformation or surface treatment is required for FRP bars.

6.2.2 Experimental Findings

The following conclusions were obtained from the experimental program.

- The modulus of elasticity of the reinforcement has an influence on splice strength. The higher the modulus of elasticity of the reinforcement, the higher the bar force reached at failure.
- For the same type of bar, as the diameter of the bar increases, the force obtained in the bar increases.
- The bar stress reached at failure increase as the splice length increases. The strength gain provided by an identical increases in splice strength is highest for steel bars, followed by carbon FRP bars, and then glass FRP bars.
- Axial stiffness of the bar is a major parameter influencing splice strength. As the axial stiffness of the reinforcement increases, the bar force at failure increases.
- The bars in the specimens reinforced with plain and uncoated reinforcement reached stresses which are approximately one third of the companion deformed

bar reinforced specimens indicating the importance of some level of surface deformation.

- Among the specimens reinforced with deformed glass FRP bars, only small differences in splice strength were observed as the surface deformation was varied.
- Bottom cast FRP reinforced specimens generally tend to yield higher ultimate bond strengths than top cast specimens as has been previously reported steel specimens.

6.3 Analytical Investigation

An analytical investigation was performed to develop a plausible model to enable calculating the splice strength of both steel and FRP bar reinforced concrete beams without confinement in the splice region. Databases, compiled for both steel and FRP splice tests, were used to develop the model.

The steel database includes 190 unconfined, uncoated, bottom cast, steel reinforced specimens while the FRP database includes 43 unconfined splice specimens reinforced with aramid, glass, and carbon FRP bars having some level of surface deformation. The FRP database consists of 36 top cast specimens and 7 bottom cast specimens. All specimens in both databases failed in splitting. Based on analysis of the specimens in both databases, it was found that the bar force at failure is a function of the axial stiffness (EA), splice length of the reinforcement, and concrete compressive strength.

Based on evaluation of the data, an equivalent splice length, L_{eq}, which is a function of the axial stiffness and the splice length of the reinforcing bar, was defined that allows comparison of test results obtain from different reinforcing materials and different cross sectional areas. The bar force at failure can be described by the following equation for steel reinforced specimens.

$$F_b \cdot \sqrt[4]{4000 / f_c'} = 1.39 \cdot L_{eq}^{0.59} \qquad (5\text{-}5)$$

where:

$$L_{eq} = \frac{L_s E_b A_b}{1800}$$

A_b = *area of spliced reinforcement, in.*^{2}

E_b = *modulus of elasticity of the spliced reinforcement, ksi*

F_b = *bar force at failure, kips*

L_s = *splice length, in.*

Based on analysis of the data with Equation (5-5), it was found that a modification factor which incorporates the effect of cover and spacing can be introduced that improves the performance of the expression. Based on this analysis, a unified modification factor, M, can be derived to incorporate the effects of the cover and bar spacing for both side and face splitting failure modes.

$$M = 0.20\left(\frac{c}{d_b}\right) + 0.75$$

where:

c = *minimum of* c_{si} *or* c_b*, in.*

c_b = *bottom cover, in.*

c_{si} = *half of the clear spacing between bars, in.*

d_b = *bar diameter, in.*

Equation (5-5) was derived using only the steel database. It was found that stresses calculated using this method vary from the experimental results provided by the FRP reinforcement. The equation modified for FRP reinforced specimens is presented as follows:

$$F_b \cdot \sqrt[4]{4000 / f_c'} = 3.64 \cdot L_{eq}^{0.41} \qquad (5\text{-}11)$$

Equations (5-5) and (5-11) can be used to satisfactorily calculate the splice strength of the steel and FRP reinforced specimens, respectively.

A unified design expression that may be used for the evaluation of the bond strength of both FRP and steel reinforced specimens was developed by analyzing the combined FRP and steel database. The equation which incorporated the modification factor for cover and bar spacing is presented as follows:

$$F_b \cdot \sqrt[4]{4000/f_c'} = 2.1 \cdot L_{eq}^{0.50} \left(0.20 \left(\frac{c}{d_b} \right) + 0.75 \right) \qquad (5\text{-}13)$$

Equation (5-13) can be used to calculate the bond strength of both FRP and steel reinforced specimens. Using Equation (5-13), 75% of the specimens in the steel database and 100 percent of the specimens in the FRP database were calculated conservatively.

Equation (5-13) can be rearranged and solved for L_s/d_b to enable direct calculation of development length.

$$\frac{L_s}{d_b} = \frac{20,280}{E_b} \frac{f_b^{\,2} d_b}{\sqrt{f_c'}} \left(\frac{1}{M} \right)^2 \qquad (5\text{-}17)$$

6.3.1 Design Recommendations

Based on the results of this study, the following design recommendations are suggested for development length and crack width calculations.

6.3.1.1 Development Length Equation

Based on the analysis conducted on the database of FRP and steel bar reinforced concrete specimens, the following design procedure is proposed for the design of FRP and steel reinforced concrete. It should be noted that the design expression was developed based on a minimum cover and bar spacing of one bar diameter. Therefore, this expression should not be considered appropriate for cover and spacings below this minimum. In addition, the cover to bar diameter ratio was limited to 3.0 for the investigated database. For larger cover to bar diameter ratios, c/d_b should be taken as 3.0. A safety factor was provided to the recommended design equation to provide a level of safety such that 95% of the data are conservative.

$$\frac{L_s}{d_b} = \frac{29,000}{E_b} \frac{f_b^2 d_b}{\sqrt{f_c'}} \left(\frac{1}{M} \right)^2 \quad (5\text{-}1)$$

where:

$$M = \left(0.20 \left(\frac{c}{d_b} \right) + 0.75 \right)$$

$$\frac{c}{d_b} \leq 3.0$$

c = minimum of c_{si} or c_b, in.

c_b = bottom cover, in.

c_{si} = half of the clear spacing between bars, in.

d_b = bar diameter, in.

E_b = modulus of elasticity of the spliced reinforcement, ksi

f_b = bar stress at failure, ksi

f_c' = concrete cylinder strength, psi

L_s = splice length, in.

The proposed design equation yields conservative results for 97.5% of the steel database. However, the constant in the equation can be adjusted so that the desired level of conservatism can be achieved. The same level of conservatism with ACI 318 and ACI 408 equations can be obtained by changing the constant from 29,000 to 20,000.

6.3.1.2 Crack Width

The crack width equation (Equation 4-12) developed by Frosch (1999) performed satisfactorily for steel reinforced specimens. For FRP reinforced specimens, the equation is consistently unconservative; therefore, the equation can be easily modified with using a modification factor to account for the material type. The calculated material factors based on this study are 1.00 for steel reinforced specimens, 1.25 for CFRP reinforced specimens and 1.4 for GFRP reinforced specimens.

It should be noted that the modified equation performed satisfactorily for both FRP and steel reinforced specimens; therefore, it can be used to calculate the crack widths of the specimens reinforced with those materials.

6.4 Further Research

The majority of research performed on bond of FRP reinforcement has been in the form of pullout tests. The bond strengths obtained from pullout specimens, however, are significantly higher than those obtained from splice tests because of confinement provided around the bar surface. Therefore, expressions developed from the test results of pullout specimens yield unconservative calculations for specimens with spliced bars. The experimental program clearly demonstrated that FRP reinforced specimens have a tendency for splitting failure for the ranges of parameters tested. This failure mode supports the need for splice tests which provide more realistic bond behavior relative to the behavior experienced in actual structures. Therefore, tests of the following splice specimens are considered important to improving the understanding of the bond behavior of FRP and steel reinforced specimens.

- Systematic testing of cover and bar spacing is needed to better define their influence on bond strength.
- Beam splice specimens with increased cover and spacing should be tested to investigate at what point pullout failure is experienced.
- Beams with confined splices should be tested to investigate the effect of confinement on splice strength. Transverse reinforcement should be constructed from FRP and steel bars to investigate the effect of material type on bond strength as well.
- Beams cast with high strength concrete should be tested to further investigate the effect of concrete compressive strength on bond behavior.
- The majority of the specimens in the steel database were reinforced with #6, #8, and #11 bars. Beam specimens reinforced with smaller size steel bars should be tested to investigate the effect of low axial stiffness on bond strength.

LIST OF REFERENCES

1. AASHTO, *AASSHTO LRFD Bridge Design Specifications*, 3rd Edition, 2004

2. AASHTO, *Standard Specifications for Highway Bridges*, 17th Edition, 2002

3. Abrams, D.A., "Tests of Bond Between Concrete and Steel," University of Illinois Bulletin, No.71, 1913, 238 pp.

4. ACI Committee 318, "Building Code Requirements for Structural Concrete and Commentary (ACI 318-05/ACI 318 R-05)," American Concrete Institute, Detroit, 2005, 430 pp.

5. ACI Committee 408, "Suggested Development, Splice, and Standard Hook Provisions for Deformed Bars in Tension," (ACI 408.1R-03), American Concrete Institute, Farmington Hills, MI, 2003, 49 pp.

6. ACI Committee 440, "Guide for the Design and Construction of Concrete Reinforced with FRP Bars," (ACI 440.1R-03), American Concrete Institute, Farmington Hills, MI, 2003, 42 pp.

7. ACI Committee 440, "Guide for the Design and Construction of Concrete Reinforced with FRP Bars," (ACI 440.1R-XX), American Concrete Institute, Farmington Hills, MI, (balloted in 2005 to be published)

8. ACI Committee 440, "Guide Test Methods for for Fiber-Reinforced Polymers (FRPs) for Reinforcing or Strengthening Concrete Structures," (ACI 440.3R-04), American Concrete Institute, Farmington Hills, MI, 2004, 40 pp.

9. Azizinamini, A., Pavel, R., Hatfield, E., and Ghosh, S. K., "Behavior of Lap-Spliced Reinforcing Bars Embedded in High-Strength Concrete," *ACI Structural Journal*, V. 96, No. 5, Sep.-Oct. 1999, pp. 826-835.

10. Azizinamini, A., Stark, M., Roller, J. J., and Ghosh, S. K., "Bond Performance of Reinforcing Bars Embedded in High-Strength Concrete," *ACI Structural Journal*, V. 90, No. 5, Sep.-Oct. 1993, pp. 554-561

11. Benmokrane, B., Tighiouart, B., and Chaallal, O. " *ACI Materials Journal*, V. 93, No. 3, May-June 1996, pp. 246-253

12. Boothby, T.E., Nanni, A., Bakis, C.E., and Huang, H., "Bond of FRP Rods Embedded in Concrete," *Engineering Mechanics*, Proc. 10th Conf., Vol. 1, S. Sture, ed., American Society of Civil Engineers, New York, 1995, pp. 114-117.

13. Brown, V. and Bartholomew C., "FRP Reinforcing Bars in R/C Members," *ACI Material Journal*, Vol. 90, No. 1, Jan-Feb 1993, pp. 34-39.

14. Canbay, E., and Frosch, R. J., "Bond Strength of Lap-Spliced Bars," *ACI Structural Journal*, V. 102, No. 4, July-Aug. 2005, pp. 605-614.

15. Chamberlin, S. J., "Spacing of Spliced Bars in Beams," *Journal of the American Concrete Institute*, V. 29, No. 8, Proceedings V. 54, Feb. 1958, pp. 689-697.

16. Chinn, J., Ferguson, P. M., and Thompson, J. N., "Lapped Splices in Reinforced Concrete Beams," *Journal of the American Concrete Institute*, V. 27, No. 2, Proceedings V. 52, Oct. 1955, pp. 201-213.

17. Choi, O. C., Hadje-Ghaffari, H., Darwin, D., and McCabe S. L., "Bond of Epoxy-Coated Reinforcement: Bar Parameters," *ACI Materials Journal*, V. 88, No. 2, Mar.-Apr. 1991, pp. 207-217.

18. Cleary, D. B., and Ramirez, J. A., "Bond Strength of Epoxy-Coated Reinforcement," *ACI Structural Journal*, V. 88, No. 2, Mar.-Apr. 1991, pp. 146-149.

19. Darwin, D., and Graham, E. K., "Effect of Deformation Height and Spacing on Bond Strength of Reinforcing Bars," *ACI Structural Journal*, V. 90, No. 6. Nov-Dec. 1993, pp. 646-657.

20. Darwin, D., McCabe, S.L., Idun, E.K., and Schoenekase, S.P., "Development Length Criteria: Bars Not Confined by Transverse Reinforcement," *ACI Structural Journal*, V. 89, No. 6, Nov.-Dec. 1992, pp. 709-720.

21. Darwin, D., Tholen, M. L., Idun, E. K., and Zuo, J., "Splice Strength of High Relative Rib Area Reinforcing Bars," *ACI Structural Journal*, V. 93, No. 1, Jan.-Feb. 1996, pp. 95-107.

22. Darwin, D., Zuo, J., Tholen, M. L., and Idun, E. K., "Development Length Criteria for Conventional and High Relative Rib Area Reinforcing Bars," *ACI Structural Journal*, V. 93, No. 3, May-June 1996, pp. 347-359.

23. DeVries, R. A., Moehle, J. P., and Hester, W., "Lap Splice Strength of Plain and Epoxy-Coated Reinforcements: An Experimental Study Considering Concrete Strength, Casting Position, and Anti-Bleeding Additives," *Report No. UCB/SEMM-91/02*, Department of Civil Engineering, University of California Berkeley, Jan. 1991, 86 pp.

24. Ehsani, M. R., Saadatmanesh, H., and Tao, S., “Design Recommendations for Bond of GFRP Rebars to Concrete,” *Journal of Structural Engineering*, Vol. 122, No 3, Mar 1996, pp. 247-254.
25. Eligehausen, R., Popov, E. P., and BerteroV. V., “Local Bond Stress-Slip Relationships of Deforrmed Bars under Generalized Excitation,” EERC 83-23, *Earthquake Engineering Research Center*, University of California, Berkeley, California, 1983.

26. Esfahani, M.R., and Rangan, B.V., “Bond between Normal Strength and High-Strength Concrete (HSC) and Reinforcing Bars in Splices in Beams,” *ACI Structural Journal*, V.95, No.3, May-June 1998, pp.272-280.

27. Faza, S., and GangaRao, H., "Bending and Bond Behavior of Concrete Beams Reinforced with Plastic Rebars," *Transportation Research Record*, No. 1290, Vol. 2, 1990, pp. 185-193.

28. Ferguson, P.M., “Bond Stress – The State of the Art,” *Journal of the American Concrete Institute*, Title No.63-53, Nov. 1966, pp.1161-1190.

29. Ferguson, P.M., and Breen, J.E., “Lapped Splices for High Strength Reinforcing Bars, Part I & II,” *Journal of the American Concrete Institute*, No. 9, Proceedings V. 62, Sept. 1965, pp. 1063-1077.

30. Ferguson, P. M., and Krishnaswamy, C. N., “Tensile Lap Splices-Part 2: Design Recommendation for Retaining Wall Splices and Large Bar Splices,” *Research Report* No. 113-2, Center for Highway Research, The University of Texas at Austin, Apr. 1971, 60 pp.

31. Ferguson, P. M., and Thompson, J. N., “Development Length of High Strength Reinforcing Bars in Bond,” *Journal of the American Concrete Institute*, Title no.59-33, July, 1962, pp.887-922.

32. Frosch, R. J., “Another Look at Cracking and Crack Control in Reinforced Concrete,” *ACI Structural Journal*, V. 96, No. 3, May-June 1999, pp.437-442.

33. Gao, D.; Benmokrane, B.; and Masmoudi, R.; 1998, “Bond Properties of FRP Rebars to Concrete,” *Technical Report*, Department of Civil Engineering, University of Sherbrooke, Sherbrooke (Quebec), Canada, 27 pp.

34. Hadje-Ghaffari, H., Choi, O. C., Darvin, D., and McCabe, S. L., “Bond of Epoxy-Coated Reinforcement: Cover, Casting Position, Slump, and Consolidation,” *ACI Structural Journal*, V. 91, No. 1, Jan.-Feb. 1994, pp. 59-68.

35. Hamad, B. S., and Itani, M. S., "Bond Strength of Reinforcement in High-Performance Concrete: The Role of Silica Fume, Casting Position, and Superplasticizer Dosage," *ACI Materials Journal*, V. 95, No. 5, Sep.-Oct. 1998, pp. 499-511.

36. Hamad, B. S., and Machaka, M. F., "Effect of Transverse Reinforcement on Bond Strength of Reinforceng Bars in Silica Fume Concrete," *Materials and Structures*, V. 32, July 1999, pp. 468-476.

37. Hamad, B., and Mansour, M., "Bond Strength of Noncontact Tension Lap Splices," *ACI Structural Journal*, V. 93, No. 3, May-June 1996, pp. 316-326.

38. Hester, C. J., Salamizavaregh, S., Darwin, D., and McCabe, S. L., "Bond of Epoxy-Coated Reinforcement: Splices," *ACI Structural Journal*, V. 90, No. 1, Jan.-Feb. 1993, pp. 89-102.

39. Hwang, S. J., Lee, Y. Y., and Lee, C. S., "Effect of Silica Fume on the Splice Strength of Deformed Bars of High-Performance Concrete," *ACI Structural Journal*, V. 91, No. 3, May-June 1994, pp. 294-302,

40. Jirsa, J. O., Breen, J. E., Luke, J. J., and Hamad, B. S., "Effect of Casting Position on Bond," *Proceedings of the International Conference on Bond in Concrete*. Paisley, UK, 1982.

41. Kanakubo, T., Yonemaru, K., Fukuyama, H., Fujisawa, M., and Sonobe, Y., "Bond Performance of Concrete Members Reinforced with FRP Bars," *International Symposium*: Fiber-Reinforced Plastic Reinforcement for Concrete Structures, SP138, ACI Proceedings, Nov. 1993, pp.767-788.

42. Larralde, J., and Silva-Rodriguez, R., "Bond and Slip of FRP Bars in Concrete," *Journal of Materials in Civil Engineering*, Vol. 5, No. 1, Feb. 1993, pp. 30-40.

43. Maeda, M., Otani, S., and Aoyama, H., "Bond Splitting Strength in Reinforced Concrete Members," *Transaction of the Japan Concrete Institute*, Vol. 13, 1991, pp. 581-588.

44. Makitani, E., Irisawa, I., and Nishiura, N., "Investigation of Bond in Concrete Members with Fiber Reinforced Plastic Bars," *International Symposium*: Fiber-Reinforced Plastic Reinforcement for Concrete Structures, ACI Proceedings, SP-138, Nov. 1993, pp. 315-331.

45. Malvar, J. L., "Technical Report: Bond Stress Slip Characteristics of FRP Bars," *Naval Facilities Engineering Service Center*, Port Hueneme, CA, Feb. 1994, 45 pp.

46. Mathey, R. G., and Watstein, D., "Investigation of Bond in Beam and Pull-out Specimens with High-Yield-Strength Deformed Bars," *Journal of the American Concrete Institute*, V. 32, No. 9, Proceedings V. 57, March 1961, pp. 1071-1090.

47. Morita, S., and Fujii, S., "Bond Capacity of Deformed Bars Due to Splitting of Surrounding Concrete," *Proceedings of the International Conference on Bond in Concrete*, 1982

48. Mosley, C. P., "Bond Performance of Fiber Reinforced Plastic (FRP) Reinforcement in Concrete," *Master Thesis*, Purdue University, Dec. 2000, 79 pp.

49. Nanni, A., Al-Zahrani, M. M., Al-Duajani, S. U., Bakis, C. E., and Boothby, T. E., "Bond of FRP Reinforcement to Concrete—Experimental Results," *Non-Metallic Reinforcement (FRP) for Concrete Structures*, Proceedings of the Second International Symposium, 1995, L. Taerwe, Editor, pp. 135-145.

50. Orangun, C. O., Jirsa, J. O., and Breen, J. E., "The Strength of Anchored Bars: A Reevaluation of Test Data on Development Length and Splices," *Research Report* No. 154-3F, Center for Highway Research, The University of Texas at Austin, 1975, 78 pp.

51. Orangun, C. O., Jirsa, J. O., and Breen, J. E., "A Reevaluation of Test Data on Development Length and Splices," *ACI Journal*, Proceedings V.74, No.3, Mar. 1977, pp. 114-122

52. Pleimann, L. G., "Tension and Bond Pullout Tests of Deformed Fiberglass Rods," *Final Report* for Marshall-Vega Corporation, Marshall, Arkansas, Civil Engineering Department, University of Arkansas, Fayetteville, Ark., 1987, pp. 5-11.

53. Pleimann, L. G., "Strength, Modulus of Elasticity, and Bond of Deformed FRP Rods," *Proceedings of the Specialty Conference on Advanced Composite Materials in Civil Engineering Structures*, Material Engineering Division, American Society of Civil Engineers, pp. 99-110.

54. Rezansoff, T., Akanni, A., and Sparling, B., "Tensile Lap Splices under Static Loading: A Review of the Proposed ACI 318 Code Provisions," *ACI Structural Journal*, V. 90, No. 4, July-Aug. 1993, pp. 374-384.

55. Tastani, S. P., and Pantazopoulou, S. J., "Exprimental Evaluation of the Direct Tension-Pullout Bond Test," Bond in Concrete- from Research to Standards, Budapest, 2002, 8 pp.

56. Tepfers, R., "Tensile lap splices with confining reinforcement," *Contribution to the International Conference on Bond in Concrete*, Paisley, Scotland, June 14th-l6th 1982, pp. 318-330.

57. Thompson, M. A., Jirsa, J. O., Breen, J. E., and Meinheit, D. F., "The Behavior of Multiple Lap Splices in Wide Sections," *Research Report* No. 154-1, Center for Highway Research, The University of Texas at Austin, Feb. 1975, 75 pp.
58. Tighiouart, B., Benmokrane, B., and Gao, D., "Investigation of Bond in Concrete Member with Fiber Reinforced Polymer (FRP) Bars," *Construction and Building Materials Journal*, Dec. 1998, 10 pp.

59. Tighiouart, B., Benmokrane, B., Mukhopadhyaya, P., "Bond Strength of Glass FRP Rebar Splices in Beams Under Static Loading," *Construction and Building Material*, Vol 13, No 7, 1999, pp. 383-392.

60. Toutanji, H. A., and Saafi, M., "Flexural Behavior of Concrete Beams Reinforced with Glass Fiber-Reinforced Polymer (GFRP) Bars," *ACI Structural Journal*, V. 97, No. 5, Sep.-Oct. 2000, pp. 712-719.

61. Treece, R. A., Jirsa, J. O., "Bond Strength of Epoxy-Coated Reinforcing Bars," *ACI Materials Journal*, V. 86, No. 2, Mar.-Apr. 1989, pp. 167-174.

62. Wambeke, B. W., "Development Length of Glass Fiber Reinforcing Polymer Bars in Concrete," *Master Thesis*, University of Minnesota, May 2003, 72 pp.

63. Zuo, J., Darwin, D., "Bond Strength of High Relative Rib Area Reinforcing Bars," *SM Report No. 46*, University of Kansas Center for Research, Lawrence, Kansas, June 1998, 350 pp.,

64. Zuo, J., Darwin, D., "Splice Strength of Conventional and High Relative Rib Area Bars in Normal and High Strength Concrete," *ACI Structural Journal*, V. 97, No.4, July-Aug. 2000, pp. 630-641.

Appendix A

Stress-Strain Curves for Reinforcement

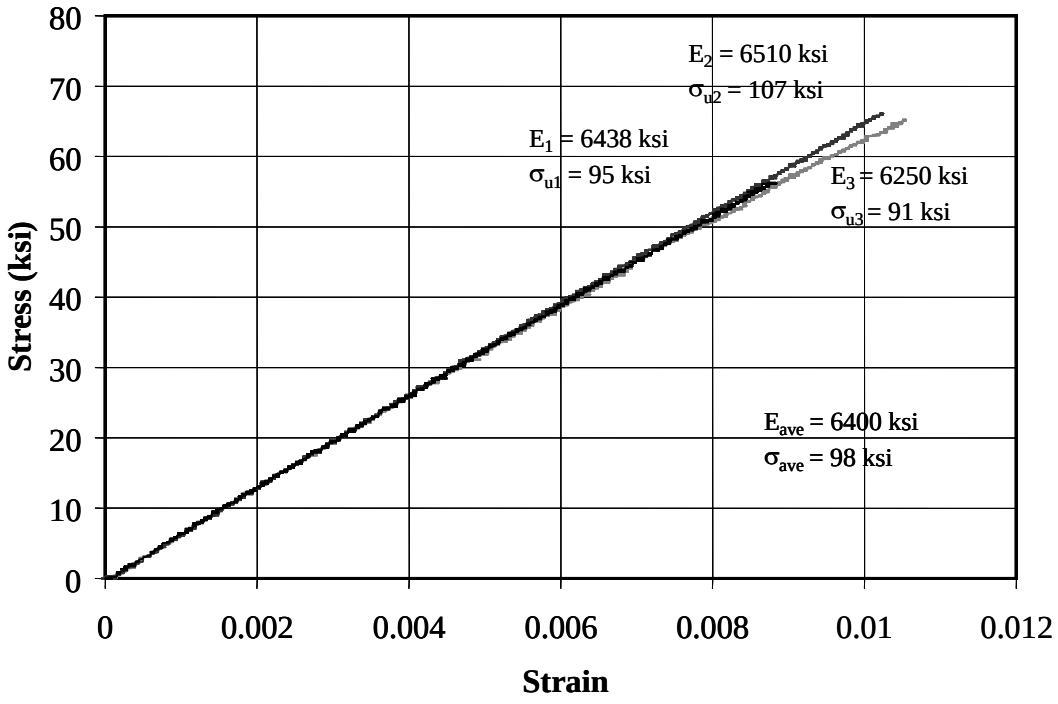

Figure A.1 Stress vs. Strain - #5 Hughes Glass (HN), Phase I

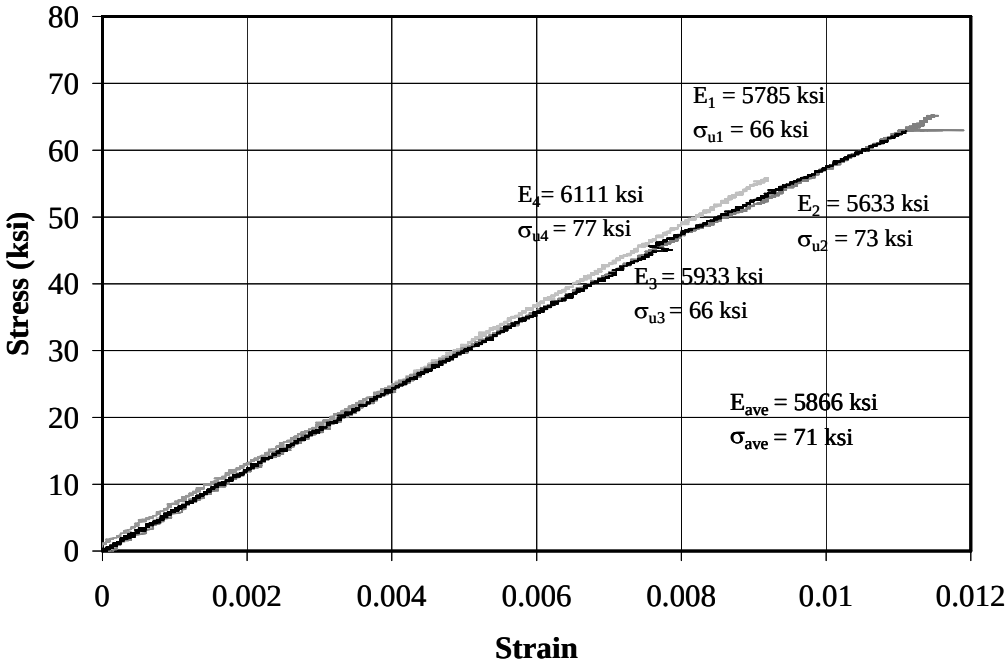

Figure A.2 Stress vs. Strain - #5 Hughes Glass (HO), Phase I

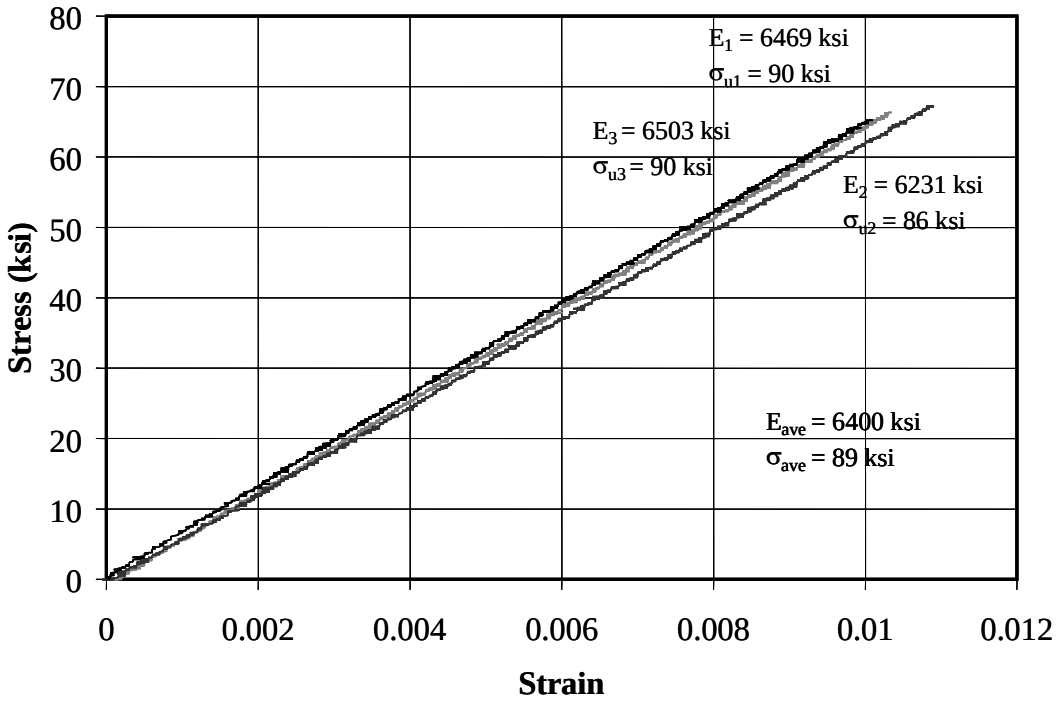

Figure A.3 Stress vs. Strain - #5 Glass Pultrall (P), Phase I

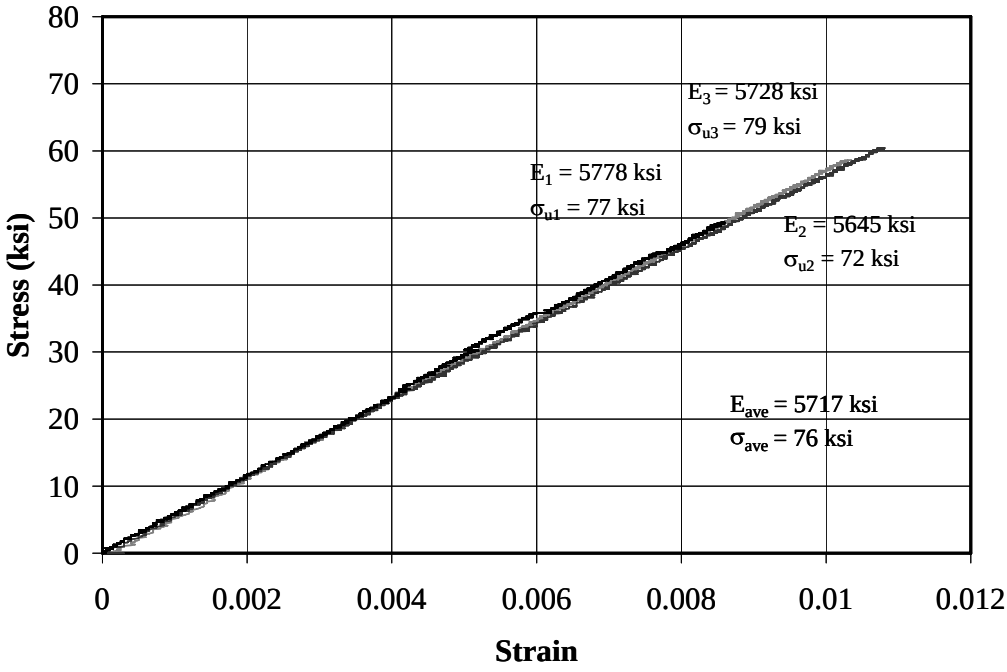

Figure A.4 Stress vs. Strain - #8 Glass Hughes (H), Phase I

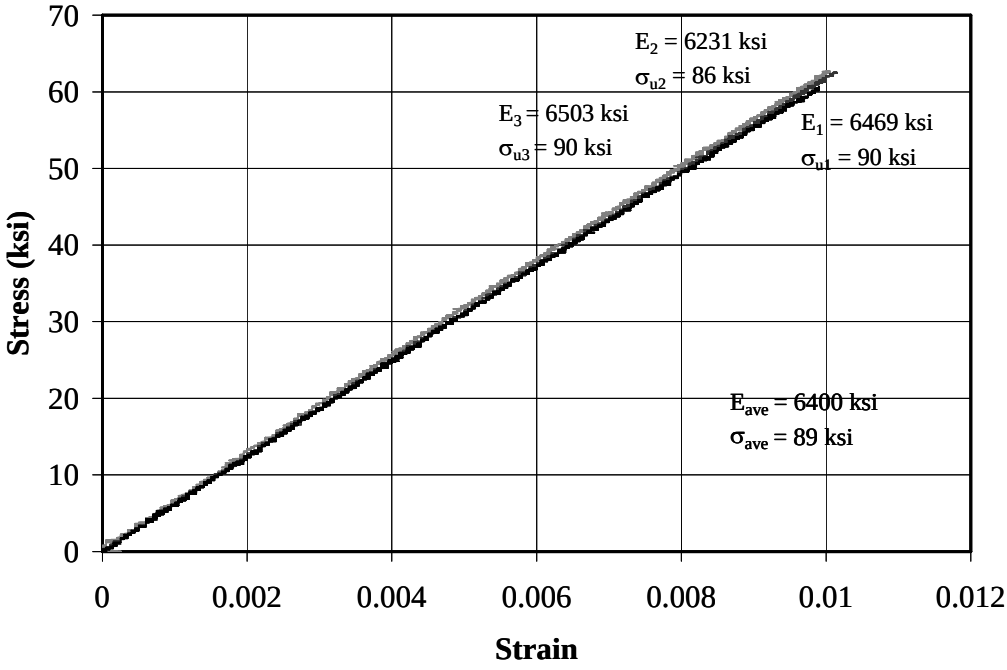

Figure A.5 Stress vs. Strain - #8 Glass Pultrall (P), Phase I

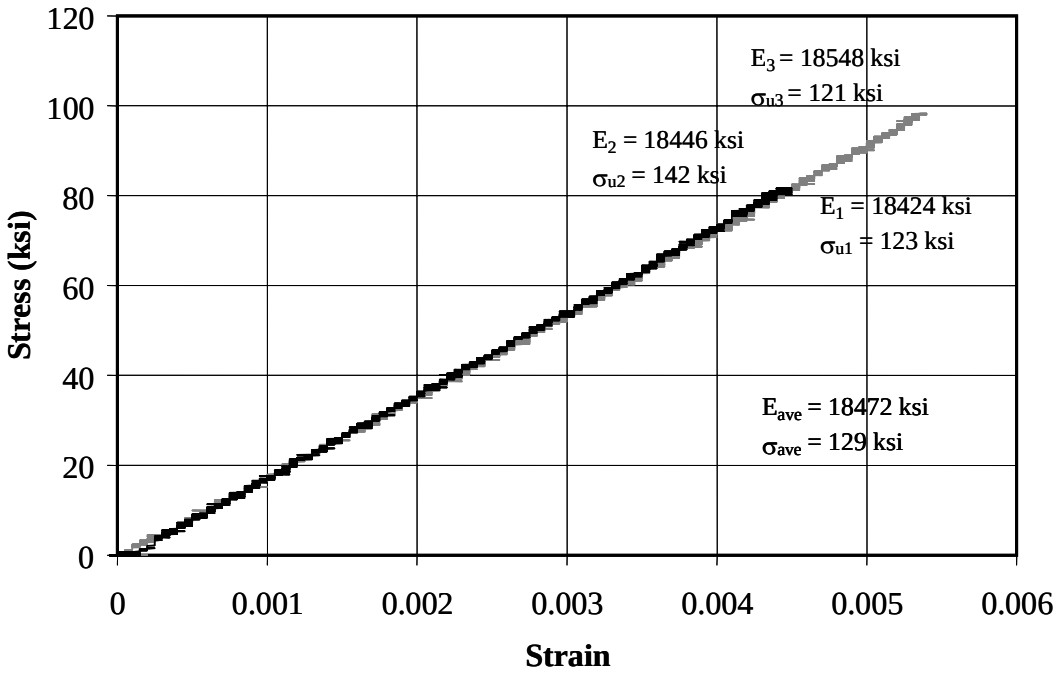

Figure A.6 Stress vs. Strain - #5 Hughes Carbon (C), Phase I

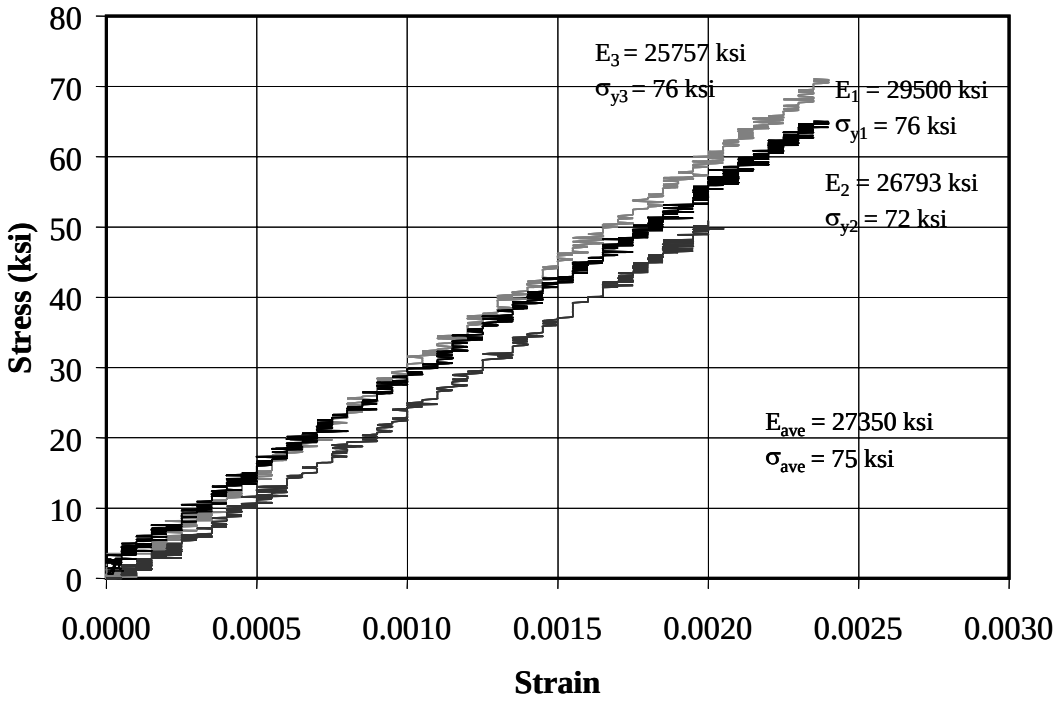

Figure A.7 Stress vs. Strain - #5 Steel (S), Phase I

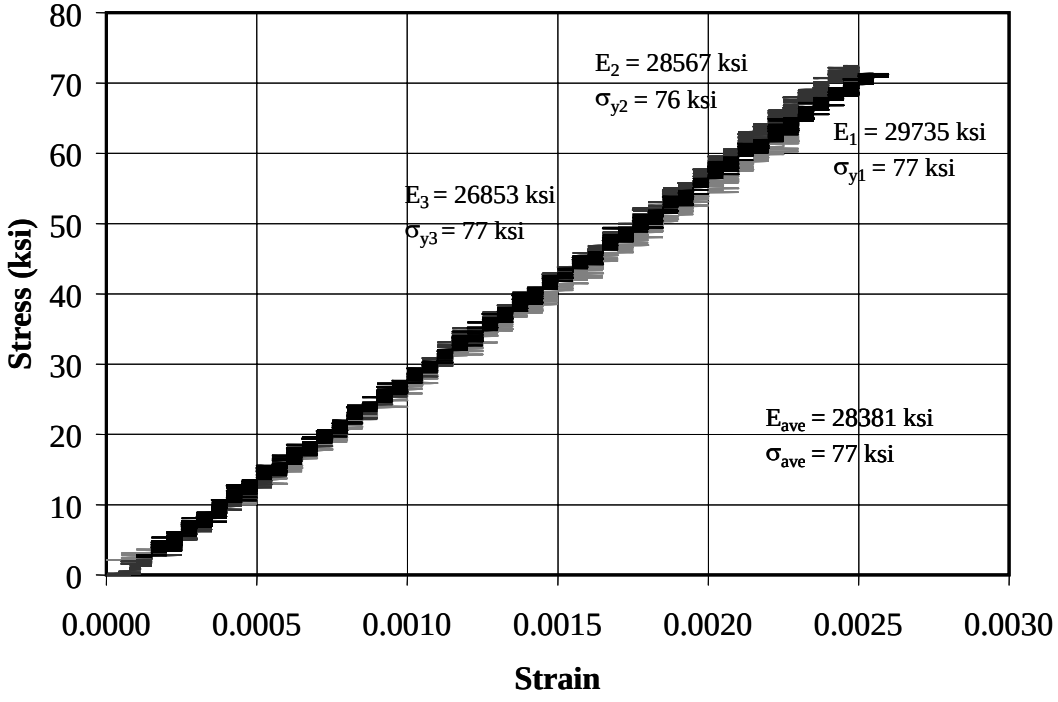

Figure A.8 Stress vs. Strain - #8 Steel (S)-Phase I

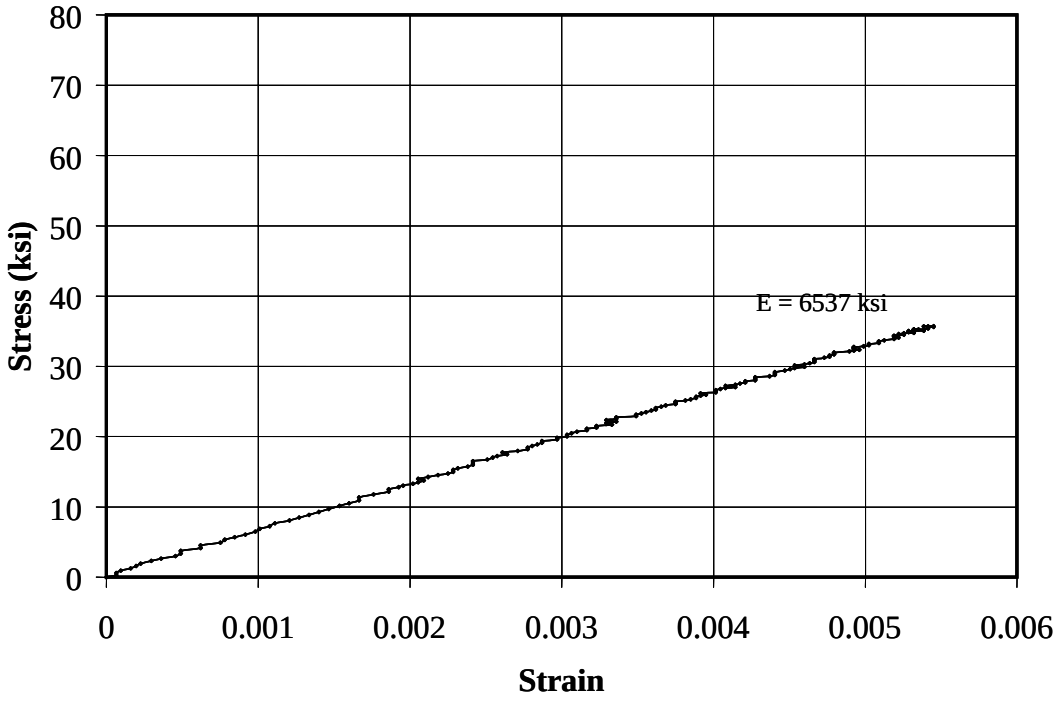

Figure A.9 Stress vs. Strain - #5 Hughes Glass (HG1), Phase II

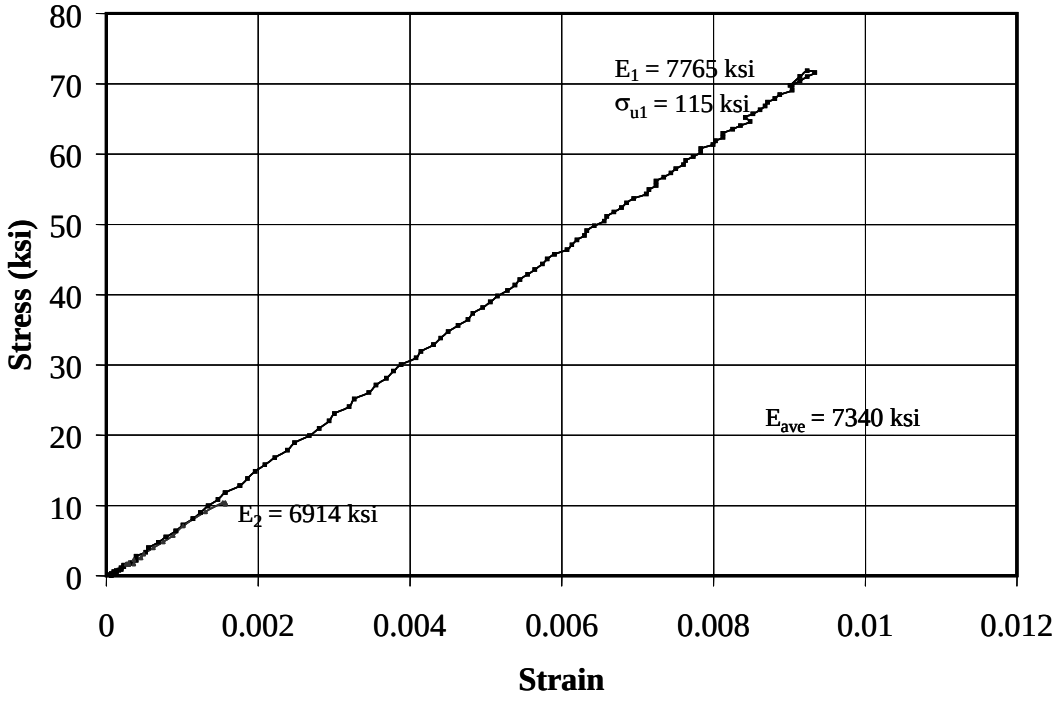

Figure A.10 Stress vs. Strain - #5 Hughes Glass (HG2), Phase II

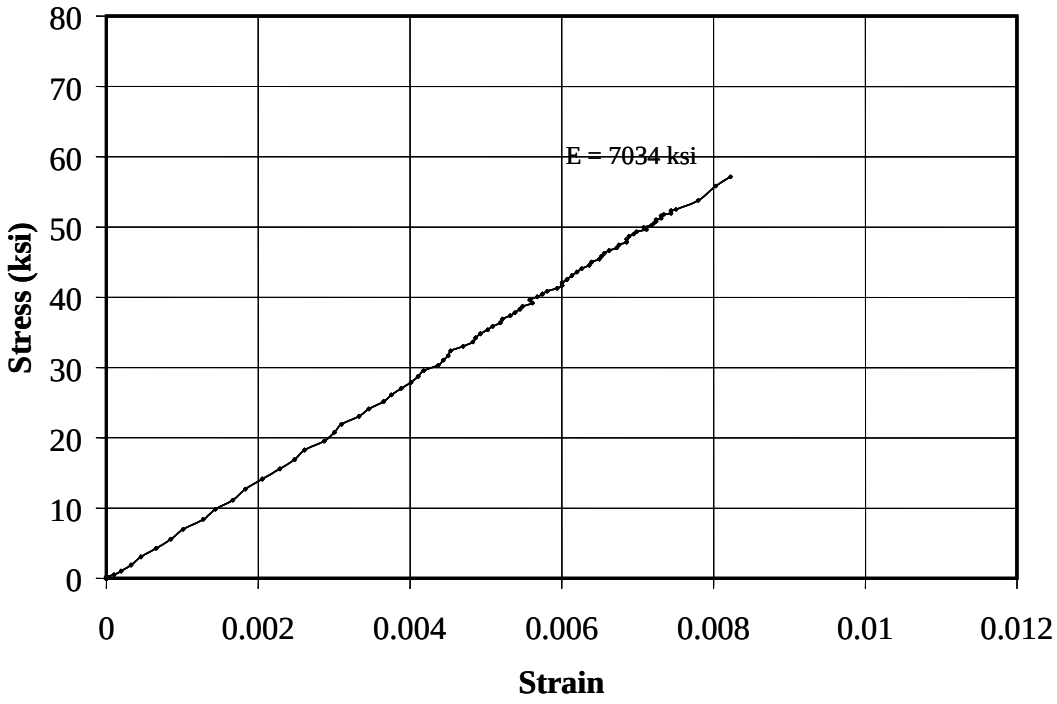

Figure A.11 Stress vs. Strain - #5 Hughes Glass (HG3), Phase II

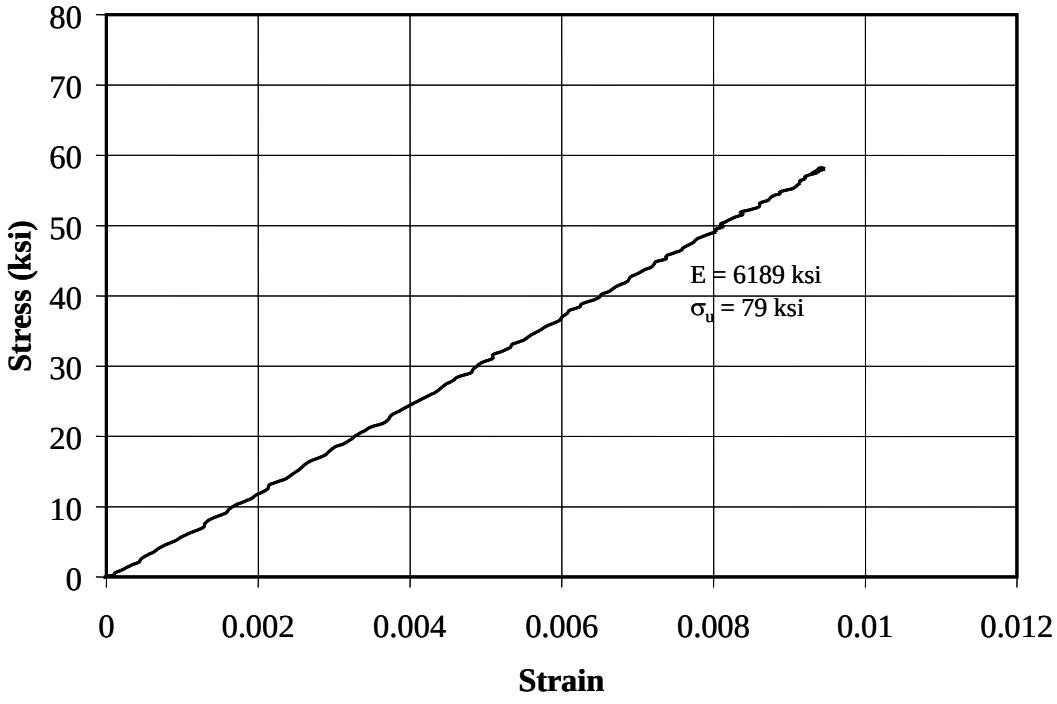

Figure A.12 Stress vs. Strain - #5 Glass Pultrall (PG1), Phase II

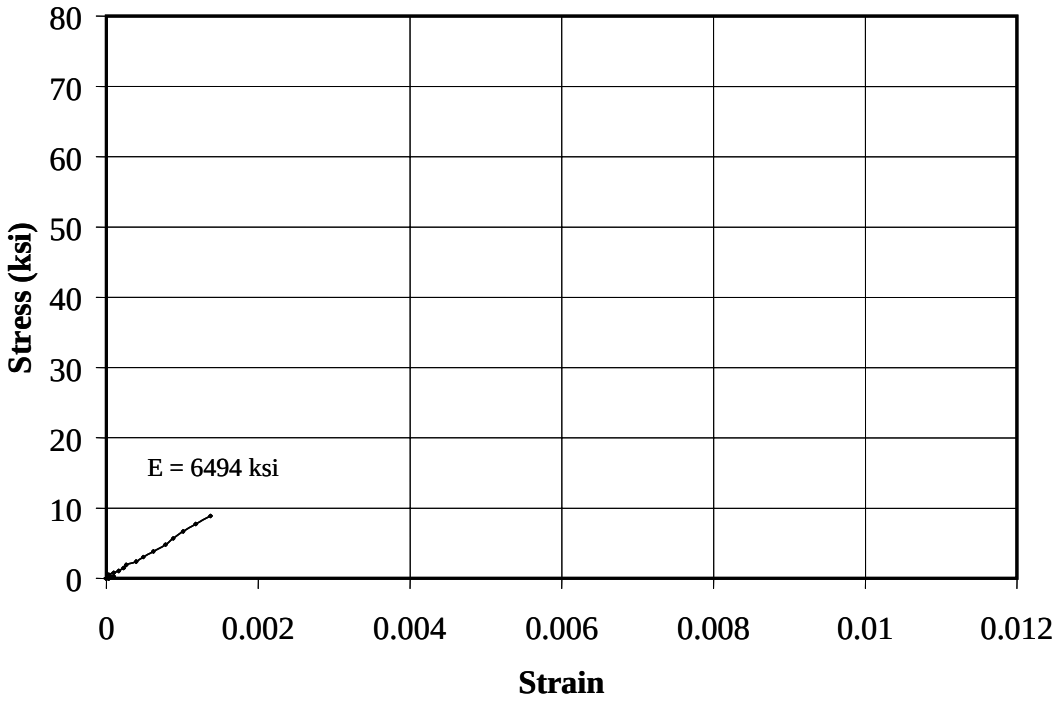

Figure A.13 Stress vs. Strain - #5 Pultrall Glass (PG2), Phase II

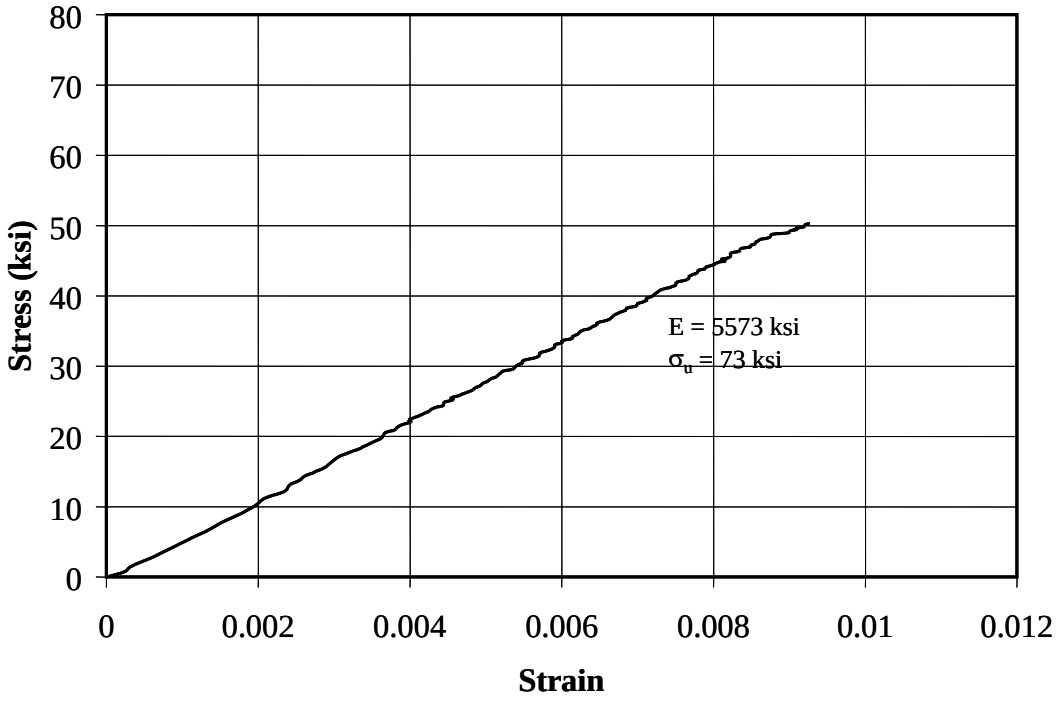

Figure A.14 Stress vs. Strain - #8 Hughes Glass (HG), Phase II

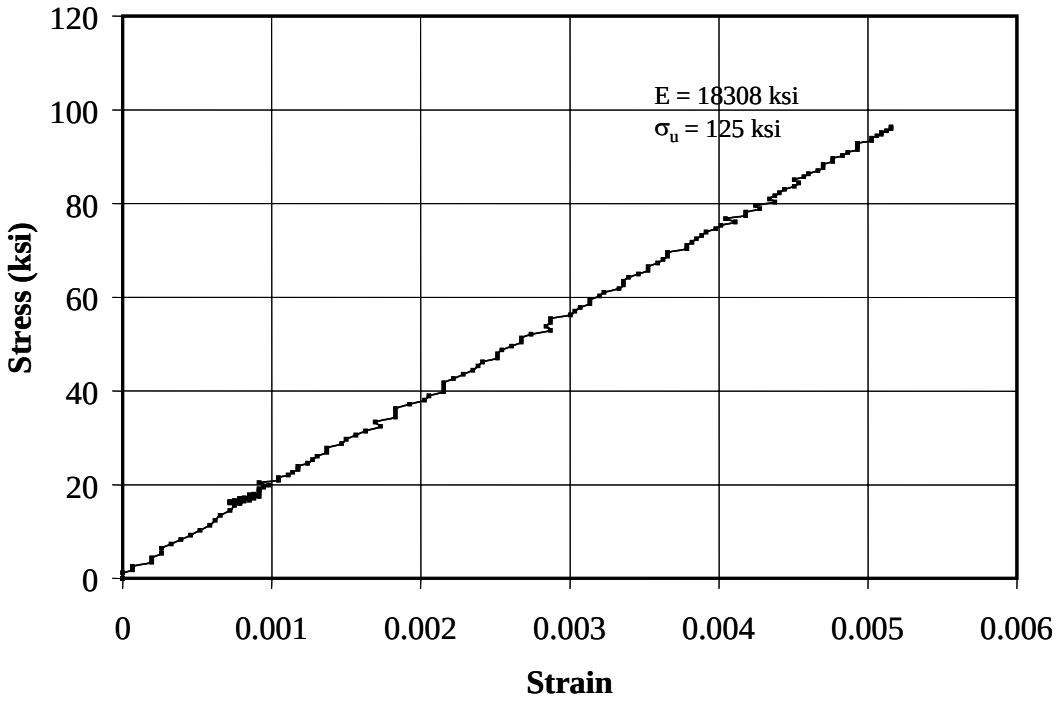

Figure A.15 Stress vs. Strain - #5 Hughes Carbon (HC), Phase II

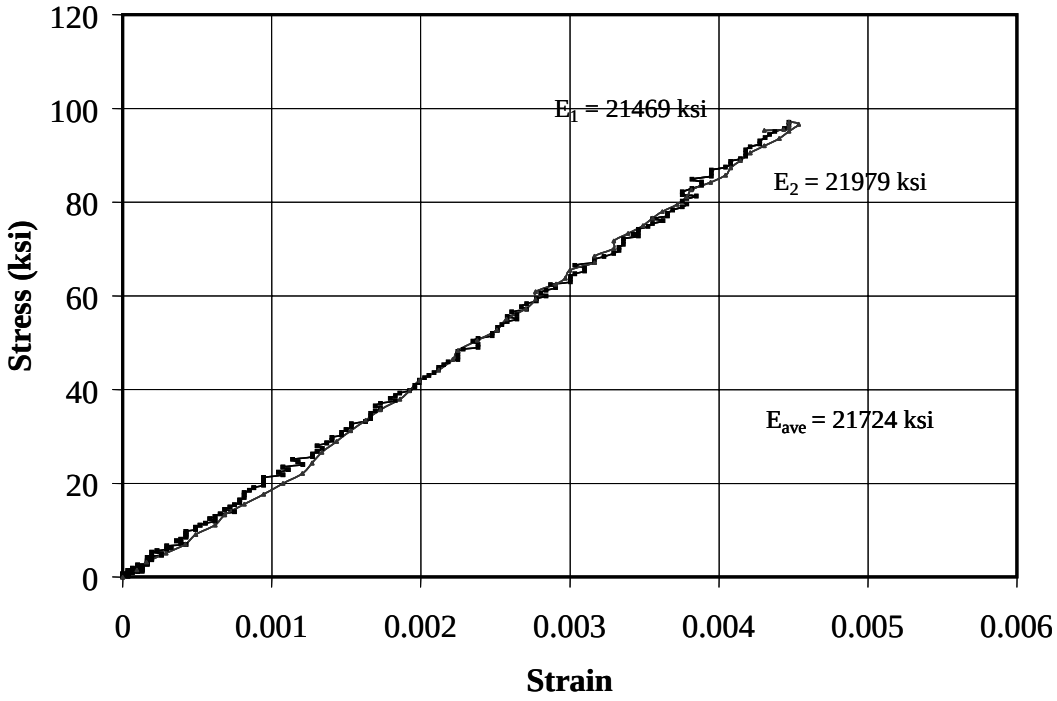

Figure A.16 Stress vs. Strain - #5 Pultrall Carbon (PC1), Phase II

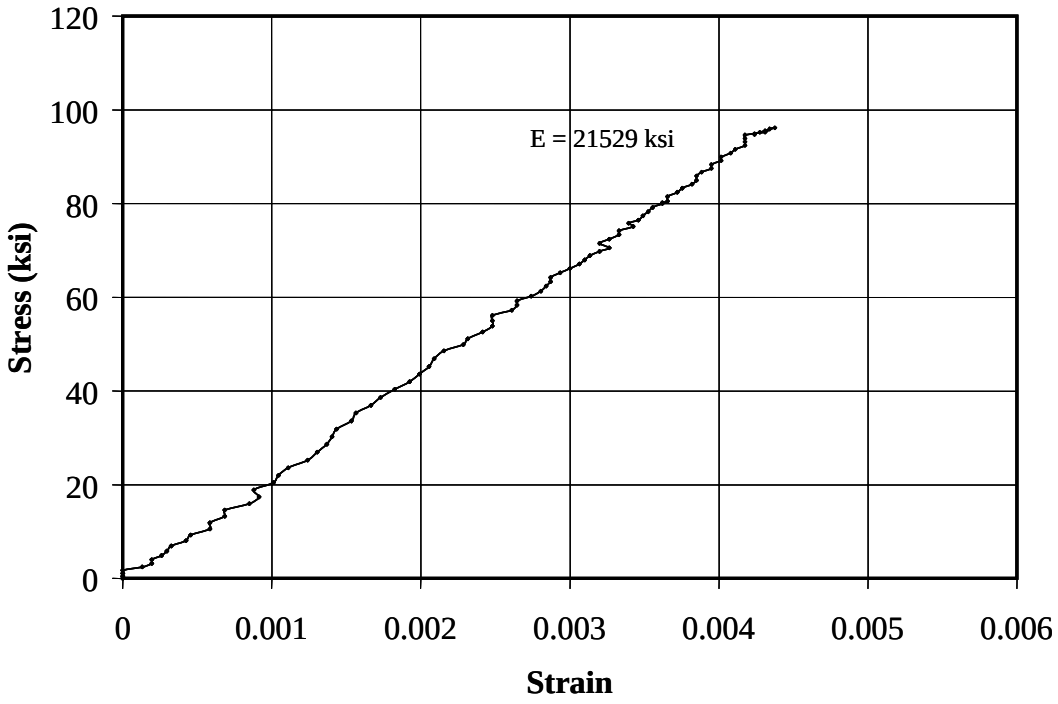

Figure A.17 Stress vs. Strain - #5 Pultrall Carbon (PC2), Phase II

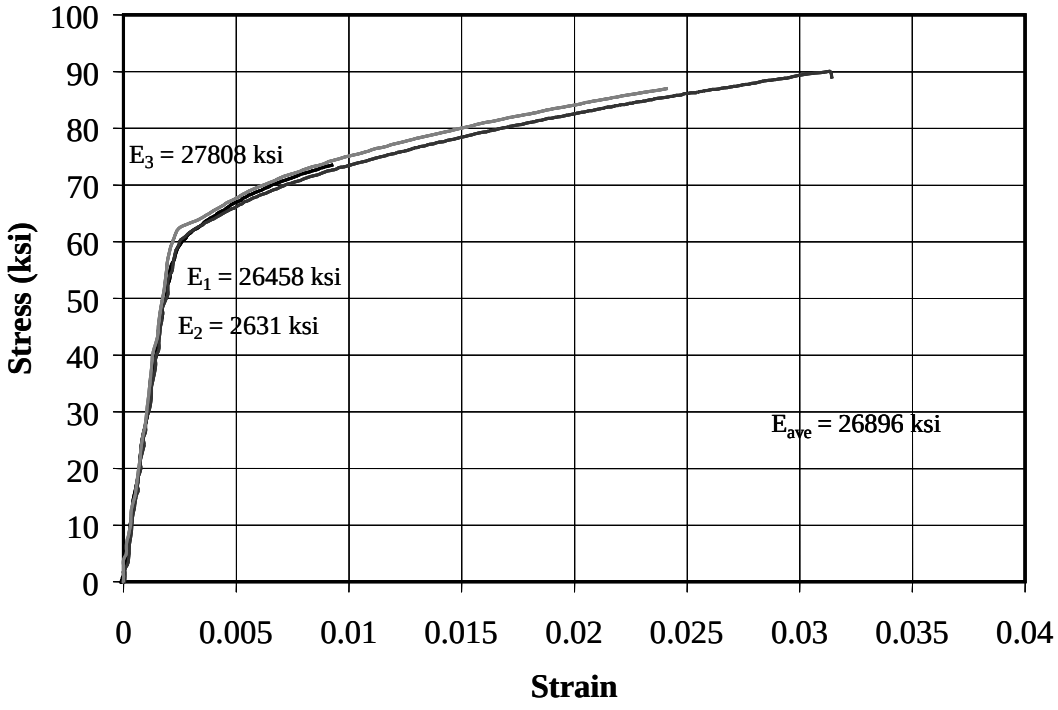

Figure A.18 Stress vs. Strain - #5 Steel (S), Phase II

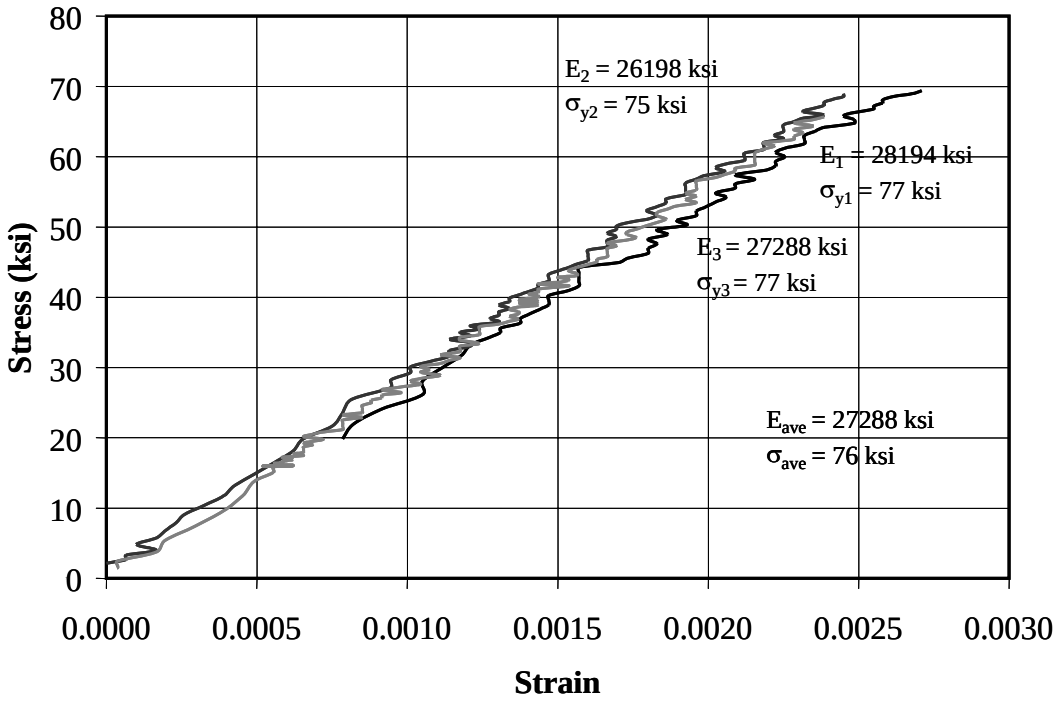

Figure A.19 Stress vs. Strain - #8 Steel (S1 and S2), Phase II

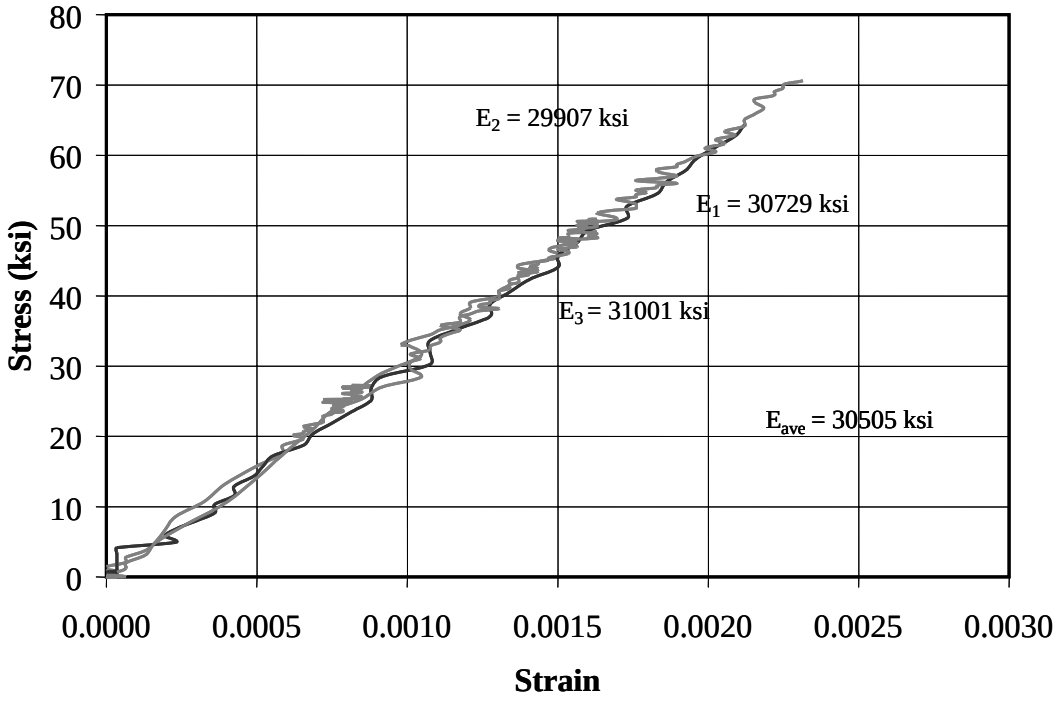

Figure A.20 Stress vs. Strain - #8 Steel Bar (S3), Phase II

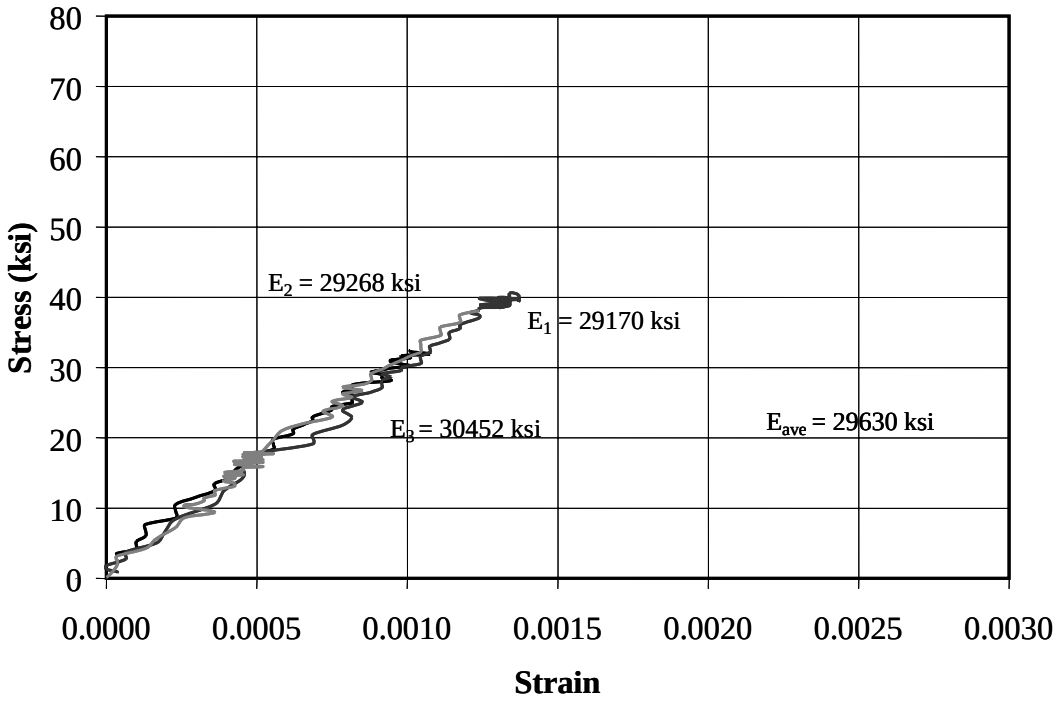

Figure A.21 Stress vs. Strain - Steel Pipe (S4), Phase II

Appendix B

Concrete Properties

Table B.1 Measured Concrete Properties

Concrete Batch	Age (days)	Concrete Compressive Strength (psi)								Tensile Strength (psi)			
		6x12 in. Cylinders				4x8 in. Cylinders				6x12 in. Split Cylinders			
		1	2	3	Average	1	2	3	Average	1	2	3	Average
I	28	5213	4948	5117	5093	-	-	-	-	587	635	620	614
	32	4903	5470	5445	5273	-	-	-	-	545	604	626	592
	38	5388	5418	5420	5409	-	-	-	-	592	568	553	571
II	28	5523	5333	5505	5454	-	-	-	-	469	497	543	503
	35	5561	5334	5510	5468	-	-	-	-	583	525	458	522
	43	5542	5445	5480	5489	-	-	-	-	562	498	514	525
III	28	-	3614	3696	3655	3600	3624	3814	3679	-	-	-	-
	109	4202	4045	4120	4122	3581	3858	3971	3803	383	380	379	381
	132	4182	3818	3993	3998	3909	3853	3891	3884	398	358	371	376
	142	3888	3952	3937	3926	3892	-	-	3892	406	363	385	385
IV	28	4035	3969	4109	4038	4425	4412	4536	4457	-	-	-	-
	131	4665	4680	4666	4670	4369	-	4117	4243	481	433	375	430
	151	4610	4481	4728	4606	4626	4814	4650	4638	491	442	454	462
	157	4481	4891	4588	4653	4704	4827	4831	4767	441	451	412	435
V	28	3700	3796	3650	3715	4000	4136	3920	4019	-	-	-	-
	156	4086	4358	4112	4185	3905	4106	4196	4069	387	424	385	399
	167	3818	3800	3888	3835	3828	3940	4002	3923	447	446	487	460
	183	4281	4107	4103	4164	4047	4163	4025	4078	410	468	418	432

Appendix C

Crack Measurement and Pattern

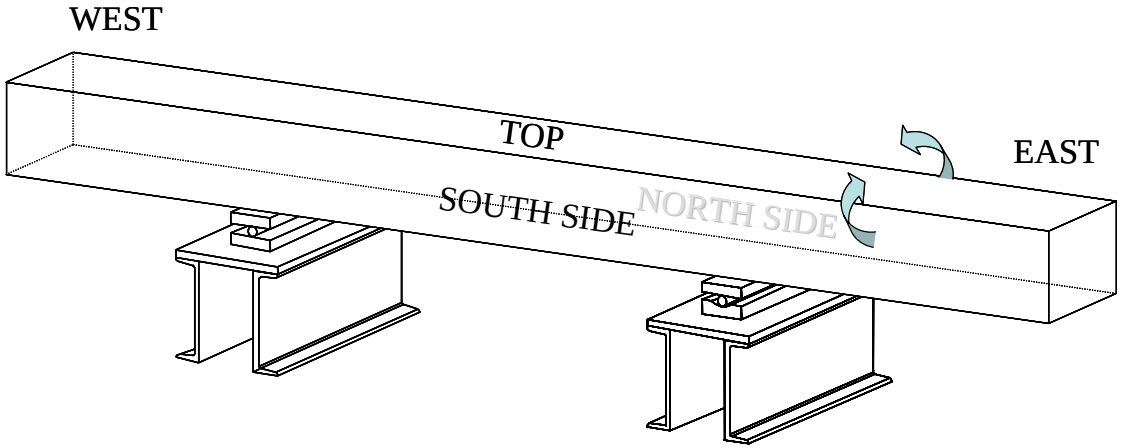

Figure C.1 Specimen Orientation (Phase I)

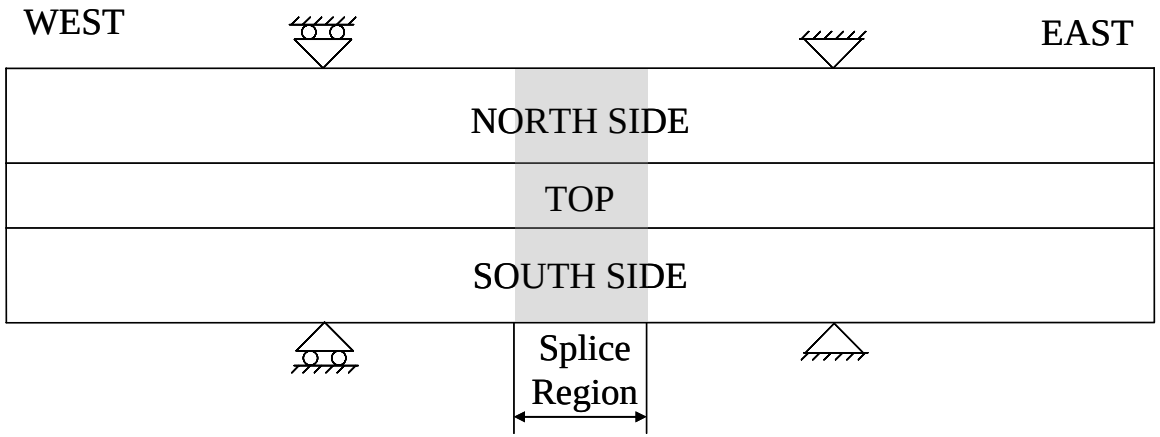

Figure C.2 Template for Crack Drawings (Phase I)

Table C.1 Crack Measurements and Pattern for Specimen B-S-8-18

Load, P (kips)	Crack Width (1/1000 in.)						
	Crack No.						
	1	2	3	4	5	6	7
12	2	2					
13	3	3					
14	3	3					
15	3	3	3	2	2	3	
16	4	3	3	3	3	3	
17	3	4	3	3	3	3	
18	4	4	3	3	4	3	
19	4	4	4	5	5	4	
20	4	5	4	5	5	4	6

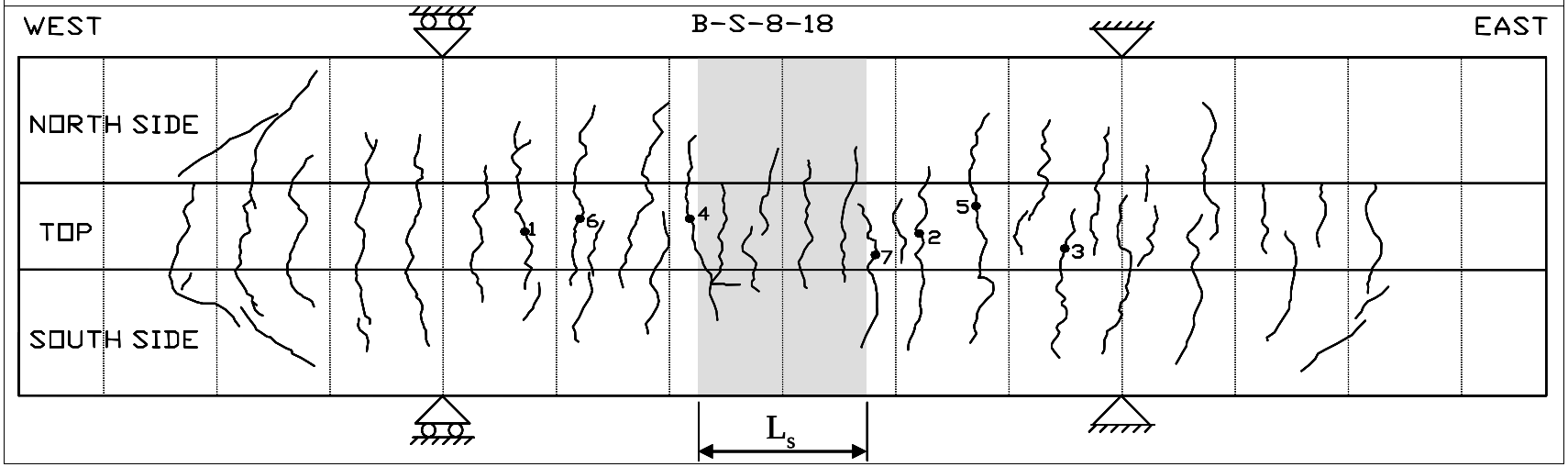

Table C.1 Crack Measurements and Pattern for Specimen B-S-8-18 (continued)

Load, P (kips)	Crack Width (1/1000 in.)						
	Crack No.						
	1	2	3	4	5	6	7
21	4	5	4	5	5	5	6
22	4	5	5	5	6	5	7
24	5	6	5	6	6	5	7
26	5	7	5	7	6	6	8
28	7	8	6	8	7	8	10

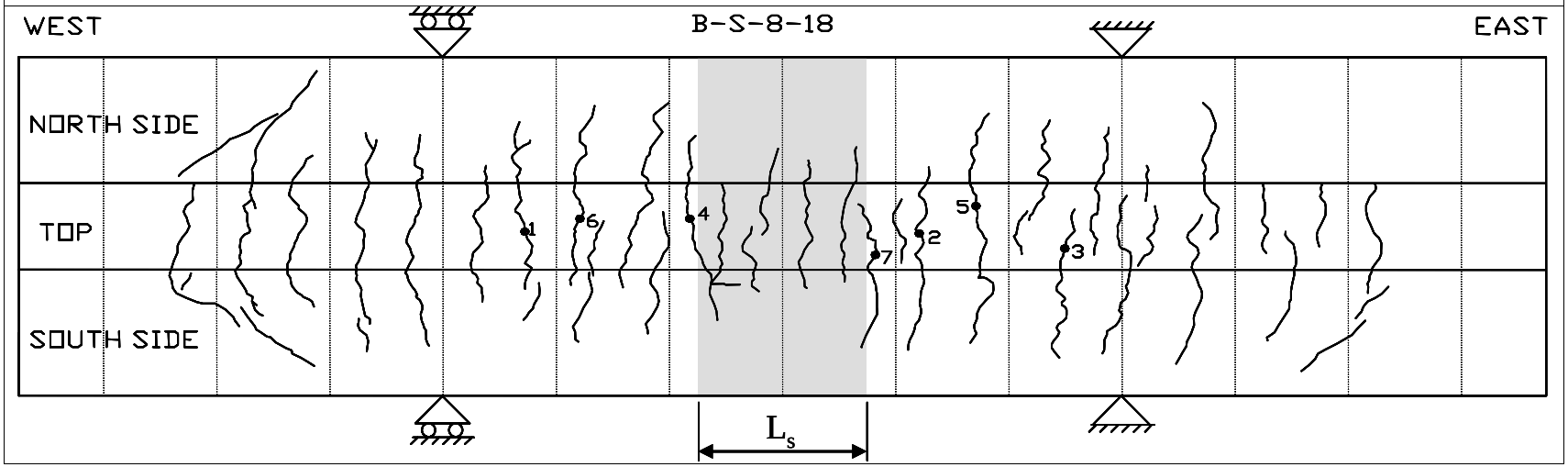

Table C.2 Crack Measurements and Pattern for Specimen B-P-8-18

Load, P (kips)	Crack Width (1/1000 in.)								
	Crack No.								
	1	2	3	4	5	6	7	8	9
7	3	5							
8	6	7	6	6	7	1			
9	7	8	7	9	9	3	5	6	5
10	10	10	8	10	10	5	6	10	9
11	15	10	10	10	10	5	9	11	10
12	18	13	10	14	15	7	10	11	15
13	22	18	10	14	17	9	11	15	16
14	24	18	12	15	18	9	12	15	18
15	24	20	12	15	19	9	12	15	20

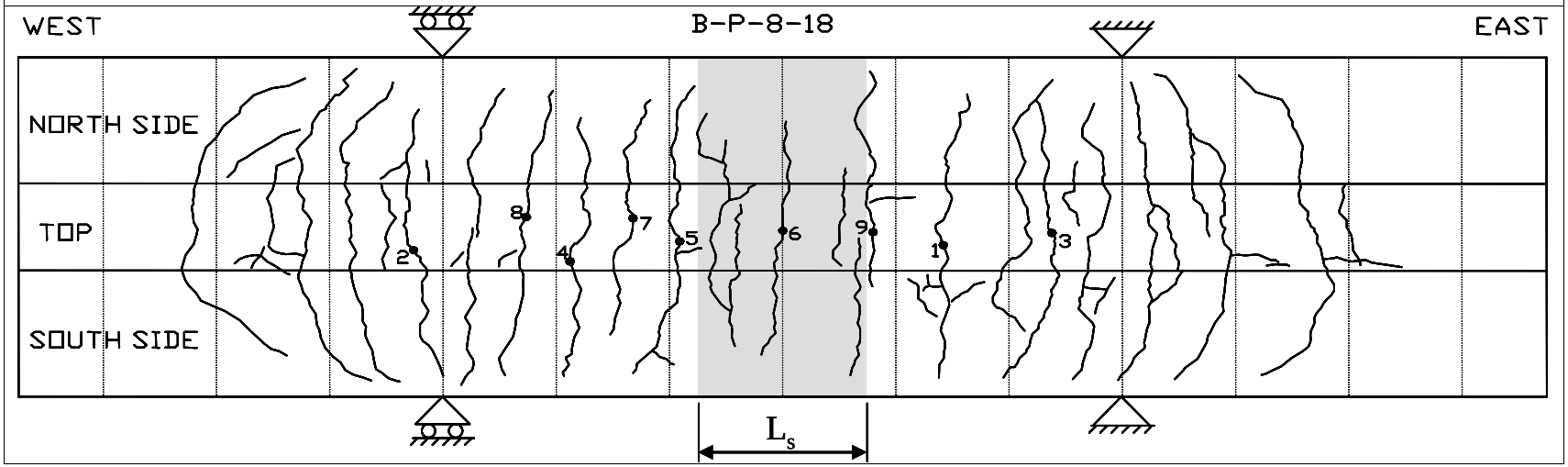

Table C.3 Crack Measurements and Pattern for Specimen B-H-8-18

Load, P (kips)	Crack Width (1/1000 in.)							
	Crack No.							
	1	**2**	**3**	**4**	**5**	**6**	**7**	**8**
7	1	4	2	4	6	4		
8	5	5	7	7	8	4	7	
9	6	7	7	7	9	9	7	3
10	8	7	9	10	10	14	10	5
11	8	8	9	12	10	16	10	8
12	10	8	10	12	14	18	11	8
13	11	10	12	17	15	23	13	9
14	14	11	12	18	16	30	15	10
15	15	11	15	20	18	32	15	12
16	15	14	15	20	19	35	15	12
17	16	16	16	25	20	40	19	13

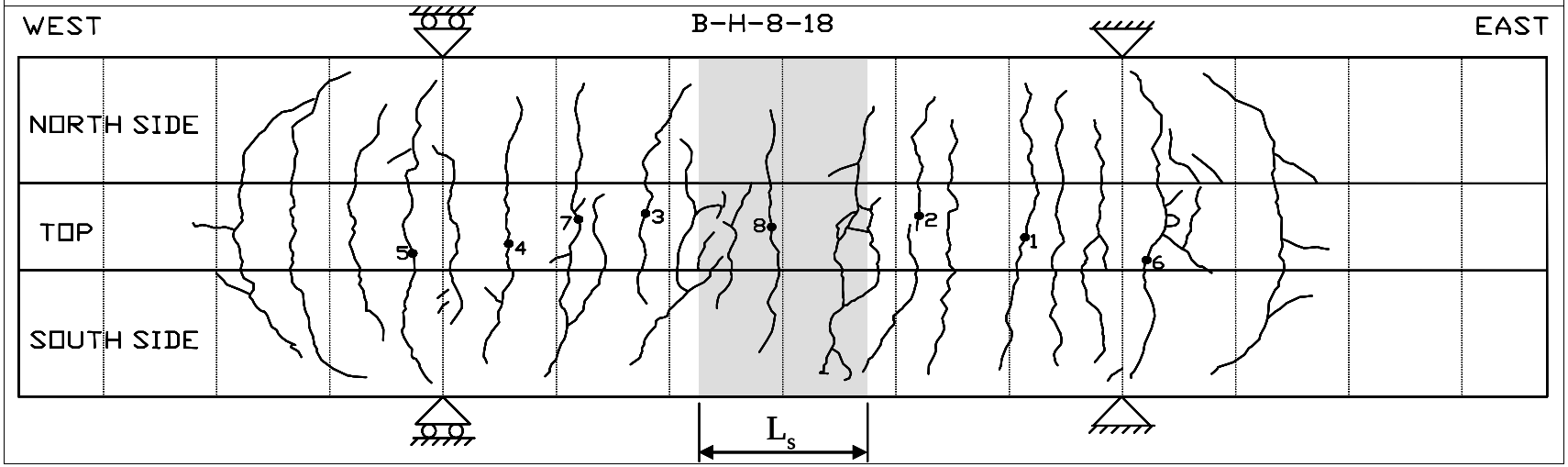

Table C.4 Crack Measurements and Pattern for Specimen B-HN-5-18

Load, P (kips)	Crack Width (1/1000 in.)								
	Crack No.								
	1	2	3	4	5	6	7	8	9
5.5	4	4	10						
6.0	12	5	18	15					
6.5	15	12	24	20	4				
7.0	16	25	35	23	4	3	13	10	
7.5	17	30	35	30	5	4	16	16	
8.0	16	30	38	34	5	5	19	18	17
8.5	15	42	42	40	7	5	20	20	17
9.0	18	45	42	40	7	8	25	20	18
9.5	18	45	45	45	8	9	29	26	20
10.0	17	42	50	45	8	12	35	30	22
10.5	16	50	50	46	9	11	40	30	22
11.0	18	50	50	50	9	11	40	30	21

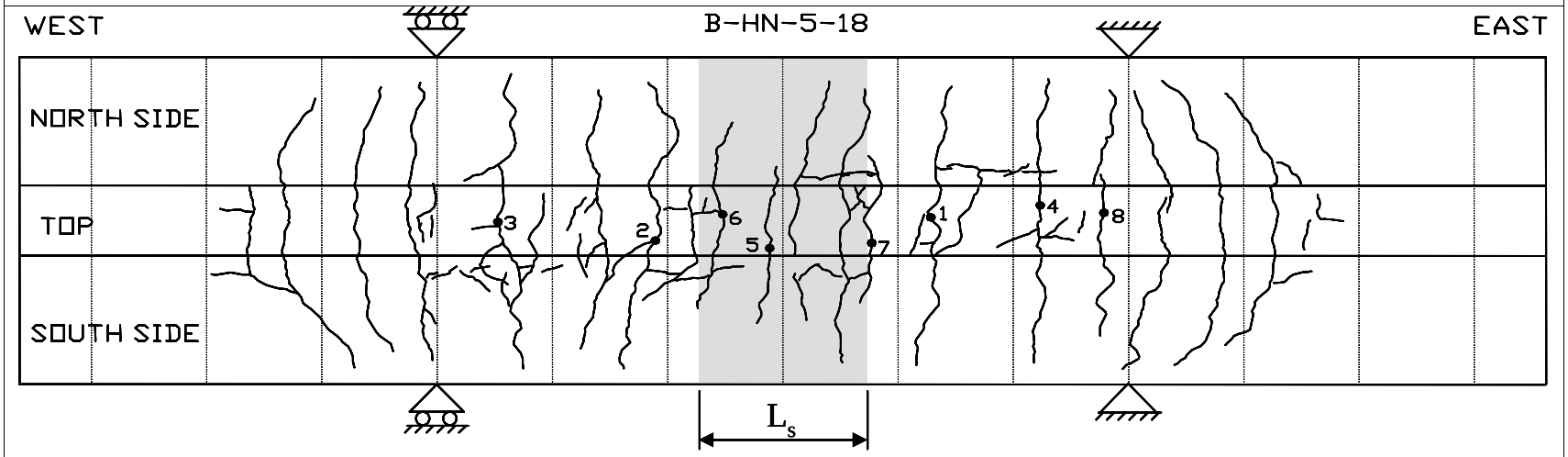

Table C.5 Crack Measurements and Pattern for Specimen B-HO-5-18

Load, P (kips)	Crack Width (1/1000 in.)								
	Crack No.								
	1	2	3	4	5	6	7	8	9
5.5	10	11	10						
6.0	20	15	17	2	7				
6.5	25	24	23	5	9	14			
7.0	27	29	25	8	12	15	15	12	
7.5	30	30	30	10	15	17	20	17	
8.0	30	34	27	11	19	18	20	18	
8.5	32	40	27	14	20	22	28	18	
9.0	34	45	25	17	20	25	30	25	
9.5	34	45	25	17	20	25	34	25	
10.0	40	54	25	17	25	25	35	25	
10.5	40	56	28	20	28	27	35	30	12
11.0	38	58	28	20	28	35	45	35	13

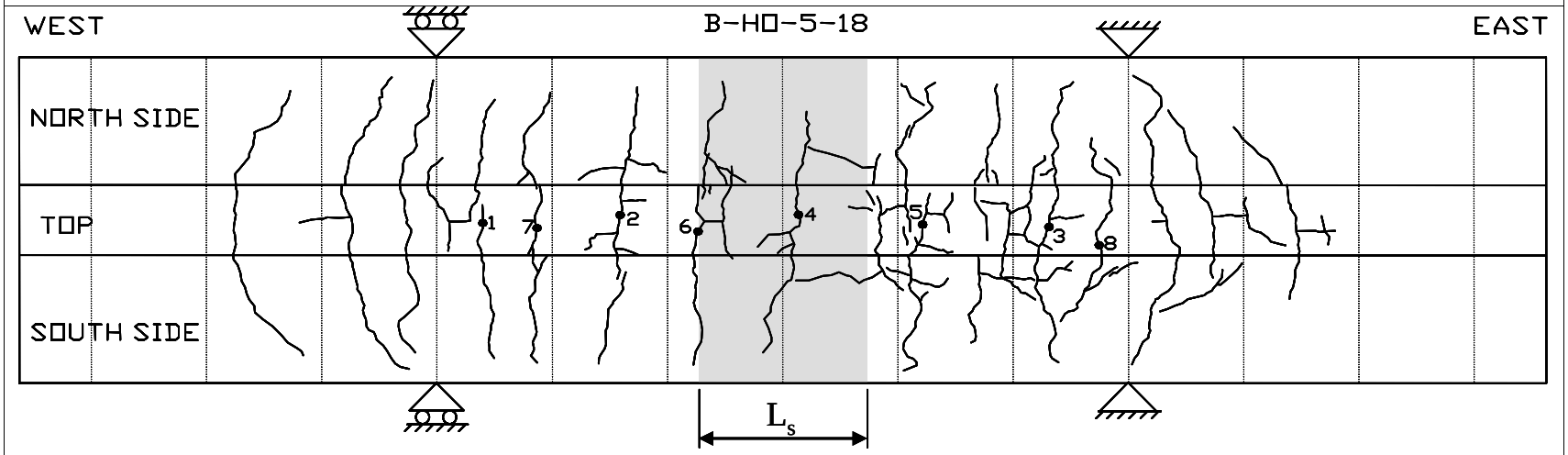

Table C.6 Crack Measurements and Pattern for Specimen B-P-5-18

Load, P (kips)	Crack Width (1/1000 in.)								
	Crack No.								
	1	2	3	4	5	6	7	8	9
5.5	7	5							
6.0	11	8	7	6					
6.5	15	10	8	17					
7.0	15	13	13	19	12	10	12		
7.5	21	15	18	20	14	13	9	4	8
8.0	24	16	18	20	17	16	10	5	8
8.5	25	18	20	25	17	18	12	7	8
9.0	27	20	21	28	20	20	15	9	8
9.5	28	20	22	26	20	23	15	10	9
10.0	30	22	24	29	22	25	15	10	10
10.5	30	22	26	30	25	25	15	13	10
11.0	38	22	28	33	28	30	15	15	10

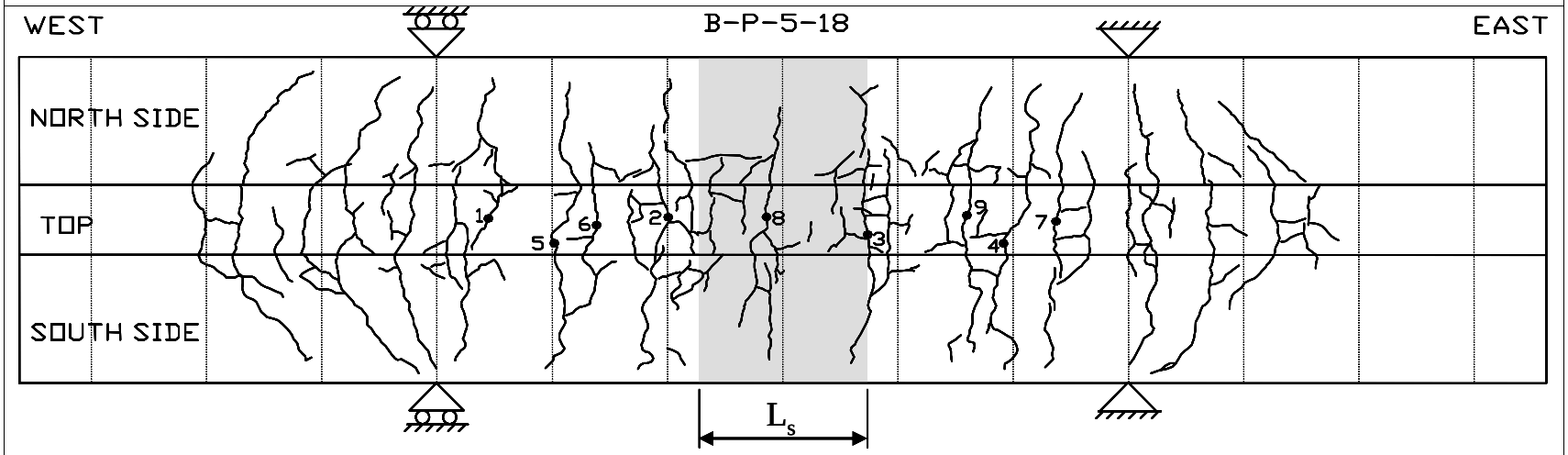

Table C.7 Crack Measurements and Pattern for Specimen B-S-5-18

Load, P (kips)	Crack Width (1/1000 in.)									
	Crack No.									
	1	**2**	**3**	**4**	**5**	**6**	**7**	**8**	**9**	**10**
7	1	2	2	2						
8	2	2	4	3	2	4	3			
9	3	4	4	4	3	5	5	1	1	1
10	5	5	6	5	5	5	5	2	1	1
11	5	8	6	5	5	8	7	3	1	2
12	8	8	8	6	5	6	6	5	1	2
13	8	9	8	6	6	10	8	5	1	2
14	9	12	10	9	9	10	10	5	2	3
15	9	12	10	9	9	10	10	7	2	4
16	10	15	10	10	9	10	13	8	2	4
17	10	16	12	11	10	10	14	10	2	4

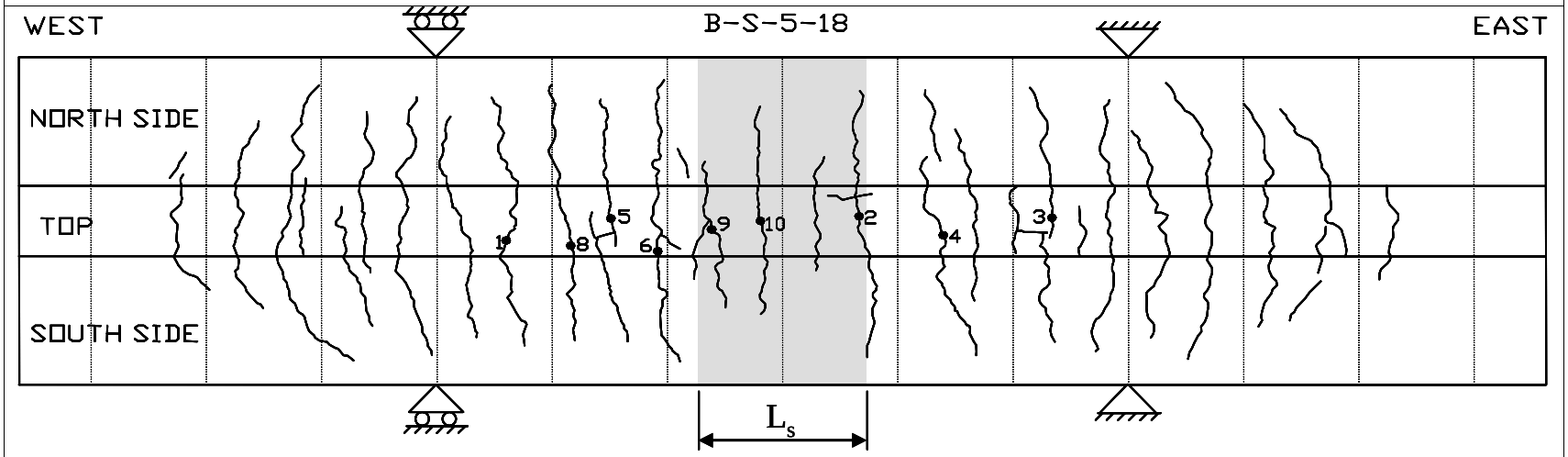

Table C.8 Crack Measurements and Pattern for Specimen B-C-5-18

Load, P (kips)	Crack Width (1/1000 in.)									
	Crack No.									
	1	2	3	4	5	6	7	8	9	10
5.5	2	4								
6.0	4	4								
6.5	6	7	2	3	1					
7.0	8	9	4	5	2	2				
7.5	8	10	5	8	3	4	5			
8.0	10	10	5	9	3	5	8	3	1	5
8.5	10	10	8	9	4	7	10	3	2	8
9.0	10	11	7	9	4	7	9	3	3	10
9.5	10	12	10	10	4	8	10	4	4	10
10.0	12	14	10	10	5	8	11	5	5	12
10.5	14	15	10	10	5	8	13	5	5	12
11.0	13	18	10	13	5	10	14	5	5	12

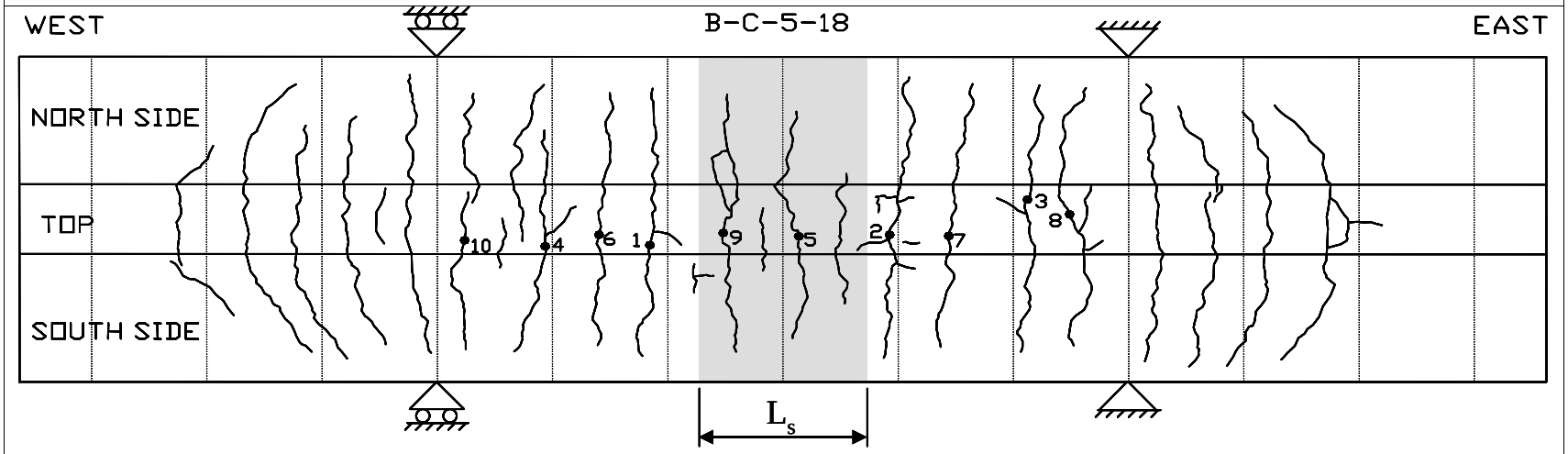

Table C.8 Crack Measurements and Pattern for Specimen B-C-5-18 (continued)

Load, P (kips)	Crack Width (1/1000 in.)									
	Crack No.									
	1	2	3	4	5	6	7	8	9	10
11.5	14	20	13	14	5	10	15	5	10	12
12.0	14	20	13	13	5	10	15	5	10	13
12.5	15	23	13	13	5	10	15	8	12	13
13.0	15	24	15	14	6	10	15	8	11	17
13.5	15	27	14	15	6	12	15	8	13	15
14.0	18	27	15	17	6	15	15	8	14	18
14.5	17	29	15	19	8	15	19	8	14	20
15.0	18	30	17	19	7	17	19	10	15	20
15.5	18	30	19	19	7	17	22	10	17	20

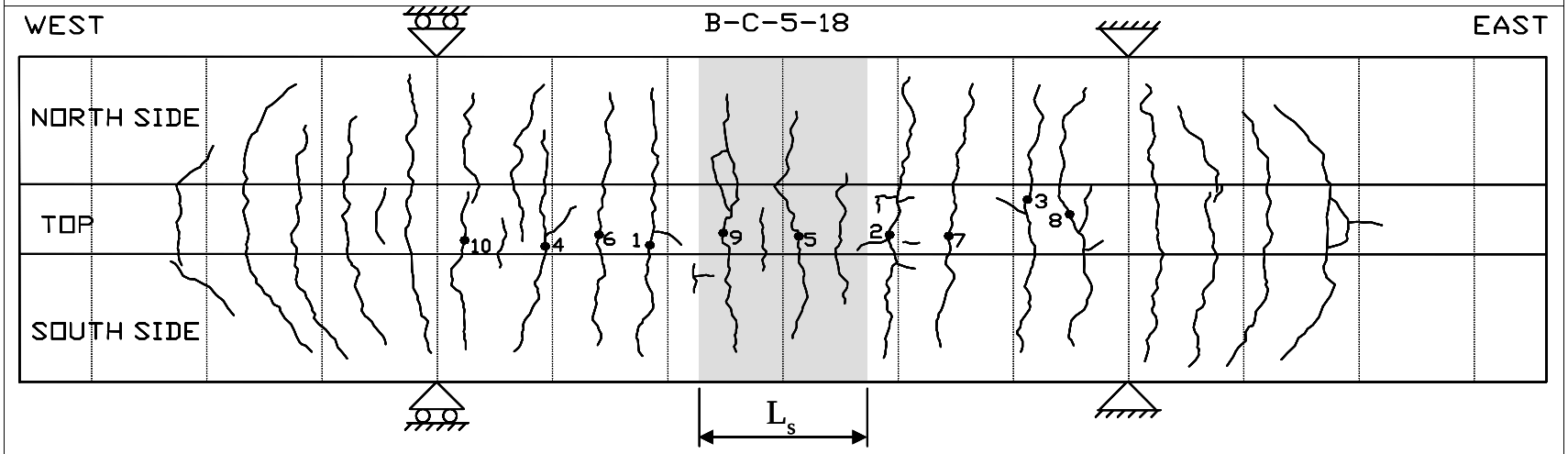

Table C.9 Crack Measurements and Pattern for Specimen B-C-5-12

Load, P (kips)	Crack Width (1/1000 in.)									
	Crack No.									
	1	2	3	4	5	6	7	8	9	10
5.0	2	3								
5.5	5	5	5	3						
6.0	6	7	5	5	3					
6.5	8	7	7	5	3	2	2	1	1	
7.0	8	8	8	7	6	2	4	5	2	
7.5	9	8	9	8	7	3	5	5	2	2
8.0	10	8	10	8	10	3	6	9	4	3
8.5	10	8	11	8	10	3	6	9	4	3
9.0	12	9	12	10	12	7	6	9	5	5
9.5	12	9	12	10	12	9	7	10	6	6
10.0	12	9	13	10	12	9	7	10	7	7

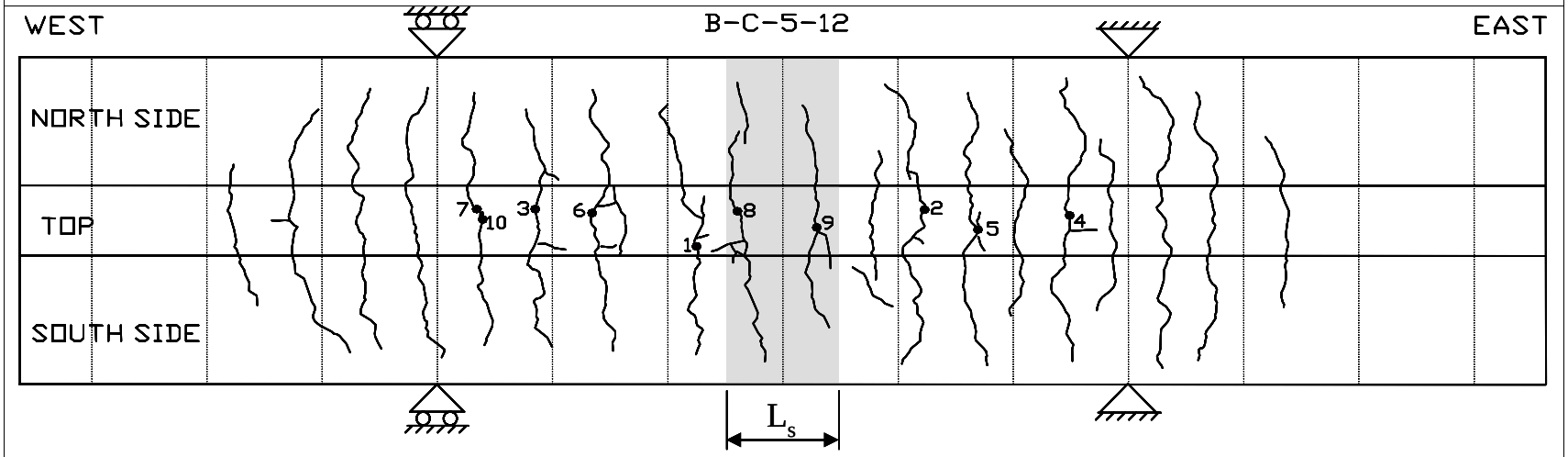

Table C.9 Crack Measurements and Pattern for Specimen B-C-5-12 (continued)

Load, P (kips)	Crack Width (1/1000 in.)									
	Crack No.									
	1	2	3	4	5	6	7	8	9	10
10.5	12	9	13	13	12	10	7	10	6	7
11.0	13	9	14	13	14	10	7	11	7	7
11.5	14	9	14	14	15	12	8	12	7	7
12.0	15	12	16	15	15	13	9	13	7	8

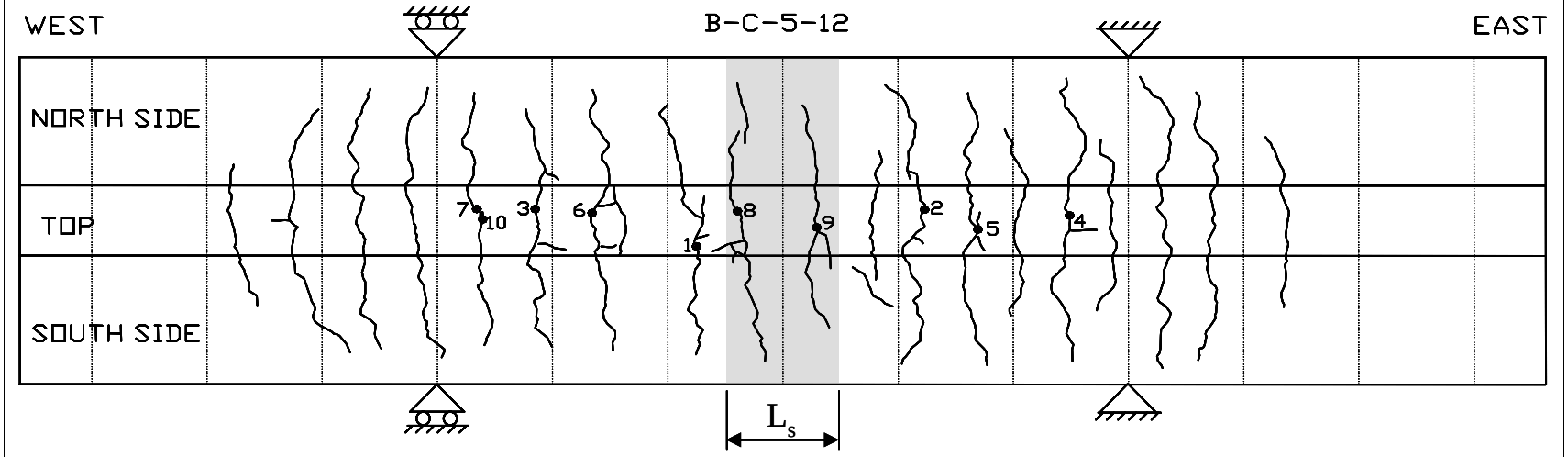

Table C.10 Crack Measurements and Pattern for Specimen B-S-8-36

Load, P (kips)	Crack Width (1/1000 in.)													
	Crack No.													
	1	2	3	4	5	6	7	8	9	10	11	12	13	14
7	2	1	2	2	2									
8	2	1	2	3	3	2	2	1						
9	2	2	3	3	3	3	2	2	1					
10	2	3	3	4	3	3	3	3	1	3	1	2	1	
11	3	3	3	4	4	3	3	3	2	3	1	2	2	
12	3	3	4	5	4	4	4	3	2	4	2	4	3	
13	4	3	4	5	4	5	4	3	2	4	2	4	3	
14	4	3	4	5	4	6	4	3	2	4	2	5	3	
15	5	5	4	5	5	6	4	4	3	4	3	5	4	
16	5	5	4	5	5	6	5	4	3	4	3	6	4	
17	5	5	4	6	6	6	5	5	3	5	3	6	4	
18	5	5	4	6	6	7	5	5	3	5	3	7	5	
19	6	5	4	8	6	7	6	5	4	5	4	7	5	

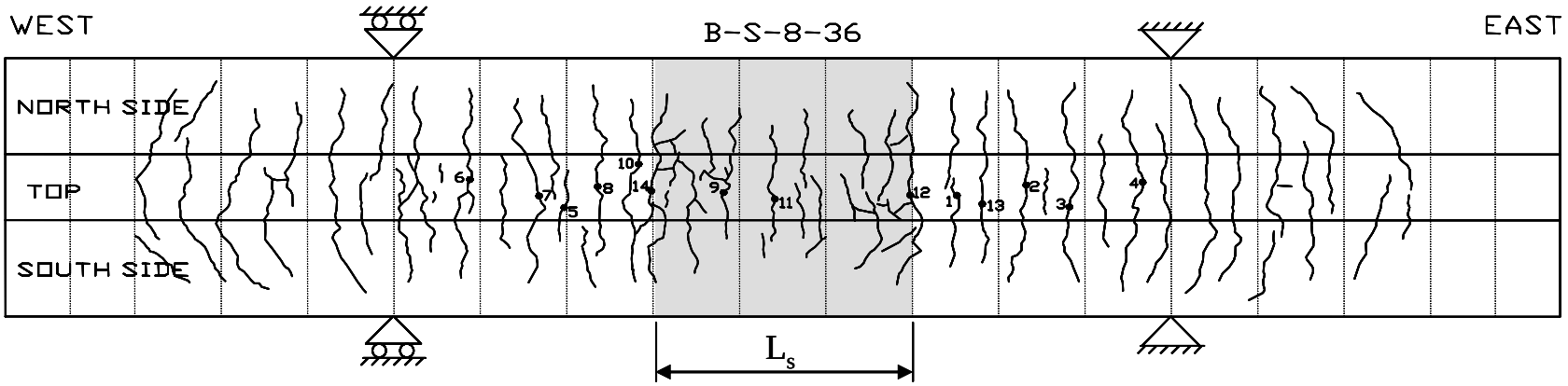

Table C.10 Crack Measurements and Pattern for Specimen B-S-8-36 (continued)

Load, P (kips)	Crack Width (1/1000 in.)													
	Crack No.													
	1	2	3	4	5	6	7	8	9	10	11	12	13	14
20	6	6	5	8	7	8	6	6	4	5	4	7	5	5
21	7	6	6	8	7	8	7	6	5	5	4	8	7	6
22	7	7	6	9	7	9	8	8	5	5	4	9	7	6
23	7	8	6	9	7	9	8	8	5	5	4	9	7	6
24	7	8	6	9	8	9	8	8	5	6	4	9	7	6
25	7	9	6	10	9	10	8	8	5	6	5	10	8	7
26	7	9	6	10	10	10	9	8	5	6	5	10	9	7
28	8	10	7	11	10	10	9	9	5	6	5	11	10	8

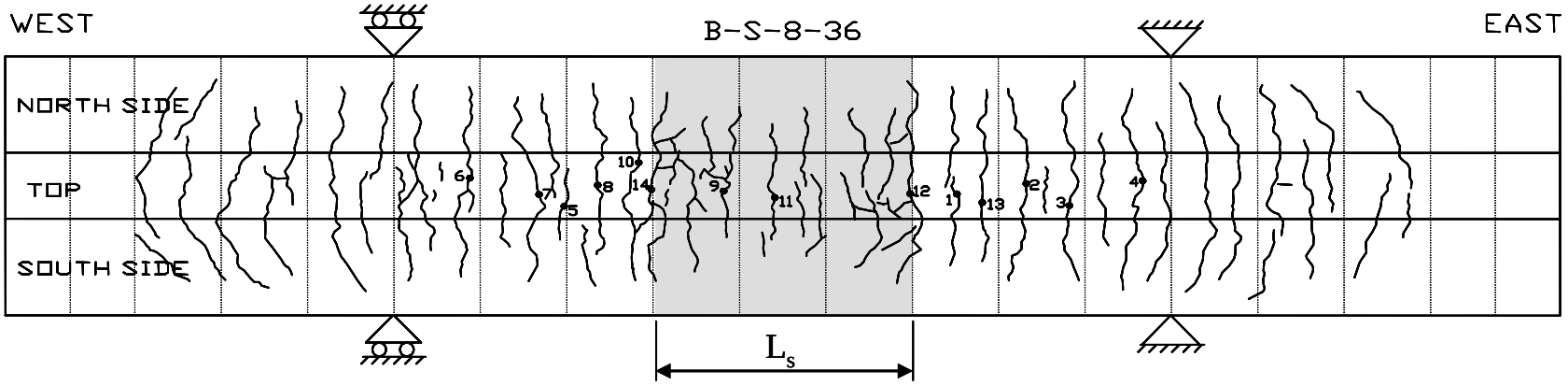

Table C.11 Crack Measurements and Pattern for Specimen B-P-8-36

Load, P (kips)	Crack Width (1/1000 in.)																	
	Crack No.																	
	1	2	3	4	5	6	7	8	9	10	11	12	13	14	15	16	17	18
5	2	2	4	4														
6	2	2	5	9	5	7	2	4	7	8								
7	8	5	9	11	11	10	4	5	8	12	5	3	3	5				
8	12	7	13	14	13	14	4	8	10	17	8	6	6	6	4			
9	16	8	18	16	16	16	4	13	11	21	9	7	7	8	5			
10	20	10	22	21	19	18	6	15	12	25	12	9	9	11	6	2		
11	21	10		23	21	20	7	16	13	30	13	10	10	13	8	4		
12	22	11	25	24	23	24	7	18	15	35	15	10	12	13	8	5		
13	25	12	27	29	26	26	7	20	17	40	18	10	13	13	9	7	4	10
14	25	14	27	29	29	29	9	20	19	42	18	10	14	14	11	9	7	15
15	25	16	28	30	30	30	10	21	20	42	21	11	15	14	12	10	10	18

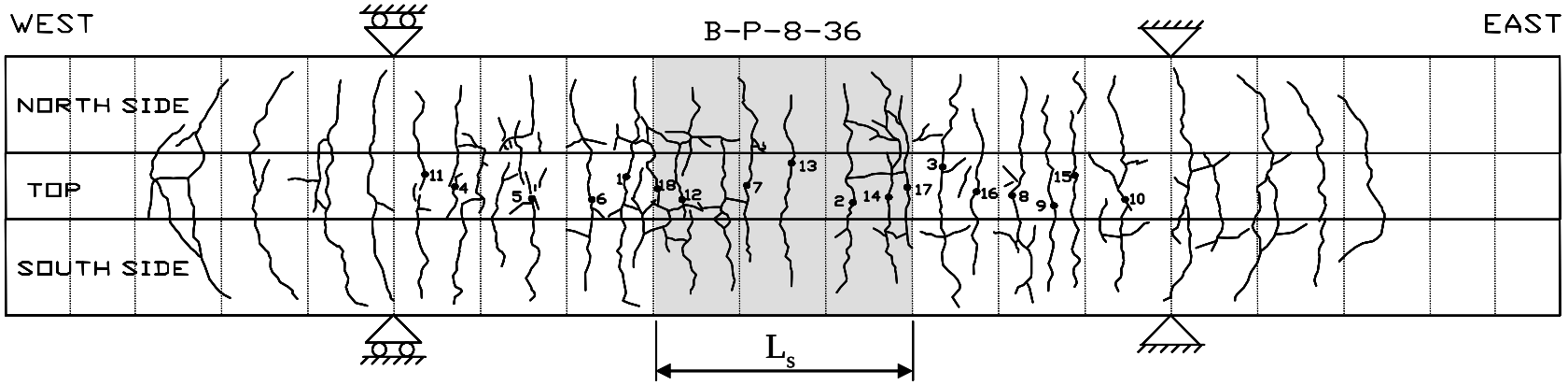

Table C.11 Crack Measurements and Pattern for Specimen B-P-8-36 (continued)

Load, P (kips)	Crack Width (1/1000 in.)																	
	Crack No.																	
	1	**2**	**3**	**4**	**5**	**6**	**7**	**8**	**9**	**10**	**11**	**12**	**13**	**14**	**15**	**16**	**17**	**18**
16	26	17	30	30	33	32	10	25	22	47	23	15	18	15	14	11	14	21
17	26	19	31	30	36	35	12	30	22	50	25	20	18	15	17	13	17	25
18	26	20	31	32	40	10	10	36	26	53	30	24	18	17	19	14	22	25

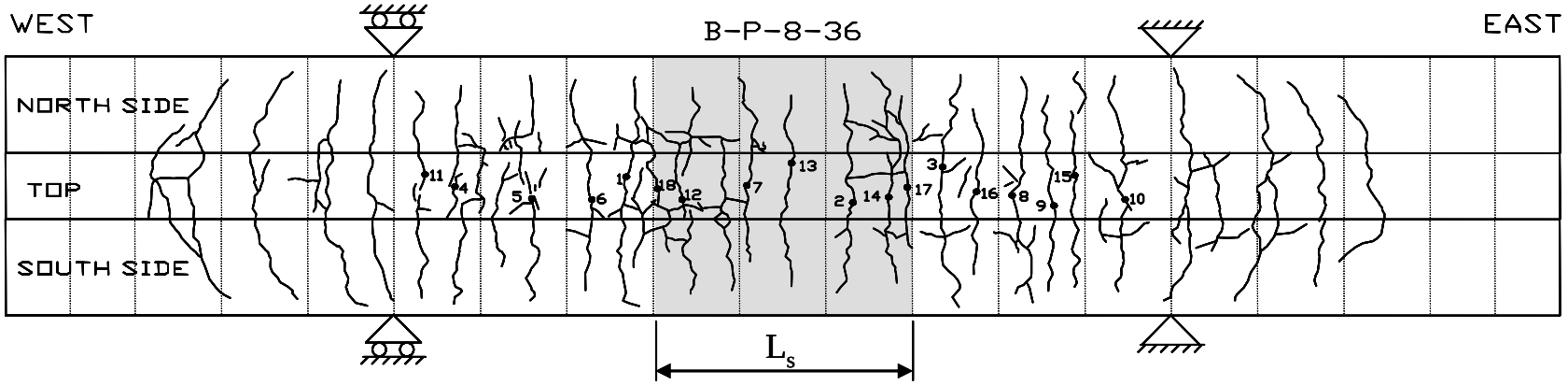

Table C.12 Crack Measurements and Pattern for Specimen B-H-8-36

Load, P (kips)	Crack Width (1/1000 in.)															
	Crack No.															
	1	**2**	**3**	**4**	**5**	**6**	**7**	**8**	**9**	**10**	**11**	**12**	**13**	**14**	**15**	**16**
5	5	4	2	5												
6	8	9	5	9	10	8	10									
7	10	12	7	12	11	9	14	4	4	2	3	6				
8	12	13	11	15	14	16	15	5	5	5	4	11	3	9	6	
9	14	16	11	18	15	19	20	6	9	5	4	13	5	11	10	
10	17	18	11	20	17	23	20	6	9	8	5	15	5	15	14	
11	18	21	12	23	20	25	23	6	9	10	6	18	6	16	16	9
12	21	22	12	26	20	29	25	8	13	11	8	20	8	20	18	12
13	24	22	13	29	22	31	25	8	13	12	8	25	8	21	22	16
14	24	24	14	34	22	34	25	9	15	14	9	25	12	24	23	20
15	24	25	15	37	25	36	25	10	17	16	10	28	12	27	25	21

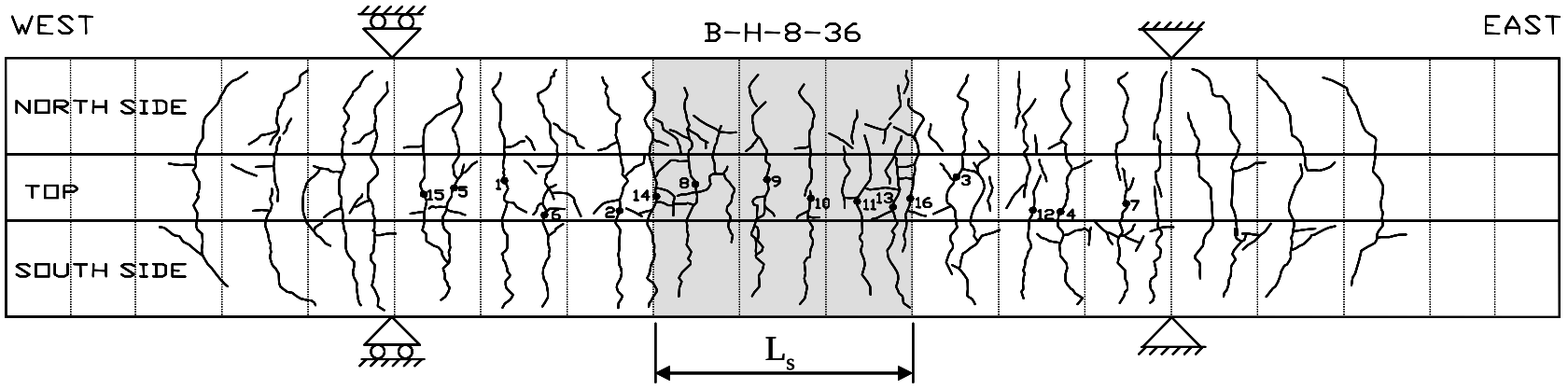

Table C.13 Crack Measurements and Pattern for Specimen B-HN-5-36

Load, P (kips)	Crack Width (1/1000 in.)													
	Crack No.													
	1	2	3	4	5	6	7	8	9	10	11	12	13	14
3.5	3													
4.0	5	6	2	8										
4.5	14	21	6	15	20	7	7	12	17	9	15			
5.0	20	28	7	16	26	8	15	17	20	13	18	6		
5.5	25	32	9	17	28	10	19	20	22	13	22	9	15	
6.0	35	37	17	17	38	10	20	22	24	16	24	9	16	11
6.5	36	40	20	22	39	10	22	26	25	19	28	10	18	15
7.0	40	45	20	22	41	10	25	26	29	22	28	13	21	17
7.5	47	51	26	22	48	10	30	30	30	22	33	15	22	20
8.0	48	52	26	24	51	12	35	32	31	27	38	17	22	24
8.5	51	60	31	24	54	12	38	37	36	28	40	17	25	27

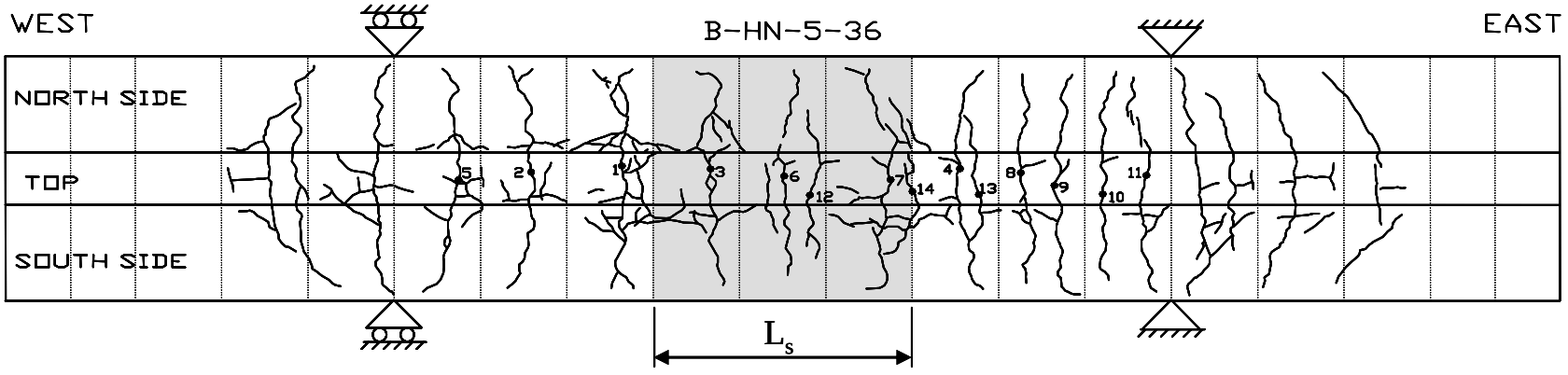

Table C.13 Crack Measurements and Pattern for Specimen B-HN-5-36 (continued)

Load, P (kips)	Crack Width (1/1000 in.)													
	Crack No.													
	1	2	3	4	5	6	7	8	9	10	11	12	13	14
9.0	53	63	31	27	63	12	41	40	36	31	44	18	27	28
9.5	60	70	31	28	70	12	45	40	39	31	45	20	29	31
10.0	60	75	35	29	80	15	53	42	40	35	50	23	30	35

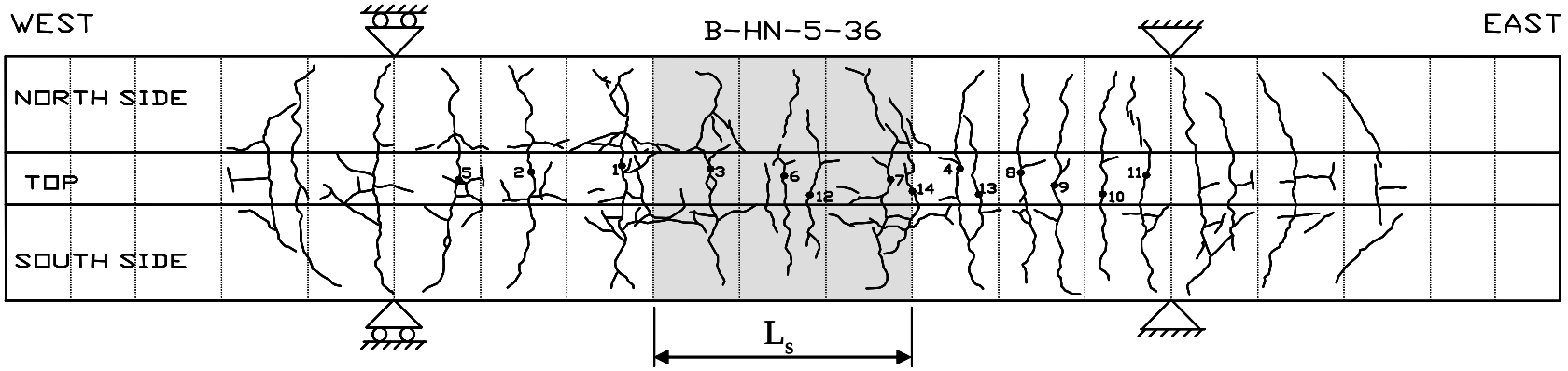

Table C.14 Crack Measurements and Pattern for Specimen B-HO-5-36

Load, P (kips)	Crack Width (1/1000 in.)																		
	Crack No.																		
	1	2	3	4	5	6	7	8	9	10	11	12	13	14	15	16	17	18	19
3.5	3	3																	
4.0	7	15	9	10															
4.5	18	19	16	15	20	14	6	4	3	15	15								
5.0	21	22	22	20	26	16	8	7	5	20	17	7	3	12					
5.5	24	23	24	20	30	20	10	7	8	23	18	10	5	15	3	2	14	8	
6.0	27	23	30	26	34	24	11	7	7	27	20	14	6	17	4	4	17	13	
6.5	31	26	24	25	36	25	12	8	8	25	20	13	8	19	4	7	19	12	5
7.0	32	26	37	27	40	27	15	12	8	35	25	14	9	20	5	7	22	18	5
7.5	35	30	45	32	45	30	15	12	9	37	25	15	10	23	6	9	24	21	6
8.0	38	30	47	36	45	31	17	13	10	39	30	17	11	24	6	9	28	25	7
8.5	40	32	50	39	50	35	18	15	11	42	30	16	15	28	7	10	30	26	10
9.0	40	32	50	40	52	36	20	15	10	45	32	15	15	30	7	11	32	32	9
9.5	40	34	50	42	55	40	20	15	12	46	32	20	15	32	7	11	35	32	10

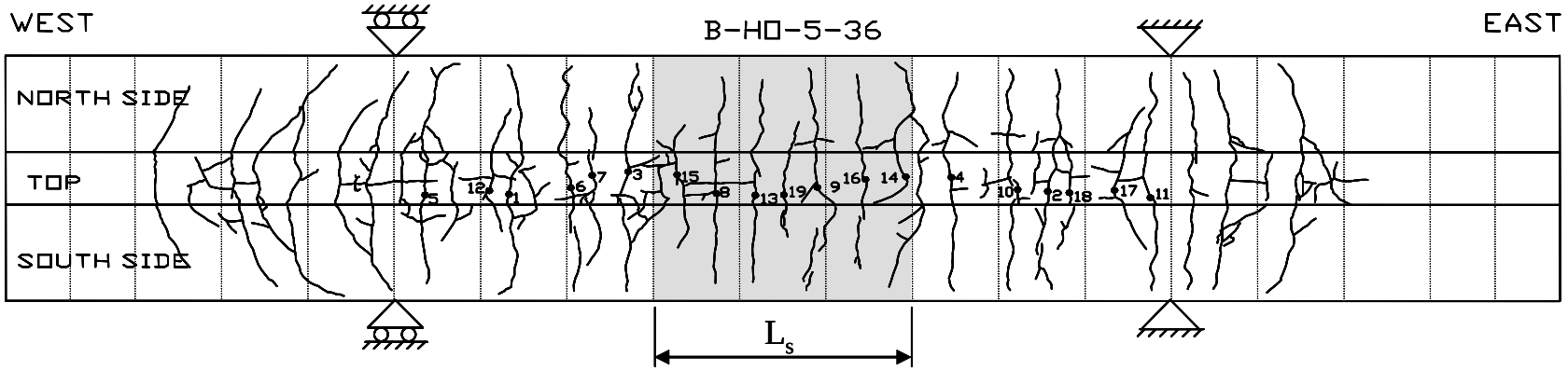

Table C.15 Crack Measurements and Pattern for Specimen B-P-5-36

Load, P (kips)	Crack Width (1/1000 in.)																			
	Crack No.																			
	1	2	3	4	5	6	7	8	9	10	11	12	13	14	15	16	17	18	19	20
3.5	3																			
4.0	12	6																		
4.5	20	16	16	18	14	7														
5.0	22	20	16	25	23	13	5													
5.5	23	25	13	25	27	18	5	8	5	8	7	22	12							
6.0	23	26	13	25	30	18	11	12	5	10	8	29	4	9	15					
6.5	25	26	13	28	36	23	15	15	6	13	8	35	20	12	18	16	3			
7.0	26	26	13	30	41	23	15	15	6	14	8	35	22	14	20	20	6	7		
7.5	29	26	13	34	45	23	15	15	7	15	10	40	25	15	22	22	8	7	21	8
8.0	30	30	13	35	45	30	15	15	8	15	10	40	29	15	22	24	10	9	25	12
8.5	32	30	13	39	47	34	15	15	11	16	11	44	32	19	22	25	12	10	26	15

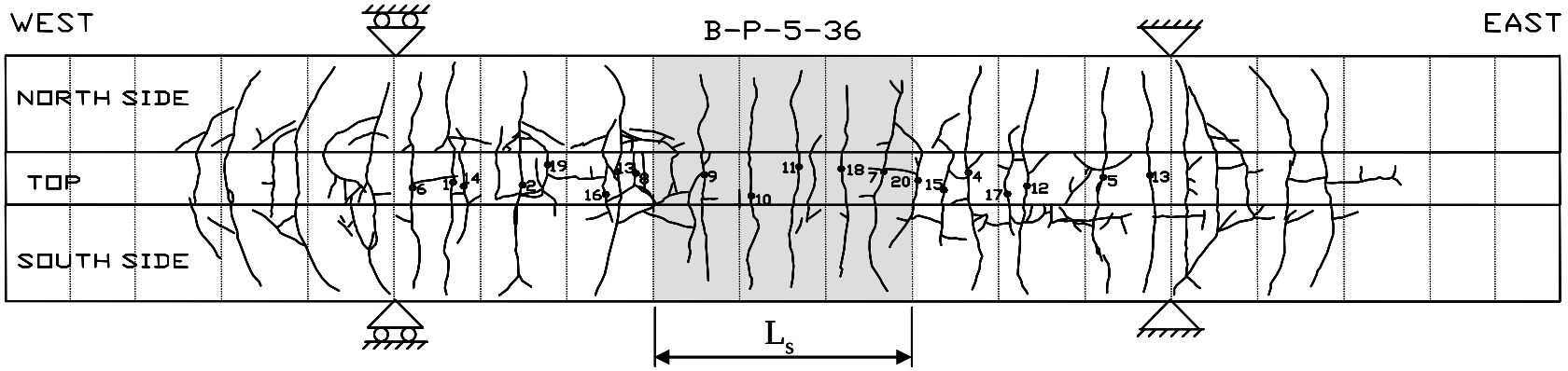

Table C.15 Crack Measurements and Pattern for Specimen B-P-5-36 (continued)

Load, P (kips)	Crack Width (1/1000 in.)																			
	Crack No.																			
	1	**2**	**3**	**4**	**5**	**6**	**7**	**8**	**9**	**10**	**11**	**12**	**13**	**14**	**15**	**16**	**17**	**18**	**19**	**20**
9.0	32	30	13	39	54	35	15	15	11	18	12	45	35	20	24	28	14	11	28	19
9.5	35	32	13	41	56	37	16	15	11	21	15	52	36	22	25	30	16	11	30	24
10.0	35	32	15	45	57	39	18	12	12	22	15	52	39	24	25	30	17	12	34	30

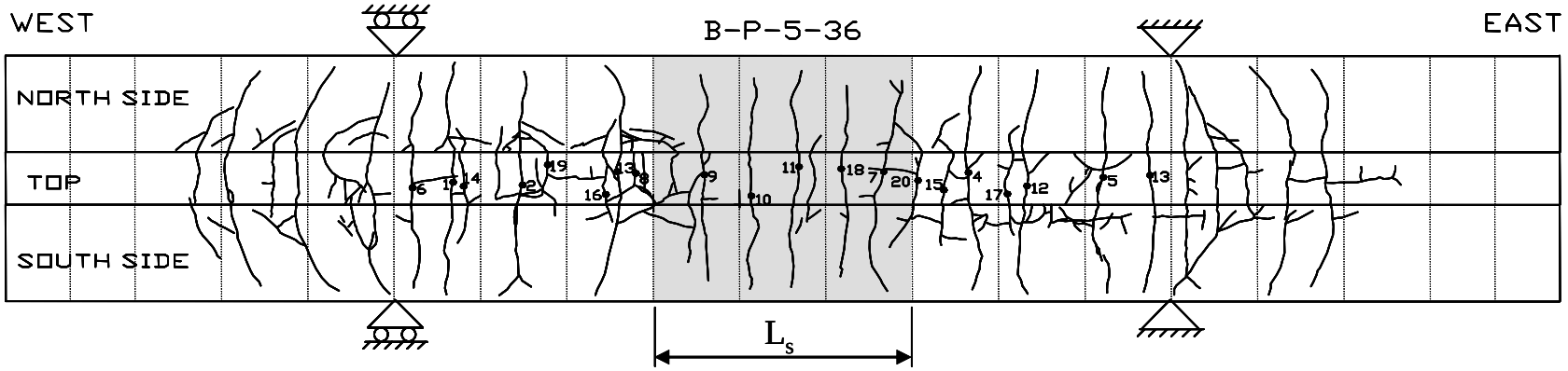

Table C.16 Crack Measurements and Pattern for Specimen B-C-5-36

Load, P (kips)	Crack Width (1/1000 in.)																				
	Crack No.																				
	1	**2**	**3**	**4**	**5**	**6**	**7**	**8**	**9**	**10**	**11**	**12**	**13**	**14**	**15**	**16**	**17**	**18**	**19**	**20**	**21**
4.5	3	3																			
5.0	4	4	7	2	3																
5.5	6	5	7	3	5	6	2	5	6	6											
6.0	6	5	10	4	5	6	3	6	7	6	4										
6.5	6	6	11	5	6	9	4	6	9	7	5	5	3	7							
7.0	10	9	13	7	7	11	5	6	10	7	6	5	4	8	4	2					
7.5	10	10	13	8	7	11	5	6	10	8	7	6	5	10	4	2					
8.0	10	12	14	10	10	11	6	7	13	8	7	7	5	10	4	2	6				
8.5	12	12	14	11	10	11	6	7	12	8	8	7	5	12	5	2	8				
9.0	13	12	14	12	11	12	6	8	14	9	8	8	5	13	5	3	8				
9.5	13	14	15	12	11	12	7	8	15	9	9	9	5	13	5	3	8	3			
10.0	14	15	17	13	13	7	9	15	10	10	10	6	15	6	4	8	5	4			

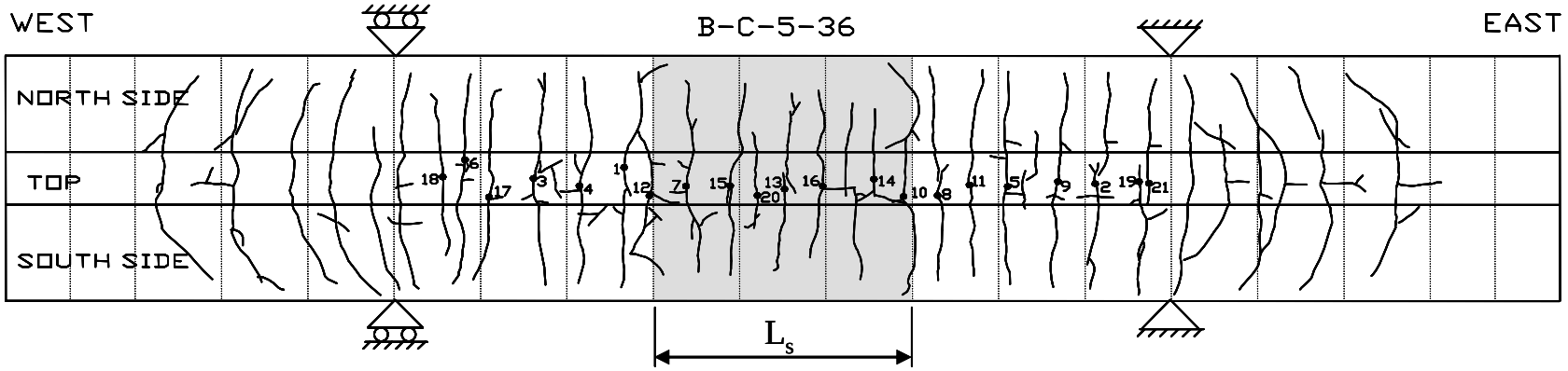

Table C.16 Crack Measurements and Pattern for Specimen B-C-5-36 (continued)

Load, P (kips)	Crack Width (1/1000 in.)																				
	Crack No.																				
	1	2	3	4	5	6	7	8	9	10	11	12	13	14	15	16	17	18	19	20	21
10.5	14	15	18	14	13	13	8	12	15	10	10	10	7	17	6	4	8	5	5	2	
11.0	15	15	20	15	15	14	8	12	16	10	11	10	7	15	7	6	10	5	5	3	
11.5	15	17	20	15	15	14	8	12	16	10	12	10	8	18	7	6	10	5	5	3	
12.0	17	19	22	16	15	14	8	12	17	11	12	12	8	18	7	6	10	6	5	3	
12.5	17	19	23	18	15	15	8	12	17	12	12	12	8	22	8	6	10	7	6	3	10
13.0	17	21	23	18	15	16	10	13	20	12	13	12	8	22	9	7	11	7	6	3	10
13.5	17	20	25	20	15	17	10	13	20	13	14	14	8	25	10	7	11	7	6	3	11
14.0	17	20	25	21	15	17	10	15	23	13	15	16	8	25	10	7	12	8	6	4	12
14.5	20	21	25	21	15	20	11	15	23	13	15	16	8	26	10	8	12	8	6	4	12
15.0	20	22	25	21	16	20	11	15	23	13	15	18	9	26	10	8	13	9	6	4	13

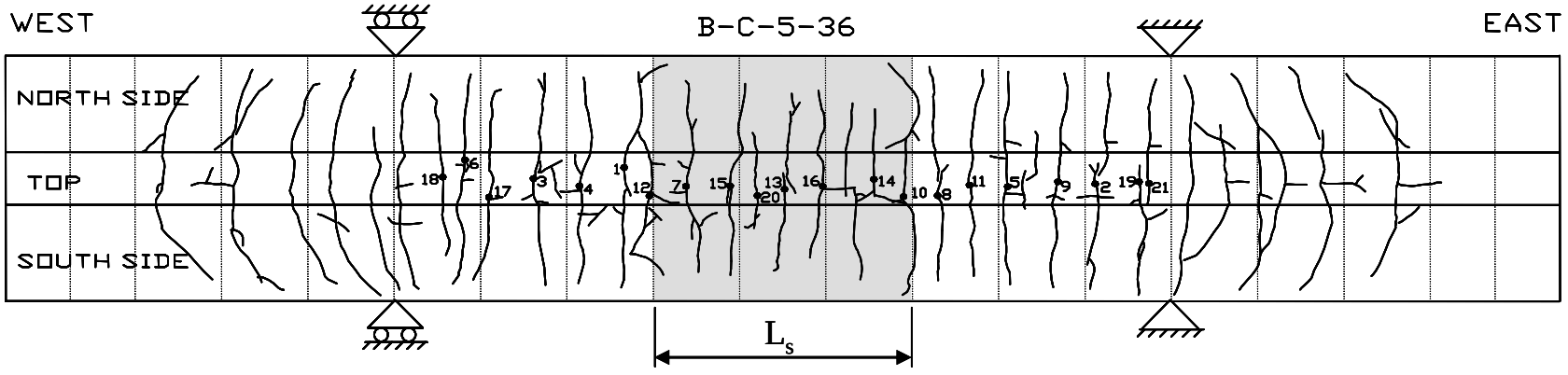

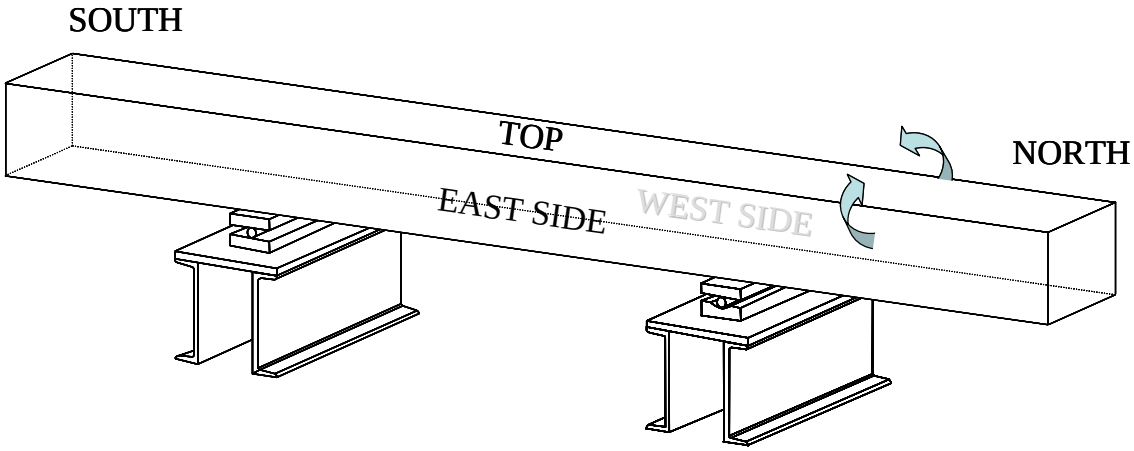

Figure C.3 Specimen Orientation (Phase II)

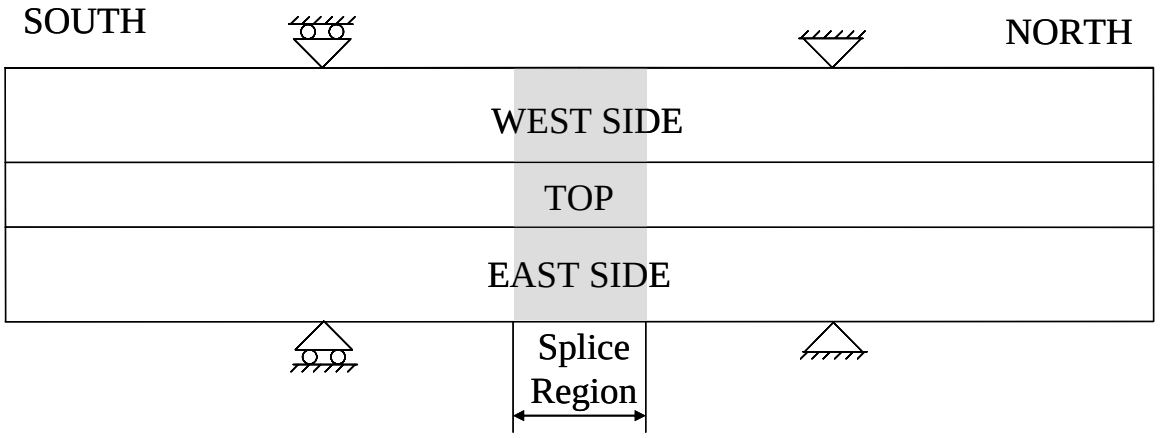

Figure C.4 Template for Crack Drawings (Phase II)

Table C.17 Crack Measurements and Pattern for Specimen B-S2-8-12

Load, P (kips)	Crack Width (1/1000 in.)								
	Crack No.								
	1	**2**	**3**	**4**	**5**	**6**	**7**	**8**	**9**
7	1	2	2	2	2	2	2		
8	1	2	3	3	2	2	3	2	
9	2	4	4	4	2	3	4	2	4
10	2	4	4	5	3	2	4	4	4
11	3	5	5	6	4	3	4	4	4
12	2	5	5	7	4	4	5	5	4
13	3	5	6	8	4	4	5	5	3
14	2	4	8	10	5	5	5	6	4
15	3	5	8	11	5	5	5	5	6
16	3	6	7	12	4	7	6	5	5
17	4	7	8	12	5	8	6	5	5

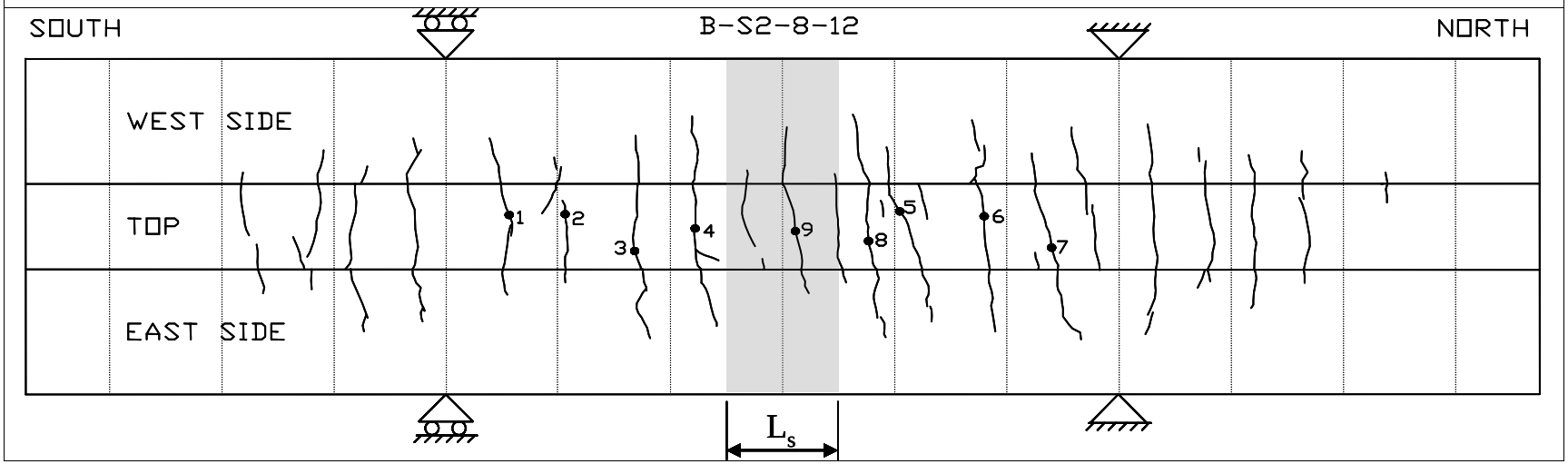

Table C.18 Crack Measurements and Pattern for Specimen B-S1-8-12

Load, P (kips)	Crack Width (1/1000 in.)										
	Crack No.										
	1	2	3	4	5	6	7	8	9	10	11
6	2	2	2	2	2						
7	2	2	2	2	2						
8	2	2	2	2	2	1					
9	2	2	3	2	2	2					
10	2	3	3	3	2	3	1	1			
11	2	3	4	3	3	3	2	2			
12	3	4	5	4	3	4	3	2	6		
13	4	4	5	4	5	5	4	3	6		
14	4	5	5	5	5	6	4	4	7		
15	5	6	6	5	5	6	4	5	9	5	
16	6	6	7	6	6	6	4	5	9	5	5
17	6	5	7	6	6	7	6	5	9	7	5
18	5	6	8	6	7	8	6	5	10	7	5

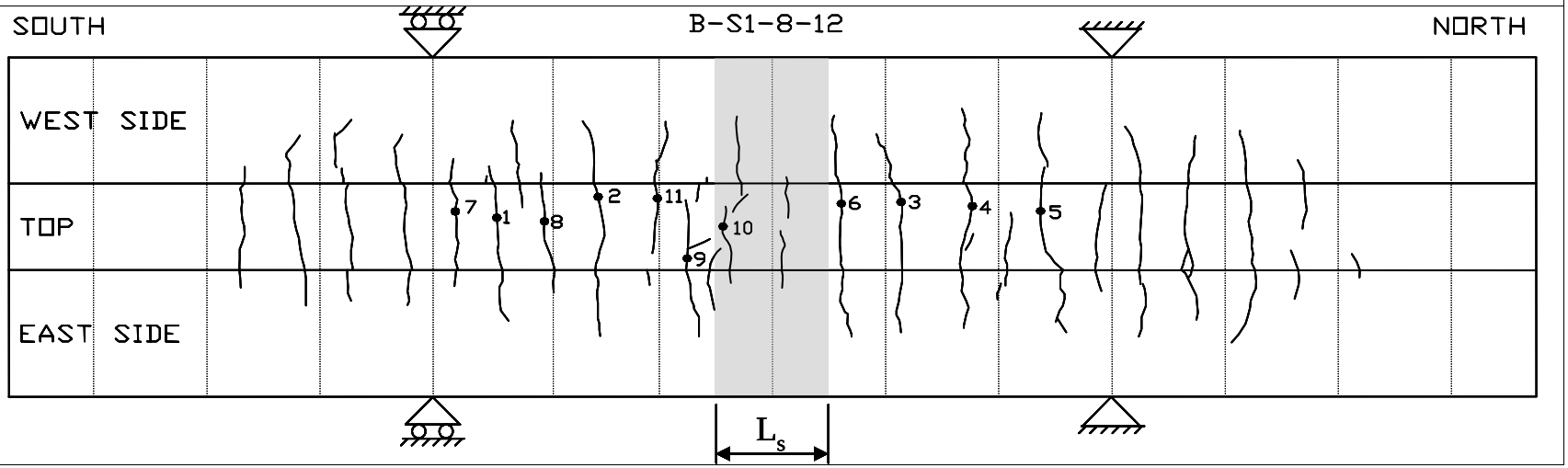

Table C.19 Crack Measurements and Pattern for Specimen B-S4-8-12

Load, P (kips)	Crack Width (1/1000 in.)					
	Crack No.					
	1	**2**	**3**	**4**	**5**	**6**
6	3	4	3	2		
7	5	5	4	4	2	4
8	5	6	5	5	3	6

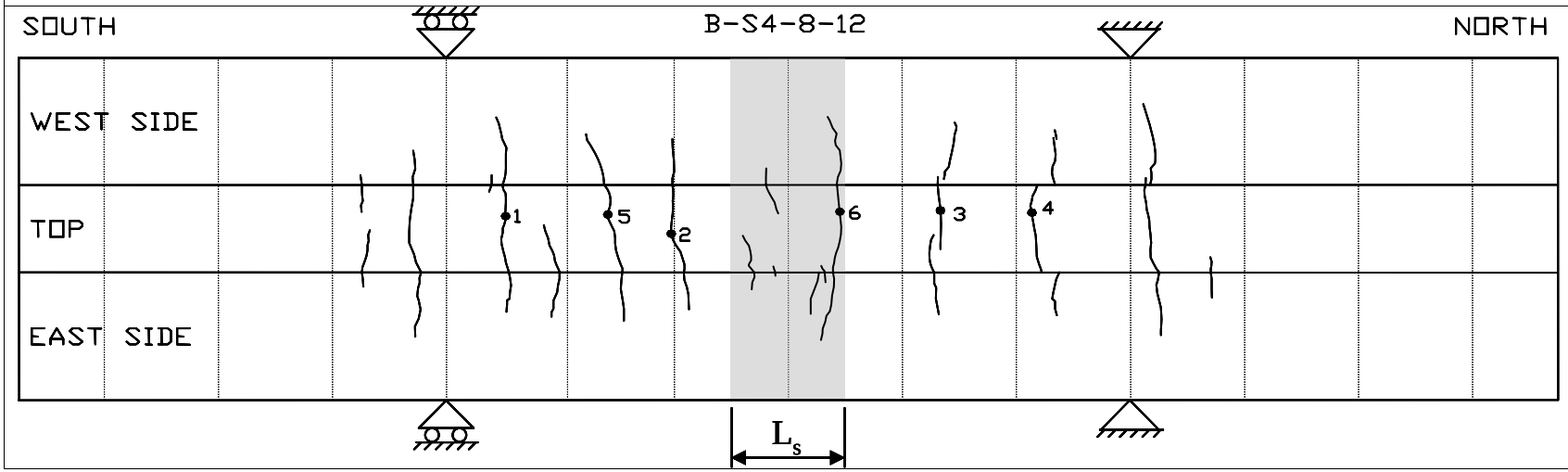

Table C.20 Crack Measurements and Pattern for Specimen B-S3-8-12

PLAIN BARS
Crack widths were not measured.

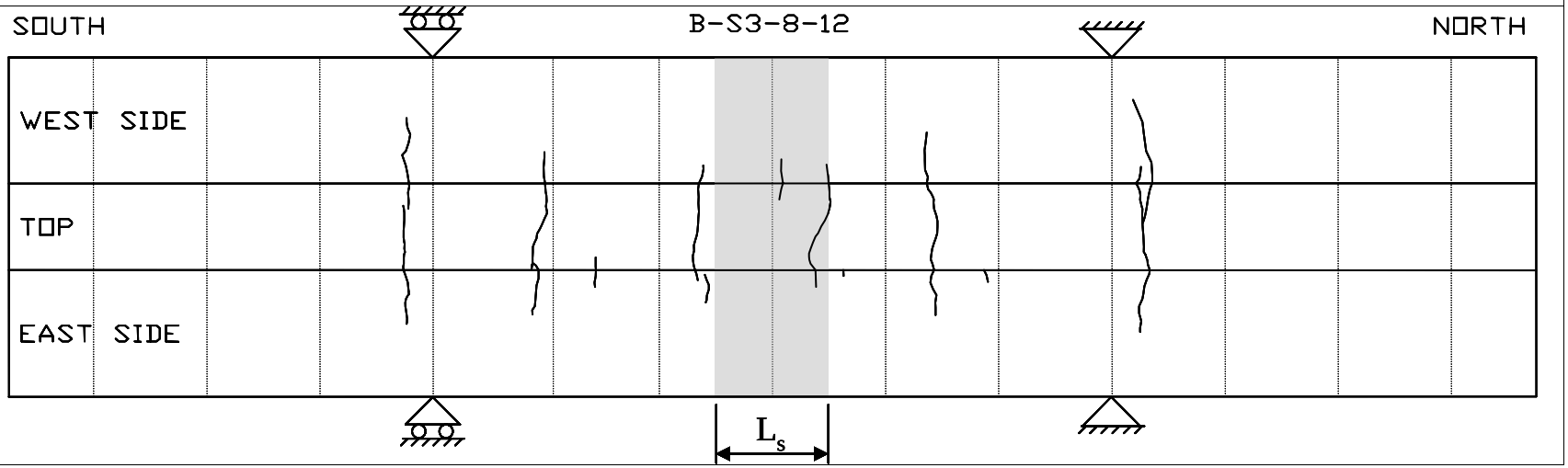

Table C.21 Crack Measurements and Pattern for Specimen B-PG-8-12

Load, P (kips)	Crack Width (1/1000 in.)											
	Crack No.											
	1	**2**	**3**	**4**	**5**	**6**	**7**	**8**	**9**	**10**	**11**	**12**
4	1	1	1									
5	2	2	2	2								
6	3	5	4	5	4	2						
7	4	7	5	8	6	2	1	5				
8	5	8	6	10	10	2	5	5	3	3	4	
9	8	8	15	18	10	3	8	8	5	3	8	
10	10	10	15	20	15	3	13	9	6	7	10	3
11	11	13	20	20	15	3	13	9	10	8	10	3
12	11	15	20	25	15	3	20	10	10	10	11	6
13	11	15	25	30	15	3	25	10	15	10	15	6
14	13	20	25	30	20	3	30	10	15	13	15	7
15	14	20	28	30	20	4	30	12	15	16	18	10
16	15	25	30	35	25	4	30	15	20	15	16	15

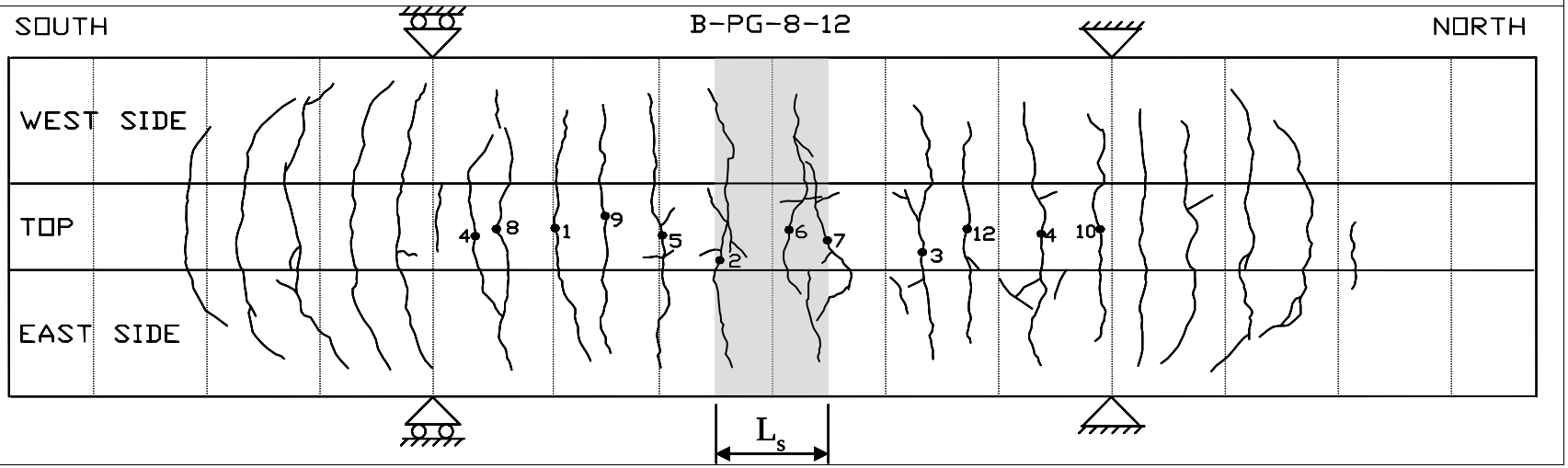

Table C.22 Crack Measurements and Pattern for Specimen B-HG-8-12

Load, P (kips)	Crack Width (1/1000 in.)										
	Crack No.										
	1	2	3	4	5	6	7	8	9	10	11
4	1	1									
5	3	2	4								
6	6	7	7	4	2	5					
7	10	8	11	7	6	10	6	7			
8	12	10	12	9	10	11	10	10	2	2	
9	15	13	14	12	10	15	12	12	4	5	
10	20	13	15	12	10	15	15	15	4	7	
11	22	15	15	15	10	20	15	15	5	9	
12	25	18	16	20	10	25	20	20	10	8	
13	25	20	20	23	10	28	20	22	13	13	15

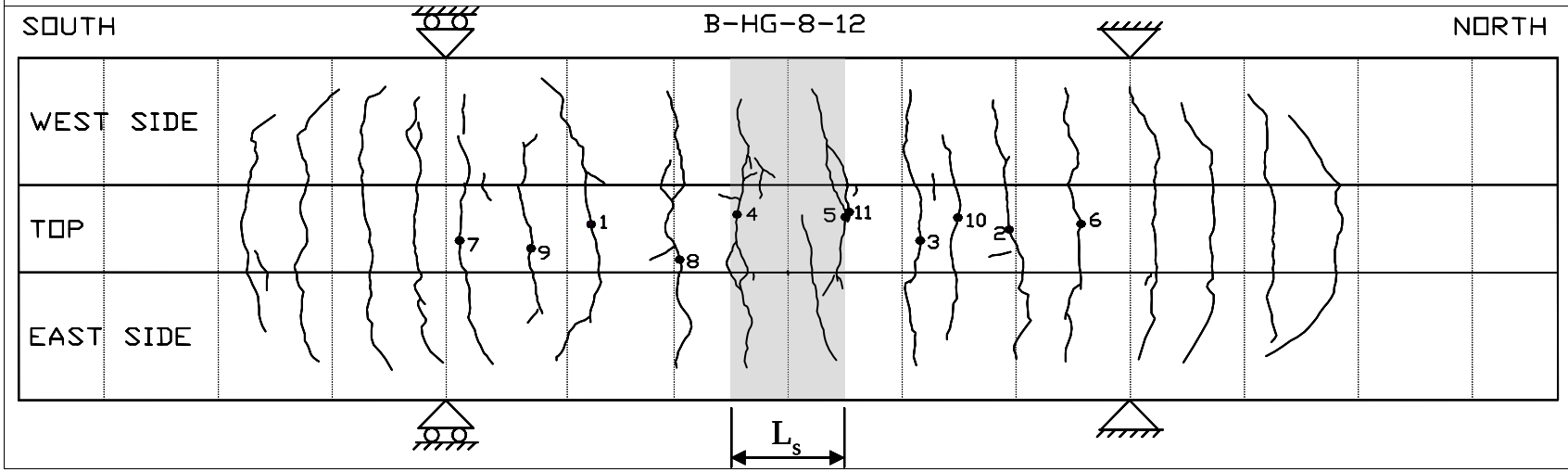

Table C.23 Crack Measurements and Pattern for Specimen B-S1-8-12b

Load, P (kips)	Crack Width (1/1000 in.)								
	Crack No.								
	1	2	3	4	5	6	7	8	9
12	2								
13	3	2	4						
14	2	2	4	2	1	3			
15	4	4	4	2	2	3			
16	4	4	6	3	2	3			
17	5	4	6	3	2	4			
18	5	5	6	3	2	4	2		
19	5	5	6	4	2	4	3	3	3
20	6	4	7	4	2	4	4	4	3

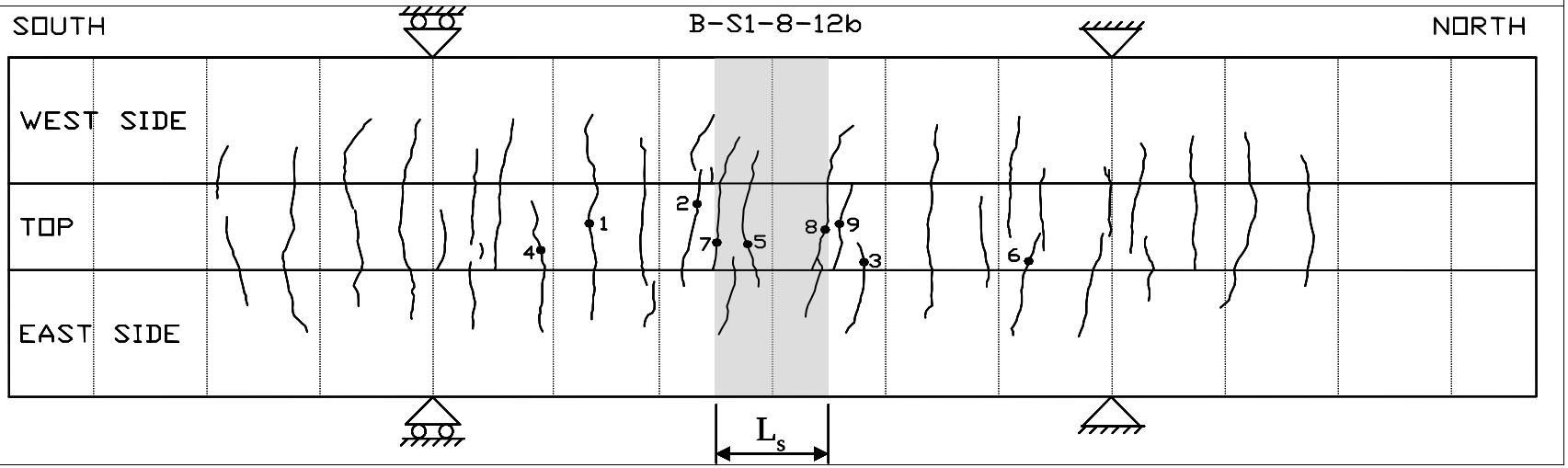

Table C.24 Crack Measurements and Pattern for Specimen B-HG-8-12b

Load, P (kips)	Crack Width (1/1000 in.)												
	Crack No.												
	1	**2**	**3**	**4**	**5**	**6**	**7**	**8**	**9**	**10**	**11**	**12**	**13**
5	3	1											
6	5	3	4	2	3								
7	8	4	7	3	6	4							
8	10	4	8	4	8	7	3	5	4				
9	8	5	9	5	10	9	4	4	5	5	8	6	
10	8	9	11	5	12	14	8	5	9	7	10	5	
11	7	11	14	7	13	16	7	4	11	12	12	10	
12	7	13	17	5	17	16	10	4	12	14	13	12	2
13	8	12	25	6	20	20	11	5	14	17	17	17	5

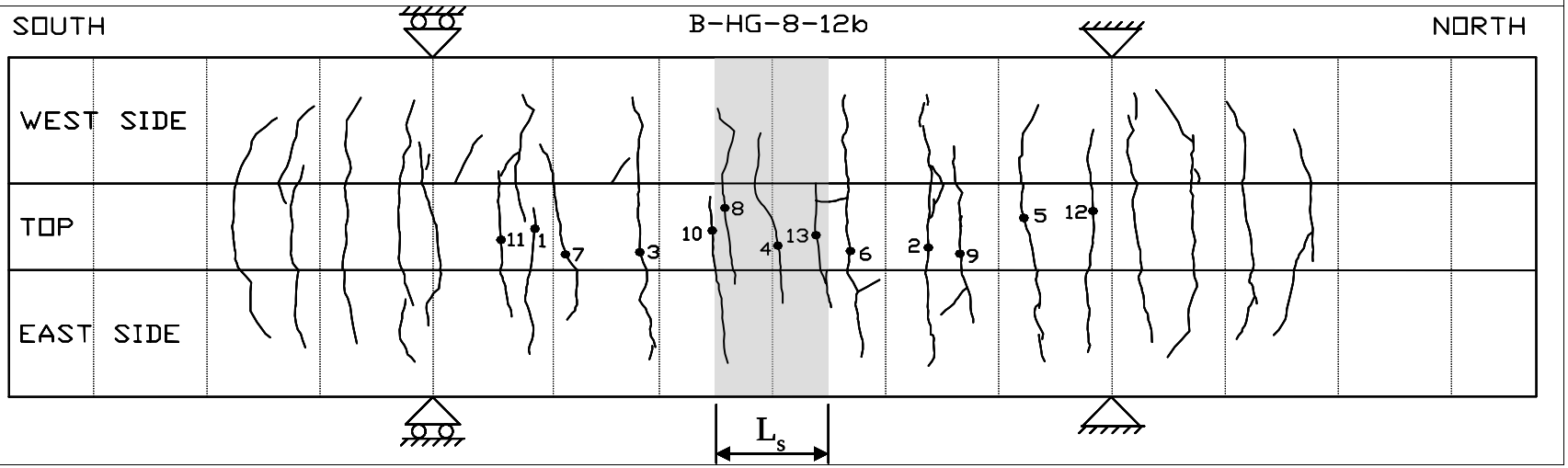

Table C.25 Crack Measurements and Pattern for Specimen B-PG-8-12b

Load, P (kips)	Crack Width (1/1000 in.)														
	Crack No.														
	1	2	3	4	5	6	7	8	9	10	11	12	13	14	15
5	3	1	2												
6	5	2	5	4											
7	8	3	6	6	6	7	1	7	9						
8	10	3	6	5	7	6	2	9	9	2					
9	9	3	8	6	7	7	2	10	10	4	2				
10	11	5	9	6	10	6	2	12	11	4	4	4	10		
11	11	4	9	6	10	10	2	12	15	5	4	6	12		
12	12	4	12	10	13	10	3	15	16	4	5	7	10	3	5
13	11	5	14	10	13	12	3	14	18	4	7	10	12	4	5
14	12	5	13	10	16	12	3	15	20	4	6	10	15	5	7
15	15	4	15	10	15	20	3	15	20	5	8	12	15	6	9

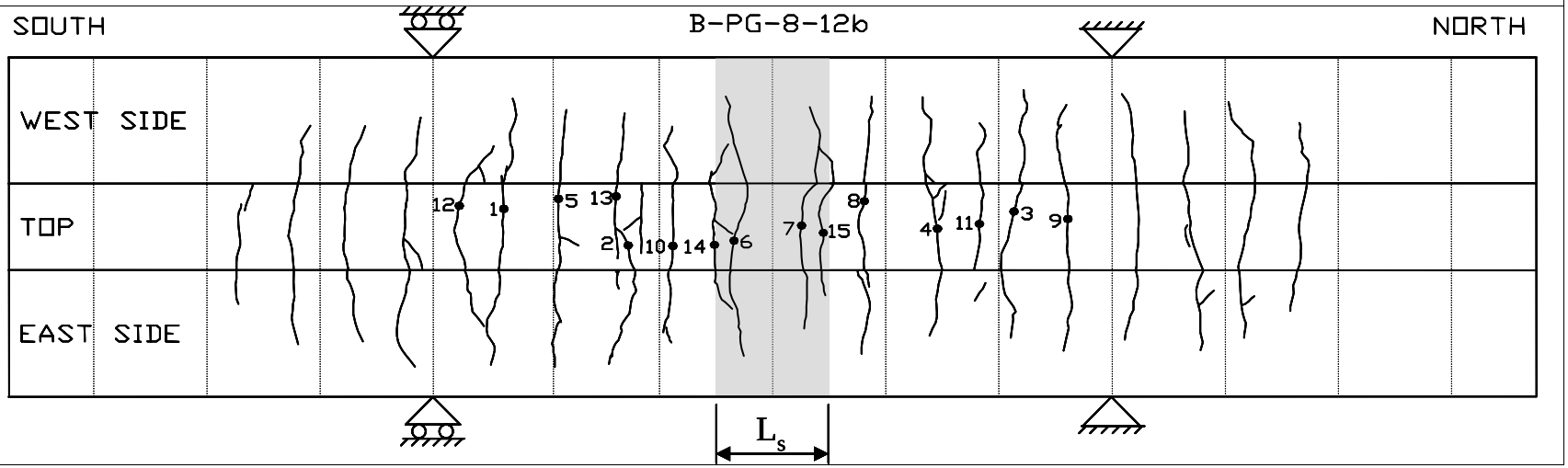

Table C.26 Crack Measurements and Pattern for Specimen B-S-5-24

Load, P (kips)	Crack Width (1/1000 in.)											
	Crack No.											
	1	**2**	**3**	**4**	**5**	**6**	**7**	**8**	**9**	**10**	**11**	**12**
5	2	2	2	2								
6	4	3	3	3	4	3	3					
7	4	5	4	4	5	3	2	3				
8	5	5	5	4	6	3	3	5				
9	8	7	8	5	7	5	5	7	3	2	3	
10	8	7	8	5	7	6	5	9	4	2	5	
11	10	7	8	6	9	5	5	10	3	3	5	
12	11	8	10	8	12	8	5	10	4	3	6	
13	14	9	10	8	13	8	5	14	3	4	7	2
14	15	10	11	10	12	8	7	13	4	3	9	2
15	15	10	12	12	13	10	6	15	5	3	9	3
16	15	12	11	12	15	10	8	17	5	4	10	3

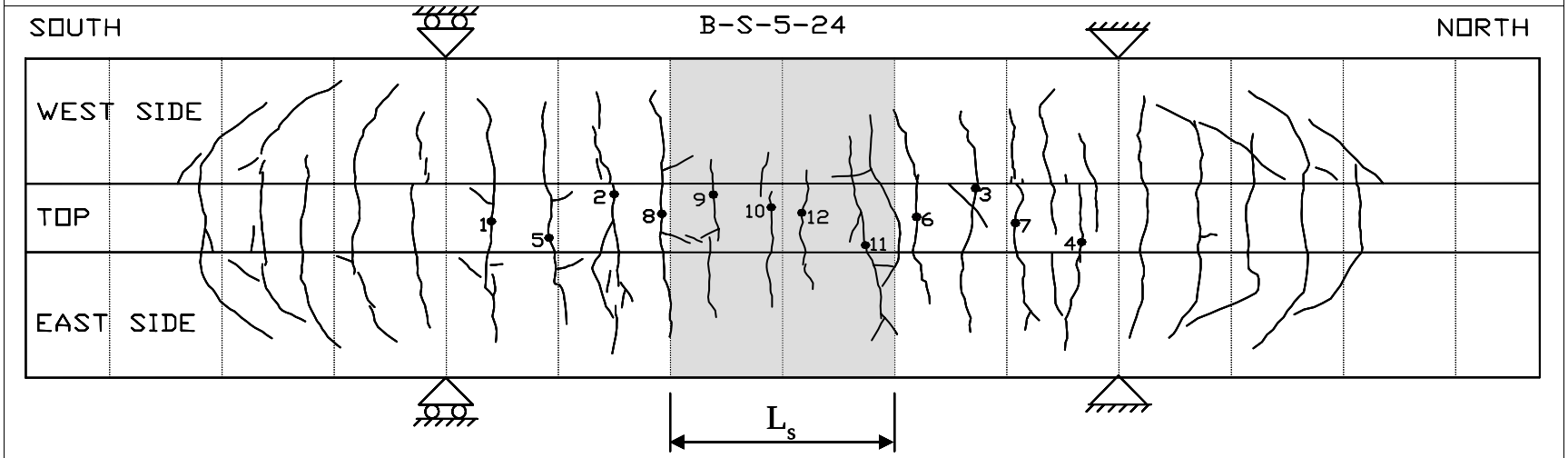

Table C.26 Crack Measurements and Pattern for Specimen B-S-5-24 (continued)

Load, P (kips)	Crack Width (1/1000 in.)											
	Crack No.											
	1	2	3	4	5	6	7	8	9	10	11	12
17	16	11	14	13	15	11	10	16	5	6	9	3
18	18	13	15	15	16	12	12	20	6	6	8	4
19	22	15	15	15	18	12	11	20	6	7	8	4
20	23	15	18	15	17	12	11	23	5	6	10	3

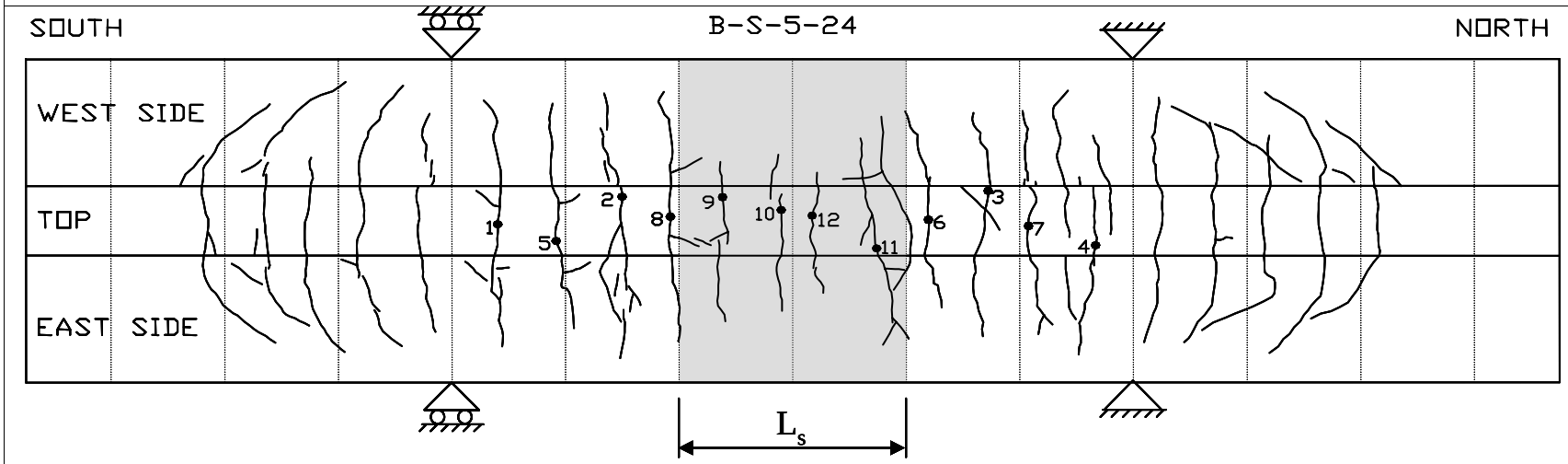

Table C.27 Crack Measurements and Pattern for Specimen B-HC1-5-24

Load, P (kips)	Crack Width (1/1000 in.)												
	Crack No.												
	1	2	3	4	5	6	7	8	9	10	11	12	13
4.0	4												
4.5	4	1	2										
5.0	4	1	3	2									
5.5	5	2	4	4	5								
6.0	5	2	6	4	8	7	3	2	4	3			
6.5	5	2	7	5	9	7	3	3	5	6	1		
7.0	5	3	8	5	10	8	4	3	6	7	3	4	
7.5	7	3	6	5	10	9	5	4	7	7	3	5	
8.0	6	3	7	6	10	9	5	6	7	8	3	6	2
8.5	8	3	7	6	11	10	5	8	6	10	4	7	3
9.0	7	5	8	7	11	12	5	8	8	11	6	8	4
9.5	7	4	8	7	12	12	6	8	9	14	7	8	6

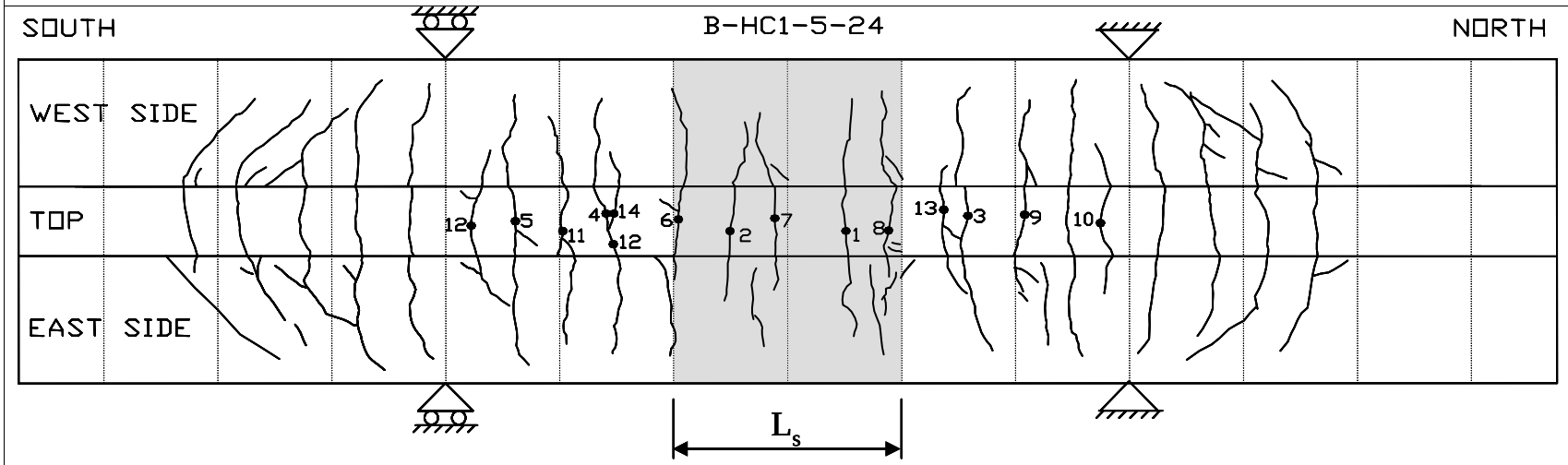

Table C.27 Crack Measurements and Pattern for Specimen B-HC1-5-24 (continued)

Load, P (kips)	Crack Width (1/1000 in.)														
	Crack No.														
	1	2	3	4	5	6	7	8	9	10	11	12	13	14	15
10.0	8	5	10	7	12	14	5	10	10	15	8	10	5	5	13
10.5	8	5	9	6	13	15	7	9	10	15	8	10	5	5	15
11.0	9	5	9	7	13	14	8	12	10	14	8	10	7	5	15
11.5	10	5	11	8	14	17	8	12	11	16	9	12	9	5	16
12.0	9	6	11	7	14	17	8	13	12	17	9	12	8	5	16
13.0	10	6	10	8	15	19	9	12	11	17	10	14	9	6	17
14.0	10	5	11	8	16	21	10	15	11	17	12	16	10	7	17
15.0	11	5	15	8	18	22	11	18	12	18	11	17	11	8	20
16.0	11	6	14	8	18	24	12	18	12	19	11	18	12	10	21

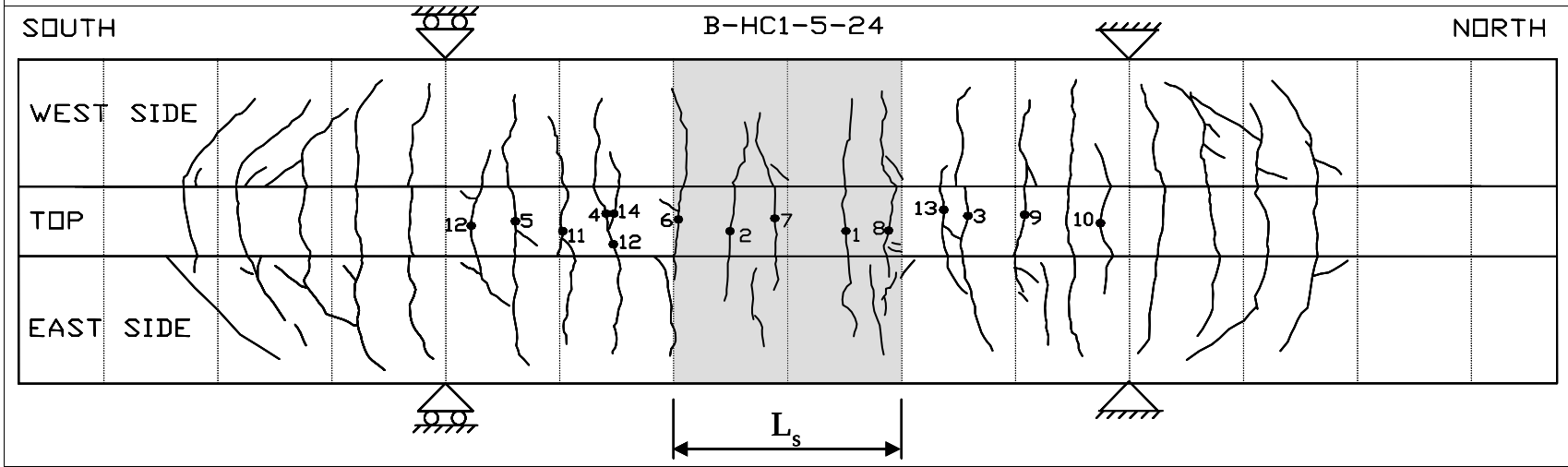

Table C.28 Crack Measurements and Pattern for Specimen B-PC2-5-24

PLAIN BARS
Crack widths were not measured.

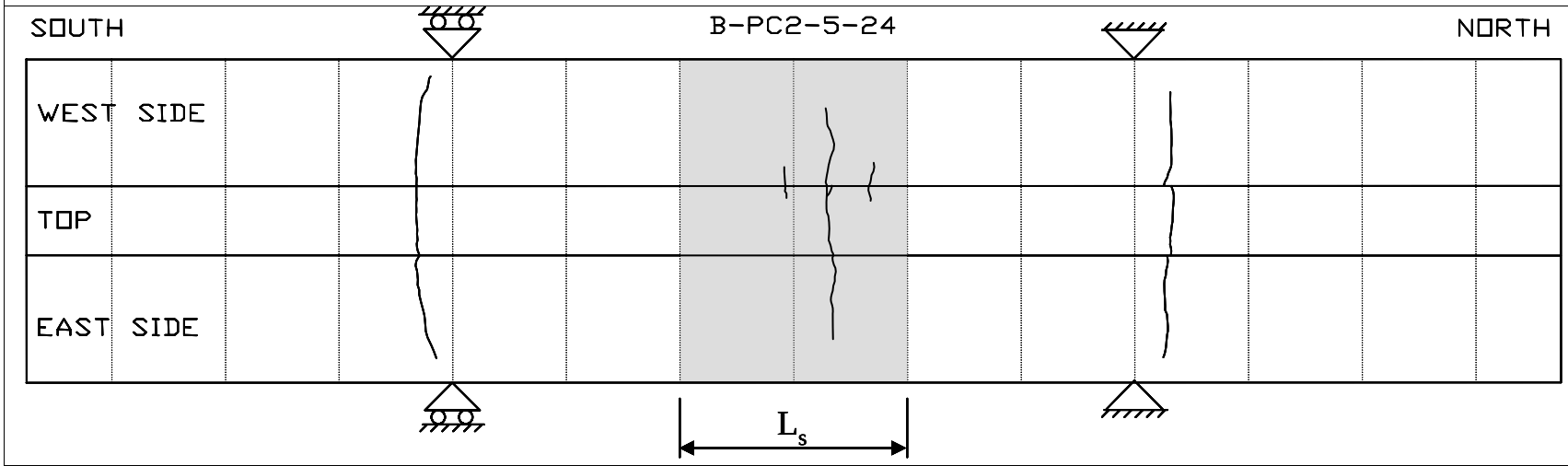

Table C.29 Crack Measurements and Pattern for Specimen B-PC1-5-24

Load, P (kips)	Crack Width (1/1000 in.) Crack No.												
	1	**2**	**3**	**4**	**5**	**6**	**7**	**8**	**9**	**10**	**11**	**12**	**13**
4.5	2	2	2										
5.0	3	4	5	4	5								
5.5	5	4	6	5	5	1	3						
6.0	6	5	8	8	7	2	4	3	4	5			
6.5	6	5	9	7	7	2	4	4	4	5			
7.0	9	5	10	10	7	2	4	5	4	6	3		
7.5	10	7	11	12	8	3	5	5	5	7	3		
8.0	10	6	11	11	9	4	5	7	6	9	4	5	
8.5	11	6	12	11	11	4	6	8	7	11	5	6	
9.0	11	7	13	14	11	5	6	8	6	10	5	6	
9.5	12	7	13	15	11	5	6	9	6	11	6	6	
10.0	12	7	14	15	12	5	6	10	6	12	7	6	2

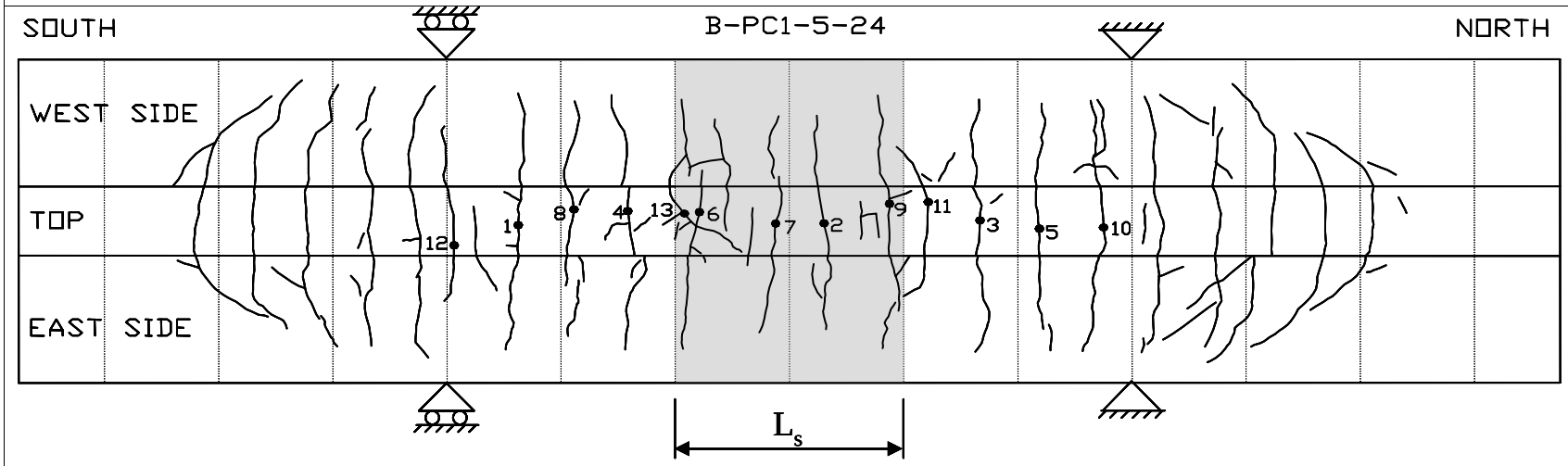

Table C.29 Crack Measurements and Pattern for Specimen B-PC1-5-24 (continued)

Load, P (kips)	Crack Width (1/1000 in.) Crack No.												
	1	**2**	**3**	**4**	**5**	**6**	**7**	**8**	**9**	**10**	**11**	**12**	**13**
10.5	14	8	14	15	12	5	6	11	9	12	8	7	3
11.0	15	9	15	15	12	4	7	12	10	12	7	8	4
11.5	15	8	15	16	14	5	7	12	10	14	8	7	5
12.0	15	8	16	16	14	5	7	13	10	15	7	8	6
12.5	16	9	17	17	16	5	7	13	12	16	8	10	7
13.0	17	9	18	17	16	5	8	12	12	15	8	10	7
13.5	18	9	18	17	17	5	8	15	12	17	9	10	8
14.0	17	10	19	19	17	5	8	16	13	18	8	10	9
14.5	18	9	20	20	17	5	9	16	13	17	8	10	10
15.0	20	10	20	21	17	6	9	16	14	19	8	11	12
15.5	20	11	21	20	17	5	9	16	15	20	7	12	10
16.0	20	11	21	22	19	6	9	17	16	21	7	12	13
17.0	21	11	22	23	21	5	9	17	16	22	7	11	15

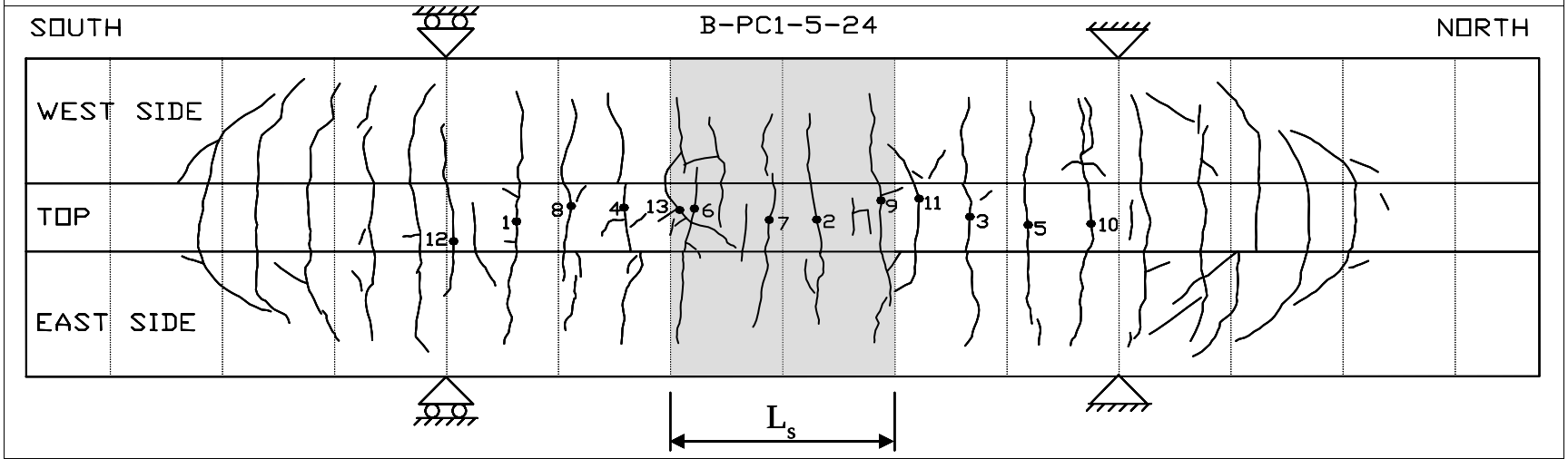

Table C.30 Crack Measurements and Pattern for Specimen B-HG3-5-24

PLAIN BARS
Crack widths were not measured.

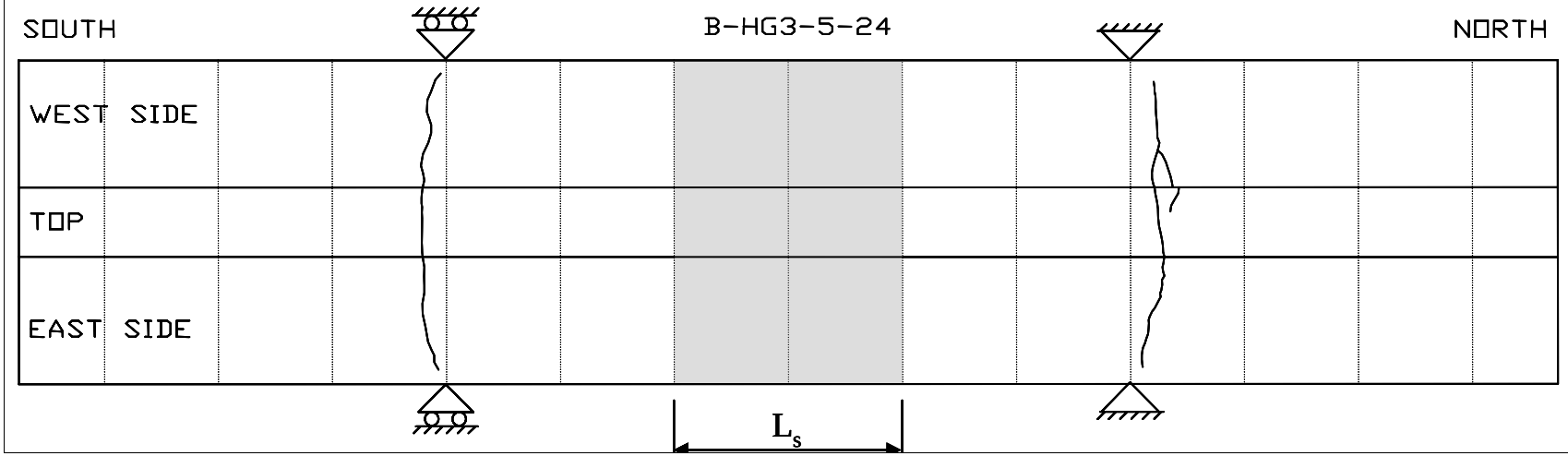

Table C.31 Crack Measurements and Pattern for Specimen B-HG1-5-24

Load, P (kips)	Crack Width (1/1000 in.) Crack No. 1	2	3	4	5	6	7	8
4.5	2	10						
5.0	7	15	15					
5.5	8	20	20	6	18			
6.0	8	25	25	12	23	12		
6.5	10	31	30	12	26	18		
7.0	18	38	35	13	31	32	9	
7.5	22	42	39	13	35	28	12	23
8.0	22	42	40	14	39	31	15	23
8.5	25	48	45	15	44	32	18	32
9.0	26	50	45	15	48	35	21	35
9.5	27	55	45	18	50	38	25	36
10.0	28	57	51	21	55	42	30	41
10.5	30	59	55	22	58	45	30	50

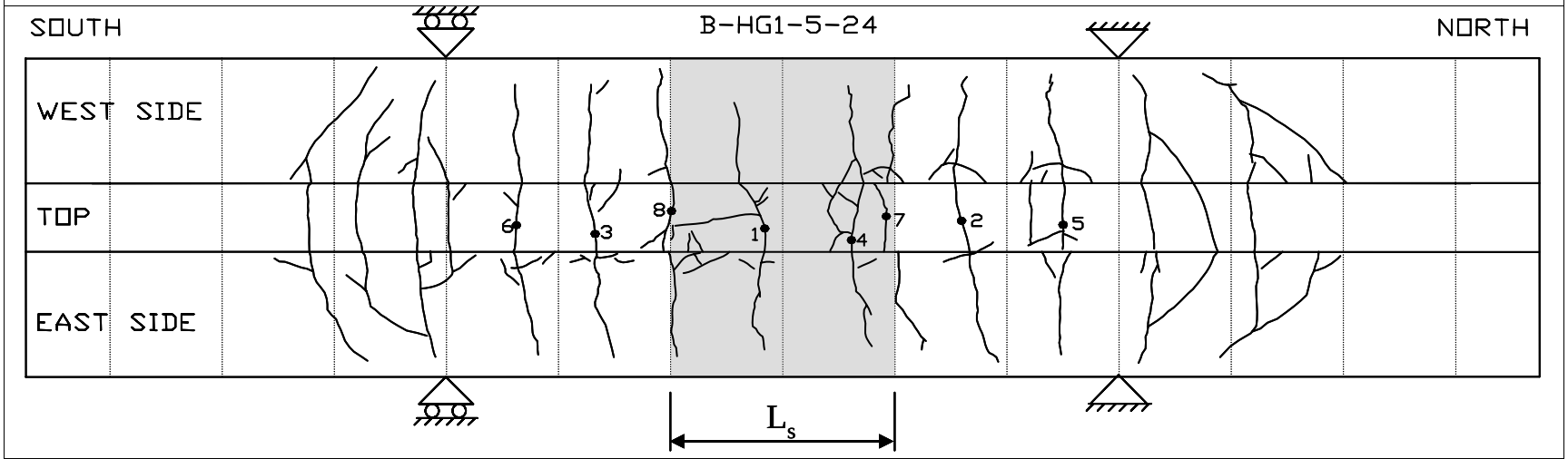

Table C.32 Crack Measurements and Pattern for Specimen B-HG2-5-24

Load, P (kips)	Crack Width (1/1000 in.) Crack No.								
	1	**2**	**3**	**4**	**5**	**6**	**7**	**8**	**9**
5.0	9								
5.5	15	14	5	5					
6.0	20	18	5	6	12				
6.5	24	22	7	12	18	6	6		
7.0	28	27	9	14	20	7	10	24	4
7.5	28	31	9	15	20	6	10	25	5
8.0	30	32	11	15	22	7	10	27	6
8.5	30	34	12	20	22	8	13	28	7
9.0	30	36	12	22	24	9	20	31	7
9.5	35	40	14	22	28	9	22	33	8
10.0	35	42	15	26	27	11	23	36	9
10.5	36	45	16	30	32	12	24	40	9

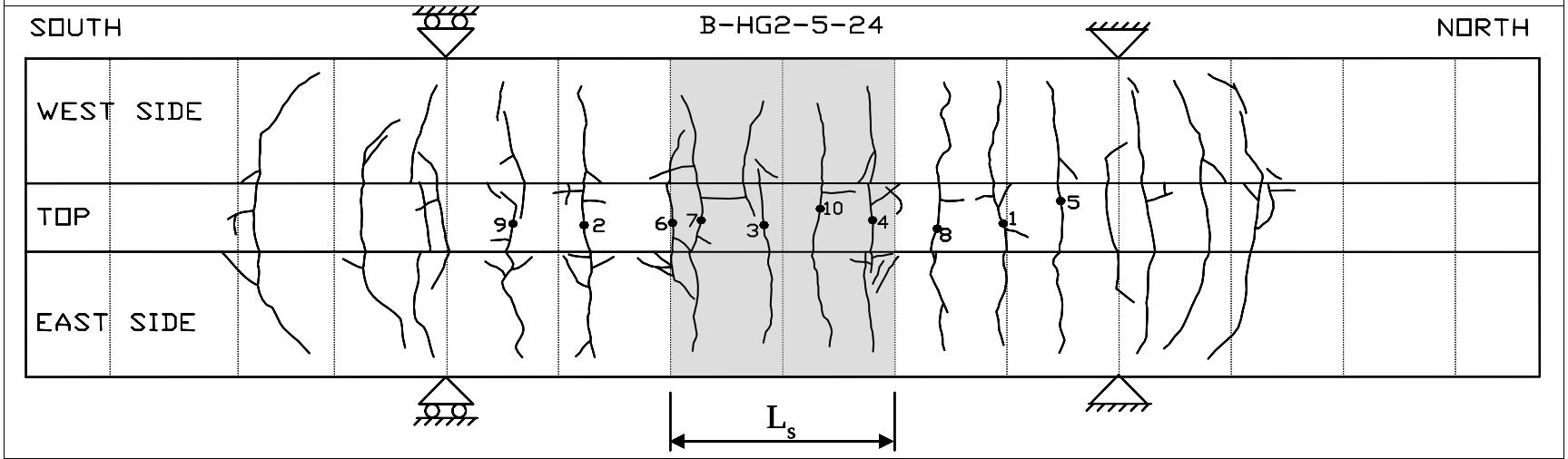

Table C.33 Crack Measurements and Pattern for Specimen B-PG2-5-24

PLAIN BARS
Crack widths were not measured.

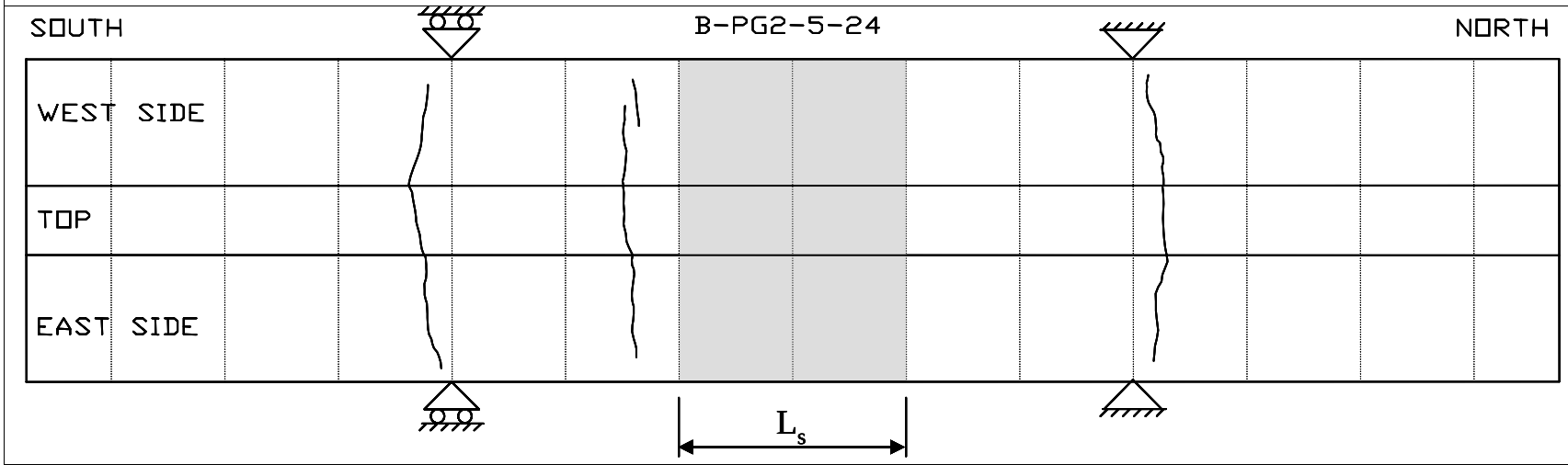

Table C.34 Crack Measurements and Pattern for Specimen B-PG1-5-24

Load, P (kips)	Crack Width (1/1000 in.) Crack No.												
	1	**2**	**3**	**4**	**5**	**6**	**7**	**8**	**9**	**10**	**11**	**12**	**13**
5.0	4	3	3										
5.5	10	5	5										
6.0	15	6	5	20	6	20	17	5					
6.5	20	5	7	22	5	24	20	7	7	11			
7.0	21	7	7	27	7	30	30	7	10	15			
7.5	27	9	7	30	8	32	30	7	11	15	2	2	
8.0	26	9	10	34	9	33	32	7	12	17	2	2	
8.5	25	11	11	38	10	40	35	7	12	20	2	2	2
9.0	25	12	11	38	11	43	36	7	14	24	8	2	3
9.5	25	12	13	40	12	50	36	7	16	24	10	2	4
10.0	25	12	14	40	15	51	35	7	19	25	12	3	8
10.5	25	15	15	45	15	52	34	8	20	26	17	3	7

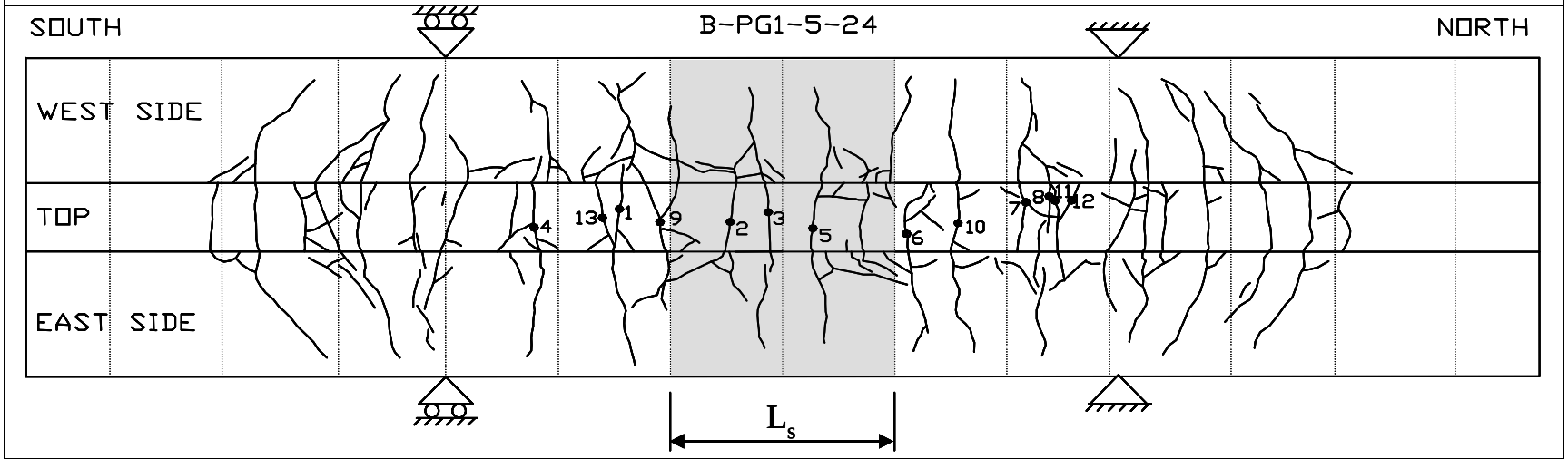

Table C.35 Crack Measurements and Pattern for Specimen B-HG1-5-24b

Load, P (kips)	Crack Width (1/1000 in.) Crack No.												
	1	**2**	**3**	**4**	**5**	**6**	**7**	**8**	**9**	**10**	**11**	**12**	**13**
5.0	9	2											
5.5	13	2	5										
6.0	18	3	5	9									
6.5	20	9	10	10	18	15							
7.0	24	12	8	12	22	20	16						
7.5	27	6	8	10	25	24	18	4	2	5	15		
8.0	32	6	7	17	27	27	25	6	4	5	23		
8.5	35	5	7	15	27	30	27	7	7	7	27	15	
9.0	40	5	7	17	31	35	30	10	10	6	33	16	4
9.5	42	5	7	18	31	35	30	10	10	6	39	20	5
10.0	43	4	7	17	32	39	35	12	10	6	39	18	10
10.5	46	4	10	16	32	41	36	13	10	5	46	18	12
11.0	46	4	10	17	32	42	42	12	11	5	50	21	14

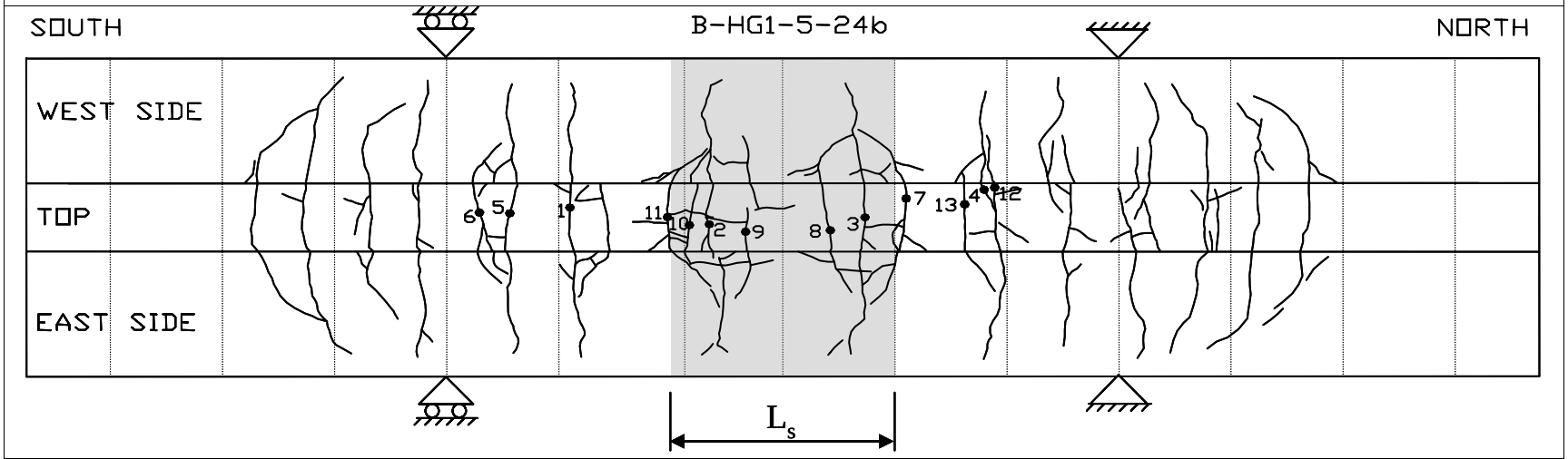

Table C.36 Crack Measurements and Pattern for Specimen B-PG1-5-24b

Load, P (kips)	Crack Width (1/1000 in.) Crack No.															
	1	**2**	**3**	**4**	**5**	**6**	**7**	**8**	**9**	**10**	**11**	**12**	**13**	**14**	**15**	**16**
5.0	1	3														
5.5	2	15	3	7	3											
6.0	2	17	20	10	5	4	2									
6.5	3	20	20	12	6	8	2	2	8							
7.0	3	20	30	12	12	8	2	2	10	1	2	6				
7.5	3	28	30	12	20	14	2	2	10	2	3	6	2	5		
8.0	4	30	30	12	23	15	2	2	14	4	4	7	2	12	13	
8.5	7	30	32	12	25	17	2	2	20	4	4	7	3	16	15	
9.0	7	33	32	12	26	17	2	2	20	5	4	7	3	15	15	
9.5	8	35	35	13	32	20	2	2	26	5	6	9	4	20	16	
10.0	7	34	35	13	36	20	2	2	25	5	6	12	4	26	16	2
10.5	7	35	35	13	36	20	2	2	25	5	6	16	4	27	20	3

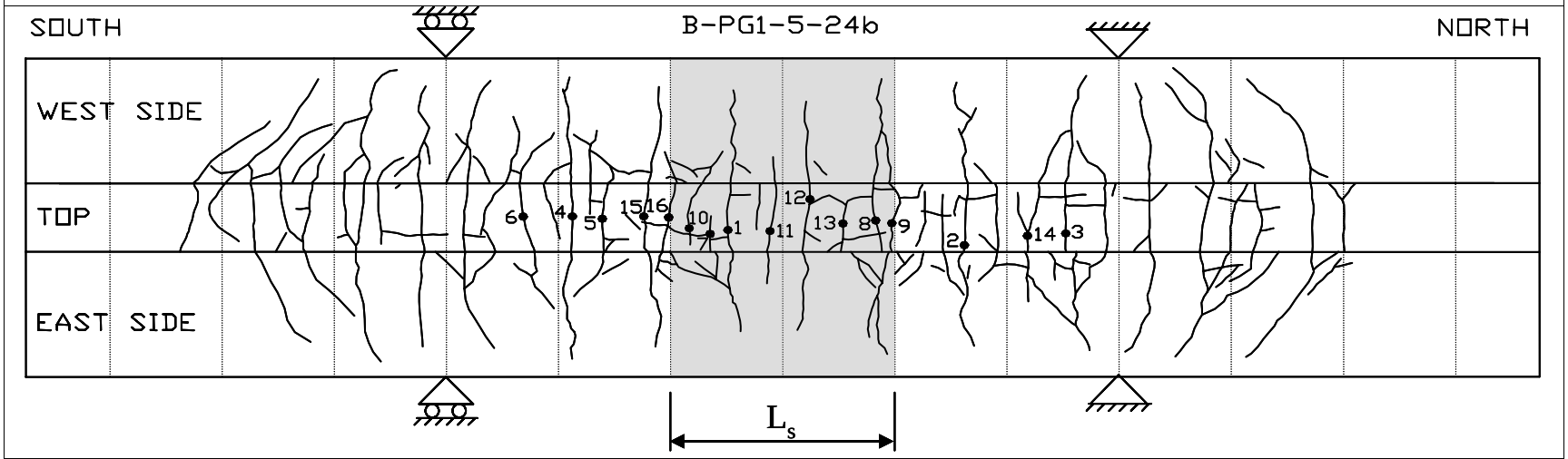

Table C.37 Crack Measurements and Pattern for Specimen B-HG1-5-12

Load, P (kips)	Crack Width (1/1000 in.) Crack No.											
	1	**2**	**3**	**4**	**5**	**6**	**7**	**8**	**9**	**10**	**11**	**12**
4.0	4	6										
4.5	11	8	5	4								
5.0	18	11	12	6	17	18	4	13				
5.5	18	13	16	6	23	21	7	20	6			
6.0	23	14	16	6	26	22	11	27	9	4	3	
6.5	27	17	19	7	30	24	12	28	13	5	4	
7.0	27	17	20	7	32	25	15	30	18	7	6	8
7.5	30	17	20	9	36	26	17	32	18	8	9	10
8.0	32	20	20	11	39	27	18	37	20	10	12	12
8.5	35	22	21	10	42	30	22	40	22	15	16	15
9.0	35	22	22	10	46	32	21	40	23	17	20	17

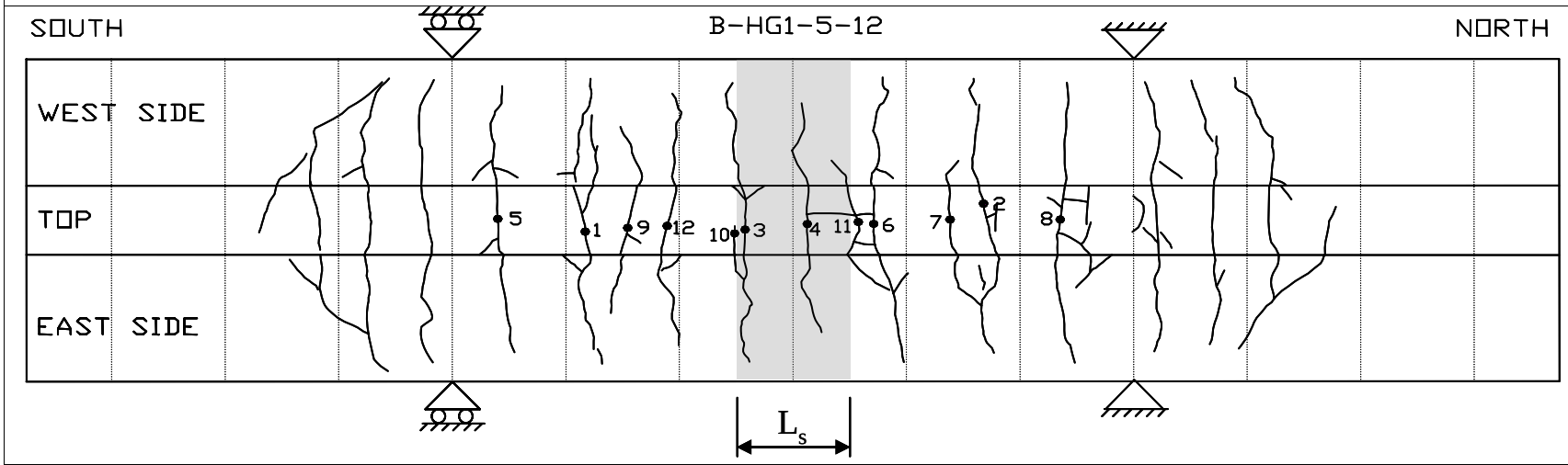

Table C.38 Crack Measurements and Pattern for Specimen B-PG1-5-12

Load, P (kips)	Crack Width (1/1000 in.) Crack No.										
	1	**2**	**3**	**4**	**5**	**6**	**7**	**8**	**9**	**10**	**11**
4.5	10	8									
5.0	16	15	16	18							
5.5	22	18	21	19	4	8					
6.0	24	22	25	22	5	10	9	7	10	8	15
6.5	26	26	25	27	7	11	11	11	10	10	18
7.0	27	29	27	28	8	12	14	15	13	14	21
7.5	29	31	31	29	8	15	16	15	14	14	22
8.0	32	31	31	29	9	15	17	20	16	16	25
8.5	34	35	33	32	10	20	20	21	17	16	26
9.0	36	37	35	34	12	21	21	21	19	16	28

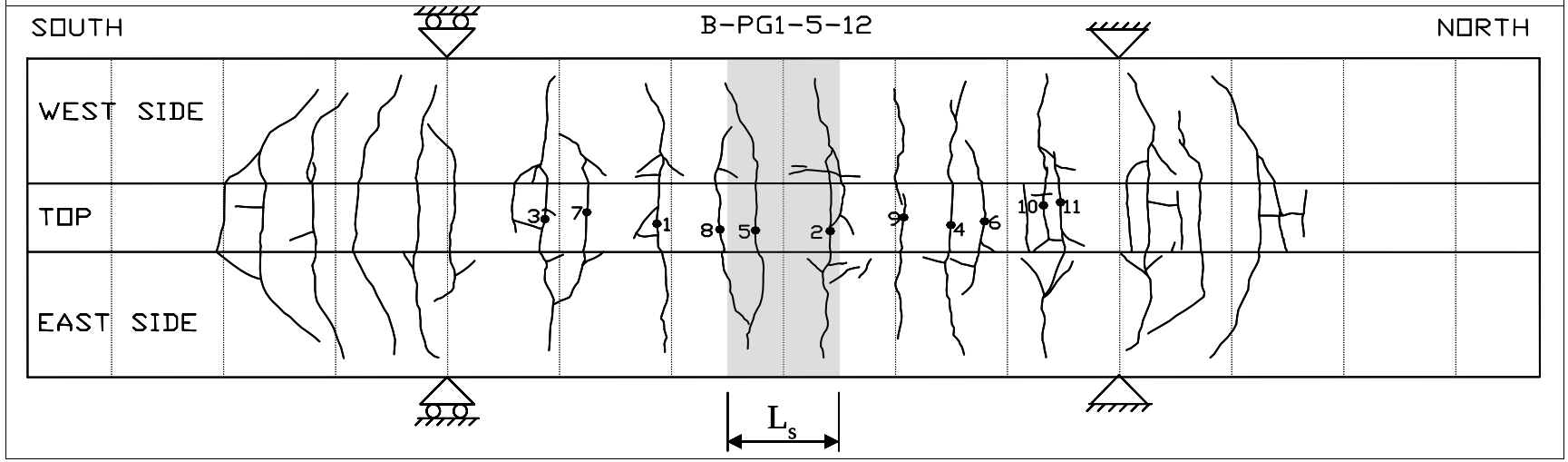

Table C.39 Crack Measurements and Pattern for Specimen B-HG-8-24

Load, P (kips)	Crack Width (1/1000 in.) Crack No.													
	1	**2**	**3**	**4**	**5**	**6**	**7**	**8**	**9**	**10**	**11**	**12**	**13**	**14**
5	2	3	3											
6	5	5	6	5										
7	6	6	7	11	9	8	7	7						
8	7	9	7	13	14	11	10	9						
9	8	10	8	14	15	13	14	12	5					
10	10	11	11	15	20	17	20	15	7	2	7			
11	11	12	10	16	20	18	20	17	9	2	7			
12	11	12	11	17	23	22	20	19	10	2	7	7		
13	11	14	12	20	25	22	22	20	11	2	7	13		
14	11	15	13	22	28	25	25	22	12	2	8	17		
15	11	14	16	24	28	24	26	26	15	2	9	21	4	
16	12	14	15	25	26	23	27	27	16	2	11	24	7	10

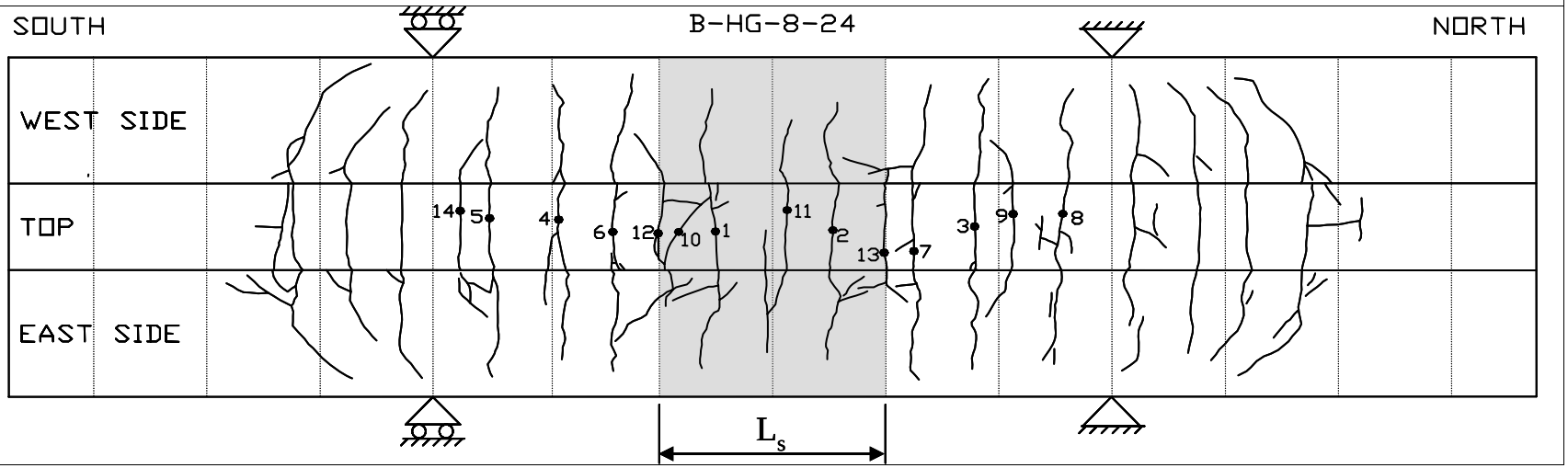

Table C.40 Crack Measurements and Pattern for Specimen B-HG-8-54

Load, P (kips)	Crack Width (1/1000 in.) Crack No.																
	1	**2**	**3**	**4**	**5**	**6**	**7**	**8**	**9**						**10**	**11**	**12**
4	5	3	2	3													
5	7	8	4	10	5	4	4	6									
6	10	10	5	12	7	7	8	11	10	7	5						
7	12	11	7	13	7	9	13	15	13	8	6	10					
8	15	14	8	15	9	11	13	18	15	9	7	10	4				
9	16	14	8	15	10	11	20	21	15	10	8	12	6	8			
10	17	14	10	20	11	12	25	22	17	11	10	16	10	8			
11	20	15	13	20	13	14	31	25	18	12	11	17	13	9			
12	25	15	14	22	14	16	32	28	20	13	11	21	16	11	3		

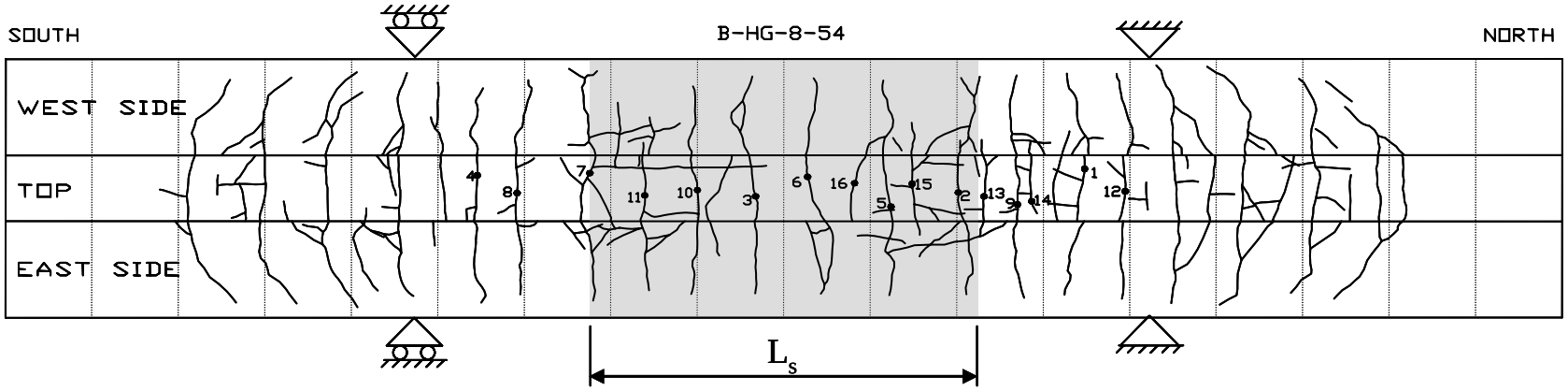

Table C.40 Crack Measurements and Pattern for Specimen B-HG-8-54 (continued)

Load, P (kips)	Crack Width (1/1000 in.)																
	Crack No.																
	1	2	3	4	5	6	7	8	9	10	11	12	13	14	15	16	17
13	25	16	14	23	14	17	35	31	22	14	13	23	17	11	4		
14	25	19	17	24	16	18	41	33	23	16	13	25	21	12	3		
15	31	20	16	33	18	20	55	36	25	16	13	27	23	13	4	5	
16	31	22	16	33	18	22	60	40	25	19	13	32	25	15	7	5	
17	33	23	18	35	18	22	70	42	26	18	14	33	30	15	5	5	2

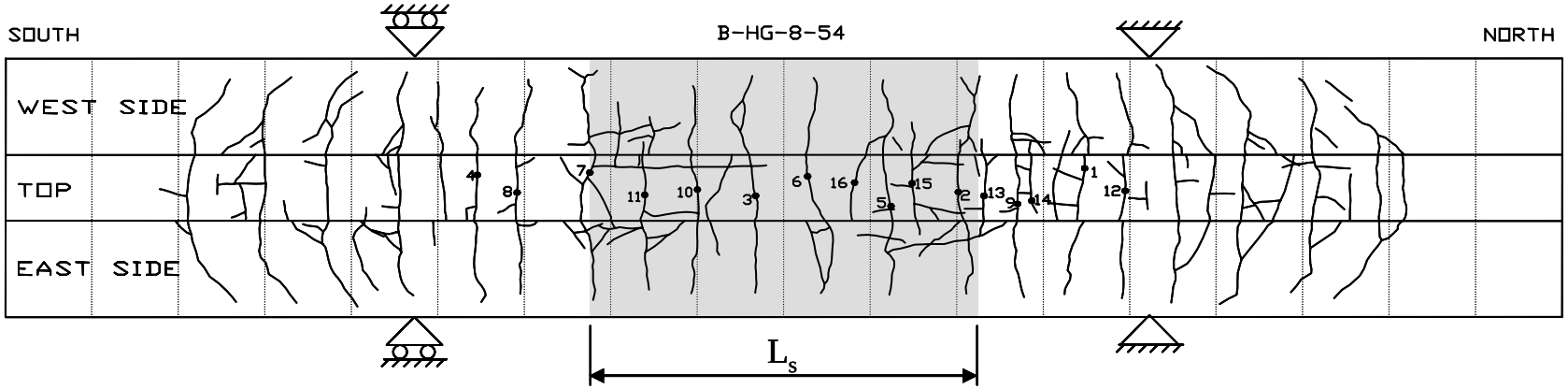

Table C.41 Crack Measurements and Pattern for Specimen B-HG1-5-54

Load, P (kips)	Crack Width (1/1000 in.)																
	Crack No.																
	1	2	3	4	5	6	7	8	9	10	11	12	13	14	15	16	17
3.0	4	2															
3.5	15	4	1	**5**	**3**	**3**											
4.0	20	5	10	6	9	4	7	9									
4.5	25	8	14	9	14	12	10	11	8	9	20						
5.0	31	10	16	10	16	13	11	18	10	10	26						
5.5	34	11	17	12	16	15	15	21	20	10	35	11					
6.0	36	15	21	15	22	16	20	27	20	16	36	14	7				
6.5	40	16	22	15	28	18	21	33	21	18	40	20	12	10			
7.0	40	17	26	17	28	20	22	35	22	19	42	22	15	14			
7.5	43	21	30	18	34	26	26	36	22	22	42	28	22	21			
8.0	43	20	33	20	33	25	28	43	22	22	43	30	25	22	4		
8.5	45	26	36	20	38	27	32	46	24	23	45	35	26	25	5		
9.0	45	26	40	22	39	27	32	50	25	26	45	36	30	25	10		
9.5	46	26	42	21	40	30	34	51	25	27	45	39	35	25	13	26	
10.0	47	26	43	24	41	30	36	55	25	30	50	39	36	25	13	31	3

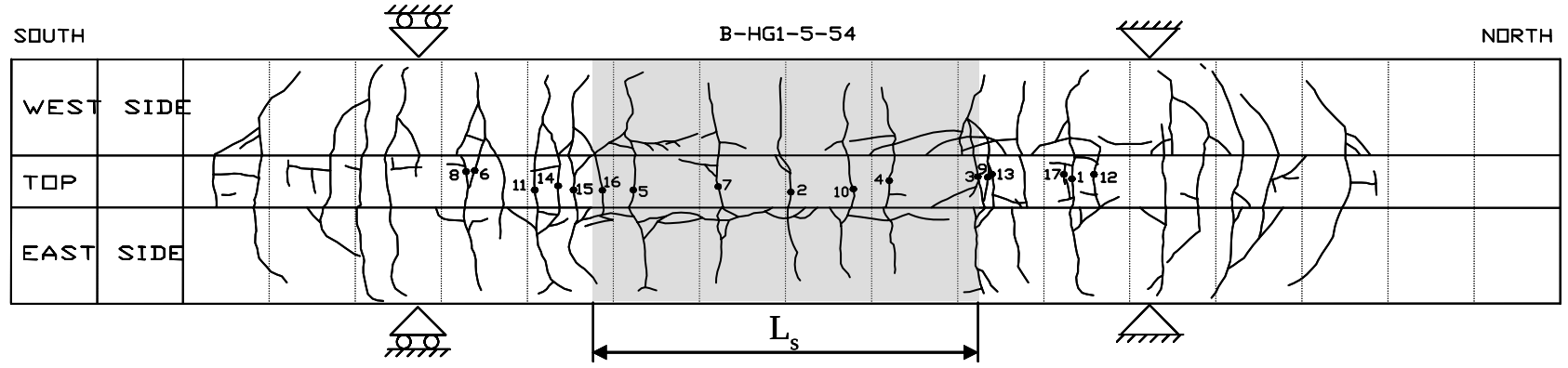

Table C.42 Crack Measurements and Pattern for Specimen B-PG1-5-54

Load, P (kips)	Crack Width (1/1000 in.)																					
	Crack No.																					
	1	**2**	**3**	**4**	**5**	**6**	**7**	**8**	**9**	**10**	**11**	**12**	**13**	**14**	**15**	**16**	**17**	**18**	**19**	**20**	**21**	**22**
3.5	7	4	4	4																		
4.0	13	6	7	8	15	2	7	6	12	15												
4.5	16	8	7	14	16	6	10	7	20	21	7	12	3	10								
5.0	21	9	11	16	18	6	10	8	22	25	13	16	3	11	2							
5.5	20	9	13	22	18	5	13	11	27	29	17	20	6	15	5	6	5	5				
6.0	27	9	13	22	17	5	14	11	36	35	18	24	6	15	5	9	5	8				
6.5	26	15	17	21	18	5	15	12	36	40	22	26	7	20	7	9	5	8	4	3		
7.0	26	15	18	24	20	5	17	12	42	45	25	28	8	20	8	11	6	10	6	3		
7.5	26	16	19	25	20	5	19	13	45	46	26	32	9	21	9	12	7	15	10	4	4	
8.0	27	15	20	26	21	5	18	15	50	49	30	32	9	25	10	11	6	15	15	4	4	
8.5	32	16	23	30	24	5	20	17	52	50	32	32	10	26	11	12	8	21	22	6	4	
9.0	32	17	23	30	26	5	21	18	56	56	35	35	9	27	12	11	7	24	25	7	4	
9.5	33	17	26	30	26	6	22	20	60	67	37	36	12	30	15	11	7	27	30	7	6	
10.0	35	17	28	31	30	6	25	20	65	67	38	40	12	32	16	11	7	28	35	7	6	3

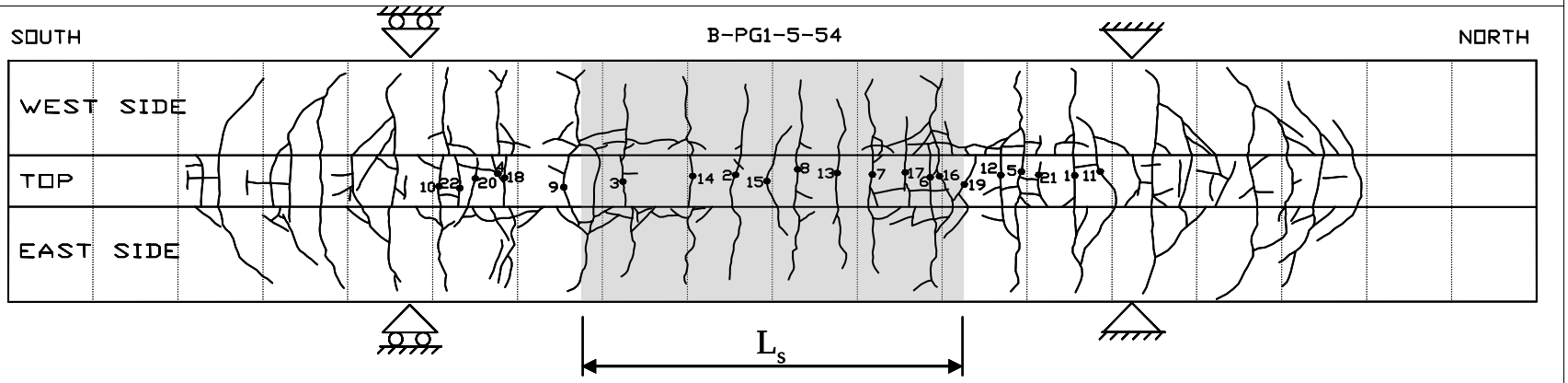

Table C.43 Crack Measurements and Pattern for Specimen B-HC1-5-54

Load, P (kips)	Crack Width (1/1000 in.)															
	Crack No.															
	1	2	3	4	5	6	7	8	9	10	11	12	13	14	15	16
2.5	3															
3.0	5	3	2	5												
3.5	5	4	3	7	6	5										
4.0	5	5	4	10	10	8										
4.5	6	5	4	10	11	9	3	4								
5.0	7	5	7	13	14	11	4	5	4	2						
5.5	7	5	7	13	15	12	5	6	5	3	4	4	5	4	5	
6.0	8	5	8	14	15	13	7	7	5	5	4	4	6	5	6	
6.5	10	11	7	15	18	15	7	8	6	7	4	4	7	6	6	
7.0	10	13	9	15	20	15	6	10	5	7	5	4	7	7	8	
7.5	11	16	10	16	20	16	7	11	6	8	5	4	9	7	11	
8.0	11	16	9	16	22	17	7	11	6	10	5	5	9	9	11	
8.5	12	16	10	17	23	18	8	12	10	11	5	5	10	9	11	
9.0	12	16	10	17	25	18	8	12	11	12	6	5	9	9	12	3

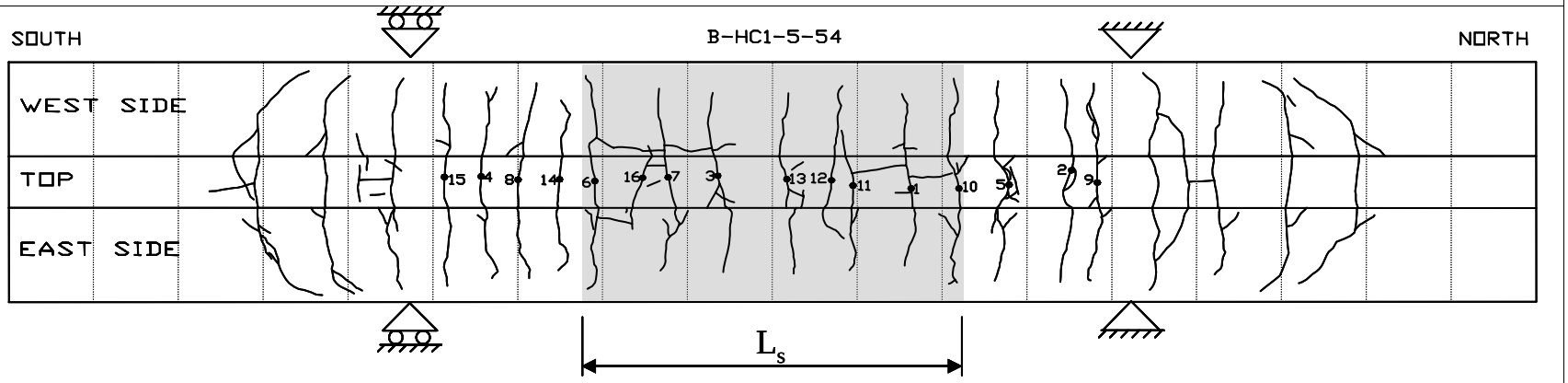

Table C.43 Crack Measurements and Pattern for Specimen B-HC1-5-54 (continued)

Load, P (kips)	Crack Width (1/1000 in.)															
	Crack No.															
	1	2	3	4	5	6	7	8	9	10	11	12	13	14	15	16
9.5	12	16	10	17	27	20	8	14	11	15	7	5	12	10	12	3
10.0	13	16	11	17	27	23	9	15	13	15	6	5	11	10	13	4
10.5	13	20	11	18	28	23	9	16	15	15	7	6	13	11	14	5
11.0	13	21	11	20	30	25	9	16	15	17	7	7	13	11	15	5
11.5	13	23	12	21	32	27	9	15	15	19	7	8	14	13	18	6
12.0	14	23	12	21	32	29	10	18	18	21	9	8	14	13	20	6
13.0	15	24	13	21	35	34	11	18	20	23	10	8	15	15	23	6
14.0	18	24	15	23	36	37	13	21	23	26	10	8	16	16	26	6
15.0	17	27	15	23	40	41	13	24	25	30	10	8	18	16	26	5
16.0	19	29	19	25	42	41	13	24	26	34	11	8	20	18	27	6
17.0	20	29	22	31	43	50	15	25	30	37	11	7	22	20	30	6
18.0	20	32	22	31	45	58	15	30	32	42	11	9	22	20	33	6
19.0	20	36	23	31	45	65	16	35	37	46	13	9	23	22	33	7

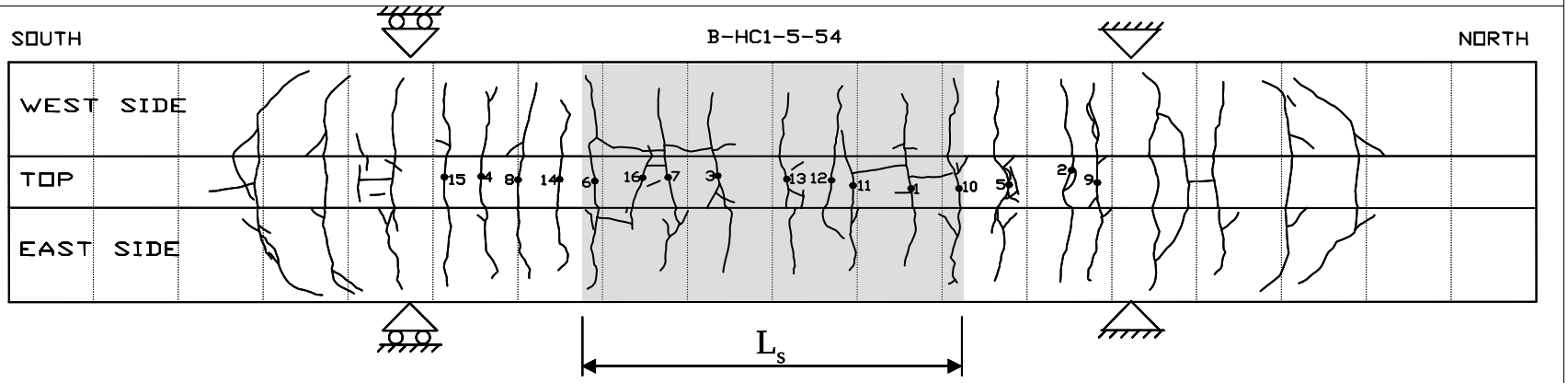

Table C.44 Crack Measurements and Pattern for Specimen B-HG1-5-12b

Load, P (kips)	Crack Width (1/1000 in.)									
	Crack No.									
	1	2	3	4	5	6	7	8	9	10
4.5	2	6								
5.0	5	8	12							
5.5	5	12	16							
6.0	6	15	22							
6.5	7	15	24	6	15	2	7	14	25	
7.0	8	16	25	9	20	2	8	18	30	
7.5	8	20	26	13	24	2	14	20	35	1
8.0	8	22	26	15	24	2	13	20	36	2
8.5	9	25	27	17	27	2	18	21	40	3
9.0	9	26	26	20	33	3	20	20	43	5

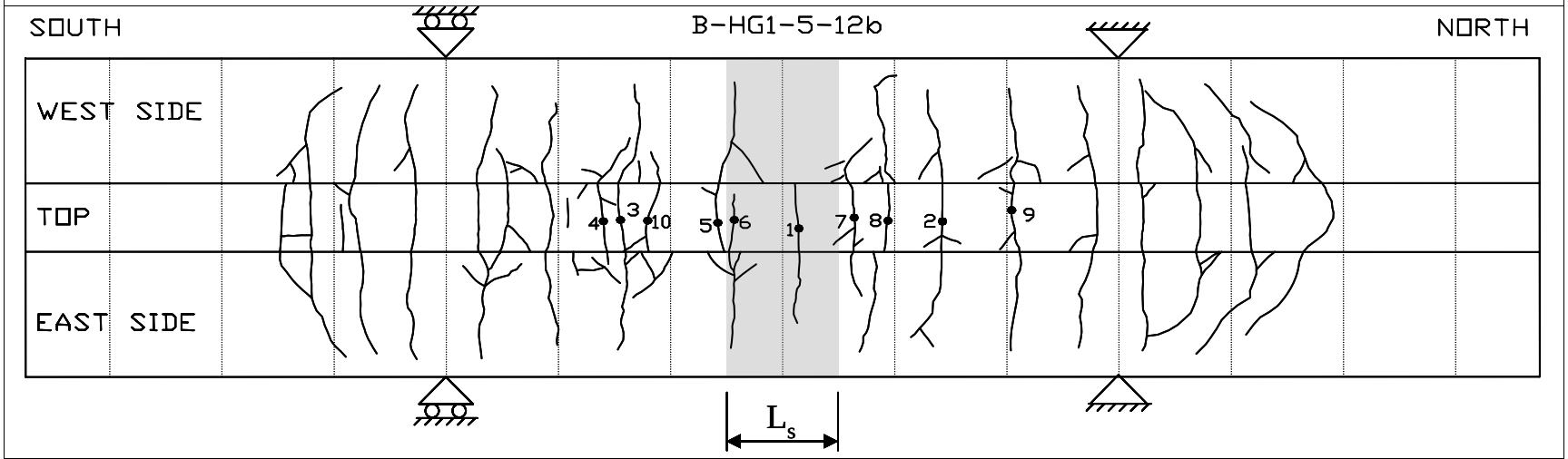

Table C.45 Crack Measurements and Pattern for Specimen B-PG1-5-12b

Load, P (kips)	Crack Width (1/1000 in.)														
	Crack No.														
	1	2	3	4	5	6	7	8	9	10	11	12	13	14	15
4.5	1	2													
5.0	3	11	5												
5.5	7	17	11	11	3										
6.0	16	20	16	12	10	5	11	2	4						
6.5	17	20	18	14	12	5	7	4	12	23	2				
7.0	22	21	21	14	17	7	8	5	15	24	4	3	1		
7.5	21	23	20	14	17	9	8	7	14	30	5	3	2	3	9
8.0	23	22	20	16	21	12	9	11	16	33	6	4	2	5	14
8.5	25	26	22	16	22	15	10	13	17	35	6	5	2	7	14
9.0	27	27	23	16	25	15	10	17	20	40	9	5	3	9	17

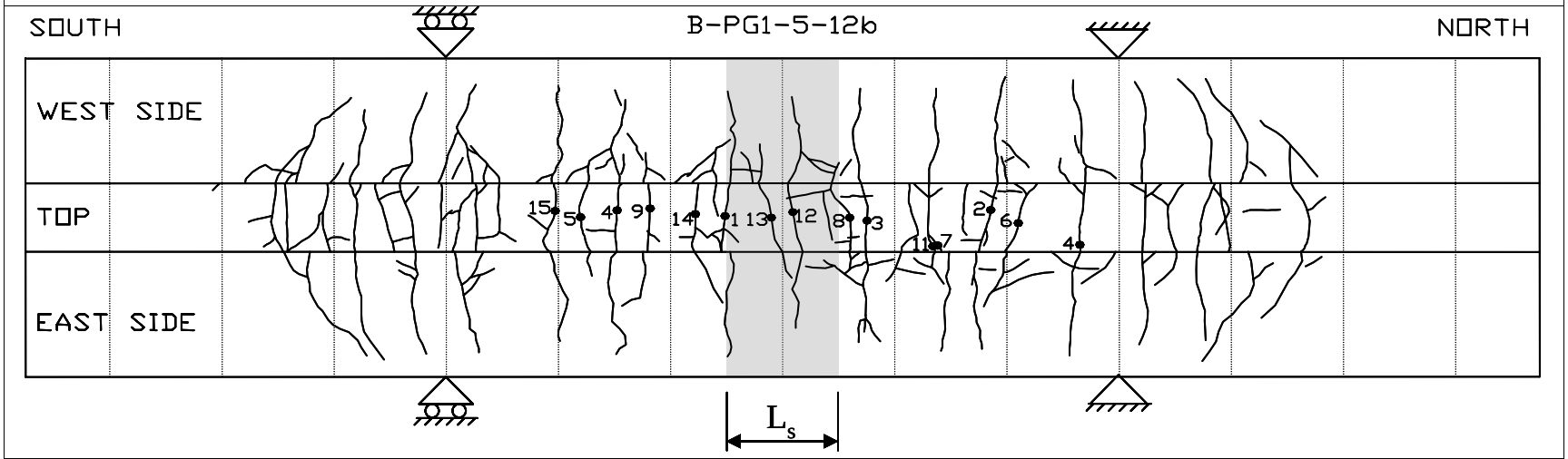

Table C.46 Crack Measurements and Pattern for Specimen B-HG-8-24b

Load, P (kips)	Crack Width (1/1000 in.)												
	Crack No.												
	1	2	3	4	5	6	7	8	9	10	11	12	13
5	3	3											
6	7	8											
7	10	10	6	4	3	5							
8	11	12	6	4	3	7	3	7	3	9			
9	12	15	14	4	3	7	5	8	3	12			
10	15	15	14	5	4	9	7	10	5	15	2	6	
11	15	17	19	5	4	9	7	12	6	16	3	8	8
12	17	18	22	8	4	10	9	15	6	20	3	10	12
13	20	16	24	8	6	10	9	17	7	22	4	12	11
14	21	16	25	7	6	12	12	22	8	26	4	12	13
15	23	17	28	10	5	12	12	25	8	30	5	16	15
16	23	17	30	11	5	12	13	25	10	31	5	16	18
17	25	20	30	11	5	15	5	27	10	36	5	15	18
18	27	22	30	12	5	16	17	32	10	40	6	18	19

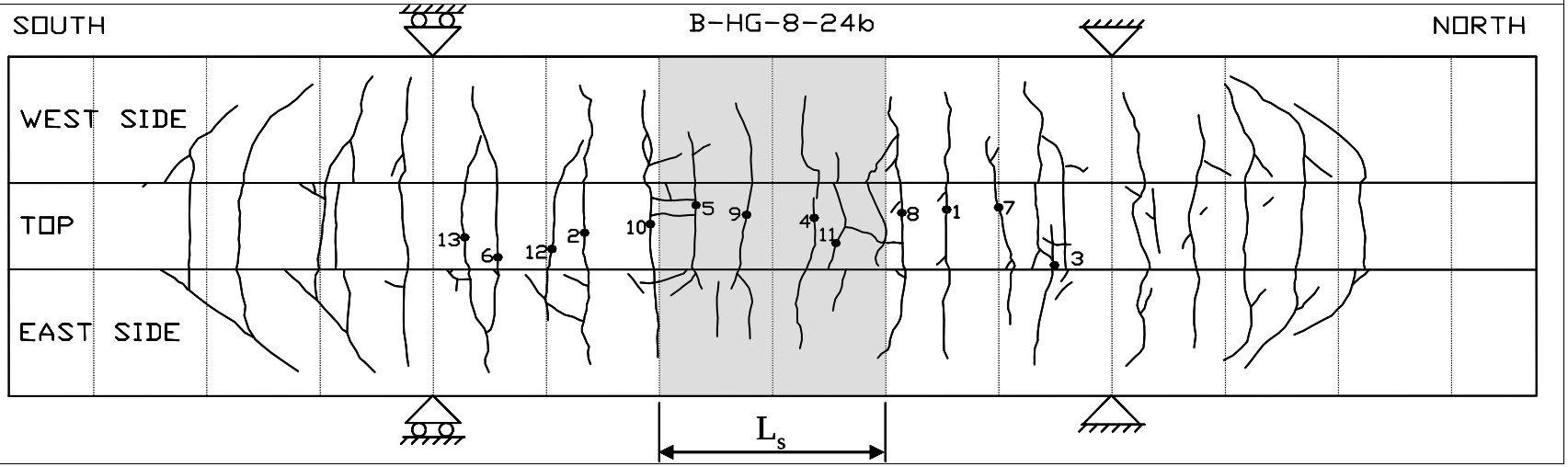

Appendix D

Strain Gage Measurements

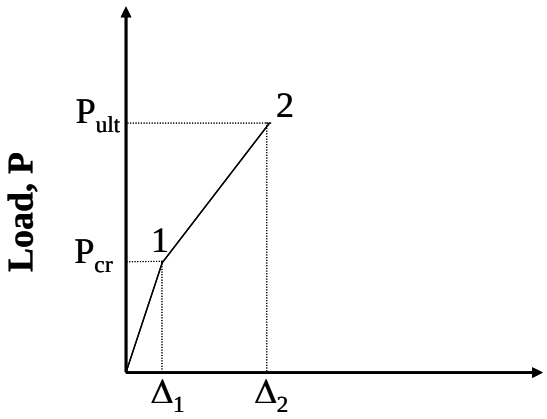

(a) Typical Load-Deflection Curve

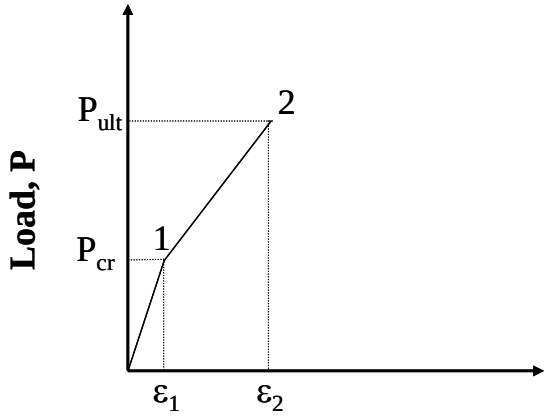

(b) Expected Load versus Strain Curve

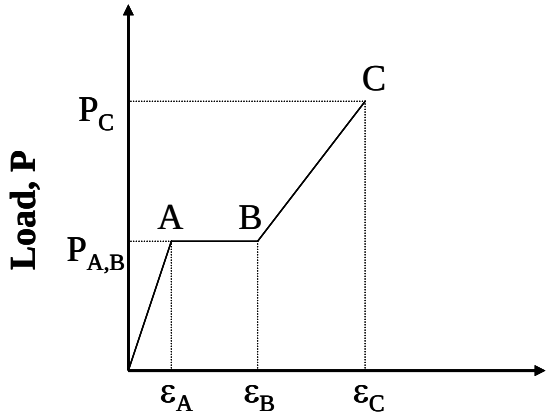

(c) Observed Load versus Strain Curve for Some of the Specimens

Figure D.1 Load-Deflection and Load-Strain Curves

In some specimens, as the bar slipped in concrete, the strain gages also slipped and read strains which were higher than expected. Therefore, the strain in the reinforcement was calculated accordingly:

$$\varepsilon = \varepsilon_C - (\varepsilon_B - \varepsilon_A)$$

or

$$\varepsilon = \varepsilon_2$$

The strain is calculated for the specimens that reached within 2% of the ultimate load, P_{ult}.

Table D. 1 Measured and Calculated Strains in the Reinforcement												
	P_A (lb)	ε_A	P_B (lb)	ε_B	P_C (lb)	ε_C	P_{ult} (lb)	$\frac{P_C - P_{ult}}{P_{ult}} \cdot 100$ (%)	ε	εE (ksi)	σ_{ave} (ksi)	σ_{test} (ksi))
B-S-8-18												
SG-1	-	-	-	-	32659	1485	33011	-1.1	1485	43.1	43.8	41.4
SG-2	-	-	-	-	32735	1539		-0.8	1539	44.6		
SG-3	-	-	-	-	-	-						
B-P-8-18												
SG-1	7861	282	7217	650	21861	4267	24094	-9.3	3899	24.0	- *	28.6
SG-2	8954	553	8368	1175	23952	5187		-0.6	4565	28.1	28.1	
SG-3	8187	233	7217	553	18915	3652		-21.5	3332	20.5	- *	
B-H-8-18												
SG-1	-	-	17926	4056	20531	3922	20531	0.0	3922	22.5	22.5	24.0
SG-2	-	-	18800	4003	20475	3950		-0.3	3950	22.6		
SG-3	-	-	-	-	17412	4596		-15.2	4596	26.3	- *	
B-HN-5-18												
SG-1	6483	469	6933	2530	14207	6045	14207	0.0	6045	38.4	41.7	41.1
SG-2	6441	978	6787	3349	14207	7067		0.0	7067	44.9		
SG-3	6948	233	6924	3156	11917	6750		-16.1	6750	42.9	- *	
B-HO-5-18												
SG-1	5960	239	5504	2531	6281	3265	11514	-45.5	973	5.7	- *	33.3
SG-2	5960	213	5466	1925	8957	4084		-22.2	2372	13.9	- *	
SG-3	5939	132	6984	3631	11415	6357		-0.9	6357	37.2	37.2	
B-P-5-18												
SG-1	-	-	-	-	10664	5378	16531	-35.5	5378	34.5	- *	48.1
SG-2	-	-	-	-	12484	6717		-24.5	6717	43.1	- *	
SG-3	5914	304	6031.3	2080	15684	8474		-5.1	6698	42.9	- *	

Table D.1 Measured and Calculated Strains in the Reinforcement (continued)

	P_A (lb)	ε_A	P_B (lb)	ε_B	P_C (lb)	ε_C	P_{ult} (lb)	$\frac{P_C - P_{ult}}{P_{ult}} \cdot 100$ (%)	ε	εE (ksi)	σ_{ave} (ksi)	σ_{test} (ksi))
B-S-5-18												
SG-1	-	-	-	-	23972	2517	24087	-0.5	2517	73.0	81.7	71.4
SG-2	-	-	-	-	23958	2828		-0.5	2828	82.0		
SG-3	-	-	-	-	23724	3104		-1.5	3104	90.0		
B-C-5-18												
SG-1	-	-	-	-	19900	3545	19903	0.0	3545	65.6	65.6	59.5
SG-2	-	-	-	-	15415	2678		-22.6	2678	49.6	-*	
SG-3	-	-	-	-	15345	2885		-22.9	2885	53.4	-*	
B-C-5-12												
SG-1	-	-	-	-	14896	3155	15071	-1.2	3155	58.4	52.9	44.9
SG-2	6939	587	6787	1032	14964	2738		-0.7	2738	50.7		
SG-3	-	-	-	-	14945	2683		-0.8	2683	49.7		
B-S-8-36												
SG-1	-	-	-	-	37089	2086	37089	0.0	2086	60.5	65.5	58.3
SG-2	-	-	-	-	37089	2428		0.0	2428	70.4		
SG-3	-	-	-	-	34173	2203		-7.9	2203	63.9	-*	
B-P-8-36												
SG-1	-	-	-	-	19769	5172	19963	-1.0	5172	31.9	33.9	29.3
SG-2	-	-	-	-	19911	5844		-0.3	5844	36.0		
SG-3	-	-	-	-	17861	4947		-10.5	4947	30.5	-*	
B-H-8-36												
SG-1	7908	500	8826	2253	15638	4825	21042	-25.7	3072	17.6	-*	30.8
SG-2	7435	675	7248	2043	14098	4233		-33.0	2865	16.4	-*	
SG-3	7755	497	8984	2230	12892	3480		-38.7	1747	10.0	-*	

Table D.1 Measured and Calculated Strains in the Reinforcement (continued)												
	P_A (lb)	ε_A	P_B (lb)	ε_B	P_C (lb)	ε_C	P_{ult} (lb)	$\frac{P_C - P_{ult}}{P_{ult}} \cdot 100$ (%)	ε	ε E (ksi)	σ_{ave} (ksi)	σ_{test} (ksi))
B-HN-5-36												
SG-1	4301	278	6405	5087	6405	5087	12362	-48.2	5087	32.3	-*	44.8
SG-2	4879	1223	5932	4178	9776	7259		-20.9	4304	27.4	-*	
SG-3	4426	429	5870	4877	5870	4877		-52.5	4877	31.0	-*	
B-HO-5-36												
SG-1	4890	637	5691	2995	5761	4555	13297	-56.7	2197	12.8	-*	48.3
SG-2	3863	115	6399	4277	6383	5800		-52.0	1638	9.6	-*	
SG-3	4807	653	4991	2658	4991	2658		-62.5	653	3.8	-*	
B-P-5-36												
SG-1	5923	632	6783	3264	6754	3928	13939	-51.5	3928	25.2	-*	50.6
SG-2	4550	621	5983	3412	10489	5969		-24.8	5969	38.3	-*	
SG-3	5856	566	8548	4504	8548	5007		-38.7	5007	32.1	-*	
B-C-5-36												
SG-1	6442	472	6541	1046	18478	4533	22923	-19.4	3959	73.3	-*	85.8
SG-2	-	-	-	-	15218	3330		-33.6	3330	61.6	-*	
SG-3	6466	410	6477	1085	15390	3450		-32.9	2775	51.4	-*	

* Not considered in the average stress calculation

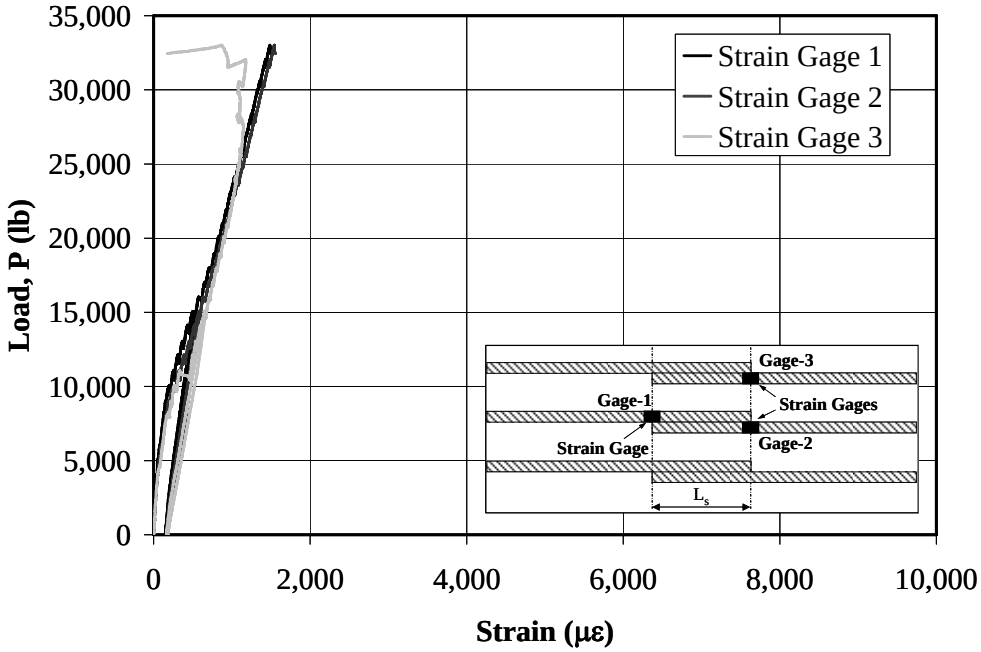

Figure D.2 Strain Gage Measurements for Specimen B-S-8-18

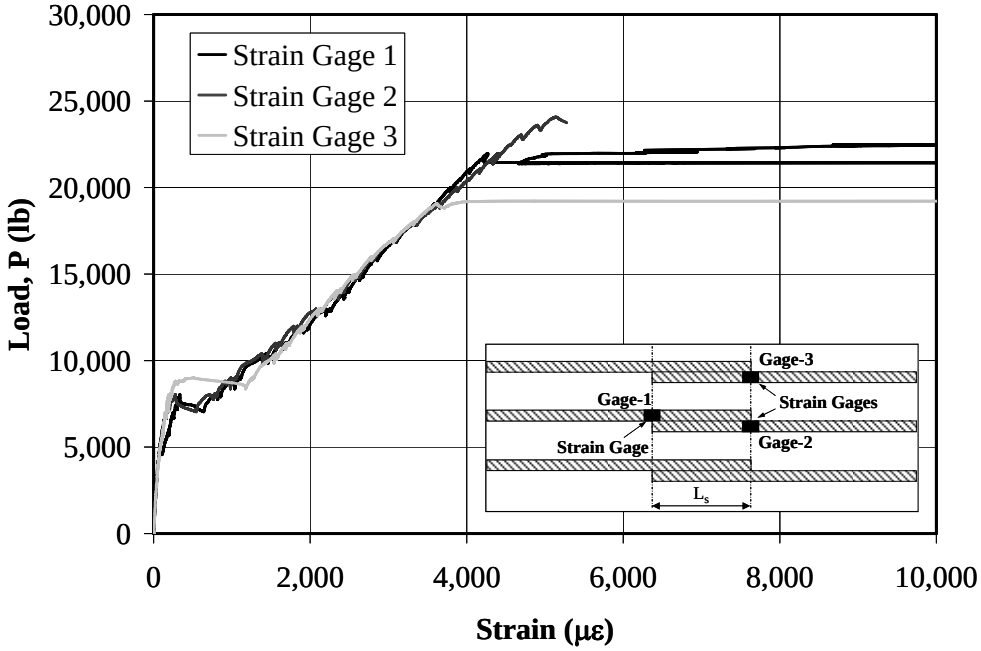

Figure D.3 Strain Gage Measurements for Specimen B-P-8-18

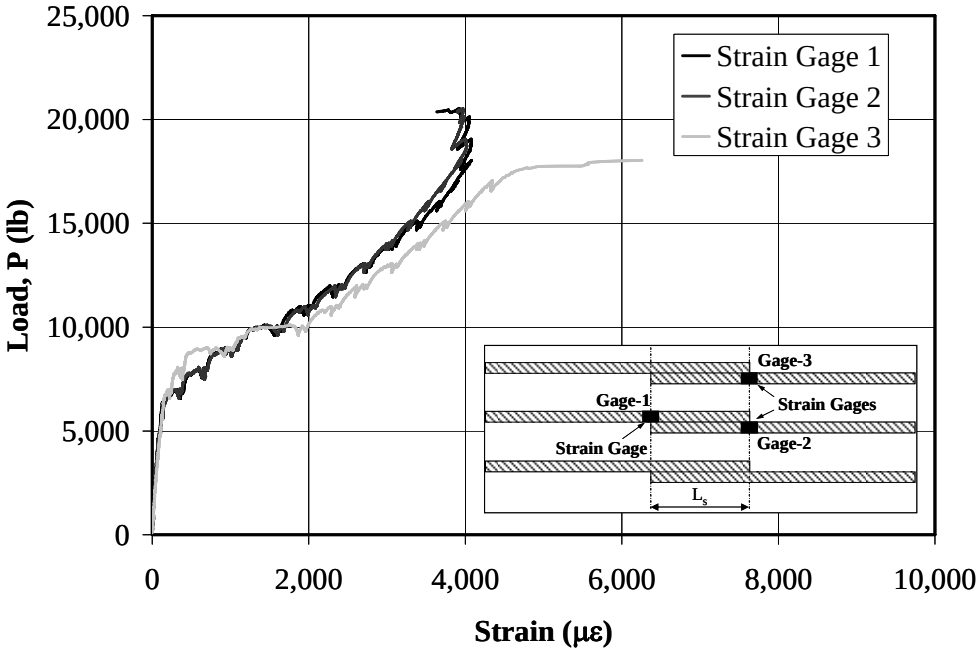

Figure D.4 Strain Gage Measurements for Specimen B-H-8-18

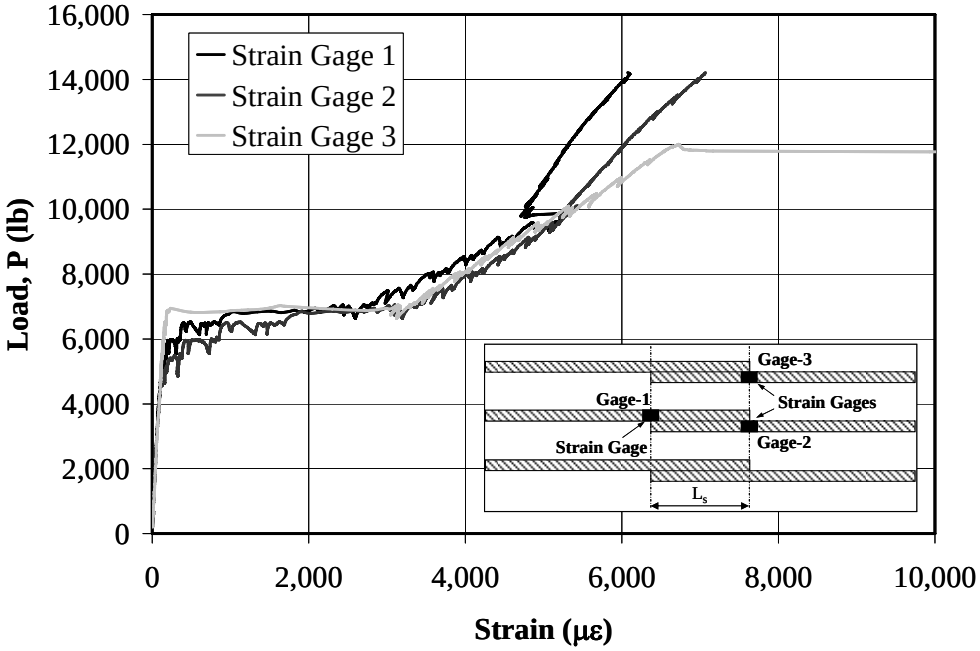

Figure D.5 Strain Gage Measurements for Specimen B-HN-5-18

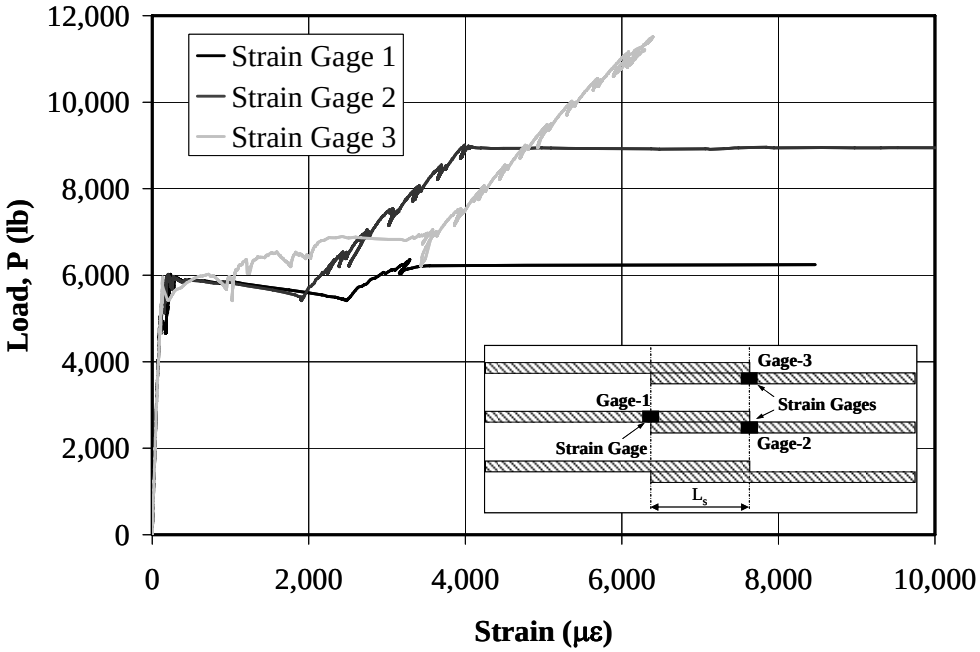

Figure D.6 Strain Gage Measurements for Specimen B-HO-5-18

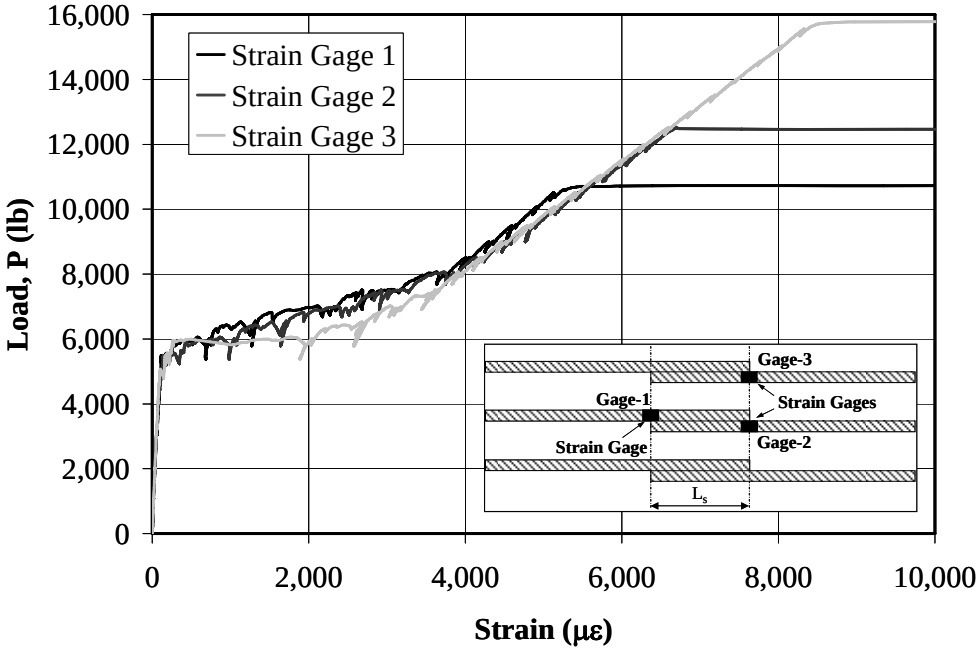

Figure D.7 Strain Gage Measurements for Specimen B-P-5-18

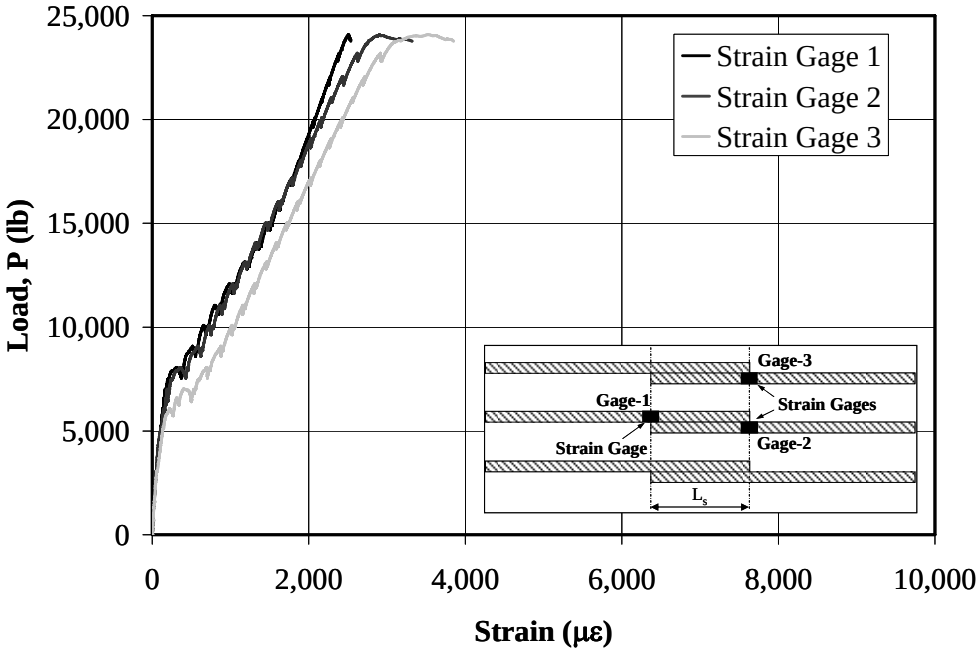

Figure D.8 Strain Gage Measurements for Specimen B-S-5-18

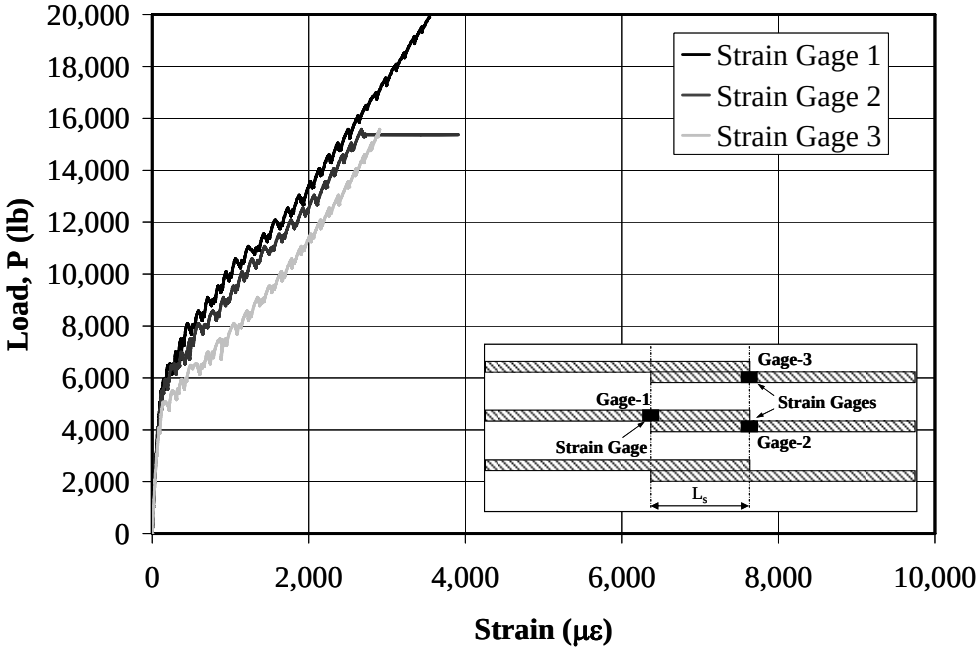

Figure D.9 Strain Gage Measurements for Specimen B-C-5-18

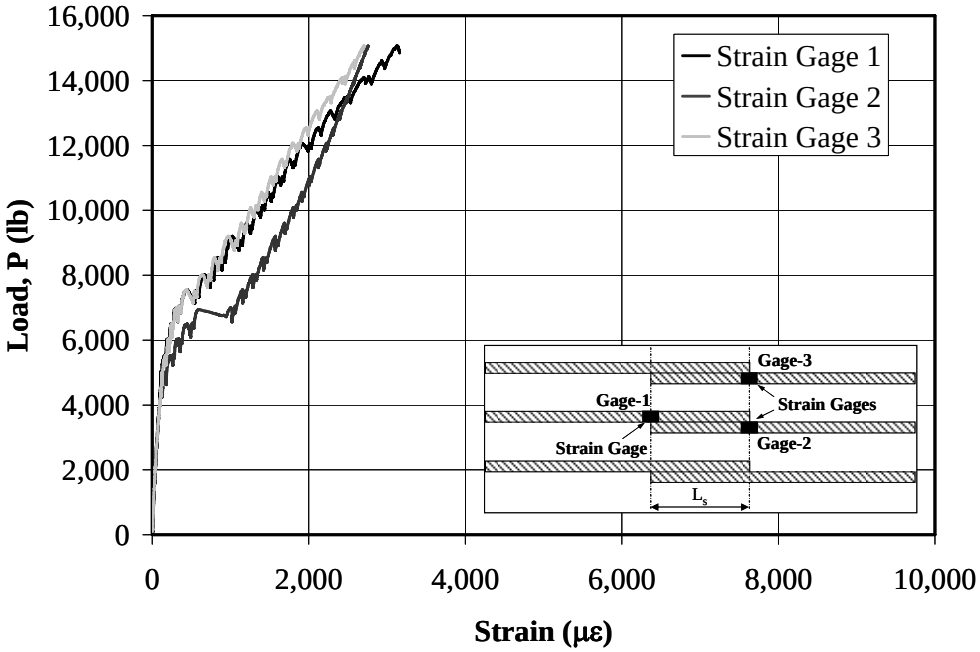

Figure D.10 Strain Gage Measurements for Specimen B-C-5-12

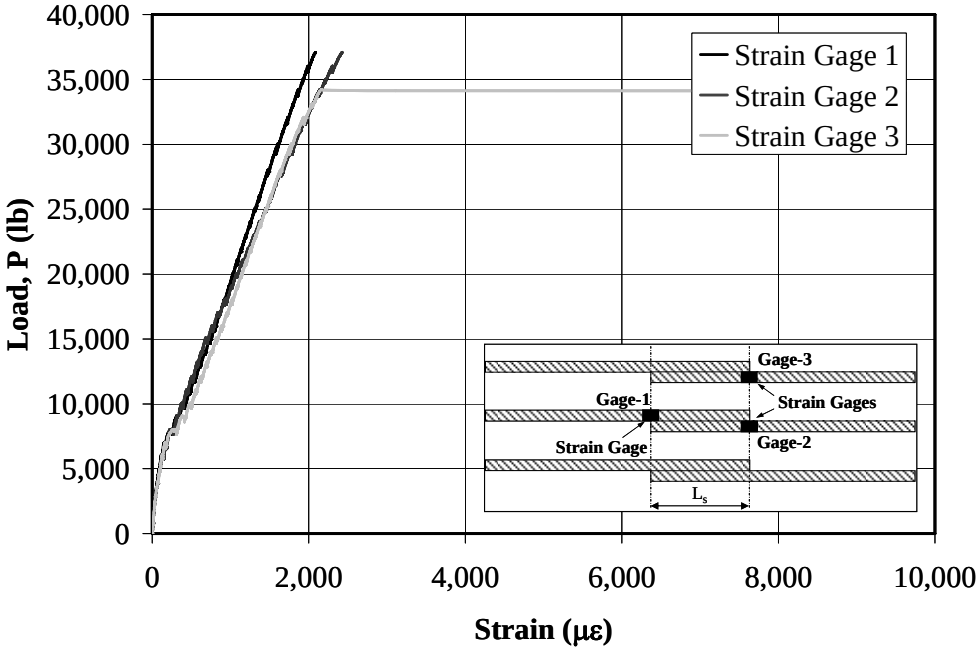

Figure D.11 Strain Gage Measurements for Specimen B-S-8-36

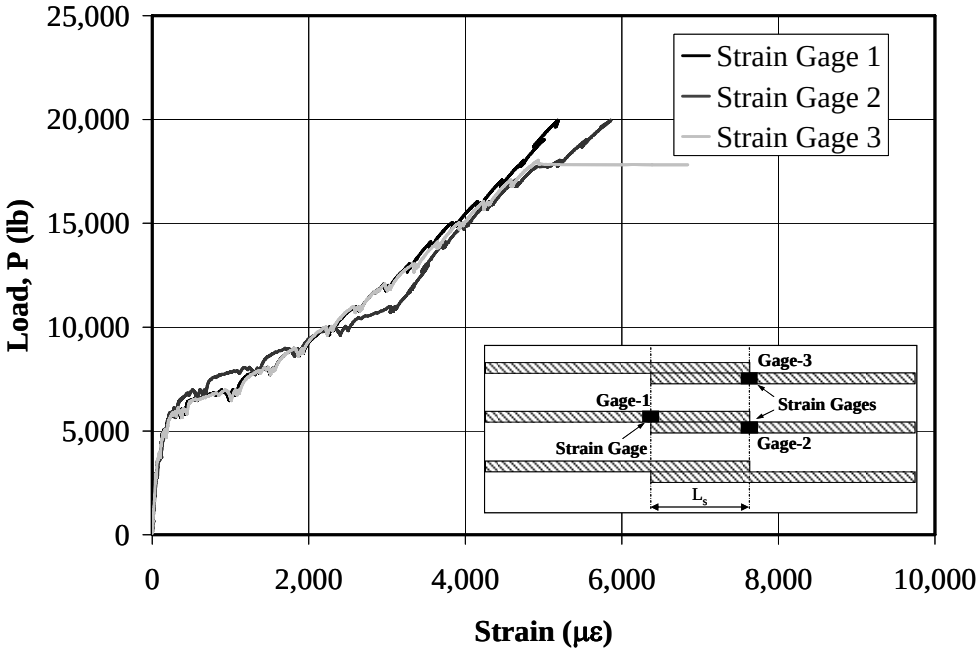

Figure D.12 Strain Gage Measurements for Specimen B-P-8-36

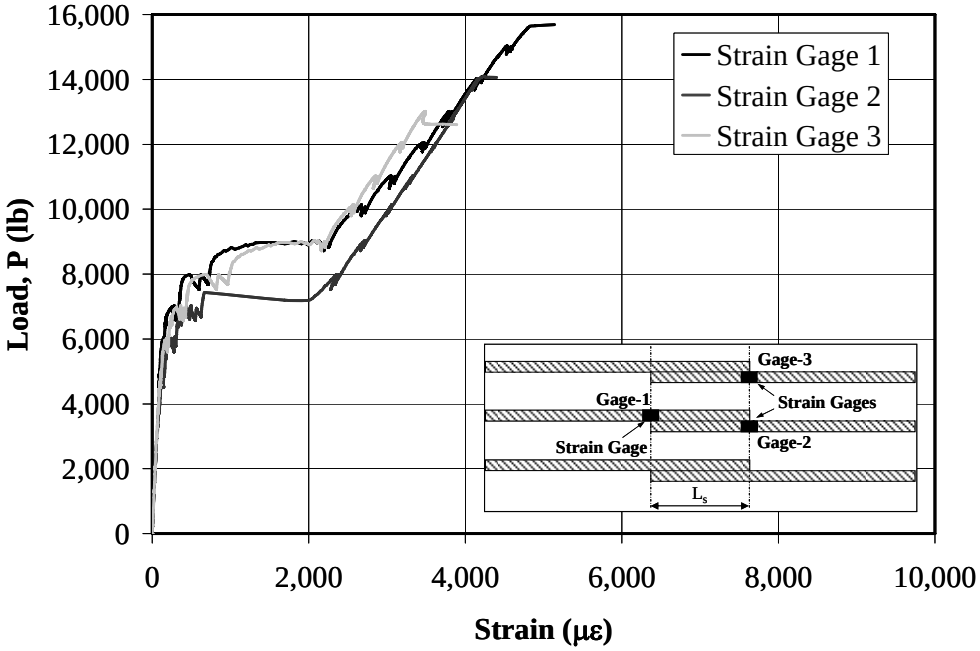

Figure D.13 Strain Gage Measurements for Specimen B-H-8-36

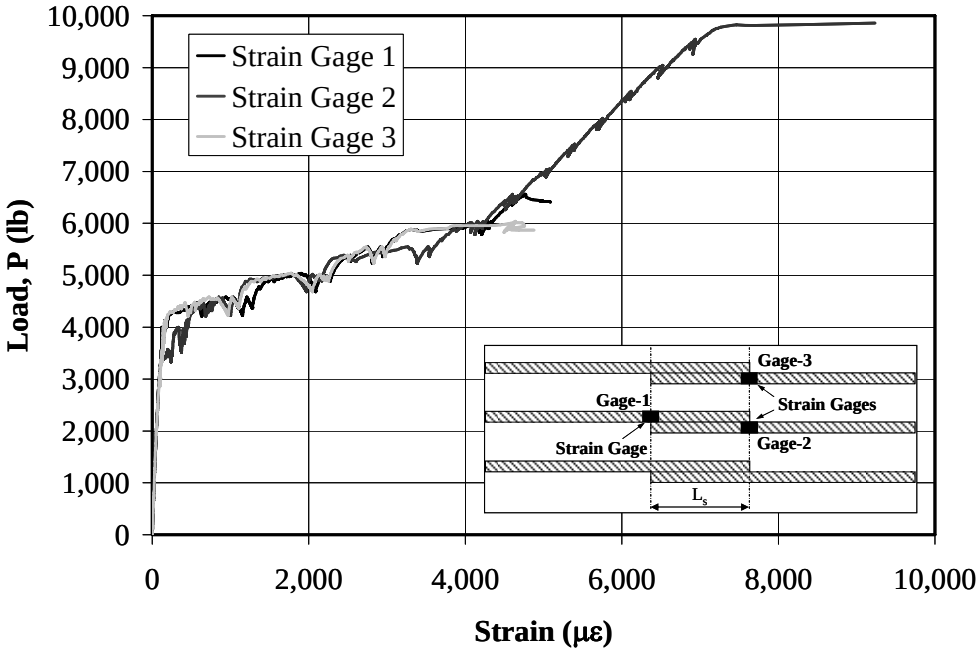

Figure D.14 Strain Gage Measurements for Specimen B-HN-5-36

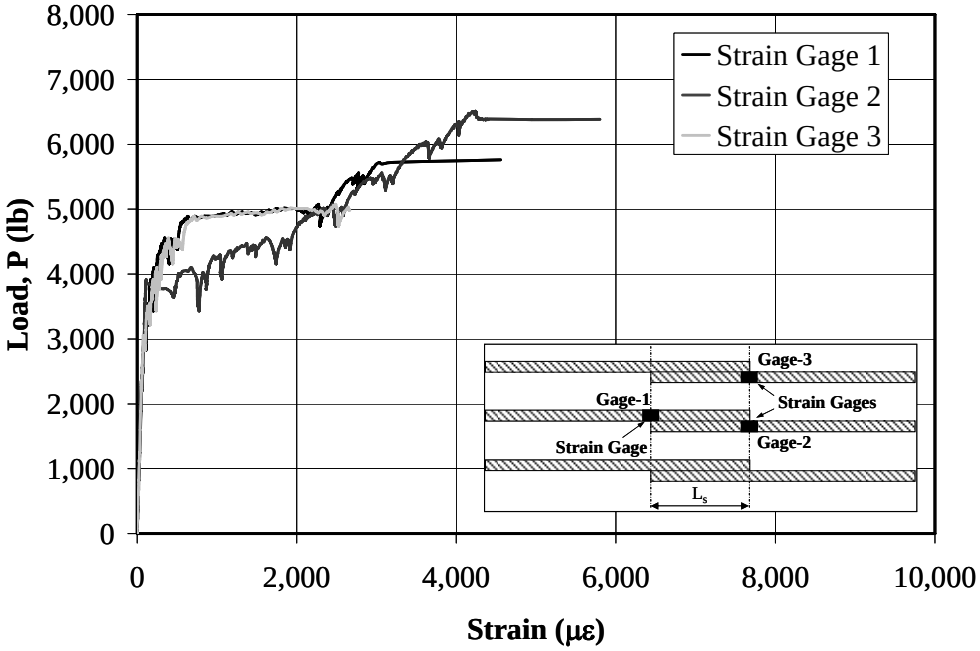

Figure D.15 Strain Gage Measurements for Specimen B-HO-5-36

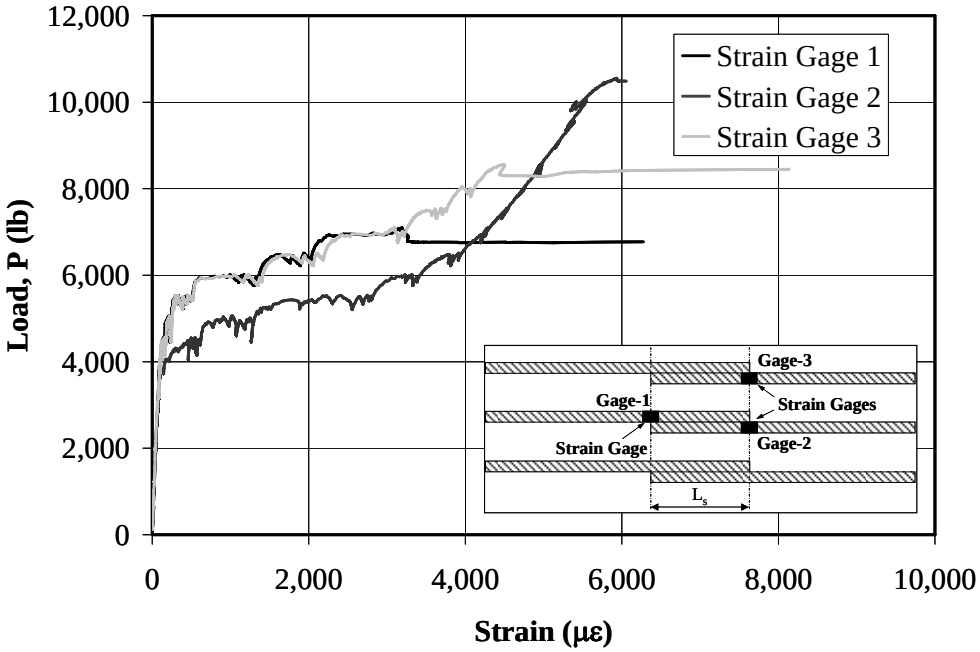

Figure D.16 Strain Gage Measurements for Specimen B-P-5-36

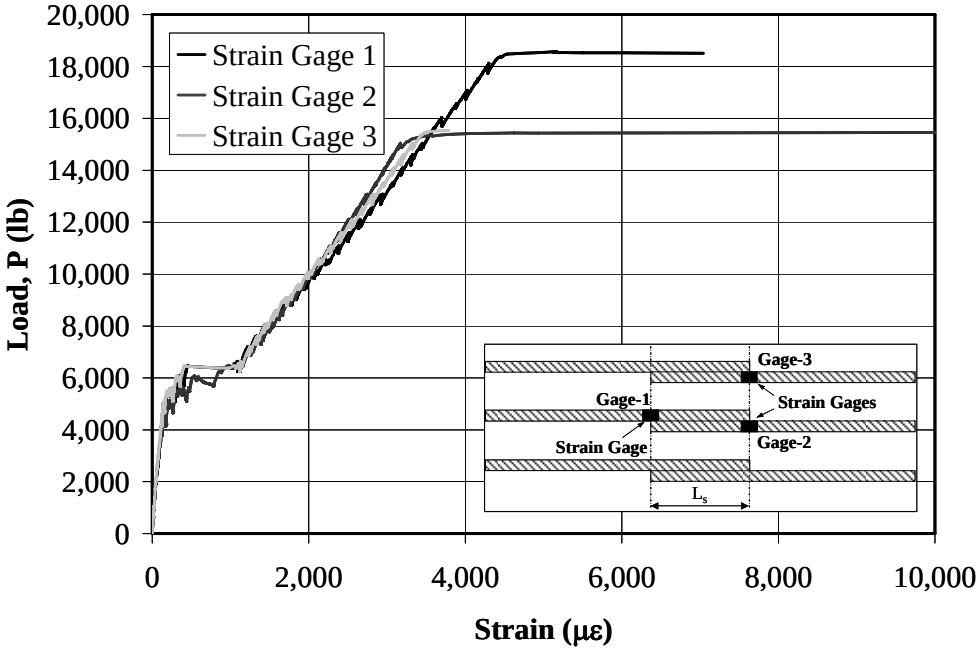

Figure D.17 Strain Gage Measurements for Specimen B-C-5-36

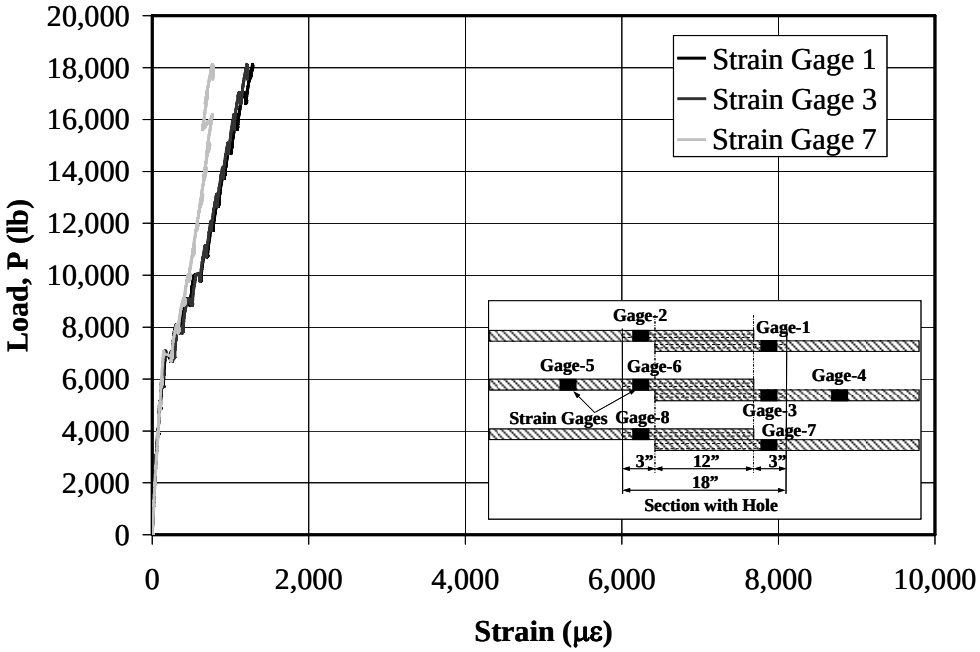

Figure D.18 Strain Gage Measurements for Specimen B-S2-8-12 (Strain Gages 1, 3, and 7)

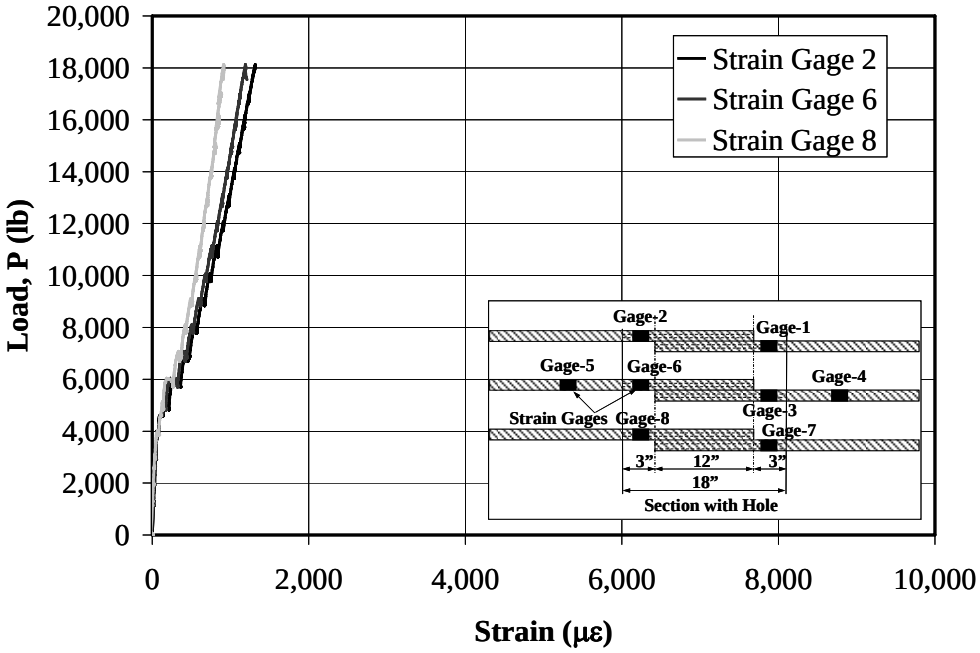

Figure D.19 Strain Gage Measurements for Specimen B-S2-8-12 (Strain Gages 2, 6, and 8)

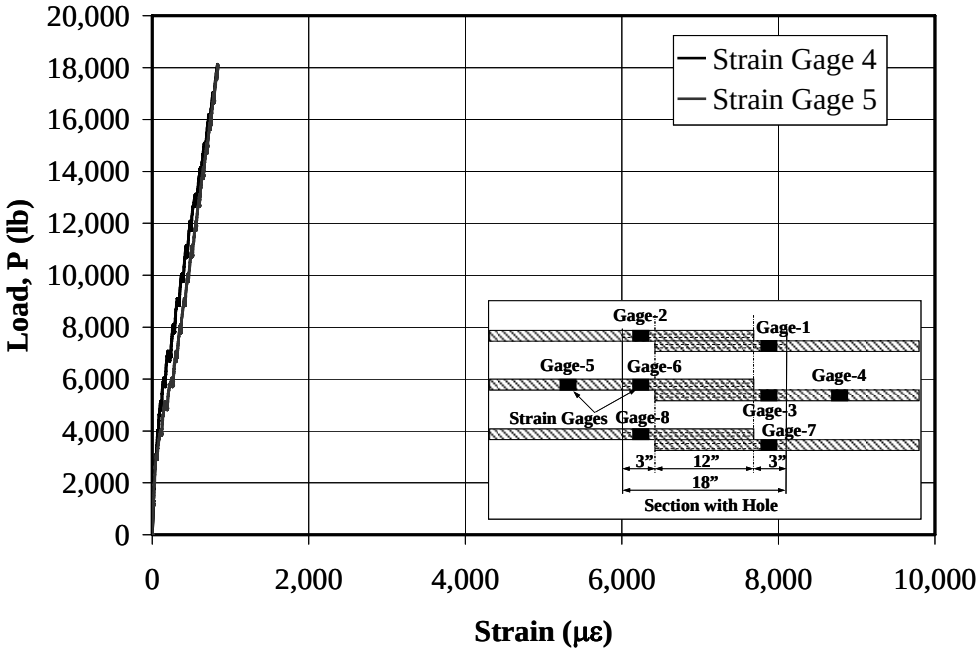

Figure D.20 Strain Gage Measurements for Specimen B-S2-8-12 (Strain Gages 4 and 5)

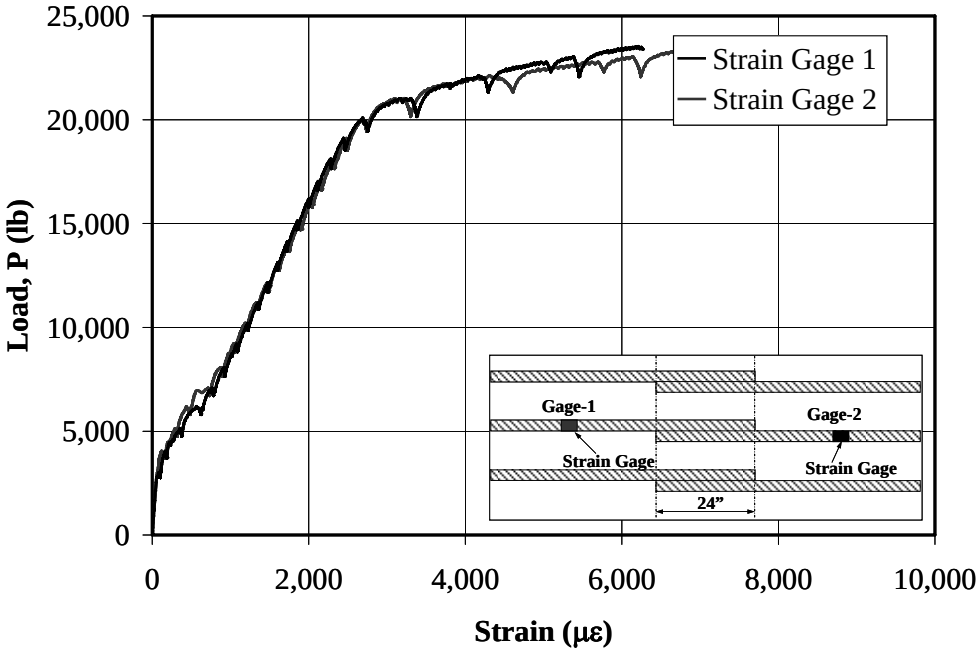

Figure D.21 Strain Gage Measurements for Specimen B-S-5-24

Appendix E

Load-Deflection Curves

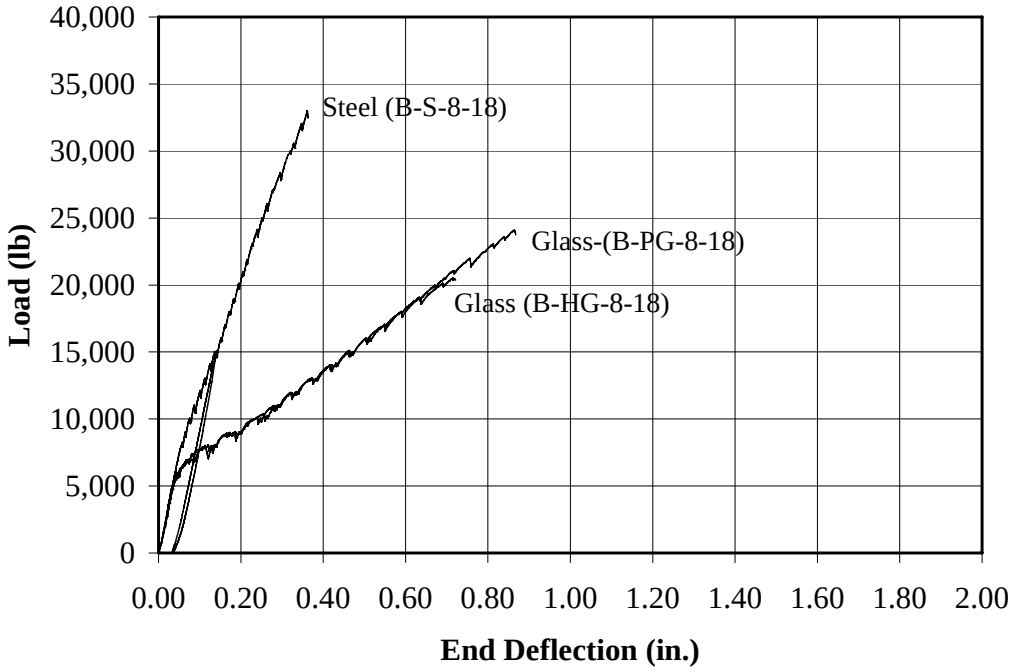

(a) Specimens Reinforced with #8 Bars (18 in. Splice)

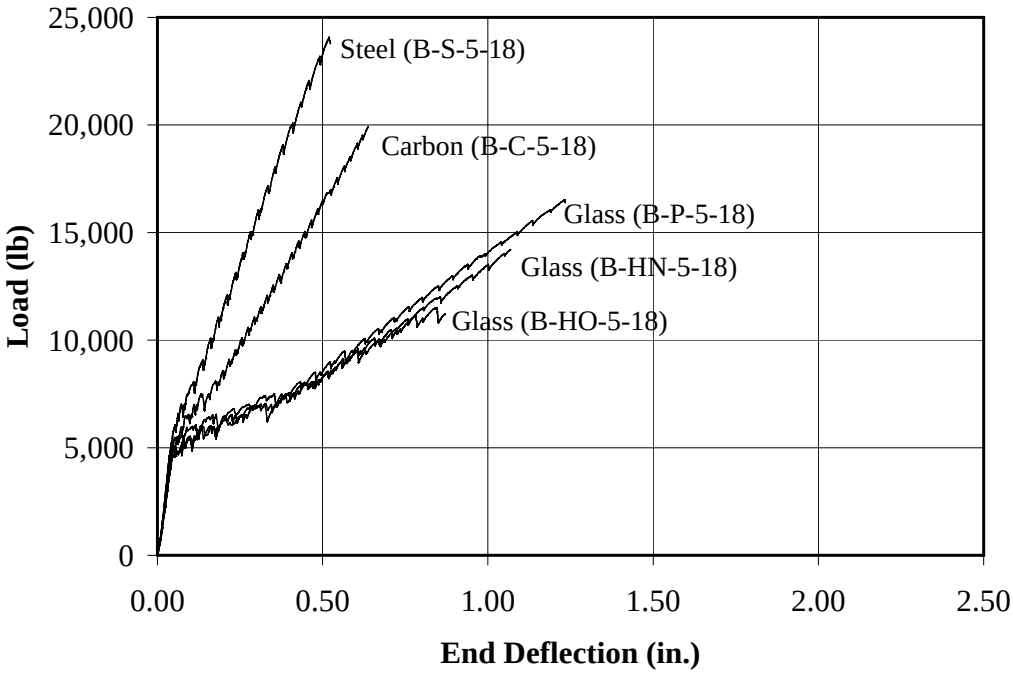

(b) Specimens Reinforced with #5 Bars (18 in. Splice)

Figure E.1 Load-Deflection for Specimens in Series I

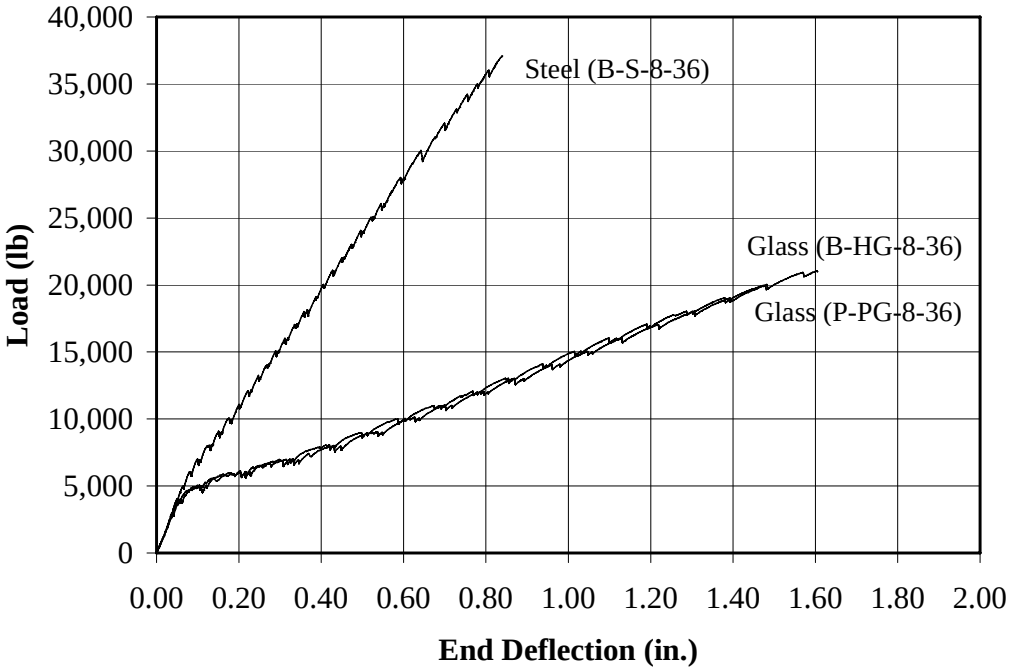

(a) Specimens Reinforced with #8 Bars (36 in. Splice)

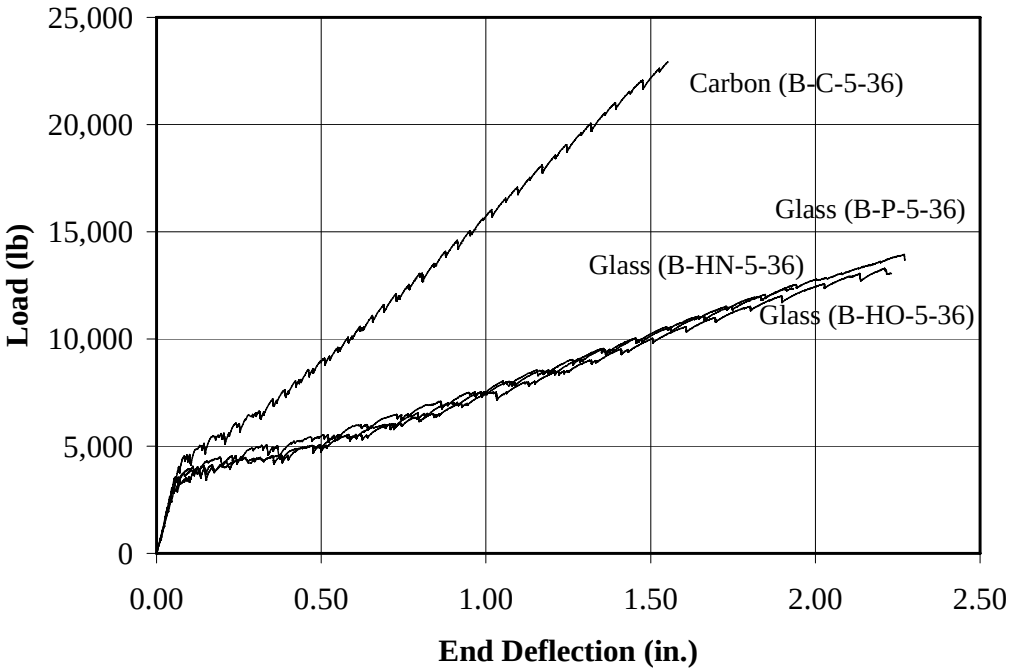

(b) Specimens reinforced with #5 Bars (36 in. Splice)

Figure E.2 Load-Deflection for Specimens in Series II

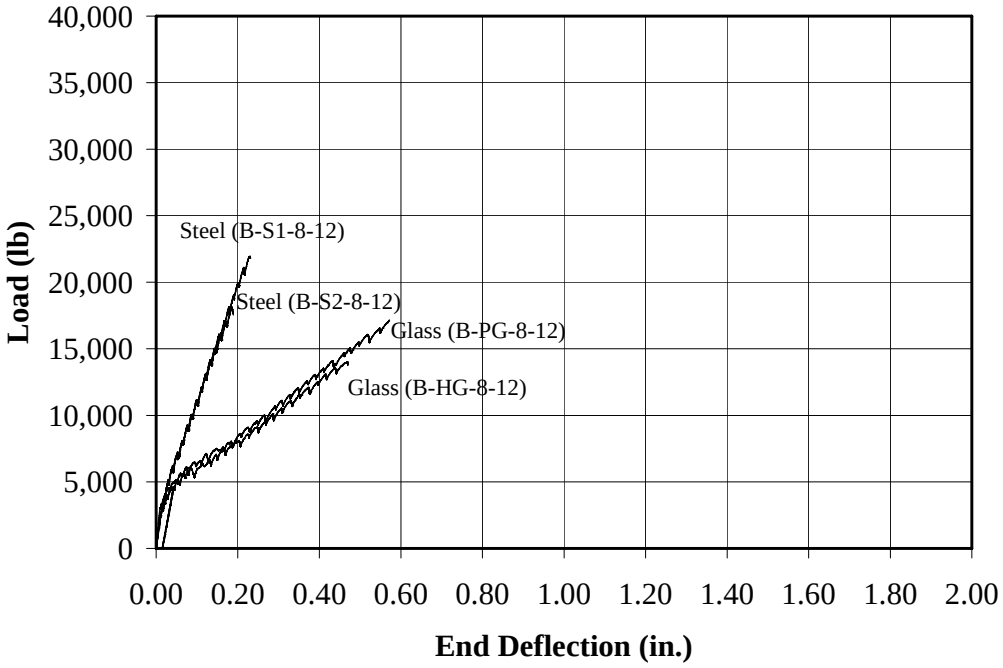

(a) Specimens Reinforced with #8 Top Cast Bars (12 in. Splice)

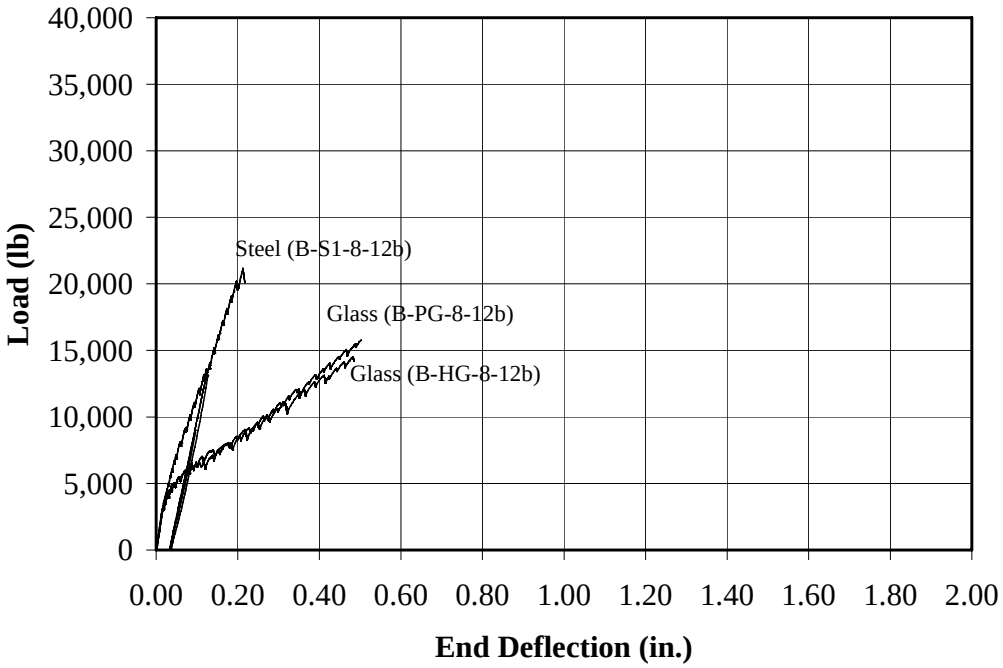

(b) Specimens Reinforced with #8 Bottom Cast Bars (12 in. Splice)

Figure E.3 Load-Deflection for Specimens in Series III

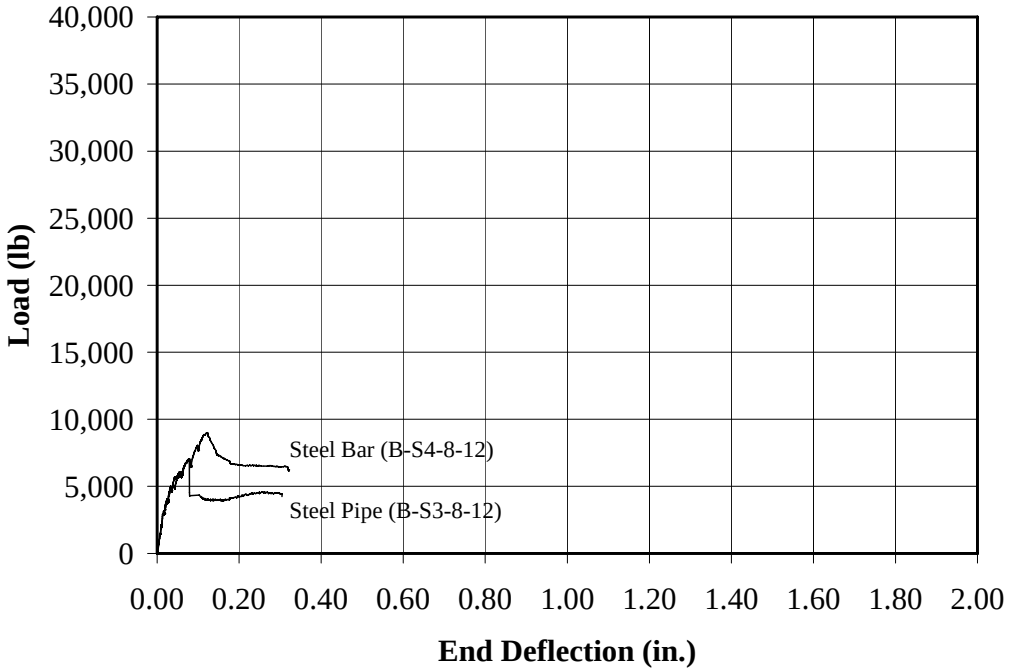

(c) Specimens Reinforced with #8 Bottom Cast Plain Bars (12 in. Splice)

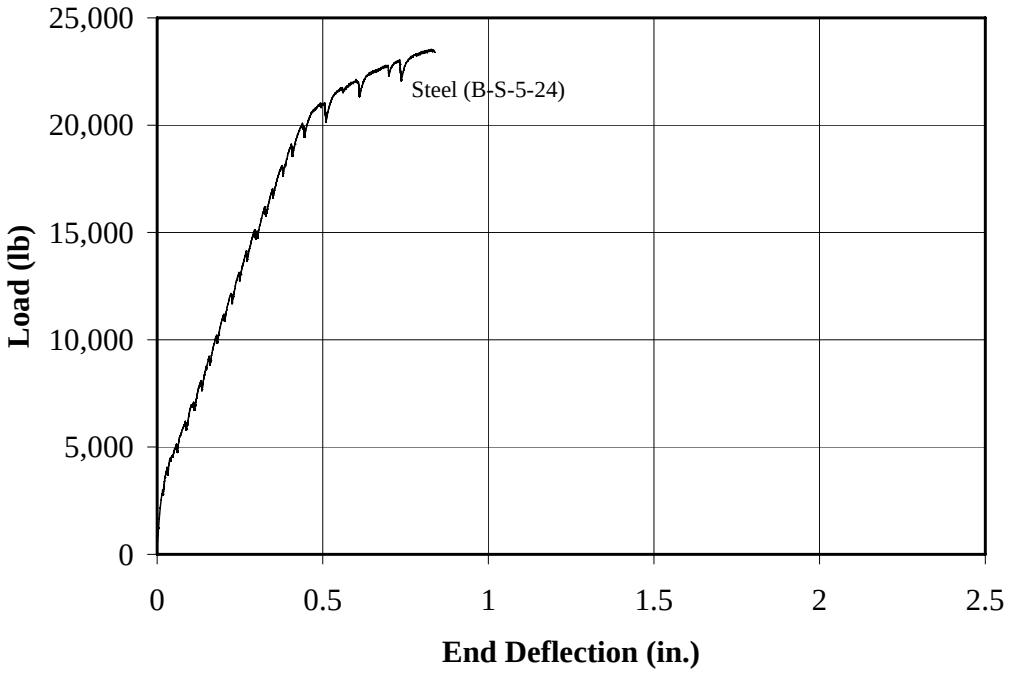

(d) Specimens Reinforced with #5 Top Cast Bar (24 in. Splice)

Figure E.3 Load-Deflection for Specimens in Series III (continued)

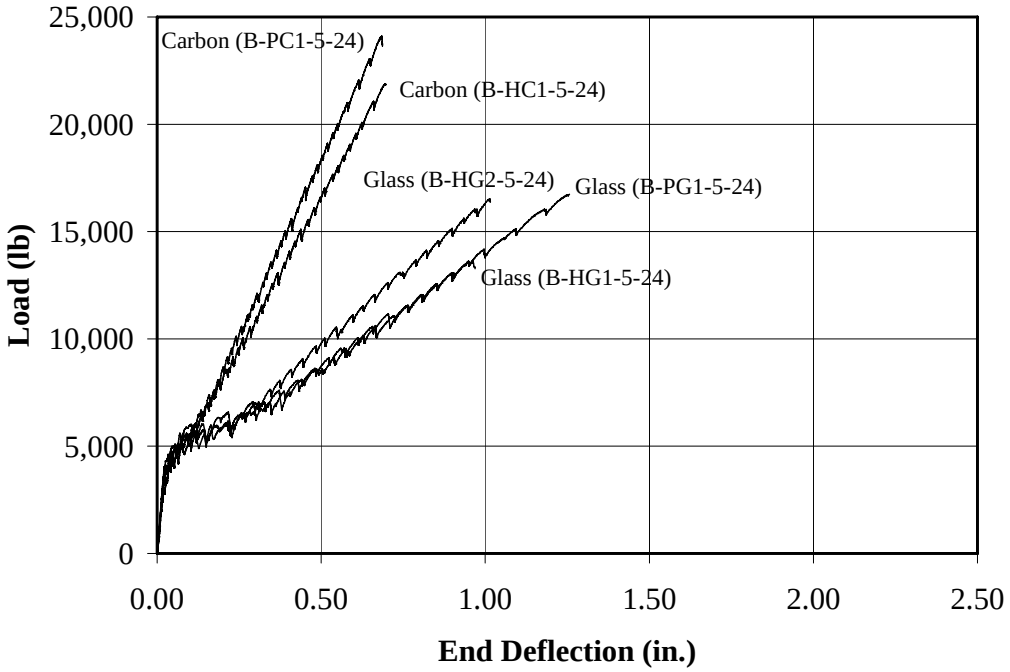

(a) Specimens Reinforced with #5 Top Cast Bars (24 in. Splice)

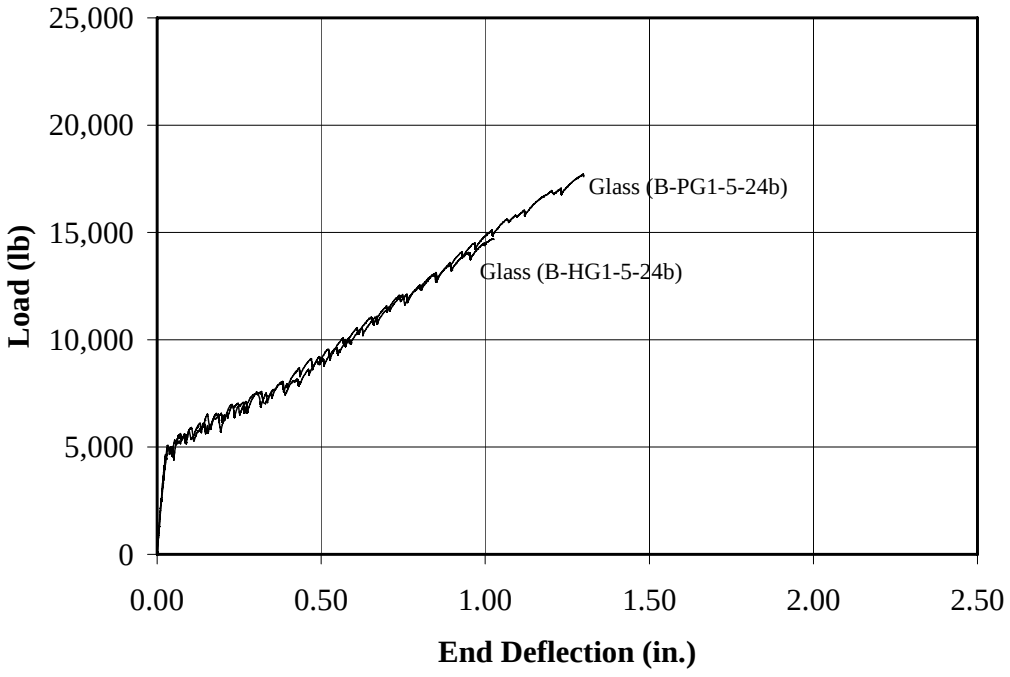

(b) Specimens Reinforced with #5 Bottom Cast Bars (24 in. Splice)

Figure E.4 Load-Deflection for Specimens in Series IV

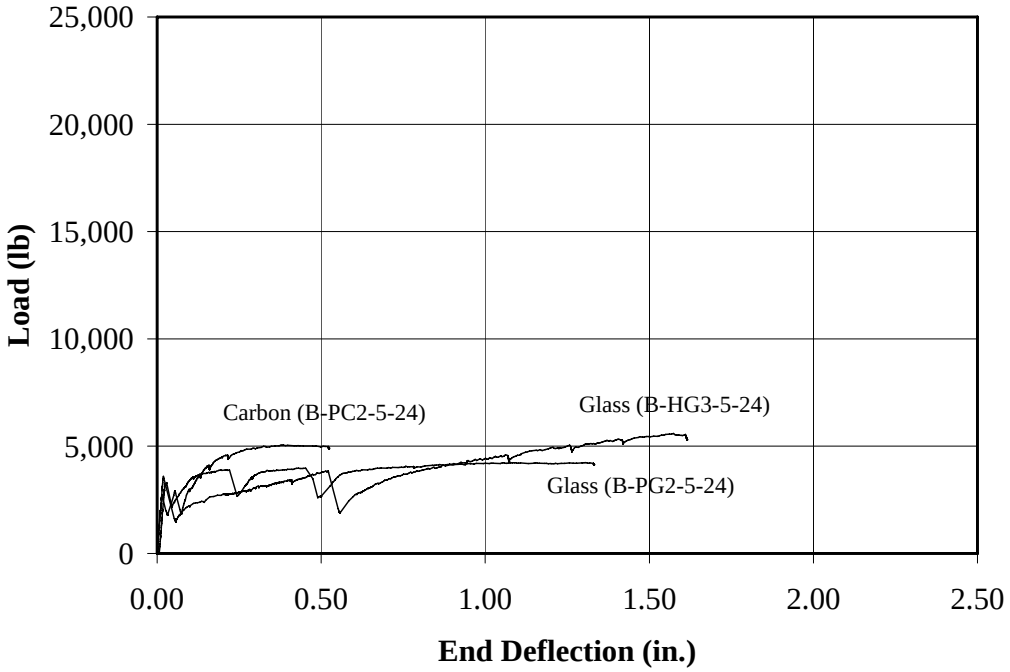

(c) Specimens Reinforced with #5 Top Cast Smooth Bars (24 in. Splice)

Figure E.4 Load-Deflection for Specimens in Series IV (continued)

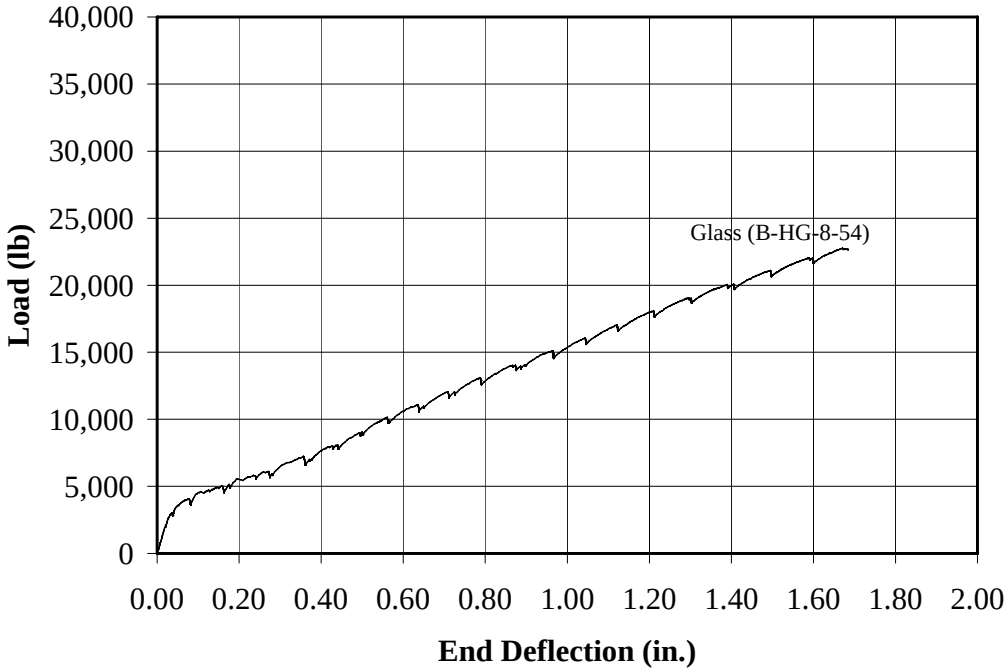

(a) Specimens Reinforced with #8 Top Cast Bars (54 in.)

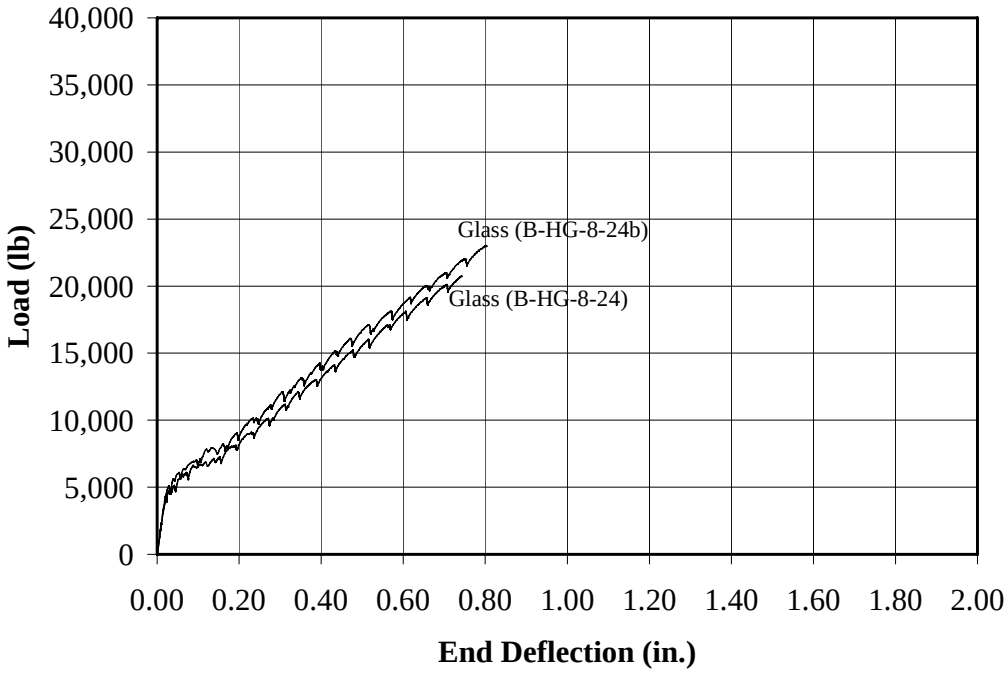

(b) Specimens Reinforced with #8 Bars (24 in. Splice)

Figure E.5 Load-Deflection for Specimens in Series V

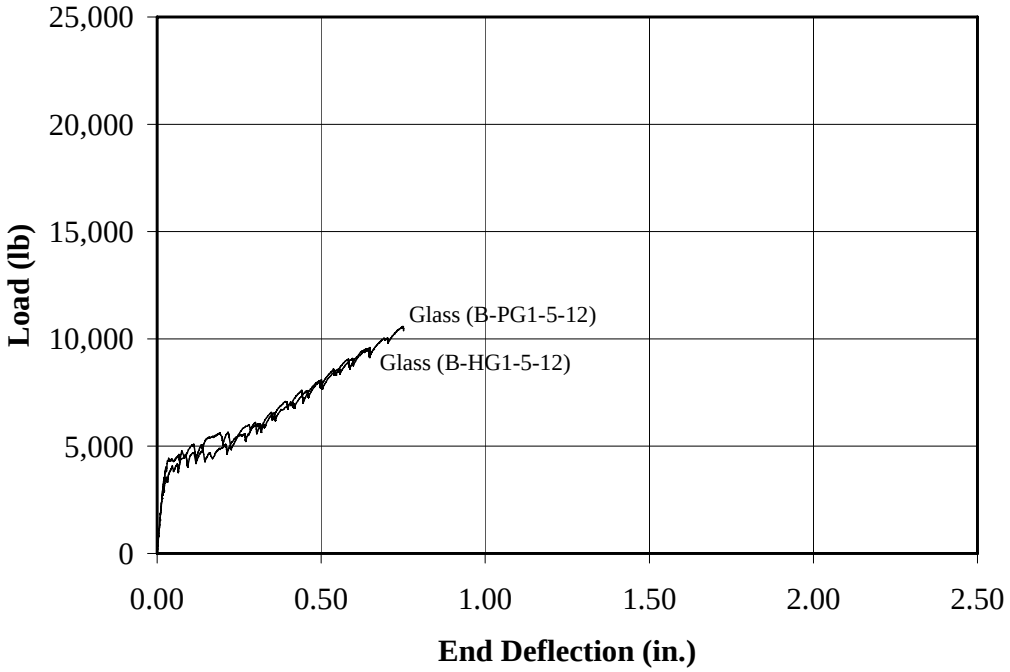

(c) Specimens Reinforced with #5 Top Cast Bars (12 in. Splice)

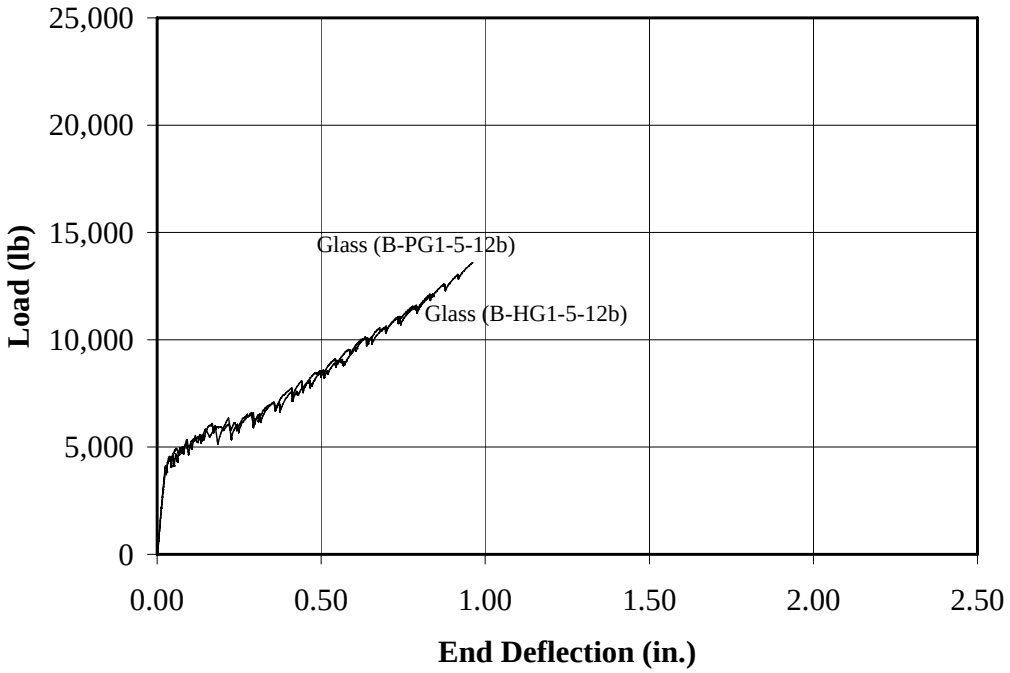

(d) Specimens Reinforced with #5 Bottom Cast Bars (12 in. Splice)

Figure E.5 Load-Deflection for Specimens in Series V (continued)

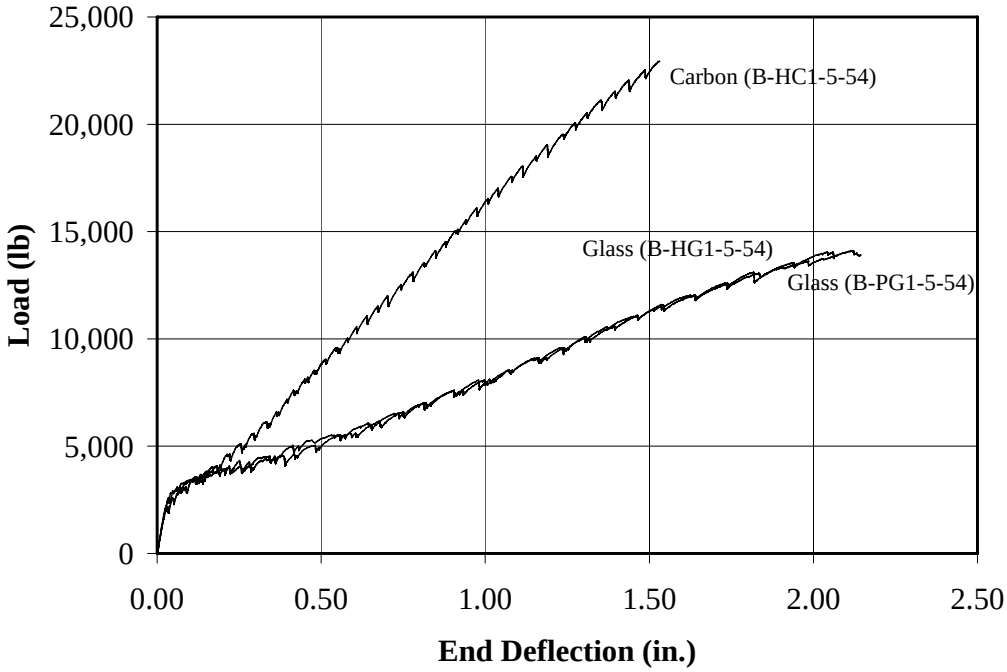

(e) Specimens Reinforced with #5 Top Cast Bars (54 in. Splice)

Figure E.5 Load-Deflection for Specimens in Series V (continued)

Appendix F

Specimen Dimensions after Testing

Table F.1 Specimen Dimensions after Testing

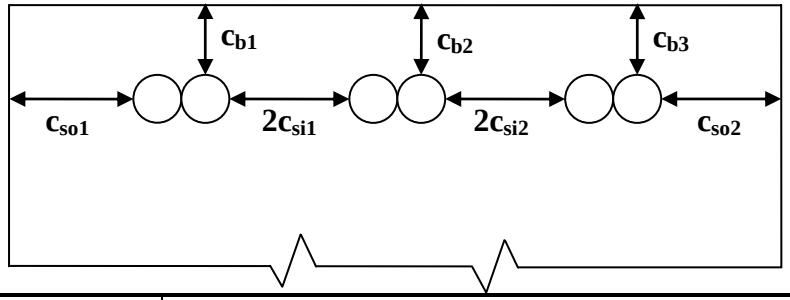

Series	Specimen	Cover and Spacing Dimensions (in.)							b_w (in.)
		c_{b1}	c_{b2}	c_{b3}	c_{so1}	$2c_{si1}$	$2c_{si2}$	c_{so2}	
I	B-S-8-18	1.43	1.52	1.55	1.46	0.73	1.14	1.34	11.03
	B-P-8-18	1.64	1.61	1.69	1.37	0.96	0.94	1.34	11.03
	B-H-8-18	1.76	1.54	1.53	1.32	0.94	1.14	1.39	10.97
	B-HN-5-18	1.52	1.48	1.38	1.57	0.98	0.93	1.30	8.72
	B-HO-5-18	1.59	1.77	1.73	1.55	0.89	0.91	1.65	8.75
	B-P-5-18	1.61	1.44	1.63	1.26	0.91	0.84	1.53	8.75
	B-S-5-18	1.47	1.43	1.62	1.78	0.77	0.78	1.51	8.74
	B-C-5-18	1.67	1.50	1.67	1.78	0.89	0.79	1.48	8.73
II	B-C-5-12	1.50	1.62	1.66	1.62	0.91	1.04	1.67	8.78
	B-S-8-36	1.66	1.69	1.70	1.50	1.04	1.02	1.34	11.06
	B-P-8-36	1.89	1.94	2.09	1.40	1.11	1.04	1.34	11.08
	B-H-8-36	1.69	1.54	1.72	1.25	1.18	0.77	1.62	11.11
	B-HN-5-36	1.57	1.85	1.70	1.51	0.91	1.19	1.23	8.75
	B-HO-5-36	1.67	1.55	1.58	1.38	1.04	0.97	1.66	8.76
	B-P-5-36	1.72	1.77	1.74	1.48	0.97	1.08	1.41	8.86
	B-C-5-36	1.55	1.57	1.60	1.73	1.17	0.93	1.48	8.77

Table F.1 Specimen Dimensions after Testing (continued)									
Series	**Specimen**	**Cover and Spacing Dimensions (in.)**							**b_w (in.)**
		c_{b1}	**c_{b2}**	**c_{b3}**	**c_{so1}**	**$2c_{si1}$**	**$2c_{si2}$**	**c_{so2}**	
III	B-S2-8-12	1.63	1.63	1.75	1.38	1.13	0.88	1.50	11.06
	B-S1-8-12	1.63	1.63	1.63	1.63	0.94	0.94	1.38	11.06
	B-S4-8-12	-	-	-	-	-	-	-	-
	B-S3-8-12	-	-	-	-	-	-	-	-
	B-PG-8-12	1.56	1.56	1.56	1.50	1.00	1.00	1.50	11.00
	B-HG-8-12	1.50	1.50	1.50	1.50	0.94	1.06	1.50	11.00
	B-S1-8-12b	1.44	1.56	1.53	1.50	0.88	1.00	1.63	11.00
	B-HG-8-12b	1.53	1.63	1.50	1.38	1.00	1.00	1.63	11.00
	B-PG-8-12b	1.56	1.63	1.50	1.63	1.00	1.06	1.44	11.00
	B-S-5-24	1.53	1.63	1.44	1.44	0.94	0.88	1.63	8.75
IV	B-HC1-5-24	1.56	1.63	1.69	1.44	1.00	1.00	1.63	8.75
	B-PC2-5-24	-	-	-	-	-	-	-	-
	B-PC1-5-24	1.53	1.56	1.50	1.50	0.94	0.94	1.56	8.84
	B-HG3-5-24	-	-	-	-	-	-	-	-
	B-HG1-5-24	1.63	1.63	1.69	1.50	0.94	0.94	1.56	8.75
	B-HG2-5-24	1.50	1.53	1.63	1.63	1.13	0.88	1.63	8.75
	B-PG2-5-24	-	-	-	-	-	-	-	-
	B-PG1-5-24	1.63	1.59	1.69	1.50	0.94	0.88	1.50	8.75
	B-HG1-5-24b	1.53	1.53	1.50	1.44	0.94	1.00	1.63	8.75
	B-PG1-5-24b	1.50	1.50	1.47	1.50	1.00	0.94	1.56	8.75

Table F.1 Specimen Dimensions after Testing (continued)									
Series	**Specimen**	**Cover and Spacing Dimensions (in.)**							**b_w (in.)**
		c_{b1}	**c_{b2}**	**c_{b3}**	**c_{so1}**	**$2c_{si1}$**	**$2c_{si2}$**	**c_{so2}**	
V	B-HG1-5-12	1.47	1.50	1.50	1.63	0.94	0.75	1.63	8.81
	B-PG1-5-12	1.63	1.50	1.50	1.38	1.25	0.94	1.38	8.75
	B-HG-8-24	1.63	1.63	1.66	1.50	0.88	1.00	1.63	11.00
	B-HG1-5-12b	1.50	1.50	1.47	1.56	1.06	1.06	1.56	8.75
	B-PG1-5-12b	1.47	1.47	1.47	1.44	0.94	1.06	1.63	8.75
	B-HG-8-24b	1.47	1.50	1.47	1.38	1.00	1.13	1.50	11.00
	B-HG-8-54	1.63	1.63	1.56	1.50	1.00	1.00	1.69	11.13
	B-HG1-5-54	1.56	1.59	1.53	1.38	0.56	1.38	1.50	8.81
	B-PG1-5-54	1.50	1.50	1.53	1.44	1.00	1.06	1.44	8.75
	B-HC1-5-54	1.63	1.63	1.63	1.69	0.94	0.94	1.69	8.81

Appendix G

Steel Database

Table G.1 Steel Database

Ref.	Specimen ID	Variables and Experimental Results											Calculated f_{test}/f_{calc}			
		L_s (in.)	d_b (in.)	b (in.)	c_{so} (in.)	c_{si} (in.)	c_b (in.)	N_b	AE (kips)	f'_c (psi)	f_y (ksi)	f_{test} (ksi)	ACI 318	ACI 408	Proposed	
													Eq. 4-4	Eq. 4-5	Eq. 5-10	Eq. 5-15
16	D3	11.0	0.75	9.0	1.50	0.50	1.50	2	12760	4350	57.0	36.9	1.96	1.10	0.94	0.97
16	D4	16.0	0.75	9.0	1.50	0.50	1.50	2	12760	4470	57.0	46.8	1.69	1.17	0.96	1.01
16	D5	11.0	0.75	5.5	2.00	-	1.50	1	12760	4180	57.0	44.3	1.12	1.12	1.29	1.39
16	D6	11.0	0.75	7.3	1.50	0.63	1.16	2	12760	4340	57.0	33.2	1.54	1.01	0.83	0.84
16	D7	11.0	0.75	3.6	1.06	-	1.27	1	12760	4450	57.0	33.9	1.09	0.98	0.97	1.04
16	D8	11.0	0.75	7.3	1.50	0.63	1.48	2	12760	4570	57.0	36.0	1.63	1.05	0.88	0.90
16	D9	11.0	0.75	3.6	1.06	-	1.44	1	12760	4380	57.0	35.0	1.13	1.00	1.01	1.08
16	D10	7.0	0.75	3.6	1.06	-	1.48	1	12760	4370	57.0	26.3	1.33	0.90	0.99	1.02
16	D12	16.0	0.75	3.8	1.13	-	1.62	1	12760	4530	57.0	45.7	0.95	1.03	1.05	1.16
16	D13	11.0	0.75	7.3	2.91	-	1.44	1	12760	4820	57.0	48.9	1.19	1.14	1.38	1.48
16	D14	11.0	0.75	3.7	1.10	-	0.83	1	12760	4820	57.0	32.6	1.20	0.99	0.92	0.98
16	D15	11.0	0.75	7.3	2.88	-	0.62	1	12760	4290	57.0	42.2	1.99	1.17	1.22	1.31
16	D17	16.0	0.75	3.7	1.10	-	0.80	1	12760	3580	57.0	39.7	1.19	1.09	0.97	1.07
16	D19	16.0	0.75	7.3	2.91	-	1.70	1	12760	4230	57.0	59.9	1.04	1.10	1.40	1.55
16	D20	7.0	0.75	3.8	1.13	-	1.42	1	12760	4230	57.0	26.9	1.33	0.93	1.02	1.05
16	D21	11.0	0.75	7.3	2.91	-	1.47	1	12760	4480	57.0	43.3	1.08	1.02	1.24	1.33
16	D22	7.0	0.75	3.7	1.10	-	0.80	1	12760	4480	57.0	23.9	1.46	0.87	0.89	0.92
16	D23	16.0	0.75	3.6	1.06	-	0.78	1	12760	4450	57.0	39.2	1.07	1.03	0.90	1.00
16	D24	16.0	0.75	7.3	2.88	-	0.81	1	12760	4450	57.0	43.2	1.15	0.93	0.99	1.10
16	D25	24.0	0.75	3.6	1.06	-	1.53	1	12760	5100	57.0	58.3	0.80	1.02	1.02	1.17
16	D26	24.0	0.75	3.7	1.10	-	0.75	1	12760	5100	57.0	55.9	0.98	1.14	0.98	1.13
16	D29	11.0	0.75	3.7	1.10	-	1.39	1	12760	7480	57.0	44.6	1.08	1.11	1.12	1.21
16	D30	16.0	0.75	3.7	1.10	-	1.56	1	12760	7480	57.0	52.9	0.88	1.06	1.07	1.19

Table G.1 Steel Database (continued)

Ref.	Specimen ID	Variables and Experimental Results											Calculated f_{test}/f_{calc}			
		L_s (in.)	d_b (in.)	b (in.)	c_{so} (in.)	c_{si} (in.)	c_b (in.)	N_b	AE (kips)	f'_c (psi)	f_y (ksi)	f_{test} (ksi)	ACI 318	ACI 408	Proposed	
													Eq. 4-4	Eq. 4-5	Eq. 5-10	Eq. 5-15
16	D31	5.5	0.38	3.7	1.47	-	0.83	1	3203	4700	79.0	60.4	1.44	1.36	1.44	1.30
16	D32	11.0	0.75	7.3	2.88	-	1.47	1	12760	4700	57.0	46.0	1.12	1.07	1.30	1.40
16	D33	20.3	1.41	6.8	1.99	-	1.55	1	45240	4830	57.0	28.2	1.33	0.86	0.94	1.18
16	D34	12.5	0.75	3.6	1.06	-	1.49	1	12760	3800	57.0	36.9	1.13	1.02	1.02	1.11
16	D35	24.0	0.75	3.6	1.06	-	1.45	1	12760	3800	57.0	55.0	0.87	1.04	1.04	1.19
16	D36	5.5	0.38	3.7	1.47	-	0.56	1	3203	4410	79.0	48.9	1.51	1.22	1.19	1.07
16	D38	11.0	0.75	4.6	1.56	-	1.52	1	12760	3160	57.0	28.2	0.82	0.78	0.88	0.94
16	D39	11.0	0.75	3.7	1.10	-	1.56	1	12760	3160	57.0	27.6	1.03	0.84	0.86	0.93
16	D40	16.0	0.75	7.4	2.94	-	0.75	1	12760	5280	57.0	50.6	1.30	1.07	1.12	1.24
15	3a	6.0	0.50	6.0	0.50	1.50	1.00	2	5800	4450	50.0	32.8	1.64	1.05	0.73	0.60
15	4a	6.0	0.50	6.0	2.50	-	1.00	1	5800	4370	50.0	42.6	1.29	1.06	1.26	1.20
29	8R18a	18.0	1.00	17.0	3.25	3.27	1.75	2	22910	3470	99.0	41.3	1.30	0.98	0.95	0.97
29	8R24a	24.0	1.00	17.1	3.25	3.31	1.67	2	22910	3530	99.0	58.9	1.43	1.19	1.16	1.21
29	8F30a	30.0	1.00	17.1	3.25	3.30	1.53	2	22910	3030	74.0	52.8	1.18	0.99	0.98	1.03
29	8F36a	36.0	1.00	17.2	3.25	3.33	1.41	2	22910	4650	63.5	66.3	1.06	1.01	1.02	1.09
29	8F36b	36.0	1.00	16.9	3.25	3.22	1.40	2	22910	3770	74.0	61.3	1.09	0.99	0.99	1.06
29	8F39a***	39.0	1.00	17.1	3.25	3.28	1.53	2	22910	3650	63.5	72.9	1.14	1.09	1.10	1.19
29	8F42a***	42.0	1.00	17.2	3.25	3.35	1.50	2	22910	2660	63.5	65.9	1.14	1.02	1.04	1.13
29	8F42b***	42.0	1.00	17.2	3.25	3.33	1.45	2	22910	3830	63.5	73.5	1.09	1.05	1.07	1.16
29	8R42a	42.0	1.00	17.2	3.25	3.35	1.56	2	22910	3310	99.0	71.0	1.07	1.02	1.05	1.14
29	8R48a	48.0	1.00	17.0	3.25	3.27	1.48	2	22910	3040	99.0	72.9	1.04	0.99	1.03	1.14
29	8R64a	64.0	1.00	17.1	3.25	3.30	1.52	2	22910	3550	99.0	89.7	0.87	0.93	1.03	1.16
29	8R80a	80.0	1.00	17.0	3.25	3.27	1.50	2	22910	3740	99.0	96.4	0.74	0.82	0.96	1.10

Table G.1 Steel Database (continued)

Ref.	Specimen ID	Variables and Experimental Results											Calculated f_{test}/f_{calc}			
		L_s (in.)	d_b (in.)	b (in.)	c_{so} (in.)	c_{si} (in.)	c_b (in.)	N_b	AE (kips)	f'_c (psi)	f_y (ksi)	f_{test} (ksi)	ACI 318	ACI 408	Proposed	
													Eq. 4-4	Eq. 4-5	Eq. 5-10	Eq. 5-15
29	8F36k	36.0	1.00	9.7	1.42	1.43	1.38	2	22910	3460	74.0	54.7	1.03	1.02	0.91	0.97
29	11R24a	33.0	1.41	24.1	4.59	4.64	1.67	2	45240	3720	93.0	51.8	1.62	1.14	1.23	1.38
29	11R30a	41.3	1.41	24.1	4.59	4.64	1.31	2	45240	4030	93.0	58.5	1.65	1.15	1.26	1.44
29	11F36a	49.5	1.41	24.1	4.59	4.64	1.50	2	45240	4570	73.0	64.2	1.30	1.07	1.17	1.36
29	11F36b	49.5	1.41	24.0	4.59	4.61	1.47	2	45240	3350	65.0	59.2	1.42	1.07	1.17	1.36
29	11F42a	57.8	1.41	24.0	4.59	4.59	1.48	2	45240	3530	65.0	63.6	1.27	1.03	1.13	1.33
29	11F48a	66.0	1.41	24.2	4.59	4.62	1.53	2	45240	3140	73.0	74.6	1.34	1.12	1.25	1.49
29	11F48b	66.0	1.41	24.2	4.59	4.67	1.58	2	45240	3330	65.0	72.2	1.24	1.06	1.19	1.42
29	11R48a	66.0	1.41	24.2	4.59	4.67	1.50	2	45240	5620	93.0	82.2	1.12	1.08	1.20	1.43
29	11R48b	66.0	1.41	24.2	4.59	4.70	2.06	2	45240	3100	93.0	71.4	1.05	0.99	1.11	1.33
29	11F60a	82.5	1.41	24.0	4.59	4.58	1.59	2	45240	2610	73.0	80.3	1.24	1.07	1.23	1.49
29	11F60b	82.5	1.41	24.0	4.59	4.59	1.50	2	45240	4090	65.0	78.0	1.00	0.94	1.08	1.31
29	11R60a	82.5	1.41	24.0	4.59	4.59	1.41	2	45240	2690	93.0	74.6	1.23	1.01	1.17	1.41
29	11R60b	82.5	1.41	24.0	4.59	4.58	1.75	2	45240	3460	93.0	87.8	1.10	1.06	1.22	1.49
30	18S15	98.0	2.26	27.0	4.50	4.49	2.63	2	11602	2860	61.0	53.2	1.03	0.93	1.05	1.41
30	18S12	60.0	2.26	27.3	4.50	4.61	3.00	2	11602	3160	61.0	46.5	1.27	1.05	1.16	1.49
30	SP40	15.0	0.63	7.5	1.25	1.25	0.83	2	8897	3220	73.0	43.0	1.04	1.03	0.83	0.76
30	14S1	45.0	1.69	20.5	3.38	3.48	2.38	2	65283	2710	61.0	47.1	1.34	1.09	1.12	1.33
57	6-12-4/2/2-6/6	12.0	0.75	33.0	2.00	2.00	2.00	6	12760	3731	61.7	57.4	1.41	1.28	1.10	1.03
57	8-18-4/3/2-6/6	18.0	1.00	36.0	2.00	2.00	3.00	6	22910	4710	59.3	56.3	1.37	1.21	1.10	1.17
57	8-18-4/3/2.5-4/6	18.0	1.00	36.0	2.50	2.00	3.00	6	22910	2920	59.3	49.3	1.52	1.15	1.09	1.15
57	8-24-4/2/2-6/6	24.0	1.00	36.0	2.00	2.00	2.00	6	22910	3105	59.3	50.6	1.14	1.06	0.97	1.01
57	11-25-6/2/3-5/5	25.0	1.41	44.1	3.00	3.00	2.00	5	45240	3920	66.3	44.2	1.56	1.16	1.16	1.27

Table G.1 Steel Database (continued)

Ref.	Specimen ID	Variables and Experimental Results											Calculated f_{test}/f_{calc}			
		L_s (in.)	d_b (in.)	b (in.)	c_{so} (in.)	c_{si} (in.)	c_b (in.)	N_b	AE (kips)	f'_c (psi)	f_y (ksi)	f_{test} (ksi)	ACI 318	ACI 408	Proposed	
													Eq. 4-4	Eq. 4-5	Eq. 5-10	Eq. 5-15
57	11-30-4/2/2-6/6	30.0	1.41	40.9	2.00	2.00	2.00	6	45240	2865	60.5	38.0	1.30	1.03	0.97	1.08
57	11-30-4/2/4-6/6	30.0	1.41	44.9	4.00	2.00	2.00	6	45240	3350	63.4	44.4	1.41	1.14	1.09	1.21
57	11-30-4/2/2.7/4/6	30.0	1.41	40.9	2.70	2.00	2.00	6	45240	4420	63.3	57.6	1.59	1.38	1.31	1.47
57	11-45-4/1/2-6/6	45.0	1.41	40.9	2.00	2.00	1.00	6	45240	3520	60.5	45.3	1.48	1.09	1.01	1.16
57	14-60-4/2/2-5/5	60.0	1.69	37.5	2.00	2.00	2.00	5	65250	2865	57.7	45.2	1.06	0.97	0.94	1.14
57	14-60-4/2/4-5/5	60.0	1.69	41.5	4.00	2.00	2.00	5	65250	3200	57.7	56.6	1.26	1.17	1.14	1.39
61	0-11-4b	36.0	1.41	20.5	2.00	2.01	2.00	3	45282	4290	62.8	45.1	1.05	0.99	0.93	1.06
61	0-11-12b	18.0	1.41	20.5	2.00	2.01	2.00	3	45282	9600	62.8	42.7	1.34	1.10	1.08	1.16
18	U16	16.0	0.75	24.0	3.25	3.25	2.00	3	12760	5620	65.2	65.2	0.98	1.02	0.96	0.92
18	U14	14.0	0.75	24.0	3.25	3.25	2.00	3	12760	5380	65.2	65.2	1.14	1.13	1.05	0.99
18	U12	12.0	0.75	24.0	3.25	3.25	2.00	3	12760	3990	65.2	46.6	1.11	0.96	0.88	0.82
18	U10	10.0	0.75	24.0	3.25	3.25	2.00	3	12760	8200	65.2	59.5	1.18	1.14	1.05	0.96
17	1-5N0-12-0-U	12.0	0.63	10.5	2.00	2.00	1.00	2	8990	5360	63.8	61.5	1.25	1.30	1.13	1.02
17	1-5N0-12-0-U	12.0	0.63	15.8	2.00	2.00	1.00	3	8990	5360	63.8	64.0	1.30	1.35	1.17	1.06
17	2-6S0-12-0-U	12.0	0.75	11.0	2.00	2.00	1.00	2	12760	6010	71.0	45.8	1.21	1.11	0.99	0.92
17	2-6C0-12-0-U	12.0	0.75	11.0	2.00	2.00	1.00	2	12760	6010	69.0	51.4	1.36	1.25	1.12	1.04
17	3-8S0-16-0-U	16.0	1.00	12.0	2.00	2.00	1.50	2	22910	5980	71.0	42.8	1.30	1.06	0.97	0.97
17	3-8N0-16-0-U	16.0	1.00	12.0	2.00	2.00	1.50	2	22910	5980	63.8	43.0	1.30	1.07	0.98	0.98
17	4-11S0-24-0-U	24.0	1.41	13.7	2.00	2.00	2.00	2	45240	5850	71.0	40.2	1.21	1.03	0.98	1.07
17	4-11C0-24-0-U	24.0	1.41	13.7	2.00	2.00	2.00	2	45240	5850	69.0	37.8	1.14	0.96	0.92	1.01
38	1-8N3-16-0-U	16.0	1.00	16.0	2.00	1.50	2.00	3	22910	5990	63.8	50.0	1.52	1.19	1.06	1.13
38	2-8C3-16-0-U	16.0	1.00	16.0	2.00	1.50	1.84	3	22910	6200	69.0	46.2	1.38	1.10	0.97	1.04
38	3-8S3-16-0-U	16.0	1.00	16.1	2.00	1.50	2.04	3	22910	6020	71.1	46.8	1.41	1.11	0.99	1.06

Table G.1 Steel Database (continued)

Ref.	Specimen ID	Variables and Experimental Results											Calculated f_{test}/f_{calc}			
		L_s (in.)	d_b (in.)	b (in.)	c_{so} (in.)	c_{si} (in.)	c_b (in.)	N_b	AE (kips)	f'_c (psi)	f_y (ksi)	f_{test} (ksi)	ACI 318	ACI 408	Proposed	
													Eq. 4-4	Eq. 4-5	Eq. 5-10	Eq. 5-15
38	4-8S3-16-0-U	16.0	1.00	16.1	2.00	1.50	2.10	3	22910	6450	71.0	42.4	1.24	0.98	0.88	0.94
38	5-8C3-16-0-U	16.0	1.00	16.1	2.00	1.50	2.05	3	22910	5490	69.0	39.8	1.26	0.96	0.86	0.92
38	6-8C3-22 3/4-0-U	22.8	1.00	16.1	2.00	1.50	2.15	3	22910	5850	69.0	51.8	1.12	1.00	0.90	0.99
38	7-8C3-16-0-U	16.0	1.00	16.0	2.00	4.00	2.12	2	22910	5240	69.0	45.4	1.18	1.06	0.95	0.95
54	2a	29.5	0.99	13.6	1.83	0.99	2.01	3	22475	3958	64.5	58.6	1.56	1.19	1.03	1.19
54	5a	35.4	1.18	15.4	1.82	1.18	2.01	3	31465	4031	68.9	56.1	1.46	1.16	1.01	1.22
54	2b	29.5	0.99	13.6	1.83	0.99	2.01	3	22475	3799	64.5	58.6	1.60	1.20	1.04	1.20
54	5b	44.3	1.18	15.4	1.82	1.18	2.01	3	31465	3726	68.9	65.8	1.43	1.20	1.07	1.31
39	S28-N-M	11.8	1.13	9.1	1.13	1.14	1.13	2	29087	12180	69.3	44.2	1.92	1.28	1.23	1.22
39	P28-N-M	11.8	1.13	9.1	1.13	1.14	1.13	2	29087	10237	69.3	43.2	2.04	1.30	1.25	1.24
39	S33-N-U	11.8	1.13	9.1	1.13	1.14	1.13	2	29087	10310	69.3	40.2	1.89	1.21	1.16	1.15
39	P33-N-M	11.8	1.13	9.1	1.13	1.14	1.13	2	29087	9237	69.3	44.5	2.22	1.38	1.33	1.31
21	1.1	16.0	1.00	16.1	2.97	2.94	2.94	2	22910	5020	60.0	51.6	1.37	1.01	0.95	0.96
21	1.3	16.0	1.00	16.1	2.03	1.44	1.94	3	22910	5020	60.0	45.0	1.54	1.13	1.01	1.08
21	2.4	24.0	1.00	12.1	2.00	1.91	1.31	2	22910	5250	75.0	54.1	1.29	1.15	1.04	1.07
21	2.5	24.0	1.00	12.1	2.06	1.86	1.81	2	22910	5250	75.0	58.7	1.09	1.12	1.02	1.06
21	4.5	24.0	1.00	12.1	2.06	1.94	1.84	2	22910	4090	60.0	51.1	1.06	1.03	0.94	0.98
21	6.5	24.0	1.00	12.1	2.00	1.91	1.97	2	22910	4220	75.0	53.6	1.07	1.05	0.96	1.01
21	8.3	24.0	1.00	12.1	2.00	1.95	2.00	2	22910	3830	79.0	61.5	1.27	1.22	1.12	1.17
21	10.2	26.0	1.00	12.1	2.06	1.88	1.93	2	22910	4250	81.0	61.2	1.14	1.14	1.05	1.11
21	13.4	16.0	0.63	12.2	2.09	1.02	1.35	3	8990	4110	64.0	60.0	1.03	1.11	0.93	0.91
21	14.3	17.0	0.63	12.1	2.03	1.03	1.30	3	8990	4200	64.0	62.8	0.99	1.11	0.93	0.92
21	15.5	40.0	1.41	18.1	3.06	2.98	1.91	2	45240	5250	81.0	54.1	1.07	1.02	1.01	1.16

Table G.1 Steel Database (continued)

Ref.	Specimen ID	Variables and Experimental Results											Calculated f_{test}/f_{calc}			
		L_s (in.)	d_b (in.)	b (in.)	c_{so} (in.)	c_{si} (in.)	c_b (in.)	N_b	AE (kips)	f'_c (psi)	f_y (ksi)	f_{test} (ksi)	ACI 318	ACI 408	Proposed	
													Eq. 4-4	Eq. 4-5	Eq. 5-10	Eq. 5-15
21	16.2	40.0	1.41	18.1	3.02	2.97	1.90	2	45240	5180	81.0	52.4	1.04	0.99	0.99	1.13
37	S1-14-300-0	11.8	0.55	23.6	0.79	4.69	0.79	3	6931	3350	68.0	54.9	1.38	1.42	1.06	0.93
37	S7-16-300-0	11.8	0.63	23.6	0.79	4.57	0.79	3	9048	3161	69.0	46.8	1.52	1.39	1.06	0.96
37	S13-20-350-0	13.8	0.79	23.6	0.79	4.33	0.79	3	14123	2900	68.7	51.4	2.72	1.73	1.38	1.31
35	PC-00-B-SP2	12.0	0.98	10.1	1.50	1.57	1.50	2	22065	9514	61.8	53.6	1.67	1.38	1.26	1.22
35	SC-05-B-SP2	12.0	0.98	10.1	1.50	1.57	1.50	2	22065	11124	61.8	56.7	1.64	1.41	1.28	1.24
35	SC-10-B-SP2	12.0	0.98	10.1	1.50	1.57	1.50	2	22065	11124	61.8	51.6	1.49	1.28	1.16	1.13
35	SC-15-B-SP2	12.0	0.98	10.1	1.50	1.57	1.50	2	22065	9730	61.8	54.9	1.69	1.41	1.28	1.25
35	SC-20-B-SP2	12.0	0.98	10.1	1.50	1.57	1.50	2	22065	10660	61.8	56.2	1.66	1.41	1.28	1.25
35	PC-00-B-SP4	12.0	0.98	10.1	1.50	1.57	1.50	2	22065	7585	61.8	46.0	1.61	1.26	1.14	1.11
35	SC-10-B-SP4	12.0	0.98	10.1	1.50	1.57	1.50	2	22065	10254	61.8	49.1	1.48	1.24	1.13	1.10
35	SC-20-B-SP4	12.0	0.98	10.1	1.50	1.57	1.50	2	22065	11081	61.8	38.7	1.12	0.96	0.87	0.85
36	C0S0	12.0	0.98	8.2	1.02	1.10	1.02	2	22069	6772	69.9	41.7	2.02	1.31	1.18	1.14
36	C0S8	12.0	0.98	8.2	1.02	1.10	1.02	2	22069	13459	69.9	52.2	1.79	1.38	1.24	1.20
36	C0S16	12.0	0.98	8.2	1.02	1.10	1.02	2	22069	12415	69.9	40.2	1.44	1.08	0.97	0.94
9	1	41.0	1.00	9.0	1.00	1.50	1.00	2	22910	15120	77.9	69.9	0.69	0.97	0.80	0.87
9	2	36.0	1.00	12.0	1.00	1.00	1.00	3	22910	14450	72.2	70.5	0.81	1.07	0.89	0.95
9	3	32.0	1.00	9.0	1.00	1.50	1.00	2	22910	15591	72.2	69.1	0.86	1.11	0.91	0.96
9	4	32.0	1.00	9.0	1.00	1.50	1.00	2	22910	15591	72.2	67.3	0.84	1.08	0.89	0.94
9	5	30.0	1.00	12.0	1.00	1.00	1.00	3	22910	15034	72.2	67.1	0.91	1.13	0.93	0.98
9	6	25.0	1.00	9.0	1.00	1.50	1.00	2	22910	15324	72.2	62.7	1.01	1.17	0.96	0.99
9	7	23.0	1.00	9.0	1.00	1.50	1.00	2	22910	5290	77.9	44.5	1.33	1.13	0.93	0.96
9	8	20.0	1.00	9.0	1.00	1.50	1.00	2	22910	15324	72.2	52.6	1.06	1.10	0.92	0.93

Table G.1 Steel Database (continued)

Ref.	Specimen ID	Variables and Experimental Results											Calculated f_{test}/f_{calc}			
		L_s (in.)	d_b (in.)	b (in.)	c_{so} (in.)	c_{si} (in.)	c_b (in.)	N_b	AE (kips)	f'_c (psi)	f_y (ksi)	f_{test} (ksi)	ACI 318	ACI 408	Proposed	
													Eq. 4-4	Eq. 4-5	Eq. 5-10	Eq. 5-15
9	16	36.0	1.00	12.0	2.00	2.00	2.00	2	22910	14450	72.2	73.2	0.51	0.79	0.75	0.81
9	17	20.0	1.00	12.0	2.00	2.00	2.00	2	22910	15034	72.2	71.1	0.87	1.13	1.02	1.05
9	18	19.0	1.00	12.0	2.00	2.00	2.00	2	22910	15591	72.2	67.0	0.85	1.08	0.98	1.00
9	19	19.0	1.00	12.0	2.00	2.00	2.00	2	22910	15591	72.2	67.3	0.85	1.09	0.99	1.01
9	20	15.0	1.00	12.0	2.00	2.00	2.00	2	22910	15324	72.2	65.0	1.05	1.21	1.10	1.10
9	21	10.0	1.00	12.0	2.00	2.00	2.00	2	22910	15324	72.2	41.3	1.00	0.94	0.89	0.85
9	29	80.0	1.41	12.0	1.41	1.77	1.41	2	45240	15120	73.7	70.9	0.51	0.78	0.73	0.89
9	30	57.5	1.41	12.0	1.41	1.77	1.41	2	45240	13870	73.7	67.6	0.70	0.96	0.87	1.02
9	31	45.0	1.41	18.0	1.41	1.68	1.41	3	45240	15750	71.5	72.3	0.90	1.16	1.03	1.19
9	32	45.0	1.41	12.0	1.41	1.77	1.41	2	45240	15513	71.5	68.4	0.86	1.10	0.98	1.13
9	33	45.0	1.41	12.0	1.41	1.77	1.41	2	45240	15513	70.8	69.5	0.87	1.12	1.00	1.15
9	34	45.0	1.41	18.0	1.41	1.68	1.41	3	45240	10900	70.8	48.8	0.73	0.86	0.77	0.88
9	36	40.0	1.41	12.0	1.41	1.77	1.41	2	45240	13000	70.8	58.6	0.91	1.06	0.94	1.08
9	37	40.0	1.41	18.0	1.41	1.68	1.41	3	45240	13600	70.8	45.7	0.69	0.82	0.73	0.83
9	39	40.0	1.41	12.0	1.41	1.77	1.41	2	45240	5080	70.8	42.9	1.06	0.98	0.87	1.00
9	40	36.0	1.41	18.0	1.41	1.68	1.41	3	45240	14550	70.8	57.2	0.93	1.07	0.95	1.08
9	42	36.0	1.41	18.0	1.41	1.68	1.41	3	45240	14550	70.8	57.5	0.93	1.07	0.96	1.08
9	43	36.0	1.41	18.0	1.41	1.68	1.41	3	45240	6170	70.8	46.6	1.16	1.08	0.96	1.09
9	45	24.0	1.41	12.0	1.41	1.77	1.41	2	45240	12730	70.8	44.6	1.16	1.05	0.97	1.06
9	46	24.0	1.41	12.0	1.41	1.77	1.41	2	45240	5080	70.8	29.7	1.22	0.88	0.81	0.89
9	48	13.0	1.41	12.0	1.41	1.77	1.41	2	45240	14330	73.7	28.0	1.27	0.81	0.85	0.88
9	58	42.0	1.41	18.0	2.82	3.36	2.82	2	45240	15034	71.5	76.2	0.63	0.93	0.94	1.09
9	59	36.0	1.41	18.0	2.82	3.36	2.82	2	45240	14450	71.5	70.7	0.69	0.97	0.97	1.10

Table G.1 Steel Database (continued)

Ref.	Specimen ID	Variables and Experimental Results											Calculated f_{test}/f_{calc}			
		L_s (in.)	d_b (in.)	b (in.)	c_{so} (in.)	c_{si} (in.)	c_b (in.)	N_b	AE (kips)	f'_c (psi)	f_y (ksi)	f_{test} (ksi)	ACI 318	ACI 408	Proposed	
													Eq. 4-4	Eq. 4-5	Eq. 5-10	Eq. 5-15
9	60	28.0	1.41	18.0	2.82	3.36	2.82	2	45240	15034	71.5	69.9	0.86	1.11	1.10	1.22
64	19.1-B-S-U	36.0	1.00	18.1	1.95	1.93	1.96	3	22910	4250	80.6	72.4	0.95	1.07	1.02	1.10
64	19.2-B-N-U^^	36.0	1.00	18.1	2.02	1.88	1.93	3	22910	4250	80.6	67.0	0.90	0.99	0.95	1.03
64	20.6-B-S-U	40.0	1.00	12.1	1.52	0.67	1.30	3	22910	5080	80.6	56.5	1.27	1.04	0.83	1.00
64	23a.5-B-S-U	22.0	1.00	18.2	2.00	1.89	1.94	2	22910	9320	80.6	62.7	0.93	1.07	0.97	1.01
64	23a.6-B-S-U	29.0	1.00	12.2	2.03	1.88	1.92	2	22910	9320	80.6	75.9	0.86	1.08	1.00	1.07
64	23b.3-B-S-U	19.5	1.00	18.2	3.03	3.86	3.06	2	22910	8370	80.6	71.8	1.21	1.07	1.02	1.05
64	24.1-B-S-U	32.0	1.00	12.1	2.00	1.88	1.90	2	22910	4300	79.1	61.3	0.92	0.99	0.93	1.00
64	25.1-B-S-U	16.5	0.63	12.2	1.98	1.02	1.56	3	8700	4490	63.0	63.2	1.00	1.10	0.93	0.91
64	26.3-B-S-U	40.0	1.00	12.1	1.55	0.65	1.89	3	22910	4956	79.1	61.6	1.42	1.08	0.92	1.11
64	26.5-B-S-U	40.0	1.00	12.2	1.50	0.68	1.89	3	22910	4956	78.0	63.4	1.43	1.10	0.94	1.13
64	28.5-B-S-U	30.0	1.41	18.1	1.98	4.03	2.00	2	45240	12610	77.8	51.2	0.85	0.96	0.90	1.01
64	30.5-B-S-U	30.0	1.41	18.1	2.06	4.02	1.96	2	45240	13220	77.8	67.3	1.09	1.25	1.18	1.31
64	31.5-B-S-U	22.0	1.00	12.3	1.83	0.51	1.49	3	22910	12890	79.1	61.8	1.84	1.28	1.05	1.22
64	31.6-B-S-U	22.0	1.00	12.2	1.72	0.54	1.49	3	22910	12890	69.5	63.7	1.84	1.31	1.08	1.25
64	32.1-B-S-U	32.0	1.41	12.2	2.00	0.98	1.90	2	45240	14400	77.8	63.6	1.46	1.26	1.09	1.36
64	32.2-B-S-U	32.0	1.41	12.1	2.00	1.06	1.92	2	45240	14400	66.7	61.8	1.36	1.21	1.05	1.30
64	32.3-B-S-U	32.0	1.41	18.1	1.97	4.02	1.95	2	45240	14400	77.8	61.0	0.89	1.07	1.01	1.13
64	32.4-B-S-U	28.0	1.41	18.2	2.03	4.05	1.94	2	45240	14400	66.7	61.4	1.03	1.16	1.10	1.22
64	34.1-B-S-U	24.0	1.00	18.1	2.06	1.94	1.94	3	22910	5440	79.1	57.6	1.00	1.06	0.97	1.01
64	34.2-B-N-U^^	24.0	1.00	18.2	2.07	1.95	1.92	3	22910	5440	79.1	61.7	1.08	1.14	1.04	1.08
64	34.3-B-S-U	24.0	1.00	18.1	2.08	1.84	1.98	3	22910	5440	69.5	58.7	1.06	1.07	0.98	1.04
64	34.4-B-N-U^^	24.0	1.00	18.2	2.05	1.88	1.94	3	22910	5440	69.5	58.2	1.04	1.07	0.98	1.03

Table G.1 Steel Database (continued)

Ref.	Specimen ID	Variables and Experimental Results											Calculated f_{test}/f_{calc}			
		L_s (in.)	d_b (in.)	b (in.)	c_{so} (in.)	c_{si} (in.)	c_b (in.)	N_b	AE (kips)	f'_c (psi)	f_y (ksi)	f_{test} (ksi)	ACI 318	ACI 408	Proposed	
													Eq. 4-4	Eq. 4-5	Eq. 5-10	Eq. 5-15
64	36.3-B-S-U	26.0	1.00	18.2	2.02	1.84	2.00	3	22910	5060	69.5	62.3	1.08	1.09	1.01	1.09
64	36.4-B-N-U^^	26.0	1.00	18.1	2.03	1.83	1.99	3	22910	5060	69.5	59.8	1.04	1.05	0.97	1.04
64	38.1-B-N-U^^	26.0	1.00	18.2	1.94	1.95	1.80	3	22910	5080	69.5	53.9	0.95	0.99	0.90	0.95
64	38.2-B-S-U	26.0	1.00	18.2	2.13	1.84	2.08	3	22910	5080	69.5	60.1	1.04	1.03	0.96	1.05
64	39.6-B-S-U	21.0	1.00	12.2	1.95	0.52	1.50	3	22910	14450	67.7	63.5	1.86	1.30	1.08	1.24
64	40.5-B-S-U	17.0	1.00	12.1	2.00	1.88	1.85	2	22910	15650	78.0	66.3	1.00	1.18	1.07	1.08

Appendix H

FRP Database

Table H.1 FRP Database

Specimen ID	Variables and Experimental Results												Calculated f_{test}/f_{calc}			
	Bar Type	L_s (in.)	d_b (in.)	Cast Pos.	c_{so} (in.)	c_{si} (in.)	c_b (in.)	N_b	E (ksi)	EA (psi)	f'_c (psi)	f_{test} (ksi)	ACI 440-03	ACI 440-XX	Proposed	
													Eq. 4-7	Eq. 4-9	Eq. 5-11	Eq. 5-15
B-P-8-18	Glass	18	1.00	Top	1.5	0.5	1.5	3	6200	4898	5258	27.9	0.93	0.96	1.27	1.65
B-H-8-18	Glass	18	1.00	Top	1.5	0.5	1.5	3	5700	4503	5258	23.7	0.79	0.81	1.12	1.46
B-HN-5-18	Glass	18	0.63	Top	1.5	0.5	1.5	3	6400	1984	5258	40.7	0.68	1.09	1.00	1.38
B-HO-5-18	Glass	18	0.63	Top	1.5	0.5	1.5	3	5800	1798	5258	32.9	0.55	0.88	0.84	1.17
B-P-5-18	Glass	18	0.63	Top	1.5	0.5	1.5	3	6401	1984	5258	47.3	0.79	1.27	1.16	1.61
B-C-5-18	Carbon	18	0.63	Top	1.5	0.5	1.5	3	18500	5735	5258	58.8	0.98	1.58	0.94	1.18
B-C-5-12	Carbon	12	0.63	Top	1.5	0.5	1.5	3	18500	5735	5470	44.5	1.12	1.44	0.83	1.08
B-P-8-36	Glass	36	1.00	Top	1.5	0.5	1.5	3	6200	4898	5470	28.9	0.48	0.68	0.99	1.20
B-H-8-36	Glass	36	1.00	Top	1.5	0.5	1.5	3	5700	4503	5470	30.4	0.51	0.71	1.07	1.31
B-HN-5-36	Glass	36	0.63	Top	1.5	0.5	1.5	3	6400	1984	5470	44.3	0.37	0.75	0.81	1.05
B-HO-5-36	Glass	36	0.63	Top	1.5	0.5	1.5	3	5800	1798	5470	47.5	0.40	0.80	0.90	1.19
B-P-5-36	Glass	36	0.63	Top	1.5	0.5	1.5	3	6401	1984	5470	49.9	0.42	0.84	0.91	1.19
B-C-5-36	Carbon	36	0.63	Top	1.5	0.5	1.5	3	18500	5735	5470	84.6	0.71	1.43	1.01	1.18
B-PG-8-12	Glass	12	1.00	Top	1.5	0.5	1.5	3	6200	4898	4014	20.0	1.00	0.92	1.15	1.54
B-HG-8-12	Glass	12	1.00	Top	1.5	0.5	1.5	3	5700	4503	4014	16.3	0.82	0.75	0.97	1.31
B-HG-8-12b	Glass	12	1.00	Bott	1.5	0.5	1.5	3	5700	4503	4014	16.9	0.65	0.52	1.00	1.36
B-PG-8-12b	Glass	12	1.00	Bott	1.5	0.5	1.5	3	6200	4898	4014	18.4	0.71	0.56	1.05	1.42
B-HC1-5-24	Carbon	24	0.63	Top	1.5	0.5	1.5	3	18500	5735	4643	64.7	0.81	1.56	0.95	1.16
B-PC1-5-24	Carbon	24	0.63	Top	1.5	0.5	1.5	3	21700	6727	4643	71.8	0.90	1.73	0.98	1.18
B-HG1-5-24	Glass	24	0.63	Top	1.5	0.5	1.5	3	6400	1984	4643	39.0	0.49	0.94	0.88	1.18
B-HG2-5-24	Glass	24	0.63	Top	1.5	0.5	1.5	3	7300	2263	4643	47.6	0.60	1.15	1.01	1.35
B-PG1-5-24	Glass	24	0.63	Top	1.5	0.5	1.5	3	6401	1984	4643	48.0	0.60	1.16	1.08	1.46
B-HG1-5-24b	Glass	24	0.63	Bott	1.5	0.5	1.5	3	6400	1984	4643	42.2	0.41	0.68	0.95	1.28

Table H.1 FRP Database

Specimen ID	Variables and Experimental Results												Calculated f_{test}/f_{calc}			
	Bar Type	L_s (in.)	d_b (in.)	Cast Pos.	c_{so} (in.)	c_{si} (in.)	c_b (in.)	N_b	E (ksi)	EA (psi)	f'_c (psi)	f_{test} (ksi)	ACI* 440-03	ACI* 440-XX	Proposed	
													Eq. 4-7	Eq. 4-9	Eq. 5-11	Eq. 5-15
B-PG1-5-24b	Glass	24	0.63	Bott	1.5	0.5	1.5	3	6401	1984	4643	50.8	0.49	0.82	1.14	1.54
B-HG1-5-12	Glass	12	0.63	Top	1.5	0.5	1.5	3	6400	1984	4174	27.4	0.69	1.02	0.84	1.21
B-PG1-5-12	Glass	12	0.63	Top	1.5	0.5	1.5	3	6401	1984	4174	30.4	0.76	1.13	0.93	1.34
B-HG-8-24	Glass	24	1.00	Top	1.5	0.5	1.5	3	5700	4503	4174	24.1	0.60	0.81	1.07	1.36
B-HG1-5-12b	Glass	12	0.63	Bott	1.5	0.5	1.5	3	6400	1984	4174	34.8	0.67	0.86	1.07	1.54
B-PG1-5-12b	Glass	12	0.63	Bott	1.5	0.5	1.5	3	6401	1984	4174	39.0	0.75	0.96	1.19	1.72
B-HG-8-24b	Glass	24	1.00	Bott	1.5	0.5	1.5	3	5700	4503	4174	26.7	0.52	0.60	1.19	1.51
B-HG-8-54	Glass	54	1.00	Top	1.5	0.5	1.5	3	5700	4503	4174	33.0	0.37	0.68	1.06	1.24
B-HG1-5-54	Glass	54	0.63	Top	1.5	0.5	1.5	3	6400	1984	4174	50.4	0.28	0.72	0.84	1.05
B-PG1-5-54	Glass	54	0.63	Top	1.5	0.5	1.5	3	6401	1984	4174	50.6	0.28	0.72	0.84	1.05
B-HC1-5-54	Carbon	54	0.63	Top	1.5	0.5	1.5	3	18500	5735	4174	85.0	0.47	1.21	0.92	1.04
B-G1-1	Glass	18	0.63	Top	1.5	0.5	1.5	3	5900	1829	5600	38.3	0.64	1.00	0.95	1.33
B-G2-1	Glass	18	0.63	Top	1.5	0.5	1.5	3	5900	1829	5600	32.6	0.54	0.85	0.81	1.13
B-A-1	Aramid	18	0.63	Top	1.5	0.5	1.5	3	6800	2108	5600	40.4	0.68	1.05	0.95	1.31
B-G1-2	Glass	12	0.63	Top	1.5	0.5	1.5	3	5900	1829	4100	28.9	0.73	1.08	0.92	1.34
B-G2-2	Glass	12	0.63	Top	1.5	0.5	1.5	3	5900	1829	4100	29.5	0.74	1.10	0.94	1.36
B-A-2	Aramid	12	0.63	Top	1.5	0.5	1.5	3	6800	2108	4100	31.1	0.78	1.16	0.93	1.33
B-G1-3	Glass	12	0.63	Top	2.69	2.37	1.5	3	5900	1829	5900	49.3	1.24	1.47	1.16	1.54
B-G2-3	Glass	12	0.63	Top	2.69	2.37	1.5	3	5900	1829	5900	46.8	1.17	1.39	1.10	1.46
B-A-3	Aramid	12	0.63	Top	2.69	2.37	1.5	3	6800	2108	5900	51.7	1.30	1.54	1.15	1.50

* ACI design expressions incorporated the modification factors